



Universitat Autònoma de Barcelona

Escola d'Enginyeria

Departament d'Enginyeria Química

# Scale-up opportunities of microbial electrolysis cells for hydrogen production from wastewater

- PhD Thesis –

Programa de Doctorat en Ciència i Tecnologia Ambientals

Memòria per a obtenir el Grau de Doctor  
per la Universitat Autònoma de Barcelona  
sota la direcció del Dr. Albert Guisasola i Canudas  
i del Dr. Juan Antonio Baeza Labat

Yolanda Ruiz Franco

13 d'abril del 2015





Universitat Autònoma de Barcelona

Escola d'Enginyeria

Departament d'Enginyeria Química

# Scale-up opportunities of microbial electrolysis cells for hydrogen production from wastewater

Programa de Doctorat en Ciència i Tecnologia Ambientals

Memòria per a obtenir el Grau de Doctor  
per la Universitat Autònoma de Barcelona  
sota la direcció del Dr. Albert Guisasola i Canudas  
i del Dr. Juan Antonio Baeza Labat

Yolanda Ruiz Franco

Albert Guisasola i Canudas

Juan Antonio Baeza Labat

Bellaterra, 13 d'abril del 2015



**GENOCOV**  
Departament d'Enginyeria Química  
Escola d'Enginyeria  
Universitat Autònoma de Barcelona  
Tel: 93 5811587



ALBERT GUIASOLA i CANUDAS, professor agregat interí i JUAN ANTONIO BAEZA LABAT, professor agregat, del Departament d'Enginyeria Química de la Universitat Autònoma de Barcelona,

CERTIFIQUEM:

Que l'enginyera química Yolanda Ruiz Franco ha realitzat sota la nostra direcció, el treball que amb títol "Scale-up opportunities of microbial electrolysis cells for hydrogen production from wastewater", es presenta en aquesta memòria, i que constitueix la seva Tesi per optar al Grau de Doctor per la Universitat Autònoma de Barcelona.

I perquè en prengueu coneixement i consti als efectes oportuns, presentem a l'Escola de Postgrau de la Universitat Autònoma de Barcelona l'esmentada Tesi, signant el present certificat.

Bellaterra, 13 d'abril de 2015

Dr. Albert Guisasola i Canudas

Dr. Juan Antonio Baeza Labat



Als meus pares Carme i Jordi,  
al meu germà Jordi i a en Jonathan.

*“The world is moving so fast that the man who says it can't be done  
is generally interrupted by someone doing it.”*

-Elbert Hubbard-





## Agraïments/ Acknowledgements

---

En primer lloc voldria donar les gràcies a l'Albert i el Juan per aquests més de 4 anys junts. I no només per ajudar-me cada cop que m'he quedat estancada, sinó que també per donar-me l'oportunitat quan els la vaig demanar, valorar sempre la meva feina i donar-me lliures els divendres a la tarda ;)

També m'agradaria agrair al Javier la seva preocupació i bones paraules i a la Mireia (i a la Raquel Montes) per trobar sempre el temps per ajudar-me al començament de tot això.

També voldria agrair a tots els "MECs" els anys que hem passat junts. Molt especialment a la Núria, en part responsable que jo hagués començat aquesta tesi. Ha estat un plaer compartir laboratori, despatx i cromatògraf amb tu i espero que encara que ara visquis a Suïssa, no deixem de parlar mai!! Igualment, a la Laura també no només li agraeixo les hores compartides a la universitat, sinó també les que vam passar fora d'ella. Has estat de les persones que més m'han ajudat en les èpoques més difícils del doctorat, i d'això no me n'oblido!! Al Javi, amb qui he compartit els últims dies al laboratori, moltes gràcies per tota la feina feta! I a l'Èdgar, per començar amb tot això des de 0 i facilitar-nos una mica el camí a tots els demés. I el que són les coses! 5 anys estudiant junts i m'ha calgut una tesi per arribar a conèixer-te!!

També vull agrair als companys de grup (Mabel, Luis, Carlota, Edu, Enric...) les estones compartides al laboratori/passadissos i als companys de despatx, tant del vell com del nou (Núria, Laura i Mabel altre cop ;), Cesc, Andrea, Josep Antón, Carlos, Milja, Mariàngel i Rosmery) per fer una mica més divertit el dia a dia.

Voldria també agrair a la Miriam, la Rosa, la Loli, la Nati i la Montse les gestions fetes (que no han estat poques) i a Lorena, la Pili, la Rosi i el Manuel per estar sempre disposats a ajudar-me quan els ho he demanat.

I com no, a la mami!!!!!! gràcies per fer-me el dinar durant tot aquest temps! A més de tot el que he après durant el doctorat, una de les millors coses d'haver-lo fet ha estat poder venir als migdies i veure't!! Al pare, agrair-li sempre l'interès en els meus "bitxets". I al Jordi, gràcies per ser el meu model a seguir en tot. A part de Jack Bauer, ets la persona a

la que més admiro i crec que quan et proposes alguna cosa, no hi ha ningú millor que tu!!! I com no, mil gràcies a les seves dues princesses!!! A l'una per haver-me cuidat i a l'altra per deixar-se cuidar.

També gràcies a les meves dues nenes: a la Klaineta, per tot el temps que vam passar juntes i ajudar-me a desconnectar als migdies amb els nostres passejos. I a la Hanna per alegrar-me els dies i fer-me companyia durant aquests últims mesos d'escriptura de tesi.

I evidentment, gràcies a tots els altres que ja no hi són però que m'hauria agradat poder tenir aquí. Per molt temps que passi, encara no sóc capaç de parlar de vosaltres sense llàgrimes als ulls.

I finalment al Jonathan: et podria donar les gràcies per milions de coses, però ho resumiré en quatre paraules. GRÀCIES PER FER-ME FELIÇ!!!

*The author thanks the Spanish Government for the FPU PhD grant (AP2010-1960) that allowed to conduct her research.*

Nowadays wastewater treatment is an energy-intensive process, even though wastewater contains a large amount of chemical energy stored within the organic contaminants. Microbial electrolysis cells (MEC) are able to recover part of this energy as hydrogen by applying an electric potential. However, there are still important hurdles to overcome before implementation at full-scale of this technology.

In this thesis, the scale-up potential of single-chamber MEC was first evaluated. Single-chamber configuration has as advantage the simple design and operation and lower energy requirements. However, the availability of hydrogen for other microorganisms can reduce both its recovery and purity. The long-term operation of MEC allowed quantifying hydrogen losses related to the consumption by either homoacetogens or methanogens for acetate and methane production, respectively. In both cases the recovery of hydrogen was low and therefore this configuration was excluded.

Two-chamber configuration prevents hydrogen to be consumed, but on the drawback side, the presence of a membrane causes potential losses associated to pH gradients. For this reason, much of the reported experiments at lab-scale have been carried out with media with high buffering capacity when compared to that in wastewater. The performance of MEC with non-buffered medium was assessed and it was observed that both anode and cathode had a higher overpotential than when working with buffered media. The overpotential of the anode, however, was significantly higher as it is a biological system and thus, more sensitive to pH changes.

A pH control was implemented to improve the performance of two-chamber MEC. It was observed that the biological activity could be maintained by controlling the anodic pH at a value close to 7. Furthermore, thermodynamics of the system was favoured by controlling the cathodic pH at low values, leading to hydrogen productions with an energy content 8 times higher than the energy invested on producing it. Thereafter, pH control in the cathode was replaced by the use of an acid effluent from the dairy industry as catholyte.

During this thesis, preliminary experiments regarding inoculation and discontinuous operation were carried out in one unit that will be part of a pilot-scale MEC. The obtained

results were quite promising but some modifications are required for improving the cell performance. Hydrogen recovery must be improved and the duration of batch cycles must be reduced in order to minimize the organic matter consumption by other microorganisms and maximize therefore, the energy recovery from wastewater as hydrogen.

Finally, the resistance of exoelectrogens to starvation was also investigated. It was observed that biological activity was not affected by a period up to 10 days without substrate as long as an electric voltage was applied, thus allowing the consumption of the accumulated substrate as polymer inside the bacterial cell.

With the work developed in this thesis it was concluded that the implementation of MEC aiming at hydrogen production at full-scale has opportunities if a series of strategies are addressed: (i) working in two-chamber configuration thus, preventing hydrogen consumption by other microorganisms, (ii) avoiding a large pH drop in the anode and (iii) reducing the applied potential requirements for hydrogen production by following strategies similar to the use of acid effluents as catholytes.

El tractament d'aigües residuals és avui en dia un procés energèticament intensiu, tot i l'energia química emmagatzemada dins la matèria orgànica contaminant. Mitjançant l'aplicació d'un potencial elèctric, les cel·les d'electròlisi microbiana (MEC) permeten recuperar part d'aquesta energia en forma d'hidrogen. Aquesta tecnologia, però, encara ha de superar obstacles abans de poder ser implementada a escala real.

En aquesta tesi, es va avaluar el potencial d'ampliació de MEC en configuració d'una sola cambra, la qual presenta un disseny i operació més senzills i uns requeriments energètics inferiors. Per contra, la disponibilitat de l'hidrogen per altres microorganismes en pot reduir la recuperació i la puresa. L'operació a llarg termini d'una MEC va permetre la quantificació de les pèrdues d'hidrogen lligades al seu consum per part d'homoacetògens o metanògens per a la producció d'acetat i metà, respectivament. En tots dos casos, la recuperació d'hidrogen va ser baixa, i per tant, aquesta configuració va ser exclosa.

La configuració de MEC en doble cambra evita que l'hidrogen sigui consumit, però la presència d'una membrana provoca pèrdues de potencial associades a gradients de pH. Per això, una gran part dels experiments a escala laboratori reportats s'han dut a terme amb medis amb una alta capacitat tamponant en comparació a la de les aigües residuals. Així doncs, el funcionament de les MEC treballant amb un medi de cultiu sense tamponar va ser avaluat. Es va observar que tant l'ànode com el càtode presentaven unes pèrdues de potencial més grans que amb el medi tamponat, sent aquestes però, més elevades en el cas de l'ànode pel fet de tractar-se d'un sistema biològic i per tant, més sensible als canvis de pH.

Per tal de millorar el funcionament de les MEC en doble cambra, es va implementar una estratègia de control de pH. Controlant el pH de l'ànode a valors propers a 7, l'activitat biològica es mantenia. A més, la termodinàmica del sistema va ser afavorida controlant el pH del càtode a valors baixos, la qual cosa va permetre produir hidrogen amb un contingut energètic fins a 8 cops superior a l'energia invertida en produir-lo. Posteriorment, el control de pH al càtode va ser substituït per l'ús d'un efluent àcid de la indústria formatgera com a catòlit.

Durant aquesta tesi es van dur a terme les primeres proves d'inoculació i operació en discontinu en una unitat que formarà part d'una planta pilot MEC. Els resultats van ser satisfactoris, si bé és cert que algunes modificacions són necessàries per tal de millorar-ne el funcionament. En aquest sentit, s'haurà de millorar la recuperació de l'hidrogen i la duració d'un cicle en discontinu s'haurà de reduir per tal de minimitzar el consum de matèria orgànica per part d'altres microorganismes, i maximitzar per tant, la recuperació energètica de les aigües residuals en forma d'hidrogen.

Per últim, es va investigar la resistència dels exoelectrògens a la inanició. Es va observar que l'activitat biològica del sistema no es veia afectada per un període de fins a 10 dies sense substrat sempre i quan el potencial elèctric es mantingués aplicat, ja que d'aquesta manera, es permetia el consum del substrat acumulat com a polímer a l'interior cel·lular.

Segons el treball desenvolupat en aquesta tesi, la implementació de les MEC a escala real per a la producció d'hidrogen serà possible si: (i) es treballa en configuració de doble cambra evitant el consum d'hidrogen per part d'altres microorganismes, (ii) s'evita un gran descens en el pH de l'ànode i (iii) s'aconsegueix reduir el potencial elèctric aplicat per a la producció d'hidrogen seguint estratègies similars a la utilització d'un efluent àcid com a catòlit.

Actualmente el tratamiento de aguas residuales es un proceso energéticamente intensivo, a pesar de la energía química almacenada dentro de la materia orgánica contaminante. Mediante la aplicación de un potencial eléctrico, las celdas de electrólisis microbiana (MEC) permiten recuperar parte de esta energía en forma de hidrógeno. Sin embargo, esta tecnología aún debe superar algunos obstáculos antes de poder ser implementada a escala real.

En esta tesis, se evaluó el potencial de ampliación de MEC en configuración de una sola cámara, la cual presenta un diseño y operación más sencillos a la vez que unos requerimientos energéticos inferiores. No obstante, la disponibilidad del hidrógeno para otros microorganismos puede reducir su recuperación y pureza. La operación a largo plazo de una MEC permitió la cuantificación de las pérdidas de hidrógeno asociadas a su consumo por parte de homoacetógenos o metanógenos para la producción de acetato y metano, respectivamente. En ambos casos la recuperación de hidrógeno fue baja, y por lo tanto, esta configuración fue excluida.

La configuración de MEC en doble cámara evita que el hidrógeno sea consumido, pero la presencia de una membrana provoca pérdidas de potencial asociadas a gradientes de pH. Por esta razón, una gran parte de los experimentos a escala laboratorio reportados se han llevado a cabo con medios con una alta capacidad tamponante, en comparación a la de las aguas residuales. Así pues, el funcionamiento de las MEC trabajando con un medio de cultivo sin tamponar fue evaluado. Se observó que tanto el ánodo como el cátodo presentaban unas pérdidas de potencial mayores que con medio tamponado, siendo éstas más elevadas en el caso del ánodo por tratarse de un sistema biológico, y por lo tanto, más sensible a los cambios de pH.

Para mejorar el funcionamiento de las MEC en doble cámara se implementó una estrategia de control de pH. Controlando el pH del ánodo a valores cercanos a 7 la actividad biológica se mantenía. Además, la termodinámica del sistema fue favorecida controlando el pH del cátodo a valores bajos, lo cual permitió producir hidrógeno con un contenido energético hasta 8 veces superior a la energía invertida en producirlo.

Posteriormente, el control de pH en el cátodo fue reemplazado por el uso de un efluente ácido de la industria quesera como catolito.

Durante esta tesis se realizaron las primeras pruebas de inoculación y operación en discontinuo en una unidad que formará parte de una planta piloto MEC. Los resultados fueron satisfactorios, aunque para mejorar el funcionamiento tendrán que realizarse algunas modificaciones. En este sentido, la recuperación de hidrógeno tendrá que ser mejorada y la duración de un ciclo en discontinuo tendrá que ser reducida para minimizar el consumo de materia orgánica por parte de otros microorganismos y maximizar, por lo tanto, la recuperación energética de las aguas residuales en forma de hidrógeno.

Por último, se investigó la resistencia de los exoelectrógenos a la inanición. Se observó que la actividad biológica no se veía afectada por un período de hasta 10 días sin sustrato siempre y cuando el potencial eléctrico se mantuviera aplicado, ya que de esta manera, se permitía el consumo del sustrato acumulado como polímero en el interior celular.

Según el trabajo desarrollado en esta tesis, la implementación de las MEC a escala real para la producción de hidrógeno será posible si: (i) se trabaja en configuración de doble cámara evitando el consumo de hidrógeno por parte de otros microorganismos, (ii) se evita un gran descenso en el pH del ánodo y (iii) se consigue reducir el potencial eléctrico aplicado para producir hidrógeno siguiendo estrategias similares a la utilización de un efluente ácido como catolito.



<b>CHAPTER 1 General Introduction</b> .....	<b>1</b>
1.1 Energy from wastewater.....	3
1.2 Bioelectrochemical systems (BES).....	4
1.2.1 Principles of bioelectrochemical systems.....	4
1.2.2 Anode respiring bacteria (ARB) .....	6
1.2.3 Thermodynamics and electromotive force .....	7
1.2.3.1 Thermodynamics of MFC.....	8
1.2.3.2 Thermodynamics of MEC.....	11
1.2.4 Potential losses .....	12
1.2.4.1 Activation losses.....	13
1.2.4.2 Concentration losses.....	16
1.2.4.3 Bacterial metabolic losses .....	17
1.2.4.4 Ohmic losses.....	17
1.2.4.5 Use of potentiostats in BES .....	18
1.2.5 Major achievements in BES.....	18
1.3 Hydrogen as fuel .....	20
1.3.1 Hydrogen production in MEC.....	22
<b>CHAPTER 2 Scope of the thesis</b> .....	<b>25</b>
2.1 Background of the research group in bioelectrochemical systems .....	27
2.2 Research motivations.....	28
2.3 Objectives .....	28
2.4 Thesis overview .....	29
<b>CHAPTER 3 Materials and Methods</b> .....	<b>31</b>
3.1 Reactor configurations and inoculation procedures.....	33
3.1.1 Concentric MEC.....	33
3.1.2 Small-scale air-cathode MFC.....	34
3.1.3 Small-scale MEC .....	36
3.1.4 Two-chamber small-scale MEC .....	37

3.1.5	Inoculation procedure .....	38
3.2	Monitoring of the current intensity .....	41
3.3	Culture medium.....	42
3.4	Analytical methods.....	43
3.4.1	Acetate .....	43
3.4.2	Glucose .....	43
3.4.3	Gas composition .....	43
3.4.4	pH and conductivity.....	45
3.5	Electrochemical techniques.....	45
3.5.1	Polarization curves.....	45
3.5.2	Cyclic voltammetry .....	47
3.5.3	Linear sweep voltammetry.....	48
3.5.4	Chronoamperometry .....	48
3.5.5	Electrochemical impedance spectroscopy .....	49
3.6	System performance indexes .....	50
<b>CHAPTER 4 Long term operation of a single-chamber membrane-less microbial electrolysis cell: electron equivalent balances.....</b>		<b>53</b>
4.1	Introduction.....	55
4.2	Objectives .....	56
4.3	Materials and Methods.....	57
4.3.1	Reactor description and operation .....	57
4.3.2	Batch experiments .....	57
4.3.3	Presence of homoacetogens.....	57
4.4	Results and Discussion .....	58
4.4.1	CE and $r_{CAT}$ as MEC performance indicators.....	58
4.4.2	Including $H_2$ -recycling (with or without hydrogenotrophic methanogenesis).....	60
4.4.2.1	Contribution of the growth processes .....	62
4.4.2.2	Coulombs obtained from the oxidation of the externally added acetate, $C_{AC}$ .....	64

4.4.2.3	Coulombs consumed in the production of the measured $H_2$ , $C_{H_2}$ .....	64
4.4.2.4	Coulombs consumed in the production of $H_2$ converted to $CH_4$ , $C_{CH_4}$ .....	64
4.4.2.5	Coulombs recovered as current intensity, $C_{Cl}$ .....	65
4.4.3	Including hydrogenotrophic methanogenesis when no $H_2$ -recycling is occurring.....	67
4.4.4	Experimental study: Occurrence of $H_2$ -recycling .....	68
4.4.5	Experimental study: Presence of methanogens.....	73
4.5	Conclusions.....	80

**CHAPTER 5 Performance of microbial electrolysis cells with non-buffered and low-conductivity media ..... 81**

5.1	Introduction.....	83
5.2	Objectives .....	85
5.3	Materials and Methods.....	86
5.3.1	Reactors description and medium composition .....	86
5.3.2	Electrochemical analyses.....	86
5.3.3	Batch experiments .....	87
5.4	Results and Discussion .....	87
5.4.1	Inoculation and MFC operation with buffered medium.....	88
5.4.2	Current intensity performance in MEC.....	91
5.4.3	Analysis of single-chamber operation.....	93
5.4.4	Experimental assessment of ion exchange membranes inclusion.....	96
5.4.5	Analysis of two-chamber operation.....	99
5.4.6	Summary of the experimental results .....	101
5.5	Conclusions.....	102

**CHAPTER 6 Enhanced performance of two-chamber microbial electrolysis cells using a pH control strategy ..... 105**

6.1	Introduction.....	107
6.2	Objectives .....	109

6.3	Materials and Methods.....	109
6.3.1	Reactor description and medium composition.....	109
6.3.2	Batch experiments and pH control.....	110
6.3.3	Electrochemical analyses.....	112
6.3.4	Calculations.....	112
6.4	Results and Discussion.....	113
6.4.1	Experiments with well-buffered medium.....	113
6.4.1.1	Enhanced performance of the two-chamber MEC with pH control implementation.....	113
6.4.1.2	Effect of the cathodic pH on the two-chamber MEC performance.....	118
6.4.1.3	Operational problems with high current intensities.....	122
6.4.1.4	Hydrogen production with very low applied voltage.....	124
6.4.1.5	Effect of conductivity on MEC performance.....	125
6.4.2	Experiments with non-buffered medium.....	126
6.4.3	Assessment of the performance of cheese brine as catholyte.....	129
6.5	Conclusions.....	132
<b>CHAPTER 7 Design, building and preliminary data from a novel pilot-scale microbial electrolysis cell.....</b>		<b>133</b>
7.1	Introduction.....	135
7.2	Objectives.....	137
7.3	Materials and Methods.....	137
7.3.1	Reactors description and medium composition.....	137
7.3.2	Batch experiments.....	138
7.4	Results and Discussion.....	138
7.4.1	Reactor design.....	138
7.4.2	Reactor inoculation with anaerobic sludge.....	141
7.4.3	Reactor operation with acetate as substrate.....	144
7.4.4	Reactor operation with glucose as substrate.....	147
7.4.5	Comparison with other works.....	150
7.4.6	Performance of MEC after different starvation periods.....	152

7.5 Conclusions.....	157
<b>CHAPTER 8 General conclusions and future work.....</b>	<b>159</b>
8.1 General conclusions.....	161
8.2 Future work.....	163
<b>References.....</b>	<b>165</b>
List of Figures.....	185
List of Tables.....	193
List of Acronyms and Abbreviations.....	195
Glossary.....	197
<b>APPENDIX Understanding limitations of CV in high-surface bioanodes.....</b>	<b>203</b>
Curriculum Vitae.....	221



# CHAPTER 1

---

General Introduction





## 1.1 Energy from wastewater

Activated sludge process for domestic wastewater treatment involves high operating costs due to large energy requirements for aeration, pumping and solids disposal. In Spain, 13,592,255 m<sup>3</sup> of wastewater were daily treated in 2012 [1] with an estimated energy cost of 0.67 Kwh/m<sup>3</sup> [2], which means that approximately 1.4 % of the energy consumption in Spain was used for wastewater treatment [3].

This situation is projected to worsen in the coming decades due to the increase of the population and the economic growth, which will result in an increase of **wastewater** generated. Moreover, as fossil fuels become increasingly scarce, prices will inevitably rise leading to higher wastewater treatment costs.

However, the amount of chemical energy stored in organics within wastewater is 10-fold higher than the amount of energy to treat it [4,5] and therefore, wastewater treatment may become an energy neutral or even a net energy producer process by recovering part of the energy content of wastewater. Furthermore, the carbon footprint of wastewater treatment and the associated greenhouse emissions could be reduced.

Anaerobic digestion could be an alternative to the aerobic activated sludge treatment for domestic wastewater, by which methane can be produced from organic matter. This methane can be later combusted to produce electricity with an efficiency of 35 % [6]. In addition to energy production, the quantity of digested sludge resulting from anaerobic treatment would be much lower than with aerobic treatment and hence, the costs associated to solids disposal will be lower. However, the organic matter removal would probably not be enough and a post-treatment step would be required. Moreover, low temperatures and low organic matter concentrations have been reported as unfavourable conditions for anaerobic treatment [6].

Recently, bioelectrochemical systems (BES) have emerged as a promising technology for wastewater treatment and valorisation. Nevertheless, BES are in their early stages of development and further research is still required to increase its efficiency and to reach full-scale application.

## 1.2 Bioelectrochemical systems (BES)

BES are an emerging technology, which use microorganisms to catalyse oxidation or reduction reactions at an electrode surface to either produce electrical power in systems known as microbial fuel cells (MFC) or a wide range of value-added compounds (such as hydrogen) by applying a small voltage in systems known as microbial electrolysis cells (MEC). As previously stated, BES are being nowadays studied as an alternative for wastewater treatment, as they would allow recovering part of the energy contained in wastewater.

### 1.2.1 Principles of bioelectrochemical systems

BES are based on the capability of exoelectrogenic bacteria or anode respiring bacteria (ARB) to transfer electrons out of the cell, thus coupling their metabolic pathways to external solid electron acceptors under anaerobic conditions. In BES, ARB oxidize organic compounds from wastewater and use a solid anode, where they grow as a biofilm, as electron acceptor under anaerobic conditions. The electrons obtained from the oxidation reaction flow through an electric circuit to the cathode, where a reduction reaction takes place. Both the anodic and cathodic processes can be physically separated by an ion exchange membrane (IEM), selectively allowing cations flow (cation exchange membrane, CEM) or anions flow (anion exchange membrane, AEM).

MFC usually operate with cathodes exposed to air and thus, oxygen is reduced at the cathode. By contrast, in MEC aiming at hydrogen production, the cathode is kept also under anaerobic conditions and protons are reduced, producing hydrogen gas. Figure 1.1 shows the schematic representation of both MFC and MEC.

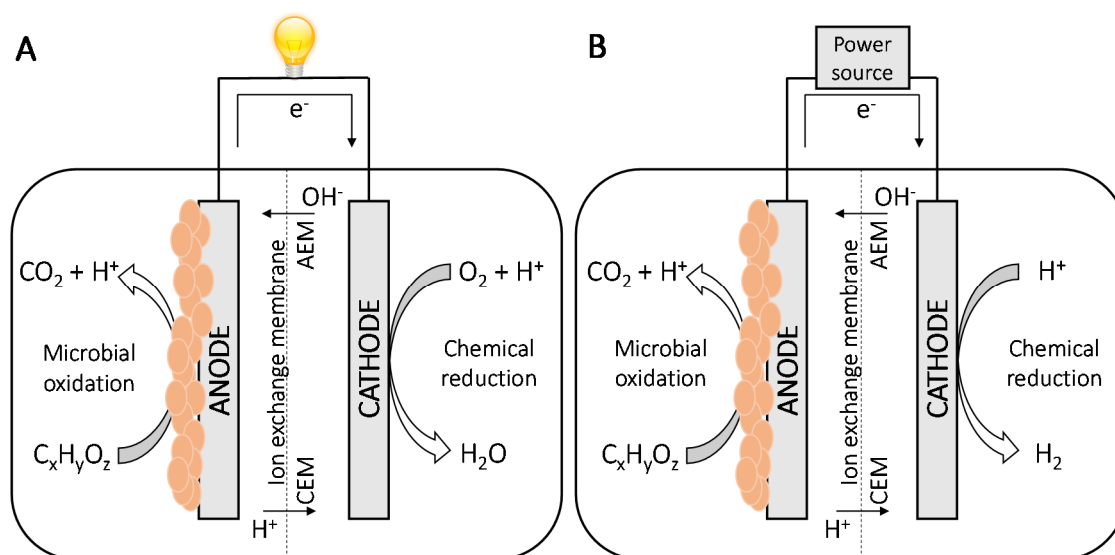


**Figure 1.1** Schematic diagram of (A) microbial fuel cell (MFC) and (B) microbial electrolysis cell (MEC) aiming at hydrogen production.

The half-reactions at the anode and cathode of an MFC with acetate as electron donor and the corresponding standard reduction potentials are summarized in Table 1.1.

**Table 1.1** Electrode half-reactions in MFC and standard reduction potentials.

Electrode	Reaction	$E^0$ (V) vs SHE
Anode	1. $CH_3COO^- + 4H_2O \rightarrow 2HCO_3^- + 9H^+ + 8e^-$	0.187
	2. $O_2 + 4H^+ + 4e^- \rightarrow 2H_2O$	1.229
Cathode	3. $O_2 + 2H_2O + 4e^- \rightarrow 4OH^-$	0.401

The half-reactions at the anode and cathode of an MEC producing hydrogen with acetate as electron donor and the corresponding standard reduction potentials are summarized in Table 1.2.

**Table 1.2** Electrode half-reactions in MEC and standard reduction potentials.

Electrode	Reaction	$E^0$ (V) vs SHE
Anode	1. $CH_3COO^- + 4H_2O \rightarrow 2HCO_3^- + 9H^+ + 8e^-$	0.187
Cathode	4. $2H^+ + 2e^- \rightarrow H_2$	0
	5. $2H_2O + 2e^- \rightarrow H_2 + 2OH^-$	-0.828

Note that the cathodic reaction in both MFC and MEC can be described either as protons consumption or hydroxyls production, since protons and hydroxyls are always in equilibrium with each other through the water dissociation constant ( $K = [H^+]\cdot[OH^-] = 1\cdot 10^{-14}$ ).

### 1.2.2 Anode respiring bacteria (ARB)

ARB have the ability of transferring electrons out of the cell and thus, they use extracellular electron acceptors. In nature, Fe(III) and Mn(III/IV) oxides are two common electron acceptors in the absence of oxygen [7]. This ability was exploited to reduce solid conductors, which led to the development of BES.

Electrical current generation has been reported for alpha-, beta-, gamma-, and delta-proteobacteria, as well as for firmicutes, acidobacteria and yeasts [8]. Examples of microorganisms with exoelectrogenic capabilities are: *Geobacter sulfurreducens* [9], *Geobacter metallireducens* [10], *Shewanella oneidensis* [11], *Pseudomonas aeruginosa* [12], *Desulfuromonas acetoxidans* [10], *Rhodospirillum rubrum* [13] and *Geothrix fermentans* [14].

Several mechanisms have been proposed for the extracellular electron transfer (EET) by ARB (Figure 1.2), which include among others direct electron transfer to the anode via c-type cytochromes located on the outer cell surface [15]. This EET mechanism requires physical contact between cells and the anode surface. However, anodic biofilms may have a relatively large thickness and bacteria at a greater distance from the anode also contribute to current intensity generation through a conductive biofilm matrix containing cytochromes or through electrically conductive pili called “nanowires” [16,17].

Electron transfer between cells and the anode can also be mediated by soluble electron shuttles: compounds that are sequentially reduced by bacteria and then oxidized by the anode. Electron shuttles can be produced by bacteria themselves or artificially added [18].

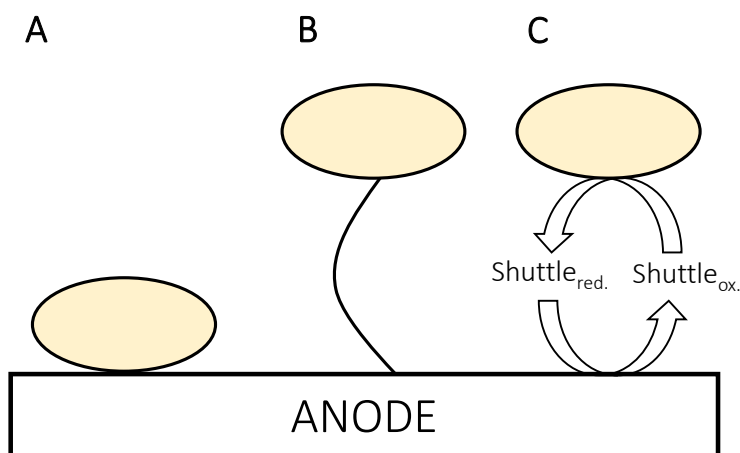


**Figure 1.2** Extracellular electron transfer for ARB (A) Direct transfer by direct contact or through a conductive biofilm matrix (B) Direct transfer by conductive pili and (C) Indirect transfer by means of electron shuttles.

Simple fermentation products, such as acetate, are the most common substrates used in BES. However, research is currently being done with a wider range of substrates with the aim of applying BES for a sustainable wastewater treatment. In this framework, studies have been carried out with substrates, such as propionate, butyrate, glucose [19], lactate [20], starch [21,22], xylose [23], oxalate [24] or even with domestic, brewery [25,26], chocolate industry [27] and paper recycling [28] wastewaters among others. As substrate-utilization capabilities of ARB are mainly limited to simple fermentation products, the development of syntrophic consortia between fermenters and ARB are required to treat complex wastewaters [22,29].

### 1.2.3 Thermodynamics and electromotive force

Electrical power will be produced in an electrochemical system if the overall reaction is thermodynamically favourable, which can be evaluated in terms of Gibbs free energy (equation 1.1). If the Gibbs free energy is positive, then the process is non-spontaneous and it requires an external energy input to drive the reactions. In contrast, if it is negative, then the process is spontaneous and occurs without an external energy input.

$$\Delta G_r = \Delta G_r^0 + RT \ln(\Pi) \quad (1.1)$$

where  $\Delta G_r$  ( $\text{J mol}^{-1}$ ) is the Gibbs free energy for the specific conditions,  $\Delta G_r^0$  ( $\text{J mol}^{-1}$ ) is the Gibbs free energy under standard conditions ( $T=298.15$  K, concentration  $=1$  mol  $\text{L}^{-1}$  and  $P=1$  atm),  $R$  is the universal gas constant ( $8.31447$  J  $\text{mol}^{-1} \text{K}^{-1}$ ),  $T$  (K) is the temperature and  $\Pi$  is the reaction quotient calculated as the activities of the products divided by those of the reactants, each raised to the power of its stoichiometric coefficient. The standard reaction Gibbs free energy can be calculated from the tabulated energies of formation of organic compounds in water.

However, thermodynamics in electrochemical systems are evaluated in terms of the electromotive force,  $E_{\text{emf}}$ , which indicates the theoretical maximum attainable potential of an spontaneous process ( $E_{\text{emf}} > 0$ ) or the voltage required to drive the reactions of a non-spontaneous process ( $E_{\text{emf}} < 0$ ). Both  $\Delta G_r$  and  $E_{\text{emf}}$  can be related by the following expression [30]:

$$E_{\text{emf}} = -\frac{\Delta G_r}{bF} \quad (1.2)$$

where  $E_{\text{emf}}$  (V) is the electromotive force,  $b$  is the number of moles of electrons transferred in the reaction (per mole of reactant or product) and  $F$  is the Faraday's constant ( $96485$  C/mol  $e^-$ ).

Moreover,  $E_{\text{emf}}$  is calculated as the difference between the theoretical cathodic and anodic potentials (equation 1.3) [30]. Therefore, a process is spontaneous only if the cathodic potential is higher than the anodic potential.

$$E_{\text{emf}} = E_{\text{cathode}}^{\text{eq}} - E_{\text{anode}}^{\text{eq}} \quad (1.3)$$

where  $E_{\text{cathode}}^{\text{eq}}$  (V) and  $E_{\text{anode}}^{\text{eq}}$  (V) are the theoretical cathodic and anodic potentials (equilibrium potentials) at specific conditions.

### 1.2.3.1 Thermodynamics of MFC

The standard reduction potential ( $E^0$ ) of a certain half-reaction is tabulated relative to the standard hydrogen electrode (SHE), which, by convention, is zero at all temperatures to form a basis for comparison with all other electrode reactions. These values, however, must be corrected by means of the Nernst equation when the conditions are other than

standard. The Nernst equation is function of the activities of the species involved in the redox equation. However, since the activity coefficients tend to be unity at low concentrations, activities in this equation are frequently replaced by simple concentrations.

The theoretical reduction potential for an anode in which acetate is oxidized according reaction 1 in Tables 1.1 and 1.2 at specific conditions can be calculated as follows [30]:

$$E_{\text{anode}}^{\text{eq}} = E_{\text{anode}}^0 - \frac{RT}{b_{\text{Ac}^-} F} \ln \left( \frac{C_{\text{CH}_3\text{COO}^-}}{C_{\text{HCO}_3^-}^2 C_{\text{H}^+}^9} \right) \quad (1.4)$$

where  $E_{\text{anode}}^0$  (V) is the standard reduction potential for reaction 1 (0.187 V vs SHE),  $b_{\text{Ac}^-}$  is the moles of electrons transferred per mole of acetate (8 mol  $e^-$  mol $^{-1}$   $\text{Ac}^-$ ), and  $C_{\text{CH}_3\text{COO}^-}$ ,  $C_{\text{HCO}_3^-}$  and  $C_{\text{H}^+}$  (mol L $^{-1}$ ) are the concentrations of acetate, bicarbonate and protons, respectively. By assuming standard conditions at a pH of 7, the theoretical reduction potential of acetate is -0.27 V vs SHE.

The theoretical reduction potential for a cathode in which oxygen is reduced to water according reactions 2 and 3 can be calculated as in equations 1.5 and 1.6 [30,31].

$$E_{\text{cathode}}^{\text{eq}} = E_{\text{cathode\_H}^+}^0 - \frac{RT}{b_{\text{O}_2} F} \ln \left( \frac{1}{p_{\text{O}_2} \cdot C_{\text{H}^+}^4} \right) \quad (1.5)$$

$$E_{\text{cathode}}^{\text{eq}} = E_{\text{cathode\_OH}^-}^0 - \frac{RT}{b_{\text{O}_2} F} \ln \left( \frac{C_{\text{OH}^-}^4}{p_{\text{O}_2}} \right) \quad (1.6)$$

where  $E_{\text{cathode\_H}^+}^0$  and  $E_{\text{cathode\_OH}^-}^0$  are the standard reduction potentials for reactions 2 (1.229 V vs SHE) and 3 (0.401 V vs SHE), respectively,  $b_{\text{O}_2}$  is the moles of electrons transferred per mole of oxygen (4 mol  $e^-$  mol $^{-1}$   $\text{O}_2$ ),  $p_{\text{O}_2}$  (atm) is the partial pressure of oxygen and  $C_{\text{OH}^-}$  (mol L $^{-1}$ ) is the concentration of hydroxyls. By assuming a temperature of 293.15 K, a pH of 7 and atmospheric oxygen concentration (0.21 atm), the theoretical reduction potential of oxygen is 0.81 V vs SHE. Note that the theoretical reduction potential is the same using either of the two equations.

The  $E_{\text{emf}}$  for an MFC with acetate as electron donor at pH 7, calculated by means of equation 1.3 as the difference between the theoretical cathodic and anodic potentials, is

1.1 V, which indicates that the overall process is spontaneous and that a maximum voltage of 1.1 V is attainable.

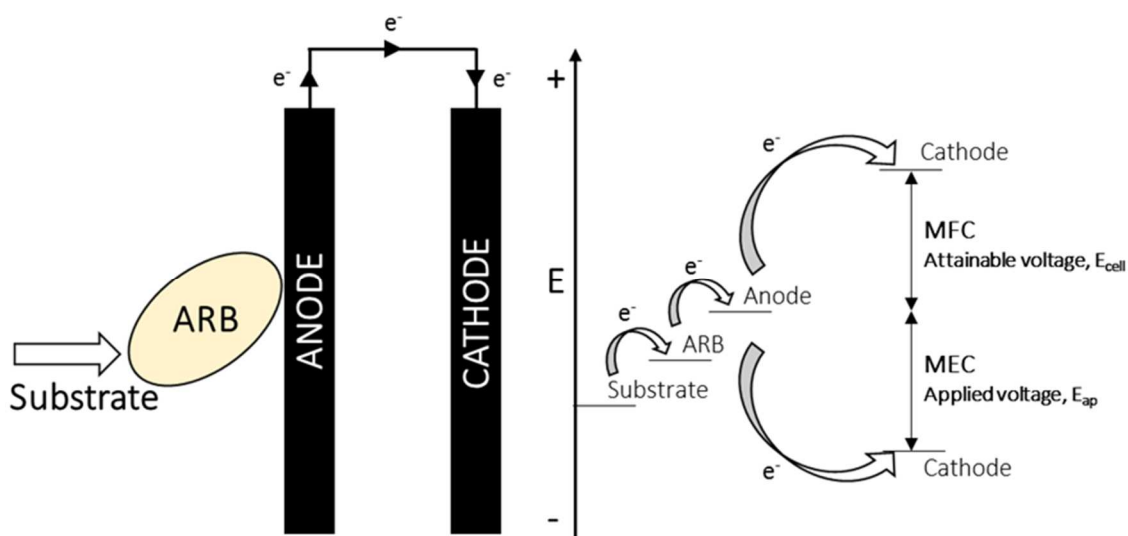


**Figure 1.3** Electron flow according to electrodes potentials. Arrows indicate the direction of electron flow, which is spontaneous only from lower to higher potentials.

Figure 1.3 shows a schematic diagram of the electron flow according to electrode potentials. For an MFC, the anodic potential is lower than the cathodic potential, thus the reaction is spontaneous and the electron flow is favoured.

According to equations 1.4, 1.5 and 1.6, the reduction potentials of reactions 1, 2 and 3 are pH-dependent. In addition, the anodic pH would not only affect thermodynamics, but also the performance of the anodic biofilm, since it is a biological system and thus, sensitive to pH changes. The effect of pH on the theoretical reduction potential of the oxygen reduction reaction (ORR) in the cathode and the  $E_{emf}$  of MFC is displayed in Figure 1.4. An increase of the cathodic pH entails a more negative cathodic potential (Figure 1.4A), which in turn, reduces the attainable voltage (Figure 1.4B).



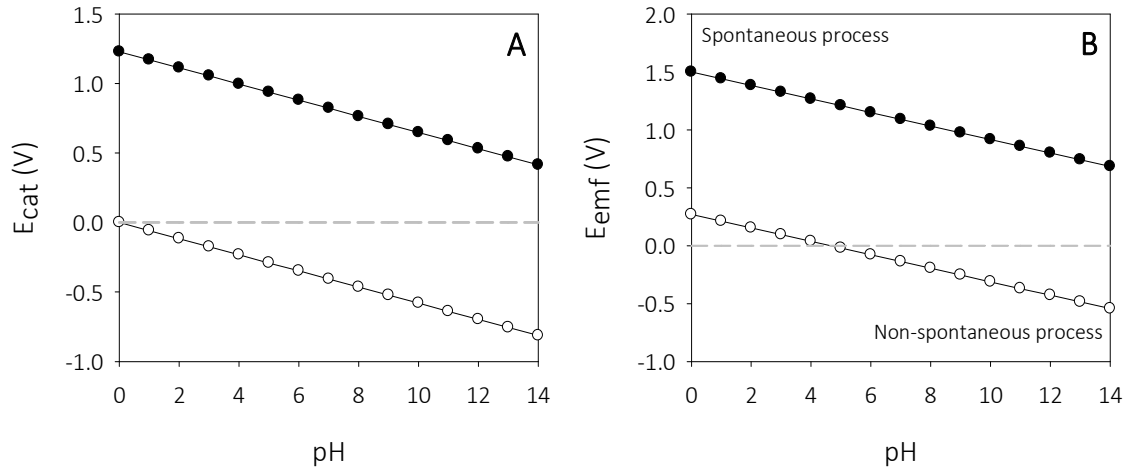


**Figure 1.4** Effect of pH on the (A) theoretical reduction potential of the cathode ( $E_{cathode}^{eq}$ ) and (B) cell electromotive force ( $E_{emf}$ ). For spontaneous processes,  $E_{emf}$  is above the dashed line, whereas for non-spontaneous processes  $E_{emf}$  is below. MFC (●) and MEC (○). For the  $E_{emf}$  calculation, biological standard conditions (pH of 7) were assumed for the anode (adapted from Rozendal [31]).

### 1.2.3.2 Thermodynamics of MEC

The anodic reaction in an MEC is the same as in an MFC, thus the theoretical reduction potential of acetate would be 0.27 V vs SHE at pH 7.

For the hydrogen evolution reaction (HER), the theoretical reduction potential can be calculated by means of either equation 1.7 (reaction 4) or equation 1.8 (reaction 5) [31,32].

$$E_{cathode}^{eq} = E_{cathode\_H^+}^0 - \frac{RT}{b_{H_2}F} \ln \left( \frac{p_{H_2}}{C_{H^+}^2} \right) \quad (1.7)$$

$$E_{cathode}^{eq} = E_{cathode\_OH^-}^0 - \frac{RT}{b_{H_2}F} \ln \left( p_{H_2} C_{OH^-}^2 \right) \quad (1.8)$$

where  $E_{cathode\_H^+}^0$  is the theoretical cathode potential at standard conditions for reaction 4 (0 V vs SHE) and  $E_{cathode\_OH^-}^0$  is the theoretical cathode potential at standard conditions for reaction 5 (-0.828 V vs SHE),  $b_{H_2}$  represents the moles of electrons transferred per mole of hydrogen (2 mol  $e^-$  mol $^{-1}$   $H_2$ ) and  $p_{H_2}$  (atm) is the partial pressure of hydrogen.

By assuming standard conditions at a pH of 7, the theoretical reduction potential of hydrogen is -0.41 V vs SHE. Again,  $E_{\text{cathode}}^{\text{eq}}$  is the same using either of the two equations.

The  $E_{\text{emf}}$  at pH 7 for an MEC with acetate as electron donor, calculated by means of equation 1.3 as the difference between the theoretical cathodic and anodic potentials, is -0.14 V.  $E_{\text{emf}}$  is negative, since the anodic potential is higher than the cathodic potential (Figure 1.3) and then, the overall process is non-spontaneous. According thermodynamics, a minimum applied voltage of -0.14 V will be required to drive the reactions.

The theoretical reduction potential of HER is also pH-dependent and the higher the pH, the more negative the cathodic reaction potential is (Figure 1.4). Moreover, the higher the cathodic pH, the higher the energy requirements to drive the process. In fact, at a very low cathodic pH the process in an MEC aiming at hydrogen production could even be spontaneous according to thermodynamics.

#### 1.2.4 Potential losses

In practice, the voltage that can be achieved in an MFC or that it is required in an MEC differs from the thermodynamic values. This is due to a whole variety of voltage losses occurring in the system (overpotentials), which decrease the attainable voltage in MFC and increase the voltage requirements in MEC.

The real voltage obtained in an MFC can be expressed as follows [30]:

$$E_{\text{cell}} = E_{\text{emf}} - \eta_{\text{cathode}} - \eta_{\text{anode}} - \eta_{\text{ohm}} \quad (1.9)$$

where  $E_{\text{cell}}$  (V) is the real voltage of an MFC,  $\eta_{\text{cathode}}$  (V) and  $\eta_{\text{anode}}$  (V) are the overpotentials at the cathode and the anode, respectively, and  $\eta_{\text{ohm}}$  (V) is the ohmic overpotential.

Similarly, the real voltage requirements for an MEC can be calculated as in equation 1.10 [32].

$$E_{\text{ap}} = E_{\text{emf}} - \eta_{\text{cathode}} - \eta_{\text{anode}} - \eta_{\text{ohm}} \quad (1.10)$$

where  $E_{ap}$  (V) is the applied voltage requirements of an MEC. Note that  $E_{ap}$  is negative in value according to the previous equation.

The overpotentials of both the cathode and the anode can be calculated as the difference between the real (measured) electrode potential and the theoretical reduction potential at specific conditions:

$$\eta_{cathode} = E_{cathode} - E_{cathode}^{eq} \quad (1.11)$$

$$\eta_{anode} = E_{anode} - E_{anode}^{eq} \quad (1.12)$$

where  $E_{cathode}$  (V) and  $E_{anode}$  (V) are real electrode potentials for the cathode and the anode, respectively.

Moreover, overpotentials are a combination of activation, concentration and bacterial metabolic losses. Thus, the following can be stated [30,32]:

$$\eta_{cathode} = \eta_{act,c} + \eta_{conc,c} \quad (1.13)$$

$$\eta_{anode} = \eta_{act,a} + \eta_{conc,a} + \eta_{bact} \quad (1.14)$$

where  $\eta_{act,c}$  (V) and  $\eta_{act,a}$  (V) are the activation losses for the cathode and the anode, respectively,  $\eta_{conc,c}$  (V) and  $\eta_{conc,a}$  (V) are the concentration losses for the cathode and the anode, respectively and  $\eta_{bact}$  (V) are the bacterial metabolic losses for the anodic biofilm.

#### 1.2.4.1 Activation losses

The activation losses represent the voltage loss required to initiate a reaction, i.e. the overpotential required to overcome the activation energy of an electrochemical reaction on a catalytic surface. The activation losses depend on the type of catalyst used: a better catalyst decreases the activation energy and hence causes lower activation losses. The relation between the activation losses and the current intensity is described by the Butler-Volmer equation, which is the key equation in electrochemical kinetics [33]. For instance, the Butler-Volmer equation for the ORR of MFC according reactions 2 and 3 is [34]:

$$I = I_{0,c} \left[ \left( \frac{C_{O_2}^*}{C_{O_2}^B} \right) \left( \frac{C_{H^+}^*}{C_{H^+}^B} \right)^4 \exp \left( \frac{-\alpha b_{O_2} F \eta_{act,c}}{RT} \right) - \exp \left( \frac{(1-\alpha) b_{O_2} F \eta_{act,c}}{RT} \right) \right] \quad (1.15)$$

$$I = I_{0,c} \left[ \left( \frac{C_{O_2}^*}{C_{O_2}^B} \right) \exp \left( \frac{-\alpha b_{O_2} F \eta_{act,c}}{RT} \right) - \left( \frac{C_{OH^-}^*}{C_{OH^-}^B} \right)^4 \exp \left( \frac{(1-\alpha) b_{O_2} F \eta_{act,c}}{RT} \right) \right] \quad (1.16)$$

where  $I$  (A) is the current intensity,  $I_{0,c}$  (A) is the exchange current intensity (background current or current intensity at zero overpotential),  $C^*$  (mol L<sup>-1</sup>) stands for the concentration at the catalyst surface,  $C^B$  (mol L<sup>-1</sup>) indicates concentrations at the bulk solution and  $\alpha$  is the transfer coefficient. Both  $I_{0,c}$  and  $\alpha$  are parameters related to the catalyst activity and should be determined for each specific case. A low exchange current intensity corresponds to a high activation energy [35]. A concentration gradient of oxygen from the bulk solution to the catalyst surface can be neglected in MFC cathodes, since oxygen transport limitations occur at very high intensities, which have not been yet achieved in MFC [34,36]. Therefore, the term ( $C_{O_2}^*/C_{O_2}^B$ ) in equations 1.15 and 1.16 could be eliminated.

For the HER at the cathode of an MEC, this relation can be written as in equations 1.17 and 1.18 for reactions 5 and 6, respectively.

$$I = I_{0,c} \left[ \left( \frac{C_{H^+}^*}{C_{H^+}^B} \right)^2 \exp \left( \frac{-\alpha b_{H_2} F \eta_{act,c}}{RT} \right) - \left( \frac{C_{H_2}^*}{C_{H_2}^B} \right) \exp \left( \frac{(1-\alpha) b_{H_2} F \eta_{act,c}}{RT} \right) \right] \quad (1.17)$$

$$I = I_{0,c} \left[ \exp \left( \frac{-\alpha b_{H_2} F \eta_{act,c}}{RT} \right) - \left( \frac{C_{OH^-}^*}{C_{OH^-}^B} \right)^2 \left( \frac{C_{H_2}^*}{C_{H_2}^B} \right) \exp \left( \frac{(1-\alpha) b_{H_2} F \eta_{act,c}}{RT} \right) \right] \quad (1.18)$$

There are several approximations to the Butler-Volmer equation such as the high-field approximation (or Tafel equation) or the low-field approximation (or the linear current-potential equation). However, the conditions for its applicability must be validated in each case.

In the anode of both MFC and MEC, ARB serve as catalysts and therefore, reduce the activation losses of the oxidation reaction. Hence, differences between a well-inoculated

and a non-inoculated anode are found in the activation losses. As previously stated, the Butler-Volmer relationship describes electron transfer kinetics. However, the process occurring at the anode is governed by both enzyme kinetics (conversion of organics into carbon dioxide, protons and electrons) and electron transfer kinetics (electron transfer from microorganisms to the anode). In this context, several works have dealt with the kinetics of the bioanodes and proposed several models.

The Nernst-Monod model, for instance, is a modified version of the Monod model by considering the anode as a final electron acceptor [37]. Hence, it describes the bioanode kinetics as a function of the substrate concentration and the anode potential. The Nernst-Monod model is written as follows:

$$I = I_{\max} \left( \frac{1}{1 + e^{-\frac{F}{RT}(E_{\text{anode}} - E_{\text{KA}})}} \right) \left( \frac{C_s}{K_s + C_s} \right) \quad (1.19)$$

where  $I_{\max}$  (A) is the maximum current intensity determined by the enzymatic reaction,  $E_{\text{KA}}$  (V) and  $K_s$  ( $\text{mol L}^{-1}$ ) are the anode potential and the substrate concentration at which the current intensity is half the  $I_{\max}$ , respectively and  $C_s$  is the substrate concentration ( $\text{mol L}^{-1}$ ).

The Butler-Volmer-Monod (equation 1.20), meanwhile, improves the previous model in those cases in which the electron transfer is not that fast when compared to the enzymatic reaction [38].

$$I = I_{\max} \frac{1 - e^{-\frac{F}{RT}\eta_{\text{anode}}}}{K_1 \cdot e^{-\frac{(1-\alpha)F}{RT}\eta_{\text{anode}}} + K_2 \cdot e^{\frac{F}{RT}\eta_{\text{anode}}} + \left( \frac{K_s}{C_s} + 1 \right)} \quad (1.20)$$

where  $\eta_{\text{anode}}$  is the anodic overpotential (V),  $K_1$  is a lumped parameter describing the ratio between the biochemical and the electrochemical reaction rates and  $K_2$  is a lumped parameter describing the ratio between the forward and the backward biochemical rate constants. The anodic overpotential ( $\eta_{\text{anode}}$ ) is used in the Butler-Volmer-Monod equation instead of the anodic activation losses ( $\eta_{\text{act},a}$ ), which means that the different anodic overpotentials are considered in this model. However, it has to be noted that

experiments for fitting the model were conducted avoiding mass transfer limitations, thus the anodic concentration losses ( $\eta_{\text{conc},a}$ ) could be neglected.

#### 1.2.4.2 Concentration losses

Concentration losses ( $\eta_{\text{conc}}$ ) affect the thermodynamics of a reaction and are caused by reactant or product diffusion limitations between the bulk solution and the electrode surface.  $\eta_{\text{conc}}$  can be estimated as the difference between the theoretical reduction potential calculated at the bulk solution concentrations ( $E^{\text{eq}}$ ) and at the local electrode concentrations (indicated by the superscript \*).

$$\eta_{\text{conc},c} = E_{\text{cathode}}^{\text{eq}} - E_{\text{cathode}}^* \quad (1.21)$$

$$\eta_{\text{conc},a} = E_{\text{anode}}^{\text{eq}} - E_{\text{anode}}^* \quad (1.22)$$

As previously discussed, concentration overpotentials related to oxygen on the cathodes of MFC can be neglected and, therefore, concentration losses are only associated to either protons or hydroxyls. Equation 1.23 and 1.24 can be obtained by combining equation 1.21 with equations 1.5 and 1.6, respectively.

$$\eta_{\text{conc},c} = \frac{RT}{b_{\text{O}_2} F} \ln \left( \frac{C_{\text{H}^+}^{\text{B}}}{C_{\text{H}^+}^*} \right)^4 \quad (1.23)$$

$$\eta_{\text{conc},c} = \frac{RT}{b_{\text{O}_2} F} \ln \left( \frac{C_{\text{OH}^-}^*}{C_{\text{OH}^-}^{\text{B}}} \right)^4 \quad (1.24)$$

Similarly, assuming that concentration overpotentials related to hydrogen are negligible (as its diffusivity is higher than that of oxygen), the cathodic concentration losses of MEC for reactions 5 and 6 can be obtained by combining equations 1.21 with equations 1.7 and 1.8, respectively.:

$$\eta_{\text{conc},c} = \frac{RT}{b_{\text{H}_2} F} \ln \left( \frac{C_{\text{H}^+}^{\text{B}}}{C_{\text{H}^+}^*} \right)^2 \quad (1.25)$$

$$\eta_{\text{conc},c} = \frac{RT}{b_{\text{H}_2}F} \ln \left( \frac{C_{\text{OH}^-}^*}{C_{\text{OH}^-}^B} \right)^2 \quad (1.26)$$

According to the previous equations, a local pH increase at the cathode surface entails potential losses that reduce the attainable voltage in MFC and increase the voltage requirements in MEC. In fact, the  $\eta_{\text{conc},c}$  increases 0.059 V for each unit increase of pH at 25°C.

For the anodic reaction,  $\eta_{\text{conc},a}$  can be associated to either acetate (reactant) or both bicarbonate and protons (products) mass transport limitations. In the case of proton transport limitations, the pH would decrease inside of the biofilm, which might not only affect to reaction thermodynamics, but also to the bioanodes kinetics as the anodic biofilm is a living catalyst. Hence,  $I_{\text{max}}$  in both equations 1.19 and 1.20 would be lower if proton transport limitations out of the biofilm arises.

#### 1.2.4.3 Bacterial metabolic losses

Bacterial metabolic energy is generated by transporting electrons from a substrate to a final electron acceptor, which in BES, is the anode. The difference between the anode potential and the redox potential of the substrate will determine the metabolic energy gain for bacteria [8].

#### 1.2.4.4 Ohmic losses

The ohmic overpotential,  $\eta_{\text{ohm}}$ , is caused by the resistance to the flow of ions in the electrolyte and through the ion exchange membrane (if present) and the resistance to the flow of electrons through the electrodes and interconnections. These losses can be calculated from Ohm's law (equation 1.27) [8].

$$\eta_{\text{ohm}} = I \cdot R_{\text{int}} \quad (1.27)$$

where  $R_{\text{int}}$  ( $\Omega$ ) is the internal resistance of the cell.

#### 1.2.4.5 Use of potentiostats in BES

Current intensity in BES is limited by the different presented overpotentials. However, the processes occurring at the working electrode (in most cases, the anode) can be studied separately from the other processes of the system when using a potentiostat. A potentiostat is a powerful electrochemical tool, which provides an electrical voltage to compensate for the overpotential of the auxiliary electrode (the cathode) and the ohmic losses. Therefore, current intensity is only limited by the processes at the working electrode [39,40].

In contrast, current intensity is limited by all the processes taking place within the reactor, including both the anodic and cathodic overpotentials and the ohmic losses when using an external resistance in MFC or applying a cell voltage with a power supply in MEC.

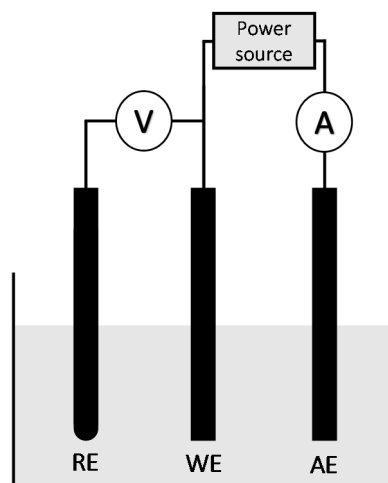


**Figure 1.5** Schematic representation of the experimental setup when using a potentiostat. RE: reference electrode, WE: working electrode, AE: auxiliary electrode, V: voltmeter, A: ammeter. The voltage between the WE and the RE is measured and controlled by modifying the applied voltage between the WE and the AE. The response of the system in terms of current intensity is measured between both the WE and the AE.

#### 1.2.5 Major achievements in BES

Since the first observation of electroactive microorganisms, many achievements and relevant applications have been developed in the field of BES, which are summarized in Table 1.3.



**Table 1.3** Major achievements and applications of BES.

Year	Achievement / Application
1911	First report on electricity generation by microbial cultures. An electrochemical potential was generated when the yeast <i>Saccharomyces cerevisiae</i> and the bacterium <i>Escherichia coli</i> were provided with different organic substrates [41].
1931	Operation of microbial fuel cells connected in series, which were capable of providing over 35 volts at a current intensity of 0.2 mA [42].
1963	MFC technology proposed by NASA as an opportunity to recycle astronauts' waste to electricity during space flights [43-45].
1993	Studies on electron mediators addition to enhance both current density and power output in MFC [46].
1999	The biggest breakthrough in MFC after discovering that chemical mediators did not need to be artificially added [47,48].
2004	Air-cathode MFC first used with the aim of increasing the energy output and reduce the operating costs of MFC. Higher power densities were obtained at expenses of lower coulombic efficiencies, i.e. less substrate recovered as current intensity [49].
2005	Development of MEC for hydrogen production by two different research groups [50-52]
2007	An MFC with a biological anode and cathode proposed for simultaneous removal of organic substrates, power production and complete denitrification [53].
2008	Development of Plant-MFC, in which plants and bacteria converted solar energy into electricity [54]. Hydrogen production in a single-chamber MEC lacking a membrane [55].
2009	MEC proposed for methane production [56]. A microbial desalination cell successfully used for desalinating water by taking advantage of the electrical field created [57]. BES for removal of recalcitrant pollutants, such as nitrobenzene [58].
2010	MFC used as biosensors, in which anodic exoelectrogenic bacteria act as the biological sensing element. MFC proposed for the measurement of biological oxygen demand (BOD) [59], microbial activity [60], toxicity [61-63] and dissolved oxygen (DO) [64]. Microbially catalysed reduction in MEC for hydrogen production by means of biocathodes [65].

Year	Achievement / Application
	<p>First report on microbial electrosynthesis, i.e. the production of organic compounds from carbon dioxide by means of biocathodes [66].</p> <p>Production of NaOH in BES both with synthetic wastewater and a real effluent of a brewery site [67].</p> <p>Development of microbial electrodialysis cells to simultaneously desalinate water and produce hydrogen by applying an electrical voltage [68].</p>
2011	First single-chamber pilot-scale MEC for hydrogen production operated with winery wastewater [26].
2013	<p>Alteration of fermentation pathways by supplying electrical current to microbial communities at the cathode of BES [69].</p> <p>Operation of a two-chamber pilot-scale MEC for simultaneously domestic wastewater treatment and hydrogen production [70].</p>

### 1.3 Hydrogen as fuel

Among all the possible renewable energy sources, hydrogen gas is one of the most attracting alternatives for the scientific community and has great potential as fuel of future. It is a clean energy carrier, without an impact on the greenhouse gas emission at the point of use and a high combustion heat ( $-143 \text{ kJ g}^{-1}$ ) when compared to other possible biofuels ( $\text{CH}_4$ ,  $-50 \text{ kJ g}^{-1}$  or ethanol,  $-26.8 \text{ kJ g}^{-1}$ ) [71]. Moreover, hydrogen can be very efficiently converted into electricity by means of chemical fuel cells when compared to biogas [72]. Besides being an important energy carrier, hydrogen is also an important feedstock to the chemical industry.

Nowadays most hydrogen is produced by steam methane reforming, a process in which steam reacts with methane to yield carbon monoxide and hydrogen at high temperatures ( $700\text{-}850^\circ\text{C}$ ) under 3-25 bar pressure in the presence of a metal-based catalyst [73]. Hydrogen can also be produced from coal by gasification. As these are non-sustainable technologies, research is focused on the development of alternatives for renewable hydrogen generation.

Among the different alternatives, electrolysis of water, i.e. the decomposition of water into oxygen ( $\text{O}_2$ ) and hydrogen gas ( $\text{H}_2$ ), is a promising technology when renewable

energy sources such as solar and wind power are used to fulfill the energy requirements of the process (minimum of 1.23 V).

Hydrogen can be also produced biologically, which has great advantages over steam methane reforming, since hydrogen would be a renewable and carbon-neutral fuel. Biological hydrogen production can be achieved by photosynthesis, dark fermentation in addition to bioelectrochemistry. Despite its great advantages, bio-hydrogen is not yet practical because of limitations inherent to each technology [74].

In photosynthesis, water is dissociated into oxygen and hydrogen using solar energy and photosynthetic microorganisms (green algae and cyanobacteria). Hydrogenase and nitrogenase are the enzymes involved in hydrogen production. However, both enzymes are very sensitive to the presence of oxygen, which is the major technical challenge of this technology.

Hydrogen is also produced when bacteria use protons as an electron sink during dark fermentation of organic substrates. The main advantages of this process are the high hydrogen production rates and the possibility to produce it from complex organic sources. On the drawback side, however, low conversions are achieved [74].

At the present time, several significant challenges must be overcome before the transition from a fossil-fuel dependent economy into a hydrogen-based economy can occur. First, the cost of an efficient and sustainable hydrogen production technology must be reduced. Hydrogen storage systems also require further development, since an efficient and cost-effective storage technology will be critical in view of commercialization of hydrogen. Nowadays, hydrogen is stored in compressed gas tanks (700 bar) and cryogenic liquid hydrogen tanks. However, up to 20 % and 40 % of the energy content of hydrogen is required to compress and liquefy the gas, respectively [75]. Hydrogen can be also stored as solid fuel, in which hydrogen atoms or molecules are tightly bound with other elements in a compound. In this sense, intensive research has been done on several different materials such as metal hydrides, adsorbent materials, and chemical hydrides. Chemical and physical solutions for hydrogen storage offers great promise, but challenges regarding capacity, uptake and release of hydrogen among

others need to be overcome [76]. The cost of hydrogen-based technologies such as fuel cells must be also reduced.

Moreover, demonstrated safety in the production, distribution and use of hydrogen will be critical to establish public confidence and successfully implement a hydrogen infrastructure.

### 1.3.1 Hydrogen production in MEC

As previously introduced, the production of hydrogen at the cathode is possible under complete anaerobic conditions and supplying an energy input. This alternative to electricity generation in BES is very attractive from an economic point of view, since the economic value of hydrogen is higher than the value of electricity [77,78]. The production of hydrogen in MEC have given very promising results at lab-scale but its feasibility at pilot and full-scale conditions is, at this moment, still to be proven. The presence of hydrogen scavengers and the need of high applied voltages are the major limiting weaknesses of this technology [79].

The development of single-chamber MEC allowed producing hydrogen with lower energy requirements [55]. However, the lack of membrane contributes to the growth of hydrogen scavengers, such as hydrogenotrophic methanogens [80], hydrogen oxidizing ARB [81] and homoacetogens [82], which limit significantly the overall performance of hydrogen production. Different operational procedures, such as periodic air exposure [83-85], low pH [83], high applied voltages [86] and low temperatures [83], have been proposed to reduce methane production in MEC. Nevertheless, none of these approaches can satisfactorily suppress hydrogenotrophic activity. Reduction of hydrogen retention time by nitrogen sparging was also proposed to avoid methanogenesis [87]. However, this strategy was not equally efficient for all substrates [22].

The presence of an IEM avoids the growth of hydrogen scavengers [26,82] at expenses of higher costs, since membranes increase the internal resistance of the cell and generate pH gradients, thus higher applied voltages are required [88].

The highest hydrogen production up to now in a single chamber MEC was reported by Call and Logan [55] ( $3.12 \text{ m}^3\text{m}^{-3}\text{d}^{-1}$ ) using a platinum based cathode at 0.8 V of applied

voltage. Nevertheless, first trials on single-chamber pilot-scale MEC could not avoid methanogens proliferation [26].

In contrast, the maximum hydrogen production in two-chamber configuration ( $50 \text{ m}^3\text{m}^{-3}\text{d}^{-1}$ ) was observed by Jeremiasse et al. [89] using a nickel foam cathode at 1 V of applied voltage. However, this hydrogen production rate was not measured but calculated based on the current densities. Moreover, the MEC performance decreased over time. First trials on two-chamber pilot-scale MEC showed a high purity gas but the electrical energy input could not be totally recovered as hydrogen [70].

The use of effective catalysts other than platinum, which is highly expensive, would be also critical in view of the real implementation of this technology. Alternative catalysts such as nickel, stainless steel or metal alloys have been also proposed [90-92].



# CHAPTER 2

---

Scope of the thesis





This thesis is framed in one of the research lines of the GENOCOV group (Research Group on Biological Treatment and Valorisation of Liquid and Gas Effluents) from the Department of Chemical Engineering at the Universitat Autònoma de Barcelona. GENOCOV was established in 1994 to research on improving biological processes for the treatment of urban and industrial water and gaseous effluents. In 2009, the research line on Bioelectrochemical Systems was born within the new focus of the group: not only optimising wastewater treatment, but also recovering most of the chemical energy contained in it as hydrogen. This is the third thesis in the research line and was started in 2011 with the initial goal of understanding the fundamentals of bioelectrochemical systems from an engineering point of view in order to bridge the gap between lab-experiments and full-scale implementation.

## 2.1 Background of the research group in bioelectrochemical systems

Although the research line of Bioelectrochemical Systems in GENOCOV was recently created, at the time this thesis began, a low-cost procedure to select ARB from anaerobic sludge was already developed [93]. Moreover, most of the analytical techniques for volatile fatty acids and hydrogen/methane analysis were already set up. The group had also incorporated polarisation curves as a routine technique for the analysis and characterization of MFC through a multi-resistance board and had studied many different cell configurations at lab scale for both MFC and MEC.

Significant research was conducted in parallel to this thesis by other PhD students in the field such as the development of a syntrophic consortia between fermentative bacteria and ARB, able to degrade different complex carbon sources (methanol, milk, starch) [22,29] and even treat real industrial effluents such as crude glycerol from the biodiesel industry or whey from the dairy industry in BES.

Moreover, the performance of different cathode materials at neutral and basic pH was also assessed [92], an strategy to avoid methanogenesis in MEC by reducing the hydrogen retention time was developed [87] and the possible degradation of the chemical inhibitor sodium 2-bromoethanesulfonate was evaluated in both MFC and MEC [94]. Finally,

techniques in molecular biology such as real-time PCR were optimized in order to analyse the microbial communities in BES [95].

During this period the group was funded by grants from the Spanish Government (Explora-Ingenio 2010, CTQ2009-06842-E/PPQ) and the Catalan Government (VALTEC13-1-0140) and by an agreement with Carburos Metálicos S.A (Air Products Group).

## 2.2 Research motivations

The full-scale implementation of MEC for hydrogen production from wastewater will be only possible if it becomes cost-effective, i.e. the energy recovered as hydrogen is higher than the energy invested to produce it, or more profitable than other technologies in direct competition. This goal will be only accomplished if high hydrogen production rates are achieved at low applied voltages and hydrogen is not lost during the process.

In a single-chamber MEC, the required potential is theoretically lower when compared to a two-chamber cell and therefore, it might seem a more suitable configuration for scale-up. However, hydrogen scavenging can become a serious obstacle in single-chamber configuration, since hydrogen usage by other microorganisms decreases hydrogen recovery and purity. In contrast, the hydrogen produced at the cathode is not consumed in a two-chamber MEC, but the energy requirements are much higher due to the presence of a membrane and the consequent pH gradients.

This previous premises motivated the study of the benefits and drawbacks of both configurations in terms of energy recovery as well as the development of a strategy to reduce the required voltage for hydrogen production. Furthermore, the fact that this technology is aimed at treating wastewaters motivated the evaluation of the performance of MEC with a culture medium similar to real wastewaters in terms of buffer capacity and conductivity.

## 2.3 Objectives

The main objective of this thesis is to investigate the potential scale-up of MEC as a cost-effective wastewater treatment for organic matter removal and hydrogen production.

This objective includes the study of different cell configurations and strategies to improve its energy efficiency. For this aim, the following specific goals have been set:

- Understanding the fate of hydrogen in membrane-less MEC through the development of electron equivalent balances.
- Assessment of MEC performance decrease with a culture medium similar to real wastewaters in terms of buffer capacity and conductivity, both in single-chamber and two-chamber MEC.
- Development of strategies to reduce the applied potential and, thus, improving the energy efficiency of MEC.
- Design, building and monitoring of an MEC at pilot-scale.

## 2.4 Thesis overview

This document is divided into eight chapters. Chapter 1 comprises a general introduction to the topic and a literature review of the state of the art. In Chapter 2, in which this section is included, the main objectives of this thesis are presented. Chapter 3 comprises the lab setups and the analytical procedures followed in this work. The main results of this thesis are presented from Chapters 4 to 7. Chapter 4 aims at quantifying hydrogen losses in a single-chamber MEC. Chapter 5 discusses the main limitations of MEC when working with non-buffered and low-conductivity media. Chapter 6 describes a pH control strategy to enhance the operation of two-chamber MEC and to reduce the energy requirements for hydrogen production. Chapter 7 details the start-up of one of the modules of the upcoming pilot-scale MEC and discusses the resistance to starvation in MEC. Chapter 8 summarizes the main conclusions drawn from all the work presented and outlines some directions for future research. Additionally, a brief study on the limitations of the cyclic voltammetry in biological anodes with large surface area is included as appendix.



# CHAPTER 3

---

Materials and Methods



### 3.1 Reactor configurations and inoculation procedures

Reactors with different configurations and volumes have been used in this thesis. The main characteristics of each one are described below:

#### 3.1.1 Concentric MEC

The concentric MEC (CC-MEC) was a single chamber membrane-less MEC consisting of a 1300 mL glass vessel provided with several lateral openings tightly sealed with polytetrafluoroethylene (PTFE) rubber caps, which were used as sampling ports (Figure 3.1).

The anode was a handmade graphite fiber brush (70 mm diameter x 70 mm length;  $\approx 0.8 \text{ m}^2$ ; fibers of  $7.2 \text{ }\mu\text{m}$  diameter; PANEX<sup>®</sup>33 160 K, ZOLTEK) wound into a titanium wire [96]. The titanium wire was protected with a plastic sheath to prevent short circuit between anode and cathode. The brush was thermally treated in a muffle furnace at  $450^\circ\text{C}$  for 30 minutes to increase the active area due to microfractures generation and thus, enhance biomass adhesion [97].

The cathode ( $340 \text{ cm}^2$ ) was carbon cloth coated with platinum in carbon powder (0.5 mg Pt/ $\text{cm}^2$ , Electrochem Inc., United States) on the inner side. The catalyst coating was prepared by mixing the platinum suspension (Pt/C) with deionized water ( $4.15 \text{ }\mu\text{L}/\text{cm}^2$ ) using borosilicate glass balls and a vortexer. Later, 2-propanol ( $16.7 \text{ }\mu\text{L}/\text{cm}^2$ , Sigma-Aldrich) and Nafion ( $33.4 \text{ }\mu\text{L}/\text{cm}^2$ , Sigma-Aldrich) were added to obtain a binding paste and the solution was mixed again. The obtained paste was applied to the carbon cloth using a paintbrush. The coating was allowed to air-dry for 24 hours [98].

Both electrodes were arranged concentrically with the cathode in the outer perimeter, so that all ends of the anode were at the same distance from the cathode. Both the titanium wires of the anode and the cathode were pierced on the lateral openings for the electrical connections. Both electrodes were connected to a power supply (TTI QL355TP), which applied the desired potential. An external resistance of  $12 \text{ }\Omega$  was serially connected to the circuit for monitoring purposes. An Ag/AgCl reference electrode ( $+210 \text{ mV}$  vs SHE, Crison reference electrode 5240) was used to monitor the electrode potentials.

The top of the cell was connected to a 0.5 L gas sample bag with a twist type valve (Cali-5-Bond, Ritter), where hydrogen was collected. Previously to its use, the gas bag was filled with nitrogen gas and vacuumed three times. The reactor operated in batch mode and with constant agitation. Both a schematic diagram and an image of the cell are presented in Figure 3.1.

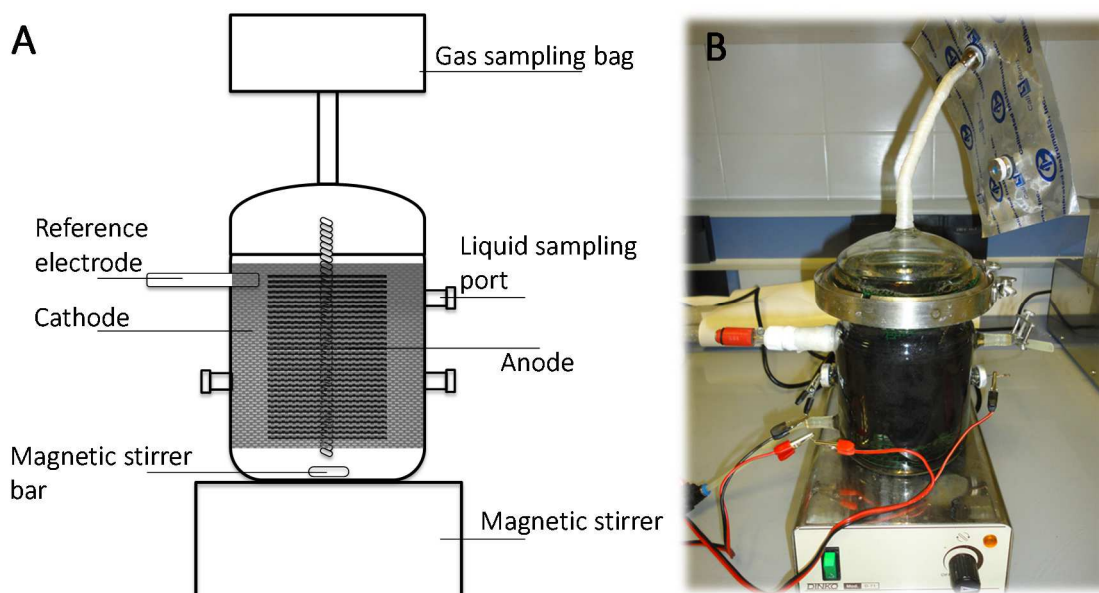


**Figure 3.1** (A) Schematic diagram and (B) image of the CC-MEC.

### 3.1.2 Small-scale air-cathode MFC

One of the drawbacks of the two-chamber MFC configuration is the aeration requirements in the cathodic chamber for the oxygen reduction reaction (ORR) to take place. In this sense, the small-scale air-cathode MFC (SSAC-MFC) configuration overcomes this disadvantage by direct exposure of the cathode to air.

SSAC-MFC were first introduced in Liu and Logan [49]. SSAC-MFC were cylindrical vessels with an empty volume of 28 mL. The body of the cell was a methacrylate cube (4.4 cm length x 5 cm width x 5 cm height) provided with a lateral aperture (3 cm diameter). The cube-shaped body was assembled with two lateral methacrylate endplates by means of O-rings and gaskets to prevent liquid leakages. Pieces were kept together by tightening wing nuts onto bolts.

One of the endplates was perforated and clamped the cathode, which, as previously described, was carbon cloth coated with platinum in carbon powder (0.5 mg Pt/cm<sup>2</sup>,



Electrochem Inc., United States) on the inner side. On the outer face of the cathode, meanwhile, a PTFE diffusion layer permitted oxygen diffusion into the cell while preventing water leakage [99,100]. For its preparation, a mixture of carbon black (1.56 mg/cm<sup>2</sup>, Vulcan XC-72) and 40 wt% PTFE solution (18.7 μL/cm<sup>2</sup>) was first applied using a paintbrush, air-dried for 2 hours and then heated at 370 °C for 30 minutes. Later, a diffusion layer was prepared by applying a coat of 60 wt% PTFE solution to the previously coated side using the paintbrush. The coating was allowed to air-dry for 10 minutes and then heated at 370 °C for about 10 more minutes. This process was repeated to obtain a total of 4 PTFE coatings [98]. The area of the cathode was 7 cm<sup>2</sup>. A lateral tiny hole was used to introduce a protruding titanium wire, which allowed the connection with the cathode. A drop of an epoxy glue was applied to seal the hole and fix the wire in place.

The anode was an industrially manufactured graphite fiber brush (20 mm diameter x 25 mm length; 0.18 m<sup>2</sup>; fibers of 7.2 μm diameter; PANEX®33 160 K, ZOLTEK) wound into a titanium wire of 2 mm diameter [96]. Industrial manufacturing ensured the same characteristics for all anodes.

The cell was also provided with two additional holes (1 cm diameter) tightly sealed by means of a silicone septum, which allowed introducing the anode and a reference electrode (RE-1B, +210 vs SHE, BAS Inc, Japan) if required. The distance between the anode and the cathode was 2 cm. Both electrodes were connected by means of an external resistance of 1000 Ω. Figure 3.2 presents a schematic diagram and an image of the SSAC-MFC.

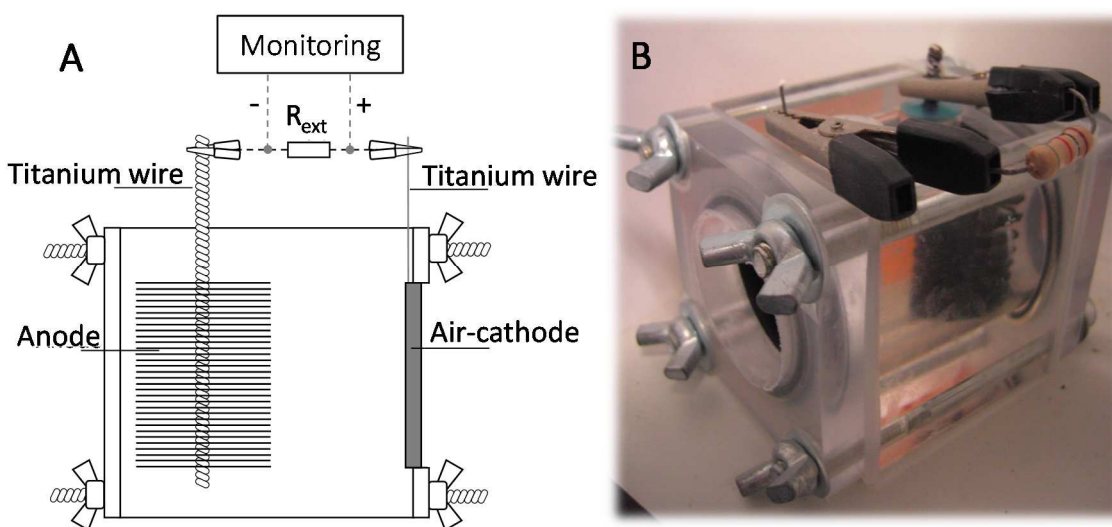


**Figure 3.2** (A) Schematic diagram and (B) image of the SSAC-MFC.

The main advantage of the cube-shaped cells was that they could be used with different configurations, and even be arranged together with other cells. Its robust design in terms of electrode position enhanced repeatability. Moreover, its smaller electrode surface area made easier the electrochemical analysis of the cells (see Appendix).

### 3.1.3 Small-scale MEC

The small-scale MEC (SS-MEC) was an adaptation of the SSAC-MFC and was first presented in Call and Logan [55]. In SS-MEC, none of the endplates was perforated, thus anaerobic conditions were kept also in the cathode.

The anode was a graphite fiber brush as in SSAC-MFC and the cathode was carbon cloth coated with platinum in carbon powder as described before. However the PTFE diffusion layer was not applied on the outer side, since when dealing with MEC the cathode is not exposed to air and therefore, neither the diffusion of air nor the prevention of water leakage are necessary.

The vessel was provided with a glass cylinder at the top, tightly sealed with a PTFE rubber cap that enables gas collection. The cell was filled with 32 mL of medium to avoid gas leakages through the junction between the glass tube and the body of the cell.

The gas produced was further collected in a 0.1 L gas sample bag with a twist type valve (Cali-5-Bond, Ritter) connected to the glass cylinder by means of a PVC tube inserted in the rubber cap. The anode and the cathode were connected to a power supply (TTI QL355TP / HQ Power PS-23023), which applied the desired potential. An external resistance of 12  $\Omega$  was serially connected to the circuit for monitoring purposes. Figure 3.3 presents a picture and a scheme of this cell.

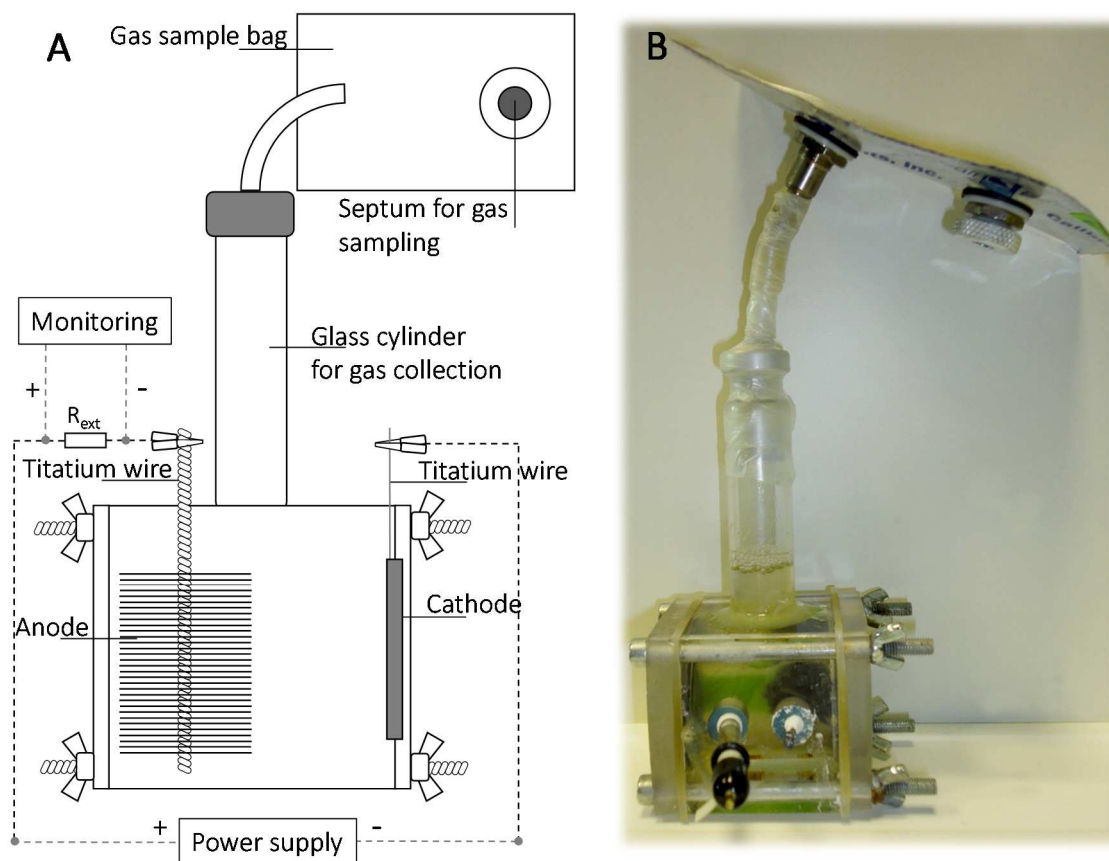


Figure 3.3 (A) Schematic diagram and (B) image of the SS-MEC.

### 3.1.4 Two-chamber small-scale MEC

SS-MEC were easily converted to a double chamber MEC by coupling an identical module and placing an ion exchange membrane in between them. Under this configuration the distance between electrodes increased to 6 cm.

Different types of ion exchange membrane were used: (i) anion exchange membrane, AEM (AMI-7001, Membranes International INC) and (ii) cation exchange membrane, CEM (Nafion N-117, fuelcellstore.com). Before its use, ion exchange membranes were pre-treated to allow for membrane hydration and expansion. The AEM was soaked overnight in a 5 wt% sodium chloride solution at 37°C according to the supplier indications. The pre-treatment procedure for the CEM, meanwhile, consisted of boiling the membrane in a 3 wt% H<sub>2</sub>O<sub>2</sub> solution, followed by boiling it in deionized water and then, boiling it in 0.5 M H<sub>2</sub>SO<sub>4</sub> for at least 1 h each step. Finally the membrane was boiled in deionized water for a further 1 h to remove the remaining H<sub>2</sub>SO<sub>4</sub> [101].

In some experiments, however, no membrane was placed in between the modules, so the cell could work as single-chamber MEC and maintain the distance between the electrodes at 6 cm for comparison purposes.

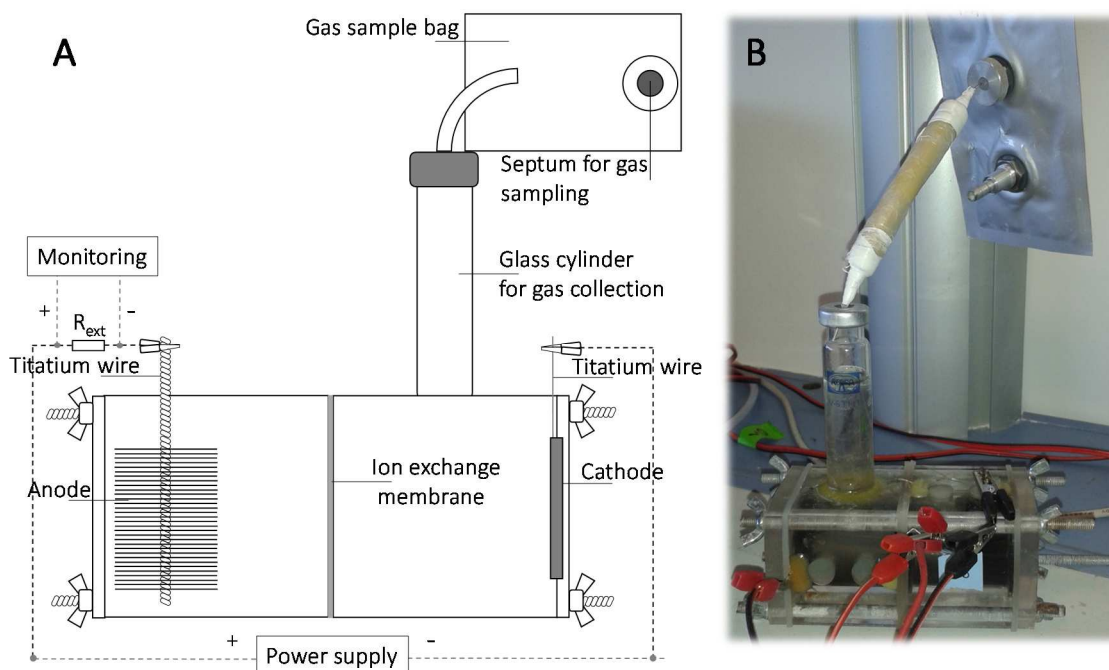


**Figure 3.4** (A) Schematic diagram and (B) image of the two-chamber SS-MEC.

### 3.1.5 Inoculation procedure

Different inoculation procedures were followed depending on the type of cell and anode. In most cases, anodes were first inoculated as MFC due to the simplicity of its operation and the enriched anodes were later transferred to MEC.

The inoculation procedure used for the handmade anodes (70 mm diameter x 70 mm length) was based on the sediment/benthic MFC (Sed-MFC) presented in Ribot-Llobet et al. [93].

This cell is an adaptation of the benthic MFC concept with a simplified lab-configuration. A benthic MFC harvest energy in natural environments by placing an anode in the sediment and connecting it with an electrical circuit to the cathode, which is placed in the overlying water layer [102-106]. The laboratory cell consisted of a plastic vessel of 1 L of capacity with the anode connected to a cathode according to Figure 3.5.

The titanium wire of the anode was protected with a plastic sheath to prevent short circuit between anode and cathode. The anode was placed in an anaerobic sludge blanket at the bottom of the cell, thus conditions were maintained anaerobic. The cathode was commercial stainless steel wool, a low-cost material with a high specific surface area, which counterbalances its low catalytic power. The cathode was floating in the upper layer of the cell in contact with the medium and the atmosphere, allowing oxygen to react on the cathode surface.

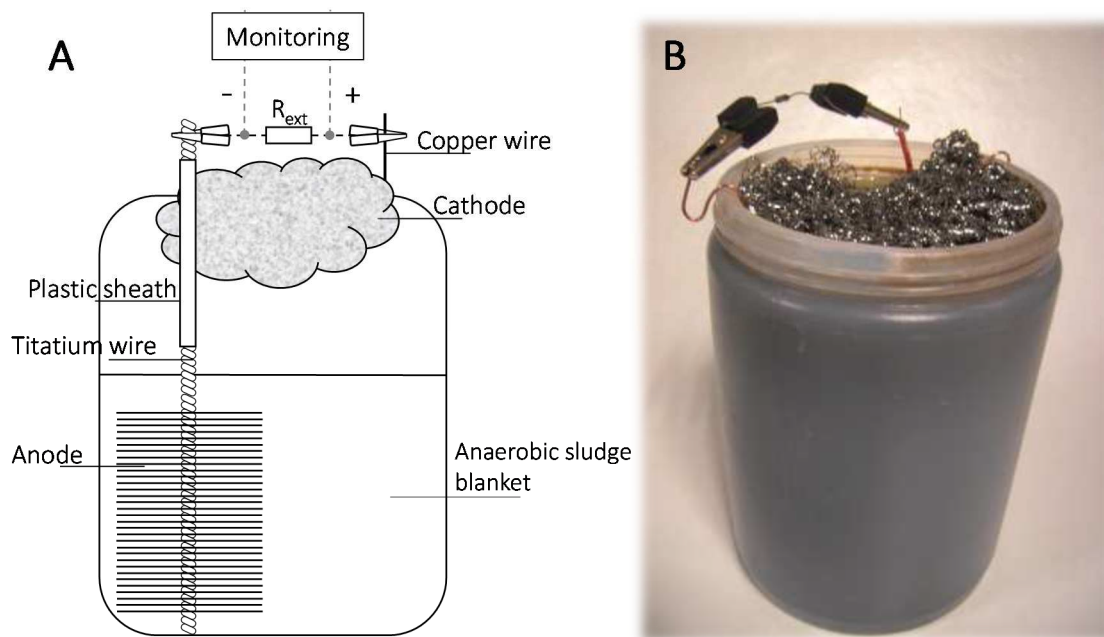


**Figure 3.5** (A) Schematic diagram and (B) image of the Sed-MFC.

The cell was filled with 500 mL of anaerobic sludge from the anaerobic digester of an urban wastewater treatment plant (Manresa, Barcelona), which was used as inoculum since it is easily available and contains a high diversity of bacterial communities, including electrochemically active strains of bacteria [107]. The vessel was filled with the usual culture medium up to 1 L. The final conductivity and pH of the cell were adjusted (when required) to be between 15-25 mS/cm and 7, respectively. The circuit was then closed by connecting an external resistance (1000  $\Omega$ ) between the anode and the cathode. During the inoculation period, fresh medium was regularly added to avoid substrate depletion and to ensure good contact between the cathode and the medium, thus otherwise reaction could not have taken place.

According to Ribot-Llobet et al. [93], a period of 30 days ensured an acceptable biofilm development. After this enrichment step, the handmade graphite fiber brush was carefully washed to remove the remaining sludge and relocated in an air-cathode MFC (AC-MFC) of 400 mL to allow ARB growth.

The design of the AC-MFC of 400 mL was based on the same concept as in SSAC-MFC, a single-chamber MFC with the cathode directly exposed to air, thus aeration was not required. The AC-MFC consisted of a 400 mL glass vessel with a lateral aperture (6.3 cm diameter). The cathode was carbon cloth with the same characteristics as in SSAC-MFC, but with an area of 31 cm<sup>2</sup>. The cathode was clamped between the glass vessel and a perforated glass endplate with a protruding titanium wire for its electrical connection. The titanium wire of the anode was pierced on a cap provided with a silicone septum used to maintain anaerobic conditions near the anode. An external resistance of 1000  $\Omega$  was used to connect both electrodes through the titanium wires. After a period of 10-15 days, the anode could be transferred to the CC-MEC. A schematic diagram and a picture of the cell are presented in Figure 3.6.

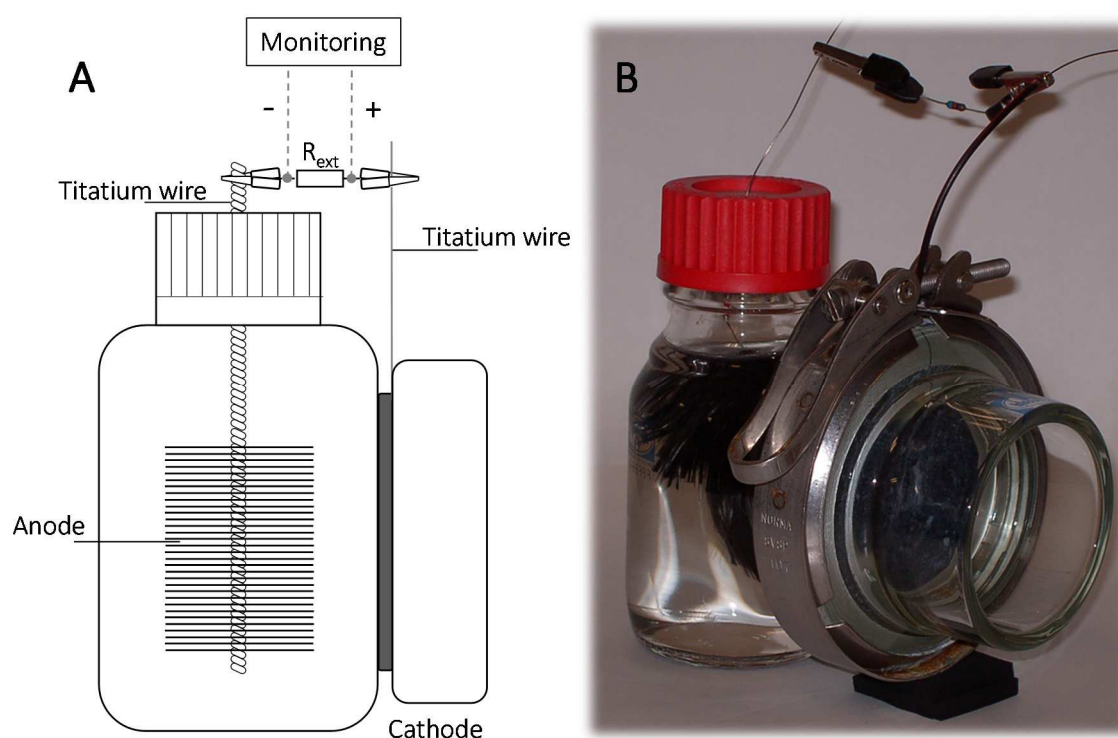


**Figure 3.6** (A) Schematic diagram and (B) image of the AC-MFC.

Cube-shaped cells were inoculated from existing MFC to reduce the startup time. In the laboratory there were four AC-MFC (called “farmhouses”) in which no experiments were carried out, but they were aimed at maintaining an ARB-enriched biomass for bioaugmentation purposes. They were fed with acetate pulses when the voltage decreased below 100 mV and the medium was renewed only once a month to maximize the concentration of ARB in suspension.

To inoculate the anode, SSAC-MFC was filled first with 15 mL of broth from the “farmhouses”, 15 mL of fresh medium and acetate at a final concentration of 1.5 g/L. As previously stated, although the objective was to work in a SS-MEC, the inoculation was conducted in a SSAC-MFC. The circuit was then closed with the external resistance. The voltage across the external resistance was monitored and when decreasing below 100 mV, the medium was replaced by fresh medium and the anode was reinoculated with 50% reactor broth of the previous batch cycle. This procedure was repeated until the behaviour of the SSAC-MFC was the same in two consecutive cycles. From that moment, the medium was completely renewed when substrate was depleted.

This inoculation procedure lasted about 15 days. Hence, it was significantly shorter than the inoculation process by means of Sed-MFC, since in this case we started from an ARB-enriched biomass.

### 3.2 Monitoring of the current intensity

The voltage across the external resistance of both MFC and MEC was monitored by using a 16-bit data acquisition card (Advantech PCI-1716) connected to a personal computer with software developed in LabWindows CVI (2010-2014) (named Addcontrol) for data acquisition. In the case of MFC, the external resistance was used for both closing the circuit and monitoring, whereas in MEC the external resistance was serially connected to the circuit exclusively for monitoring purposes. A low external resistance (12  $\Omega$ ) was used to avoid the resistance to interfere in the cell performance.

The current intensity was calculated from the voltage data according to the Ohm’s law:

$$I = V/R_{\text{ext}} \quad (3.1)$$

where  $I$  (A) is the current intensity,  $V$  (V) is the voltage drop across the resistance and  $R_{\text{ext}}$  ( $\Omega$ ) is the external resistance.

### 3.3 Culture medium

The synthetic medium used in this thesis was defined according to Parameswaran et al. [82]. This medium was chosen to ensure no lack of compounds like nitrogen and iron. Nitrogen is an essential element in the protein structure, which in turn compose the nanowires by which ARB transfer the electrons to a solid acceptor. Iron is the central atom in the heme group of cytochromes, components of the electron transport chain. In fact, electron transport in bacterial nanowires is reported to consist of a hopping/tunnelling between cytochromes [108].

The macronutrients solution contained per liter: 12.04 g  $\text{Na}_2\text{HPO}_4$  and 2.06 g  $\text{KH}_2\text{PO}_4$ , so that the final phosphate buffered saline (PBS) concentration was 100 mM, 0.2 g  $\text{NH}_4\text{Cl}$ , 4 mg  $\text{FeCl}_2$ , 6 mg  $\text{Na}_2\text{S}$  and 5 mL of a mineral media solution. The reduced form of iron ( $\text{Fe}^{2+}$  instead of  $\text{Fe}^{3+}$ ) and sulphur ( $\text{S}^{2-}$  instead of  $\text{SO}_4^{2-}$ ) were used to avoid them to be used as electron acceptor. In Parameswaran et al. [82] a concentration of 0.41 g/L  $\text{NH}_4\text{Cl}$  was used. However, this concentration had to be reduced due to inhibition problems. The macronutrients solution was stored at 4°C until use.

The mineral medium stock solution contained per liter: 1 g EDTA, 0.164 g  $\text{CoCl}_2 \cdot 6\text{H}_2\text{O}$ , 0.228 g  $\text{CaCl}_2 \cdot 2\text{H}_2\text{O}$ , 0.02 g  $\text{H}_3\text{BO}_3$ , 0.04 g  $\text{Na}_2\text{MoO}_4 \cdot 2\text{H}_2\text{O}$ , 0.002 g  $\text{Na}_2\text{SeO}_3$ , 0.02 g  $\text{Na}_2\text{WO}_4 \cdot 2\text{H}_2\text{O}$ , 0.04 g  $\text{NiCl}_2 \cdot 6\text{H}_2\text{O}$ , 2.32 g  $\text{MgCl}_2$ , 1.18 g  $\text{MnCl}_2 \cdot 4\text{H}_2\text{O}$ , 0.1g  $\text{ZnCl}_2$ , 0.02 g  $\text{CuSO}_4 \cdot 5\text{H}_2\text{O}$  and 0.02 g  $\text{AlK}(\text{SO}_4)_2$ .

Sodium 2-bromoethanesulfonate was added to chemically inhibit methanogenic growth and activity [109]. However, the utilization of this chemical inhibitor is not economically feasible at a real scale. Acetate was used as substrate in most of the experiments. The initial pH and conductivity of the medium was around 7.5 and 13 mS/cm, respectively. Cells were sparged with nitrogen for 10 minutes to remove dissolved oxygen after medium replacement in MEC.



## 3.4 Analytical methods

### 3.4.1 Acetate

Acetate concentration was analyzed with gas chromatography (Agilent Technologies, 7820-A) using a DB-FFAB column (30 m x 250  $\mu\text{m}$  x 0.25  $\mu\text{m}$ ; length x internal diameter x film thickness) and a flame ionization detector. A sample of 1  $\mu\text{L}$  was injected at a temperature of 275 $^{\circ}\text{C}$  under split conditions (29 psi). The carrier gas was helium with a split ratio of 10:1. The column temperature was set to 85 $^{\circ}\text{C}$  for 1 min, followed by a first increase of 3 $^{\circ}\text{C min}^{-1}$  until a stable value of 130 $^{\circ}\text{C}$  was reached and then 35 $^{\circ}\text{C min}^{-1}$  up to 220 $^{\circ}\text{C}$ . The detector temperature was set at 275 $^{\circ}\text{C}$ , with 350  $\text{mL min}^{-1}$  air, 40  $\text{mL min}^{-1}$  hydrogen and 30  $\text{mL min}^{-1}$  make up gas (helium) supplied. The run time was 19 min.

The procedure for the sample preparation consisted of pipetting 0.6 mL of 0.22- $\mu\text{m}$  filtered samples in a glass vial of 1.5 mL together with 0.75 mL of deionized water and 0.15 mL of a preserving solution. Sample vials were then stored in the freezer (-20 $^{\circ}\text{C}$ ) until being analysed.

The preserving solution used in sample preparation was used as internal standard as well as for sample storage purposes. It contained the following components in 1 L of deionized water: 2 g of  $\text{HgCl}_2$ , 2 g of hexanoic acid and 33.7 g of orthophosphoric acid. The solution was sonicated in an ultrasonic bath for a complete dissolution of the compounds. Hexanoic acid was used as internal standard in peaks quantification analysis.

### 3.4.2 Glucose

Glucose concentration was measured with an YSI Biochemistry Analyser (2700 SELECT Biochemistry Analyser).

### 3.4.3 Gas composition

Hydrogen, oxygen, nitrogen and methane were analysed with the same gas chromatograph using a HP-mole sieve column (30m x 320  $\mu\text{m}$  x 12  $\mu\text{m}$ ; length x internal diameter x film thickness) and a thermal conductivity detector. A sample of 1 mL was manually injected by means of a gas tight syringe (1 mL Hamilton Samplelock Syringe) at a temperature of 200 $^{\circ}\text{C}$  under split conditions (8 psi). The carrier gas was argon with a

split ratio of 44:1. The column temperature was set to 40°C. The detector was set at 220°C, with 20 mL min<sup>-1</sup> reference flow (argon) and negative polarity signal. The run time was 6 min.

The total hydrogen or methane production was calculated using the “Gas Bag Method” presented in Ambler and Logan [110]. The procedure followed consisted of first analysing the initial composition of the gas in the bag. After that, a known volume of a tracer gas (nitrogen) was added in the gas bag using a gastight syringe (10 mL Hamilton Samplelock Syringe) and then, the new composition was also analysed. From these two analyses and as shown in the following calculation procedure, the initial total volume of gas within the bag and therefore, the volumes of hydrogen and methane could be estimated.

#### *Calculation procedure for the Gas Bag Method*

The initial volume of nitrogen in the gas bag ( $V_{T,b,i}$ ) can be calculated as the product of the initial nitrogen mole fraction in the gas bag ( $X_{T,b,i}$ ) and the initial total volume of gas in the bag ( $V_{b,i}$ ) as shown in equation 3.2.

$$V_{T,b,i} = X_{T,b,i} \cdot V_{b,i} \quad (3.2)$$

After the analysis of the initial composition of the gas (which implies gas volume losses) and the addition of a certain volume of nitrogen, the mole fraction of nitrogen can be calculated as follows:

$$X_{T,b,f} = \frac{V_{T,b,i} + V_{T,b,a} - V_L \cdot X_{T,b,i}}{V_{b,i} + V_{T,b,a} - V_L} \quad (3.3)$$

where  $X_{T,b,f}$  is the mole fraction of nitrogen after the addition of a known volume of nitrogen ( $V_{T,b,a}$ ) and  $V_L$  is the total gas volume lost from the bag due to the analysis.

By combining equations 3.2 and 3.3 and rearranging the terms, the initial total volume of the gas in the bag can be calculated from the data obtained from both analyses.

$$V_{b,i} = \frac{-V_{T,b,a} + V_L \cdot X_{T,b,i} + V_{T,b,a} \cdot X_{T,b,f} - V_L \cdot X_{T,b,f}}{X_{T,b,i} - X_{T,b,f}} = V_L + V_{T,b,a} \frac{1 - X_{T,b,f}}{X_{T,b,f} - X_{T,b,i}} \quad (3.4)$$

The total volume of hydrogen and methane can be calculated as the product of their initial mole fraction and the volumes of gas in the bag and the headspace of the reactor (previous tests showed that the gas composition of the headspace was practically the same as that on the gas bag).

$$V_{\text{H}_2} = X_{\text{H}_2, \text{b}, \text{i}} \cdot (V_{\text{b}, \text{i}} + V_{\text{h}}) \quad (3.5)$$

where  $V_{\text{H}_2}$  is the volume of hydrogen produced,  $V_{\text{h}}$  is the volume of the headspace of the reactor and  $X_{\text{H}_2, \text{b}, \text{i}}$  is the initial mole fraction of hydrogen in the gas bag.

$$V_{\text{CH}_4} = X_{\text{CH}_4, \text{b}, \text{i}} \cdot (V_{\text{b}, \text{i}} + V_{\text{h}}) \quad (3.6)$$

where  $V_{\text{CH}_4}$  is the volume of methane produced and  $X_{\text{CH}_4, \text{b}, \text{i}}$  is the initial mole fraction of methane in the gas bag.

The moles of hydrogen and methane corresponding to that volume were calculated assuming a pressure of 1 atm in the reactor-bag system and room temperature.

### 3.4.4 pH and conductivity

A pHmeter (Crison micropH 2001) and a conductimeter (Crison microCM 2100) were used for routine pH and conductivity measurements at the initial and the final time of a batch experiment.

## 3.5 Electrochemical techniques

### 3.5.1 Polarization curves

The performance of MFC in terms of internal resistance ( $R_{\text{int}}$ ) and maximum power output ( $P_{\text{max}}$ ) was assessed by means of polarization and power curves. Polarization curves were obtained with a multi-resistance board which allowed changing the external resistance of the cell. The set of external resistances used was 470 k $\Omega$ , 218 k $\Omega$ , 44.2 k $\Omega$ , 24.1 k $\Omega$ , 12.1 k $\Omega$ , 6600  $\Omega$ , 3300  $\Omega$ , 2000  $\Omega$ , 1650  $\Omega$ , 1000  $\Omega$ , 825  $\Omega$ , 470  $\Omega$ , 250  $\Omega$ , 218  $\Omega$ , 100  $\Omega$ , 50  $\Omega$  and 25  $\Omega$ .

The medium was renewed previous to the recording of polarization curves to ensure substrate availability during the experiments. The cells were then connected to their

usual external resistance and once a steady state current was achieved, they were left in open circuit (OC) for 30 minutes. After that, a polarization curve was performed by changing the resistances from the highest to the lowest one. A 10 min period was used for voltage stabilization at each resistance. The voltage drop across each resistance was measured by means of a multimeter. Current intensity was calculated by Ohm's Law (equation 3.1) and power by the following relationship:

$$P = V \cdot I \quad (3.7)$$

where  $P$  (W) is the power output.

An example of a polarization and power curve is presented in Figure 3.7. The overpotentials are current dependent and as a result, the polarization curve can be divided into three clearly differentiated regions (Figure 3.7A) with different prevailing potential losses [30]. In the first region, where the voltage undergoes a rapid decrease at low current intensities, the activation losses become especially apparent. In the second region, the ohmic losses prevail over the others and produce a nearly linear decrease in voltage. Finally, in the third region the voltage drops back quickly at high current intensities due to the concentration overpotentials.

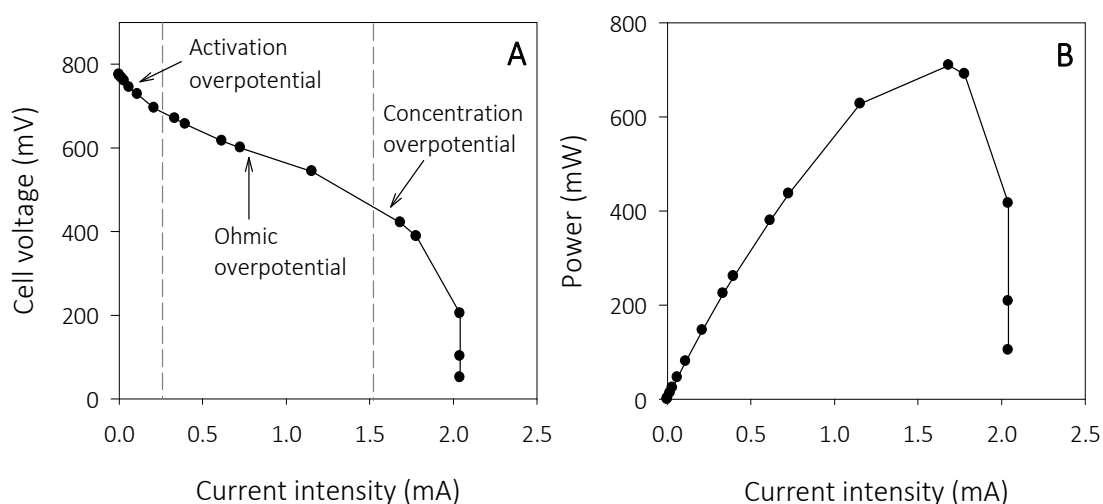


**Figure 3.7** Example of a polarization curve (A) and a power curve (B) in an MFC.

In the second region, the current-voltage curve follows the Ohm's law, since the decrease in voltage is linear. Hence, the slope of the curve can be assumed to be the  $R_{int}$  of the cell.

The  $P_{\max}$  can be easily deduced from the maximum value in the power curve of Figure 3.7B.

### 3.5.2 Cyclic voltammetry

Cyclic voltammetry (CV) is an electrochemical technique that is used to characterize the electron transfer processes. The application of CV is nowadays a very common practice in the study of BES to characterize the electron transfer interactions between microorganisms and anodes [111].

In a CV, the reaction occurring at the working electrode is studied through the analysis of the current response when a cyclic potential sweep is imposed on this electrode (i.e. the working electrode potential is ramped linearly versus time and when it reaches a set potential, the ramp is reversed) (Figure 3.8A). The working electrode potentials ( $E$ ) are measured relative to the reference electrode, whereas intensity is measured between the working and the auxiliary electrode (Figure 3.8B). The applied potential sweep is characterized by four parameters: the scan rate and the initial ( $E_i$ ), switching ( $E_s$ ) and final ( $E_f$ ) potentials. The scan rate is the rate of the sweep of potential, while  $E_i$ ,  $E_s$ , and  $E_f$  set the potentials at which ramp is started, reversed and finished, respectively.  $E_i$  and  $E_f$  usually have the same value. CV is represented by the plot of the current versus the potential at the working electrode (Figure 3.8C) [112].

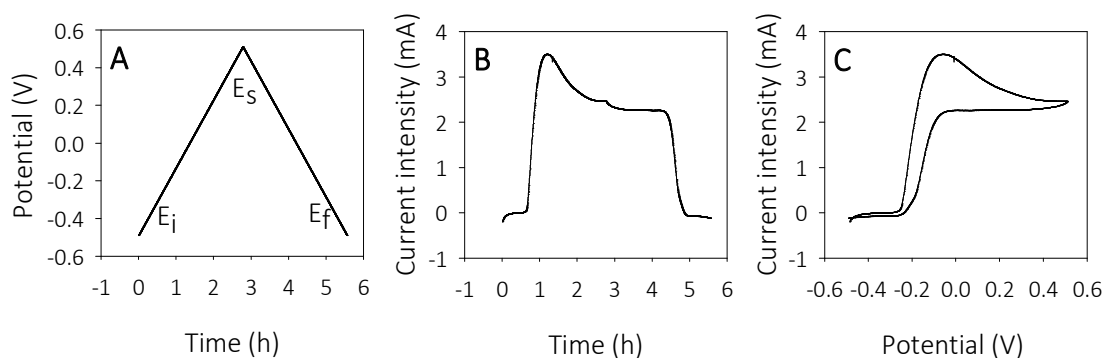


**Figure 3.8** (A) Potential waveform (B) current-time and (C) current-potential representations for a CV experiment.

CV was conducted by using a Multi Autolab system (Ecochemie, Utrecht, Netherlands). CV were recorded either in two or three-electrode mode. In the two-electrode configuration the anode was the working electrode and the cathode was used as both

the auxiliary and the reference electrodes, thus current intensity was obtained for each applied cell potential. CV were recorded from 0 V to 1.2 V. In the three-electrode mode, the anode was the working electrode and the cathode was the auxiliary one. An Ag/AgCl, NaCl 3M electrode (BAS Inc, Japan) was used as reference electrode. CV were recorded from the anode open circuit potential to 0.5 V vs SHE unless otherwise specified. In most experiments, the scan rate was set at either 0.1 mV/s or 1 mV/s. As with polarization curves, medium was renewed before CV recording to ensure substrate availability during the experiment. In the same way, cells were operated at their usual operating conditions until reaching a steady current intensity. Then, cells were left 30 minutes in OC.

### 3.5.3 Linear sweep voltammetry

Linear sweep voltammetry (LSV) was recorded by means of a power supply (TTI QL355TP). The cell applied potential was swept from 0 V to 1.0 V in steps of 0.1 V. A 10 min period was used for current stabilization at each voltage. In single-chamber configuration, an Ag/AgCl was placed in the cell allowing the measurement of the individual electrode potentials with a multimeter. In two-chamber configuration, a second reference electrode was required to measure the potential of both anode and cathode.

LSV was also recorded by means of a Multi Autolab system (Ecochemie, Utrecht, Netherlands) in three electrode configuration, so that the anode was the working electrode and the cathode the auxiliary one. An Ag/AgCl electrode was used as reference. The potential of the working electrode was ramped from the anode open circuit potential to 0.5 V vs SHE at a scan rate of 1 mV/s.

### 3.5.4 Chronoamperometry

A chronoamperometric (CA) method of the Multi Autolab system (Ecochemie, Utrecht, Netherlands) was used in MEC to poise the anode at a potential instead of applying a cell potential by a power supply. The anode was used as the working electrode and the cathode as the auxiliary one. The same Ag/AgCl was used as reference electrode.

In some of the experiments (CV and CA) a special 3-Divider cable was connected to the potentiostat. This cable allowed to monitor the cell applied potential when controlling the working electrode at a certain value.

### 3.5.5 Electrochemical impedance spectroscopy

Electrochemical impedance spectroscopy (EIS) is a powerful electrochemical technique, which also is being widely used in BES. In EIS, a small AC voltage signal is applied to the system and the AC current response is analysed to determine the impedance of the cell at a certain frequency. The different sources of polarization can be separately quantified when performed over a wide frequency range [113].

The graphical representation of the impedance measurements is made by means of Nyquist and Bode plots. Nyquist plots are obtained by plotting the real part of the impedance (X-axis) versus the imaginary part (Y-axis). In Figure 3.9A the Nyquist plot shows a semicircle. Each point of the plot represents the impedance of a certain frequency (although frequency is not explicit in such plots). The impedance at the high-frequency limit is the ohmic resistance ( $R_{\Omega}$ ), whereas the diameter of the semicircle is the polarization resistance ( $R_p$ , associated to the activation overpotentials). Thus, the impedance at the low frequency limit is  $R_{\Omega} + R_p$ . The Bode plot, meanwhile, presents information of the impedance modulus, frequency and phase angle (Figure 3.9B).

Impedance data can be adjusted to equivalent circuits consisting of resistors, capacitors and inductors for obtaining more refined values of each of the individual impedances [113].

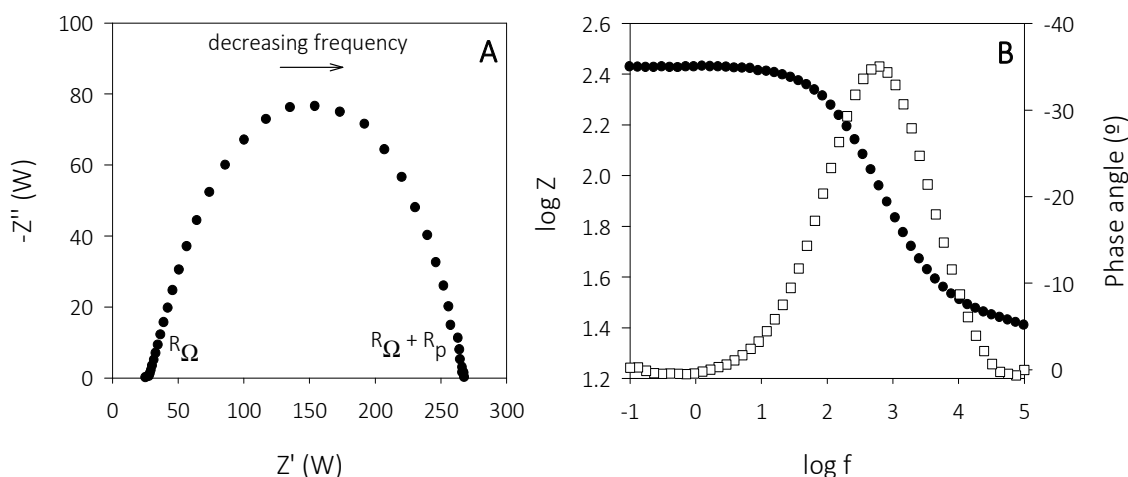


**Figure 3.9** Example of impedance measurement of the cathode of an MEC (A) Nyquist plot and (B) Bode plot: logarithm of impedance modulus (●) and phase angle (□).

In this thesis, EIS was only used for the quantification of  $R_{\Omega}$ . Impedance was measured by means of a Multi Autolab system equipped with a FRA32M module (Ecochemie, Utrecht, Netherlands) using a two-electrode configuration. The anode was used as the working electrode and the cathode as both the auxiliary and reference electrodes. EIS analyses were recorded at the cell open-circuit voltage (OCV) in a frequency range from 100 kHz to 10 mHz and with an amplitude of the AC perturbation of 10 mV. Cells were acclimated to the applied potential for 30 min previous to any impedance measurement.

### 3.6 System performance indexes

The performance of both MFC and MEC was evaluated by means of coulombic efficiency (CE), i.e. the ratio of the coulombs recovered as current intensity to the coulombs that could be theoretically generated from the substrate oxidation. CE was calculated as in equation 3.8.

$$CE = \frac{\int_{t_0}^{t_F} I dt}{F b_S V_L \Delta c M_S^{-1}} \quad (3.8)$$

where  $t_0$  and  $t_F$  (s) are the initial and final times of a batch experiment,  $F$  is the Faraday's constant (96485 C/mol  $e^-$ ),  $b_S$  is the number of  $e^-$  transferred per mole of substrate,  $\Delta c$  ( $g L^{-1}$ ) is the substrate concentration change over a batch cycle,  $M_S$  ( $g mol^{-1}$ ) is the molecular weight of the substrate and  $V_L$  (L) is the volume of liquid in the reactor (or in the anodic chamber if working in two-chamber configuration).

Moreover, MEC performance was also assessed by means of the cathodic gas recovery and energy efficiencies. The cathodic gas recovery ( $r_{CAT}$ ) compares the coulombs consumed in hydrogen production with the coulombs arriving to the cathode as current intensity.  $r_{CAT}$  was calculated as in equation 3.9.

$$r_{CAT} = \frac{V_{H_2} b_{H_2} F V_m^{-1}}{\int_{t_0}^{t_F} I dt} \quad (3.9)$$



where  $V_{H_2}$  (L) is the volume of produced hydrogen,  $b_{H_2}$  is the number of moles of  $e^-$  transferred per mole of hydrogen ( $2 \text{ mol } e^- \text{ mol}^{-1} H_2$ ) and  $V_m$  is the molar gas volume ( $24.03 \text{ L mol}^{-1}$ ) at  $20^\circ\text{C}$ .

The energy recovery of the cell, i.e. the amount of energy produced as hydrogen with respect to the energy input, was calculated in relation to: (i) the electrical input ( $r_E$ ), (ii) the energy content of the substrate ( $r_S$ ) and (iii) both the electrical input and the energy content of the substrate ( $r_{E+S}$ ) as described in Selembo et al. [91].  $r_E$ ,  $r_S$  and  $r_{E+S}$  were calculated by means of equations 3.10, 3.11 and 3.12, respectively.

$$r_E = \frac{W_{H_2}}{W_E} = \frac{n_{H_2} \Delta H_{H_2}}{\int_{t_0}^{t_F} (IE_{ap} - I^2 R_{ext}) dt} \quad (3.10)$$

where  $W_{H_2}$  (kJ) is the energy content of the produced hydrogen,  $W_E$  (kJ) is the energy input by the power supply,  $n_{H_2}$  are the moles of produced hydrogen,  $\Delta H_{H_2}$  is the heat of combustion of hydrogen ( $-285.83 \text{ kJ mol}^{-1}$ ) and  $E_{ap}$  (V) is the applied voltage.

$$r_S = \frac{W_{H_2}}{W_S} = \frac{n_{H_2} \Delta H_{H_2}}{n_S \Delta H_S} \quad (3.11)$$

where  $W_S$  (kJ) is the energy content of the substrate,  $n_S$  are the moles of consumed substrate and  $\Delta H_S$  ( $\text{kJ mol}^{-1}$ ) is the heat of combustion of the substrate.

$$r_{E+S} = \frac{W_{H_2}}{W_E + W_S} = \left( \frac{1}{r_E} + \frac{1}{r_S} \right)^{-1} \quad (3.12)$$

Two different substrates have been used in this thesis, acetate and glucose. The following table summarizes the values of  $b_s$ ,  $M_s$  and  $\Delta H_s$  for each substrate.

**Table 3.1** Summary of the parameter values for acetate and glucose

Substrate, S	$b_s$ ( $\text{mol } e^- \text{ mol}^{-1}\text{S}$ )	$M_s$ ( $\text{g S mol}^{-1}\text{S}$ )	$\Delta H_s$ ( $\text{KJ mol}^{-1}\text{S}$ )
Acetate	8	59	-870.28
Glucose	24	180,1	-2812

Equations 3.10, 3.11 and 3.12 were also used to calculate the energy efficiency of the system when methane was recovered rather than hydrogen. In these cases, equations were modified by considering the moles of recovered methane and its heat of combustion ( $-890 \text{ KJ mol}^{-1}$ ).

# CHAPTER 4

---

Long term operation of a single-chamber membrane-less microbial electrolysis cell: electron equivalent balances

**Part of the content of this chapter was published as:**

Ruiz, Y., Baeza, J.A. and Guisasola, A. (2013) Revealing the proliferation of hydrogen scavengers in a single-chamber microbial electrolysis cell using electron balances. *International Journal of Hydrogen Energy* 38(36), 15917-15927.



One of the main hurdles that microbial electrolysis cells for hydrogen production needs to overcome is the requirement of a high applied voltage that results from voltage losses in the system. A single chamber membrane-less configuration reduces to large extent the voltage losses and has as advantage the simple construction and operation. Therefore it is, *a priori*, a more suitable configuration for scale up of the process. However, this configuration causes the proliferation of hydrogen scavengers, which drastically reduces the cell efficiency leading to unrealistic very high coulombic efficiencies (CE) and very low cathodic gas recoveries ( $r_{\text{CAT}}$ ). This chapter provides a novel theoretical approach to understand, through electron equivalent balances, the fate of hydrogen in these systems. It was validated with a long term operated single-chamber membrane-less MEC. Two clearly differentiated stages were observed in the short and in the long term, where  $\text{H}_2$ -recycling and methanogenesis prevailed, respectively.

## 4.1 Introduction

Electrical energy needs to be supplied to produce hydrogen in MEC and, therefore, real implementation of this technology will only be possible if the energy obtained as hydrogen is higher than the energy supplied or if MEC becomes more economically feasible than other existing technologies for wastewater treatment.

The energy requirements can be reduced when working in single-chamber configuration and thus it is apparently a good option for scale-up. Nevertheless, in single-chamber configuration, hydrogen is available for other microorganisms, which decreases hydrogen production and purity.

The contamination of hydrogen with methane in bioelectrochemical systems has been widely reported (e.g. [55]). Methane production from organic carbon sources results in a decrease of the system efficiency, since less electrons of those contained in the substrate are converted into current. Moreover, when working with fermentable substrates, the hydrogen generated in fermentation can be used for methanogenesis as electron donor, which can account for important electron losses [114]. This hydrogenotrophic methanogenesis becomes even more important when operating single-chamber

membrane-less systems, since the hydrogen electrochemically formed in the cathode can also be used as electron donor.

The presence of different hydrogen scavengers other than methanogens has also been observed. On the one hand, the effect of homoacetogenic bacteria (e.g. strictly anaerobic bacteria that produce acetate with hydrogen as electron donor and inorganic carbon) in two-chamber MEC with fermentable substrates was reported to have a positive effect, since they allow the electron recovery from the produced hydrogen in fermentation [114]. However, in single-chamber MEC, homoacetogens can have a detrimental effect since they can transform back to acetate the hydrogen produced in the cathode. This H<sub>2</sub>-acetate loop can result in an increase of the cycles duration and thus, more input energy requirements and lower hydrogen recoveries [82]. Nevertheless, the low hydrogen recoveries in single-chamber MEC due to H<sub>2</sub>-recycling are not only as a result of the homoacetogenic activity, but the use of hydrogen as electron donor by ARB has also been reported [80]. In this sense, Lee and Rittmann [81] studied the contribution of H<sub>2</sub>-recycling in a continuous single-chamber MEC by minimizing the methanogenic activity, obtaining that from the 62 to the 76 % of the total current intensity was as a result of H<sub>2</sub>-recycling. However, methanogenic activity was not completely suppressed and therefore, the contribution of H<sub>2</sub>-recycling could have been even higher.

A whole understanding of the competition between the different hydrogen scavengers in single-chamber MEC systems has not been reported yet, although it was found that methanogenesis inhibition could favour homoacetogenic growth [114]. Lee and Rittmann [81] observed that H<sub>2</sub>-recycling and methane production occurred in the system simultaneously. Parameswaran et al. [115] found that homoacetogens could survive in a cell working at low HRT (with high BES concentration) indicating that homoacetogens could compete with hydrogenotrophic methanogens in real systems.

## 4.2 Objectives

The aim of this chapter is to experimentally assess the long term operation of a single-chamber membrane-less MEC with continuous dosage of BES. Long and fully monitored cycles and electron equivalent balances are used to understand the existing hydrogen losses due to the competition between homoacetogens, ARB and hydrogenotrophic

methanogens for hydrogen. The effect of H<sub>2</sub>-scavenging on the energy efficiency of the system is also evaluated.

## 4.3 Materials and Methods

### 4.3.1 Reactor description and operation

A concentric MEC (CC-MEC, see Materials and Methods in Chapter 3) was used to conduct the experiments. A constant voltage of 1.2 V was applied. Acetate was used as carbon source at an initial concentration of 235 mg/L (4 mM). Sodium 2-bromoethanesulfonate was used at a concentration of 50 mM except as indicated, where it was increased to 90 and 120 mM.

### 4.3.2 Batch experiments

Batch experiments were carried out to assess the cell performance over time. Culture medium was renewed prior to each cycle monitoring. Acetate concentration, gas production/composition and current intensity were measured along the cycles (see Materials and Methods in Chapter 3). Obtaining experimental profiles in time and not only start/end measurements was essential for a better understanding of the system.

### 4.3.3 Presence of homoacetogens

The presence of homoacetogenic bacteria was tested through an experiment similar to that in Parameswaran et al. [82]. Culture medium was replaced and no acetate, but sodium bicarbonate (3 g/L) was added. The MEC was operated with the applied voltage of 1.2 V. Hydrogen, stored in a gas sampling bag of 1 L, was intermittently sparged from the bottom of the reactor and collected in another gas sampling bag located at the top of the cell. Once the bag at the top was full, the position of the bags was reversed in order to continue sparging hydrogen from the bottom of the cell. This operation was repeated nine times between hours 0 and 8 and nine times more between hours 22 and 30 of the experiment.

## 4.4 Results and Discussion

### 4.4.1 CE and rCAT as MEC performance indicators

The performance of an MEC is commonly assessed through the calculation of the coulombic efficiency (CE, equation 3.8) and the cathodic gas recovery ( $r_{\text{CAT}}$ , equation 3.9). CE compares the coulombs recovered as current intensity with the coulombs that could be theoretically generated from the substrate oxidation by ARB, while  $r_{\text{CAT}}$  compares the coulombs consumed in hydrogen production with the coulombs arriving to the cathode as current intensity.

However, under certain scenarios, these efficiencies may be misleading and some considerations need to be taken into account when analysing the results.

Hydrogen is a suitable electron donor and, as such, its presence may induce the growth of hydrogenotrophic bacteria. Hydrogen is either electrochemically produced at the cathode or appears as a subproduct from the fermentation of organic products. Then, the proliferation of hydrogen scavengers in MEC systems is frequent, particularly when operating under single-chamber configuration. The most common scenarios in acetate-fed single-chamber MEC are: i) neither methanogenesis nor  $\text{H}_2$ -recycling, ii) only  $\text{H}_2$ -recycling, iii) only methanogenesis and iv) both  $\text{H}_2$ -recycling and methanogenesis taking place.

**Table 4.1** Stoichiometry of the possible reactions occurring in an MEC.

Reaction / Microorganisms	Stoichiometry
1. Acetate oxidation / ARB	$\text{CH}_3\text{COO}^- + 4\text{H}_2\text{O} \rightarrow 2\text{HCO}_3^- + 9\text{H}^+ + 8\text{e}^-$
2. $\text{CH}_4$ formation / Acetoclastic methanogens	$\text{CH}_3\text{COO}^- + \text{H}_2\text{O} \rightarrow \text{CH}_4 + \text{HCO}_3^-$
3. $\text{CH}_4$ formation / Electromethanogenesis	$\text{CO}_2 + 8\text{H}^+ + 8\text{e}^- \rightarrow \text{CH}_4 + 2\text{H}_2\text{O}$
4. $\text{CH}_4$ formation / Hydrogenotrophic methanogens	$4\text{H}_2 + \text{CO}_2 \rightarrow \text{CH}_4 + 2\text{H}_2\text{O}$
5. Acetate formation / Homoacetogens	$4\text{H}_2 + 2\text{CO}_2 \rightarrow \text{CH}_3\text{COO}^- + \text{H}^+ + 2\text{H}_2\text{O}$
6. $\text{H}_2$ oxidation / ARB	$\text{H}_2 \rightarrow 2\text{H}^+ + 2\text{e}^-$
7. $\text{H}_2$ formation / chemical reaction	$2\text{H}^+ + 2\text{e}^- \rightarrow \text{H}_2$

In view of simplification, it has been assumed that methane formation comes only from hydrogenotrophic methanogens and thus, acetate is not a carbon source for



methanogenesis. The suppression of acetoclastic methanogenesis (reaction 2 in Table 4.1) in single-chamber acetate-fed systems has already been reported and it is justified by the ARB having higher acetate affinity than methanogens [116]. Anyway, the absence of acetoclastic methanogens in our systems was ensured by monitoring acetate concentration in a batch experiment during 70 h without applying any voltage (Figure 4.1). Acetate concentration remained practically constant indicating that acetate consumption related to non-ARB microorganisms was negligible. The absence of acetoclastic methanogens was also corroborated through advanced microbiological analyses showing that only 2 % of the *Archaea* present in the anode were acetoclastic [95]. It should be noted that if a fermentable substrate different than acetate was used, hydrogen from fermentation should be also considered and the system would become much more complex.

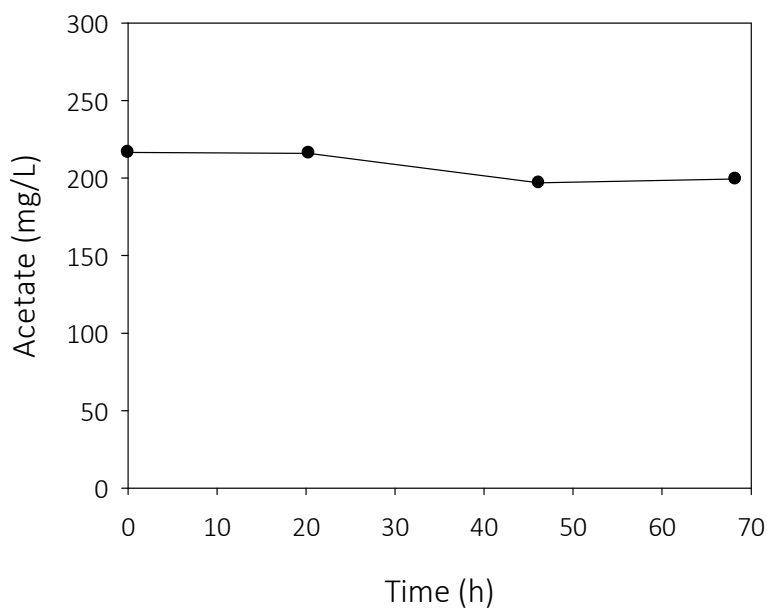


**Figure 4.1** Acetate concentration versus time in the MEC without applied voltage.

The electrochemical methane production through carbon dioxide reduction (reaction 3 in Table 4.1) has been also reported in MEC [117,118]. This process produces methane directly from carbon dioxide without hydrogen as intermediate. It can theoretically occur at a less negative cathode potential (-240 mV vs SHE) and therefore, the energy requirements could be lower [119].

Evidences for electromethanogenesis in the literature [117] are mainly based on the comparison of the performance of both a plain carbon cathode and a methanogenic biocathode. The current intensity with the abiotic cathode was lower and the measured hydrogen production rates were insufficient to explain the methane production rates with the biocathode, which suggested methane production by direct electron transfer [117].

However, electromethanogenesis has not been considered in this work, since Siegert et al. [119] claimed that with platinum cathodes, which exhibit an excellent electrocatalytic activity towards the hydrogen evolution reaction, the rate of methane production was consistent with hydrogen production rates measured in abiotic controls. Hence it could be assumed that all methane was produced by hydrogenotrophic methanogenesis.

The utilisation of CE and  $r_{\text{CAT}}$  to evaluate the MEC performance is not valid when  $\text{H}_2$ -recycling is occurring. Moreover,  $r_{\text{CAT}}$  cannot be used when hydrogenotrophic methanogenesis is taking place. In these cases, an extended approach should be used. Nevertheless, obtaining unrealistic CE and  $r_{\text{CAT}}$  results would be a good indicator of some hydrogen being lost: CE higher than 100% suggests  $\text{H}_2$ -recycling, whereas very low  $r_{\text{CAT}}$  denotes hydrogen losses probably as a consequence of methanogenesis or  $\text{H}_2$ -recycling.

#### 4.4.2 Including $\text{H}_2$ -recycling (with or without hydrogenotrophic methanogenesis)

When  $\text{H}_2$ -recycling is taking place the estimated CE values are excessively high (even higher than 100%). Then, the MEC performance becomes much more complex to evaluate and a different approach is needed. In this case, we have used electron equivalent balances (i.e. balances in terms of coulombs) for a better description of the cell performance. As it can be observed in Figure 4.2, electron equivalent balances are stated for both anodic and cathodic processes, which are linked by the coulombs recovered as current intensity and the coulombs recycled as hydrogen by ARB and homoacetogens.

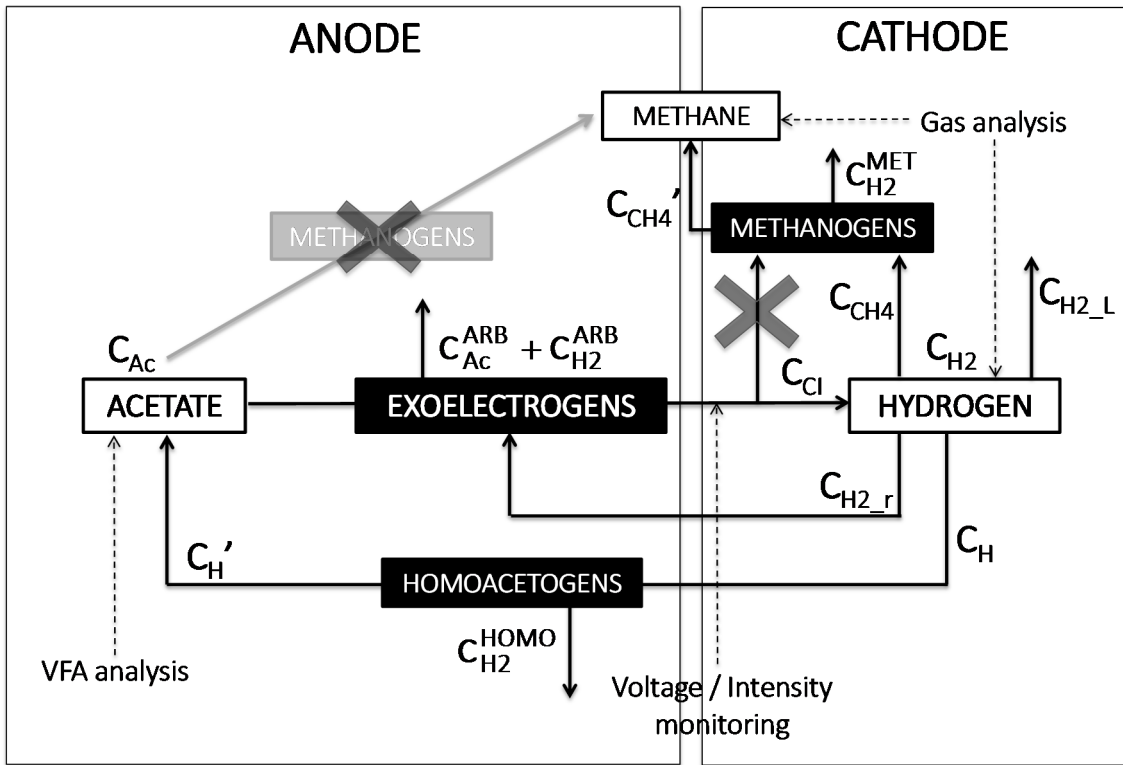


**Figure 4.2** Reaction pathways and parameters of electron equivalent balances in an acetate-fed single-chamber MEC.

Regarding anodic processes, the coulombs recovered as current intensity may come from three different sources: i) the oxidation of the external acetate initially added, ii) the oxidation of the acetate resulting from homoacetogenesis and iii) the oxidation of part of the hydrogen produced in the cathode. Moreover, it should be considered that a fraction of this acetate / hydrogen is not addressed to current intensity but to the growth of the biomass. The balance in the anodic side can be written as in equation 4.1.

$$C_{Cl} = C_{Ac} + C_{H'} + C_{H2_r} - C_{Ac}^{ARB} - C_{H2}^{ARB} \quad (4.1)$$

where  $C_{Cl}$  are the coulombs recovered as current intensity,  $C_{Ac}$  are the coulombs obtained from the oxidation of the external acetate,  $C_{H'}$  are the coulombs obtained from the oxidation of the acetate produced by homoacetogens,  $C_{H2_r}$  are the coulombs obtained from the oxidation of the hydrogen produced on the cathode by ARB while  $C_{Ac}^{ARB}$  and  $C_{H2}^{ARB}$  are the acetate and hydrogen fractions addressed to biomass growth (ARB) in terms of coulombs.

In the case of cathodic processes, the coulombs recovered as current intensity are all used for hydrogen production which, in turn, has four theoretical different endings: i) being captured in the gas bag, the most desirable, ii) being consumed by methanogens, iii) being consumed by homoacetogens, iv) being consumed by ARB. Equation 4.2 represents the previous processes in terms of coulombs.

$$C_{Cl} = C_{H_2} + C_{CH_4} + C_H + C_{H_2_r} \quad (4.2)$$

where  $C_{H_2}$  are the coulombs consumed in the production of the measured hydrogen and  $C_{CH_4}$ ,  $C_H$  and  $C_{H_2_r}$  are the coulombs consumed in the production of hydrogen subsequently consumed for the production of methane, acetate and current intensity.

Although hydrogen losses due to leakage ( $C_{H_2_l}$ ) are not considered in equation 4.2, practical knowledge suggests that, in some cases, they might be required to completely solve the equations system.  $C_{H_2_l}$  can be taken into account in terms of coulombs by modifying equation 4.2 as follows:

$$C_{Cl} = C_{H_2} + C_{CH_4} + C_H + C_{H_2_r} + C_{H_2_l} \quad (4.3)$$

Thus, the fate of the electrons would be completely described with equations 4.1 and 4.2 (or 4.3). However, each of the parameters in these equations needs to be estimated/measured.

#### 4.4.2.1 Contribution of the growth processes

The fraction of acetate addressed to ARB growth in terms of coulombs,  $C_{Ac}^{ARB}$ , can be estimated from equation 4.4.

$$C_{Ac}^{ARB} = Y_{Ac}^{ARB} \cdot (C_{Ac} + C_H) = \frac{100 - CE_{A1}}{100} \cdot (C_{Ac} + C_H) \quad (4.4)$$

where  $Y_{Ac}^{ARB}$  is the biomass/substrate yield of ARB when consuming acetate and  $CE_{A1}$  is the real coulombic efficiency of the cell, i.e., the CE of the cell when  $H_2$ -recycling does not occur and thus, current intensity is entirely produced from the oxidation of the externally added acetate. Thus, equation 4.4 calculates the product between the fraction of acetate consumed but not recovered as current intensity and the coulombs obtained from

acetate oxidation either from the externally added or the produced by homoacetogens. Note that using either  $Y_{AC}^{ARB}$  or  $CE_{A1}$  in the calculation of  $C_{AC}^{ARB}$  implicitly assumes that acetate is only consumed by ARB. Sleutels et al. [120] used CE to assess the competition between ARB and methanogens with acetate as substrate by considering the electrode and methane as the main electron sinks. As previously stated, the presence of acetoclastic methanogens in our system was negligible and therefore, it could be assumed that the acetate not recovered as current intensity was uniquely addressed to ARB growth.

The  $CE_{A1}$  could be either theoretically estimated or experimentally assessed. For the latter, two additional experiments besides the abovementioned standard monitoring are required. On the one hand, acetate evolution and current intensity are measured in a cell with constant  $N_2$  sparging to evaluate the ARB activity without  $H_2$ -recycling (experiment A1). The obtained results could be misleading if acetate stripping is simultaneously occurring and this is why the extent of this stripping is evaluated in a second experiment where acetate is monitored with constant  $N_2$  sparging and no applied voltage (experiment A2). The experimental estimation of  $CE_{A1}$  should be more reliable if it is calculated specifically for each system.

Part of the hydrogen consumed by homoacetogens (reaction 5 in Table 4.1) is also addressed to biomass growth and can be calculated as follows:

$$C_{H_2}^{HOMO} = C_H - C_H' \quad (4.5)$$

where  $C_{H_2}^{HOMO}$  are the coulombs equivalent to the hydrogen addressed to homoacetogens growth.

Similarly, part of the hydrogen oxidized by ARB is also consumed for growth and not recovered as current intensity ( $C_{H_2}^{ARB}$ ). Both  $C_{H_2}^{HOMO}$  and  $C_{H_2}^{ARB}$  can be also calculated from the biomass/substrate yield as shown in equations 4.6 and 4.7.

$$C_{H_2}^{HOMO} = Y_{H_2}^{HOMO} \cdot C_H \quad (4.6)$$

$$C_{H_2}^{ARB} = Y_{H_2}^{ARB} \cdot C_{H_2\_r} \quad (4.7)$$

where  $Y_{H_2}^{HOMO}$  and  $Y_{H_2}^{ARB}$  are the biomass/substrate yields of homoacetogens and ARB when consuming hydrogen.

$C_{Ac}$ ,  $C_{H_2}$ ,  $C_{CH_4}$  and  $C_{Cl}$  can be calculated from off-line/online measurements. The following paragraphs detail how to do so.

#### 4.4.2.2 Coulombs obtained from the oxidation of the externally added acetate, $C_{Ac}$

The moles of electrons obtained from acetate oxidation are calculated from the amount of the external acetate consumed (reaction 1 in Table 4.1) and converted to coulombs using the Faraday constant (equation 4.8). The reactor volume remained practically constant during all the experiment (less than the 2 % of the total liquid volume was extracted for sampling).

$$C_{Ac} = \Delta c \cdot M^{-1} \cdot V_L \cdot b_{Ac} \cdot F \quad (4.8)$$

where  $\Delta c$  ( $g\ Ac^{-1}\ L^{-1}$ ) is the acetate concentration change,  $M$  is the molecular weight of acetate ( $59\ g\ mol^{-1}$ ),  $V_L$  (L) is the volume of liquid in the reactor,  $b_{Ac}$  is the number of  $e^-$  transferred per mole of acetate ( $8\ mol\ e^- \cdot mol^{-1}\ Ac^-$ ) and  $F$  is the Faraday's constant ( $96485\ C\ mol^{-1}\ e^-$ ).

#### 4.4.2.3 Coulombs consumed in the production of the measured $H_2$ , $C_{H_2}$

$C_{H_2}$  is estimated by calculating the moles of electrons consumed during the production of hydrogen (reaction 7 in Table 4.1) and converting them to coulombs (equation 4.9).

$$C_{H_2} = n_{H_2,F} \cdot b_{H_2} \cdot F \quad (4.9)$$

where  $n_{H_2,F}$  are the moles of hydrogen captured and  $b_{H_2}$  is the number of  $e^-$  transferred per mole of hydrogen ( $2\ mol\ e^- \cdot mol^{-1}\ H_2$ ).

#### 4.4.2.4 Coulombs consumed in the production of $H_2$ converted to $CH_4$ , $C_{CH_4}$

$C_{CH_4}$  includes the coulombs consumed in the production of hydrogen converted to methane without considering biomass growth ( $C_{CH_4}'$ ) and the hydrogen consumed for hydrogenotrophic methanogens growth in terms of coulombs ( $C_{H_2}^{MET}$ ).  $C_{CH_4}$  can be calculated with equation 4.10.

$$C_{CH_4} = C_{CH_4}' + C_{H_2}^{MET} = n_{H_2,F}^{CH_4} \cdot b_{H_2} \cdot F \quad (4.10)$$

where  $n_{H_2,F}^{CH_4}$  are the moles of hydrogen consumed to produce methane.

$n_{H_2,F}^{CH_4}$  is calculated from the volume of hydrogen consumed to produce methane,  $V_{H_2,F}^{CH_4}$ , which, in turn, is calculated according to the proper stoichiometry (reaction 4 in Table 4.1) and considering the fraction of hydrogen consumed for biomass growth (equation 4.11).

$$V_{H_2,F}^{CH_4} = 4 \cdot \frac{V_{CH_4,F}}{1 - Y_{H_2}^{MET}} \quad (4.11)$$

where  $V_{CH_4,F}$  is the final volume of methane and  $Y_{H_2}^{MET}$  is the biomass/substrate yield of hydrogenotrophic methanogens when consuming hydrogen.

#### 4.4.2.5 Coulombs recovered as current intensity, $C_{Cl}$

$C_{Cl}$  is calculated by integrating the current intensity from the initial to the final time of the batch experiment.

$$C_{Cl} = \int_{t_0}^{t_f} I dt \quad (4.12)$$

Note that being able to calculate  $C_{Ac}$ ,  $C_{H_2}$ ,  $C_{CH_4}$  and  $C_{Cl}$  (equations 4.8, 4.9, 4.10 and 4.12) we have a system of six linear equations (4.1, 4.2, 4.4, 4.5, 4.6 and 4.7) and six degrees of freedom ( $C_{H_2}'$ ,  $C_H$ ,  $C_{H_2,r}$ ,  $C_{Ac}^{ARB}$ ,  $C_{H_2}^{HOMO}$  and  $C_{H_2}^{ARB}$ ). Thus, electron equivalent balances can be solved. All the parameters used to calculate the electron equivalent balances are summarized in Table 4.2.

Moreover, two interesting performance parameters, the fraction of the current intensity generated due to the oxidation of the externally added acetate ( $f_{Cl\_Ac}$ ) and due to recycled hydrogen ( $f_{Cl\_H_2}$ ), can be also estimated from the parameters calculated by the electron equivalent balances (equations 4.13 and 4.14).

$$f_{Cl\_Ac} = \frac{(1 - Y_{Ac}^{ARB}) \cdot C_{Ac}}{C_{Cl}} = \frac{\left(1 - \frac{100 - CE_{A1}}{100}\right) \cdot C_{Ac}}{C_{Cl}} = \frac{CE_{A1} \cdot C_{Ac}}{100 \cdot C_{Cl}} \quad (4.13)$$

$$f_{Cl_{H_2}} = \frac{(1 - Y_{Ac}^{ARB}) \cdot C_{H'} + C_{H_2_r} - C_{H_2}^{ARB}}{C_{Cl}} = \frac{CE_{A1} \cdot C_{H'} + C_{H_2_r} - C_{H_2}^{ARB}}{C_{Cl}} \quad (4.14)$$

**Table 4.2** Nomenclature and description of parameters.

Parameter	Description	Dimension
$b_{Ac}, b_{H_2}$	Number of $e^-$ transferred per mole of acetate ( $8 \text{ mol } e^- \text{ mol}^{-1} \text{ Ac}^-$ ) and $H_2$ ( $2 \text{ mol } e^- \text{ mol}^{-1} H_2$ )	$\text{mol } e^- \text{ mol}^{-1}$ substrate
$C_{Ac}$	Coulombs obtained from the oxidation of the initially added acetate	C
$C_{CH_4}$	Coulombs consumed in the production of $H_2$ converted to $CH_4$	C
$C_{CH_4}'$	Coulombs consumed in the production of $H_2$ converted to $CH_4$ (without considering hydrogenotrophic methanogens growth)	C
$C_{Cl}$	Coulombs recovered as current intensity	C
$C_H$	Coulombs consumed in the production of $H_2$ converted to acetate by homoacetogens	C
$C_{H'}$	Coulombs obtained from the oxidation of acetate produced by homoacetogens	C
$C_{H_2}$	Coulombs consumed in the production of the measured $H_2$	C
$C_{H_2_L}$	$H_2$ losses due to leakage	C
$C_{H_2_r}$	Coulombs obtained from the oxidation of $H_2$	C
$C_{Ac}^{ARB}$	Acetate consumed for ARB growth in terms of coulombs	C
$C_{H_2}^{ARB}$	$H_2$ consumed for ARB growth in terms of coulombs	C
$C_{H_2}^{HOMO}$	$H_2$ consumed for homoacetogens growth in terms of coulombs	C
$C_{H_2}^{MET}$	$H_2$ consumed for hydrogenotrophic methanogens growth in terms of coulombs	C
CE	Coulombic efficiency	-
$CE_{A1}$	Coulombic efficiency in experiment A1 (no $H_2$ - recycling)	C
$\Delta c$	Acetate concentration change over $t_F$ and $t_0$	$\text{g } Ac^- \text{ L}^{-1}$
F	Faraday constant ( $96485 \text{ C mol}^{-1} e^-$ )	$\text{C mol}^{-1} e^-$
$f_{Cl_{Ac}}$	Fraction of the current intensity generated due to the oxidation of the external acetate initially added	-
$f_{Cl_{H_2}}$	Fraction of the current intensity generated due to $H_2$ - recycling	-



Parameter	Description	Dimension
$I$	Current intensity	A
$M$	Molecular weight of the acetate ( $59 \text{ g mol}^{-1}\text{Ac}^-$ )	$\text{g mol}^{-1}$
$n_{\text{H}_2,\text{F}}$	Moles of $\text{H}_2$ at the end of a batch experiment	mol
$n_{\text{H}_2,\text{F}}^{\text{CH}_4}$	Moles of $\text{H}_2$ converted to $\text{CH}_4$ at the end of a batch experiment	mol
$r_{\text{CAT}}$	Cathodic efficiency	-
$t, t_0$ and $t_f$	Time / Initial and final times of the batch experiments	s
$V_{\text{G},\text{F}}$	Final volume of gas	L
$V_{\text{H}_2,\text{F}}$	Final volume of $\text{H}_2$	L
$V_{i,\text{F}}$	Final volume of the gas $i$	L
$V_L$	Volume of liquid in the reactor (1.3 L)	L
$V_m$	Molar gas volume ( $24.03 \text{ L mol}^{-1}$ ) at $20^\circ\text{C}$	$\text{L mol}^{-1}$
$V_{\text{H}_2,\text{F}}^{\text{CH}_4}$	Volume of the $\text{H}_2$ consumed to produce $\text{CH}_4$	L
$V_{\text{H}_2,\text{F}}^{\text{T}}$	Volume of $\text{H}_2$ produced including that consumed to produce $\text{CH}_4$	L
$x_{i,\text{F}}$	Final composition of the gas $i$	-
$Y_{\text{Ac}}^{\text{ARB}}$	Biomass/substrate yield for ARB when consuming acetate	$\text{mol e}^- \text{ biomass mol}^{-1} \text{ e}^- \text{ substrate}$
$Y_{\text{H}_2}^{\text{ARB}}$	Biomass/substrate yield for ARB when consuming $\text{H}_2$	$\text{mol e}^- \text{ biomass mol}^{-1} \text{ e}^- \text{ substrate}$
$Y_{\text{H}_2}^{\text{HOMO}}$	Biomass/substrate yield for homoacetogens when consuming $\text{H}_2$	$\text{mol e}^- \text{ biomass mol}^{-1} \text{ e}^- \text{ substrate}$
$Y_{\text{H}_2}^{\text{MET}}$	Biomass/substrate yield for hydrogenotrophic methanogens when consuming $\text{H}_2$	$\text{mol e}^- \text{ biomass mol}^{-1} \text{ e}^- \text{ substrate}$

#### 4.4.3 Including hydrogenotrophic methanogenesis when no $\text{H}_2$ -recycling is occurring

The previously developed electron equivalent balances can be used even when no  $\text{H}_2$ -recycling is occurring but most parameters would be zero. In this sense, the following simplified approach can be more practical. Thus, if hydrogenotrophic methanogens are present in the system,  $r_{\text{CAT}}$  will be underestimated since the amount of hydrogen produced and sequentially diverted to methane would not be considered. Although CE would not be affected, the calculation of  $r_{\text{CAT}}$  would need a correction by including the hydrogen theoretically converted into methane. Then, the real volume of hydrogen produced ( $V_{\text{H}_2,\text{F}}^{\text{T}}$ ) would include the measured hydrogen and the hydrogen converted to

methane according to the proper stoichiometry (reaction 4 in Table 4.1). Then,  $V_{H_2,F}^T$  should be used when estimating  $r_{CAT}$  (equation 3.9).

$$V_{H_2,F}^T = V_{H_2,F} + V_{H_2,F}^{CH_4} \quad (4.15)$$

where  $V_{H_2,F}^T$  is the total volume of hydrogen produced and  $V_{F,H_2}$  is the measured hydrogen production.

#### 4.4.4 Experimental study: Occurrence of H<sub>2</sub>-recycling

A 1.3 L MEC was operated for 8 months with BES dosage using an ARB-enriched anode. BES concentration was initially set at 50 mM, a value theoretically high enough to suppress methanogenic activity [82]. Under these conditions (i.e. single-chamber membrane-less MEC with BES and under batch operation), methanogenesis could be avoided. However, H<sub>2</sub>-recycling was favoured and then, efficient hydrogen production was still hindered. Practically from the first days of operation it was observed that the duration of the cycles was not in agreement with the monitored intensity resulting in CE higher than 100 %. Moreover, the highest hydrogen production was detected after adding fresh medium in the cell, whereas hydrogen concentration in the gas sampling bag was decreasing along the cycle, resulting in  $r_{CAT}$  values close to 0 %. Thus, the most plausible option was H<sub>2</sub>-recycling either by homoacetogens or H<sub>2</sub>-consumers ARB. Figure 4.3 shows an experiment where sodium bicarbonate and hydrogen were added as sole carbon source and sole electron donor, respectively. Acetate concentration was initially zero and it increased over time reaching values of around 70 mg/L. Meanwhile, current intensity also increased and reached values close to 9 mA. Thus, homoacetogens were present and consumed H<sub>2</sub> and CO<sub>2</sub> to form acetate. Acetate could be subsequently used by ARB to generate current from acetate. However, current intensity due to direct oxidation of hydrogen could not be ruled out.

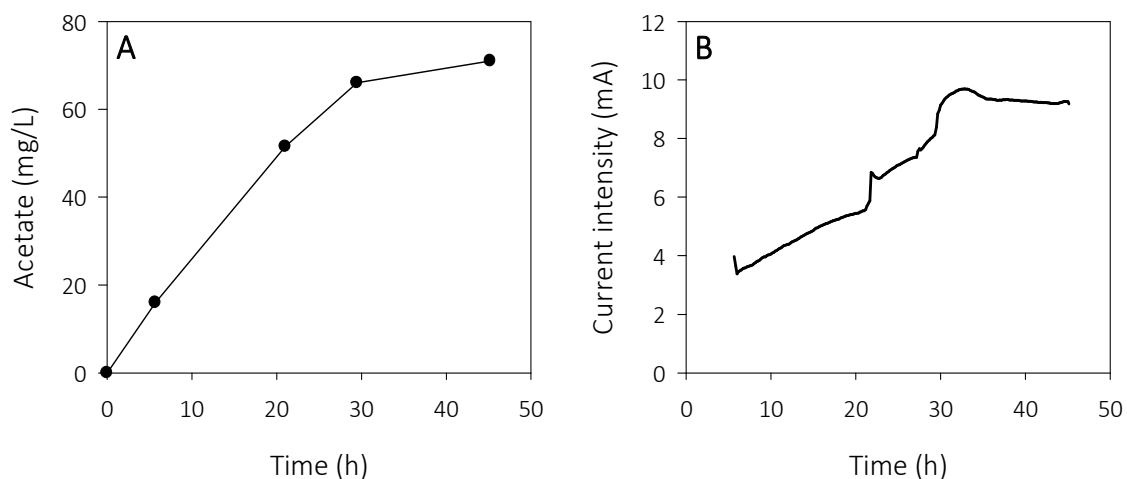


**Figure 4.3** Batch experiment with the addition of sodium bicarbonate and H<sub>2</sub> sparging (A) Acetate concentration and (B) Current intensity over time. Current intensity is shown from time 5 hours due to monitoring problems.

Electron equivalent balances were calculated to gain insight on the cell performance under H<sub>2</sub>-recycling conditions and hence a cycle was monitored during approximately 100 hours.

Figure 4.4 shows the experimental results obtained during the characterisation of the operation with H<sub>2</sub>-recycling. As previously detailed, two additional experiments were required for the calculation of  $C_{Ac}^{ARB}$ : A1) ARB activity was measured in an MEC with continuous N<sub>2</sub> sparging to avoid hydrogen utilisation by both homoacetogens and ARB and A2) acetate concentration was measured with N<sub>2</sub> sparging but with no applied voltage to estimate acetate stripping.

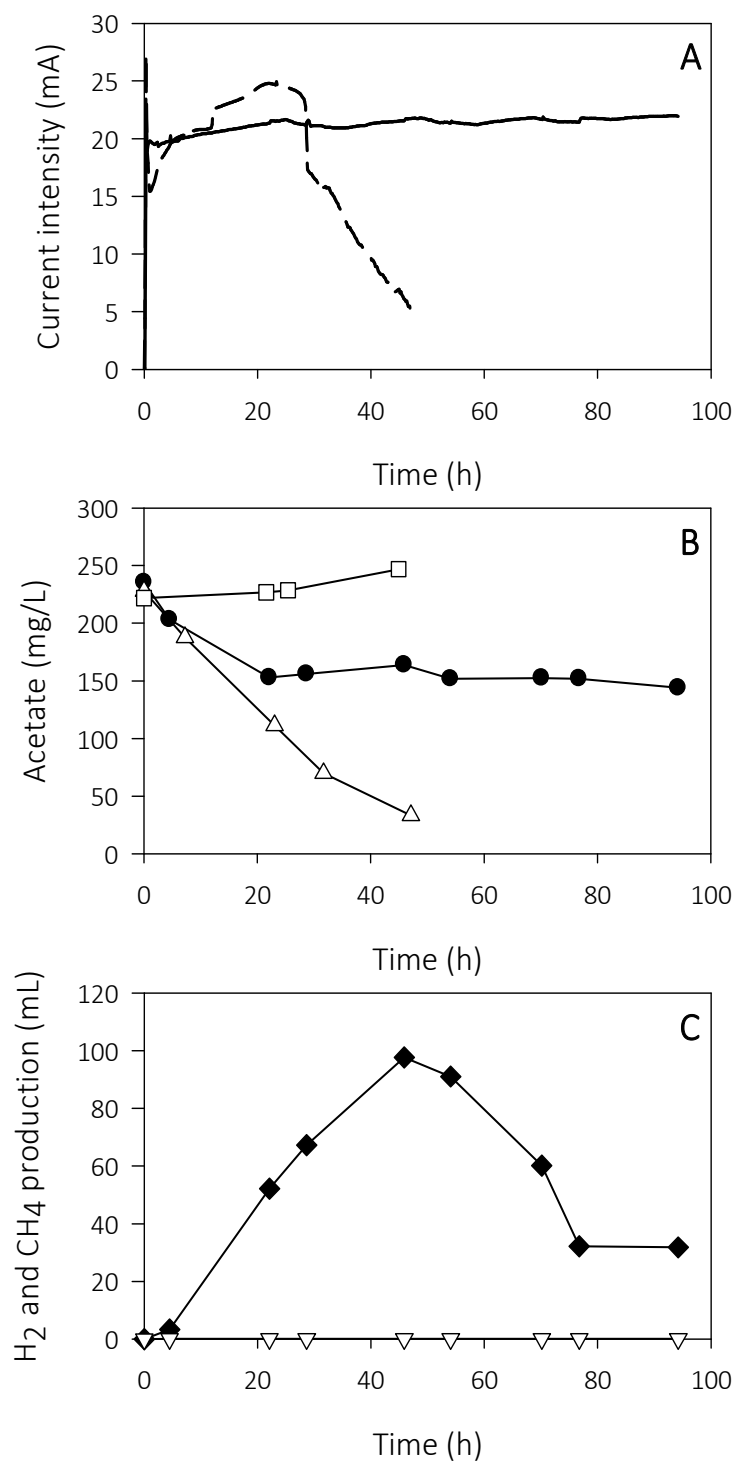


**Figure 4.4** Monitoring of the MEC with H<sub>2</sub>-recycling (A) Current intensity under conventional operation (solid) and with N<sub>2</sub> sparging (experiment A1) (dashed), (B) Acetate concentration under conventional operation (●), with N<sub>2</sub> sparging (experiment A1) (Δ) and with N<sub>2</sub> sparging and no applied voltage (experiment A2) (□) and (C) Gas production under conventional operation: H<sub>2</sub> (◆) and CH<sub>4</sub> (▽).

Figure 4.4A compares the cell current intensity with (A1) and without N<sub>2</sub> sparging (conventional operation). As it can be observed, the duration of the cycle was completely different (in spite of having the same initial acetate concentration): the cycle was completed after 50 hours with N<sub>2</sub> sparging whereas under conventional operation, the current intensity remained at values around 22 mA after 100 hours. In A1 hydrogen was removed from the system by stripping, while under conventional operation, hydrogen was used by homoacetogenic bacteria to produce acetate or by ARB to generate electricity thus, extending the cycles. Regarding acetate measurements, acetate decreased under conventional operation during the first 20 hours of the cycle and remained almost constant during the following 80 hours. In contrast, when N<sub>2</sub> was sparged, acetate was consumed in 50 hours. The decrease in acetate concentration was not related to stripping: Figure 4.4B shows that when the cell was disconnected and sparged with N<sub>2</sub> (A2), acetate concentration did not decrease but slightly increased, probably as a result of water evaporation. Finally, Figure 4.4C presents the bag composition and shows that the hydrogen increased, reached a maximum (100 mL) and then decreased. Methane concentration was scarce indicating that hydrogen consumption was not addressed to methanogenesis.

On the one hand, the CE under conventional operation was, as expected, much higher than 100 % (463 %). However, when N<sub>2</sub> was sparged, C<sub>E</sub> decreased to 90.4 %, thus only the 9.6 % of the acetate is consumed for the growth of the biomass ( $Y_{Ac}^{ARB}$ ). Therefore, CE<sub>A1</sub> (i.e. the real CE excluding the H<sub>2</sub>-recycling effect) was 90.4 %. On the other hand, r<sub>CAT</sub> was around 4 %. The coulombs generated from acetate oxidation according to the experimental acetate measurements, C<sub>Ac</sub>, were 1555 C, whereas the coulombs recovered as current intensity, C<sub>Cl</sub>, were 7203 C and the coulombs consumed in hydrogen production, C<sub>H<sub>2</sub></sub>, 292 C. For  $Y_{H_2}^{HOMO}$  and  $Y_{H_2}^{ARB}$  it was assumed a value of 0.1 mol e<sup>-</sup> biomass mol<sup>-1</sup> e<sup>-</sup> substrate, i.e. a value similar to that estimated for ARB when consuming acetate.

Substituting the values of C<sub>Ac</sub>, C<sub>H<sub>2</sub></sub>, C<sub>CH<sub>4</sub></sub>, C<sub>Cl</sub>, CE<sub>A1</sub>,  $Y_{H_2}^{HOMO}$  and  $Y_{H_2}^{ARB}$  in equations 4.1, 4.2, 4.4, 4.5, 4.6 and 4.7 it was obtained that:

$$5648 = C_H + C_{H_2_r} - C_{Ac}^{ARB} - C_{H_2}^{ARB} \quad (4.16)$$

$$6911 = C_H + C_{H2\_r} \quad (4.17)$$

$$C_{Ac}^{ARB} = 149.18 + 0.096 \cdot C_H' \quad (4.18)$$

$$C_{H2}^{HOMO} = C_H - C_H' \quad (4.19)$$

$$C_{H2}^{HOMO} = 0.10 \cdot C_H \quad (4.20)$$

$$C_{H2}^{ARB} = 0.10 \cdot C_{H2\_r} \quad (4.21)$$

The equation system (equations 4.16 to 4.21) solution is summarized in Table 4.3. The fraction of hydrogen recycled by homoacetogens, calculated as  $C_H/(C_H+C_{H2\_r})$ , was 71 %, whereas the fraction of hydrogen recycled by the direct oxidation of hydrogen by ARB, calculated as  $C_{H2\_r}/(C_H+C_{H2\_r})$ , was 29 %. Moreover, coulombic losses due to biomass growth were mainly caused by the consumption of acetate by ARB ( $C_{Ac}^{ARB}$ ) and the consumption of hydrogen by homoacetogens ( $C_{H2}^{HOMO}$ ).

$f_{Cl\_Ac}$  and  $f_{Cl\_H2}$  were 19.5 % and 80.5 % respectively (equations 4.13 and 4.14), showing that the effect of H<sub>2</sub>-recycling can be far from negligible (e.g. in our system, 80.5 % of the current intensity was generated due to H<sub>2</sub>-recycling). Moreover, the recycled hydrogen in terms of coulombs ( $C_H+C_{H2\_r}$ ) was in just five days around 1.7 times the amount of coulombs that could be generated if all the acetate externally added had been consumed.

**Table 4.3** Summary of the electron equivalent balances during a cycle with H<sub>2</sub>-recycling.

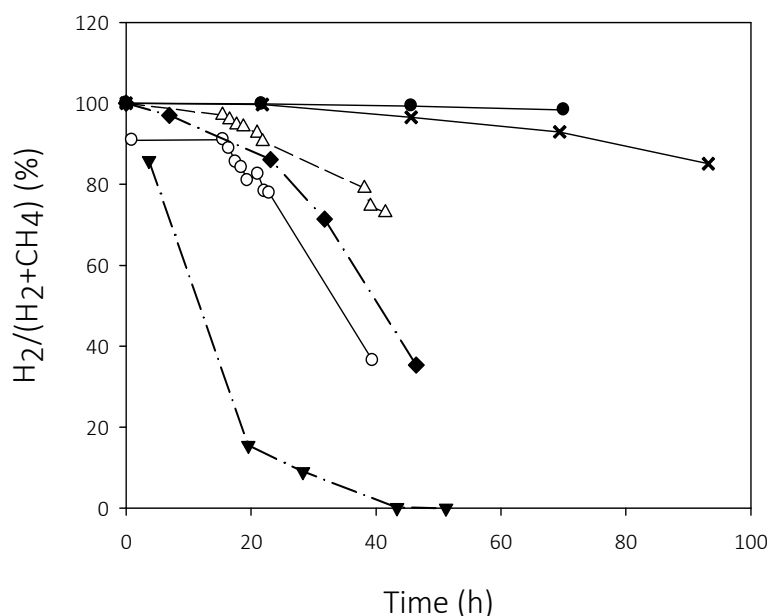
Parameter	Normal operation	With N <sub>2</sub> sparging
CE	463 %	90.4 %
$r_{\text{CAT}}$	4 %	--
$C_{\text{Cl}}$	7203 C	2989 C
$C_{\text{Ac}}$	1555 C	3306 C
$C_{\text{H}_2}$	292 C	--
$C_{\text{CH}_4}$	0 C	--
$C_{\text{H}}$	4893 C	0 C
$C_{\text{H}}'$	4403 C	0 C
$C_{\text{H}_2, \text{r}}$	2018 C	0 C
$C_{\text{Ac}}^{\text{ARB}}$	572 C	317 C
$C_{\text{H}_2}^{\text{HOMO}}$	489 C	0 C
$C_{\text{H}_2}^{\text{ARB}}$	202 C	0 C
$f_{\text{Cl}_{\text{Ac}}}$	19.50 %	100 %
$f_{\text{Cl}_{\text{H}_2}}$	80.50 %	0 %

The energy recovery of the cell under the H<sub>2</sub>-recycling scenario was calculated with respect to the electrical input ( $r_{\text{E}}$ , equation 3.10) and both the electrical input and the energy content of the substrate ( $r_{\text{E+S}}$ , equation 3.12). The results showed how detrimental H<sub>2</sub>-recycling could be, since only the 6.3 % of the invested electrical energy was recovered as hydrogen. The energy recovery in the form of hydrogen was even lower (5.0 %) when the energy content of acetate was also considered.

#### 4.4.5 Experimental study: Presence of methanogens

At week 9 of operation, batch experiments suggested growth of methanogens even though there was a BES concentration of 50 mM. It was increased to 90 and subsequently to 120 mM and, surprisingly, methane formation was detected even at those high concentrations. Our results suggest that methanogens grew in the MEC even at higher BES concentrations, either as a result of a too thick biofilm preventing BES to penetrate inside or as a result of a development of BES resistance by methanogens [121].

Figure 4.5 shows the evolution of the methanogenic activity during the cell monitoring performed at different weeks of operation. At weeks 9-10, the ratio  $H_2/(H_2+CH_4)$  only started to decrease (i.e. methane was formed) approximately 70 hours after the renewal of the medium. At week 16,  $H_2/(H_2+CH_4)$  decreased to 35 % in just 45 hours. BES concentration was increased to 120 mM at week 19 and although methanogenic activity was reduced, it was far from suppressed. At week 22 of operation, BES concentration was decreased to 50 mM to obtain results comparable to the literature. Under these operational conditions, most of the hydrogen produced was converted to methane at the end of the monitoring, as shown in Figure 4.5 for week 34. Thus, it was observed that BES may not be an adequate long term solution for methanogenic inhibition when hydrogen is widely available (i.e. batch conditions with high retention time).



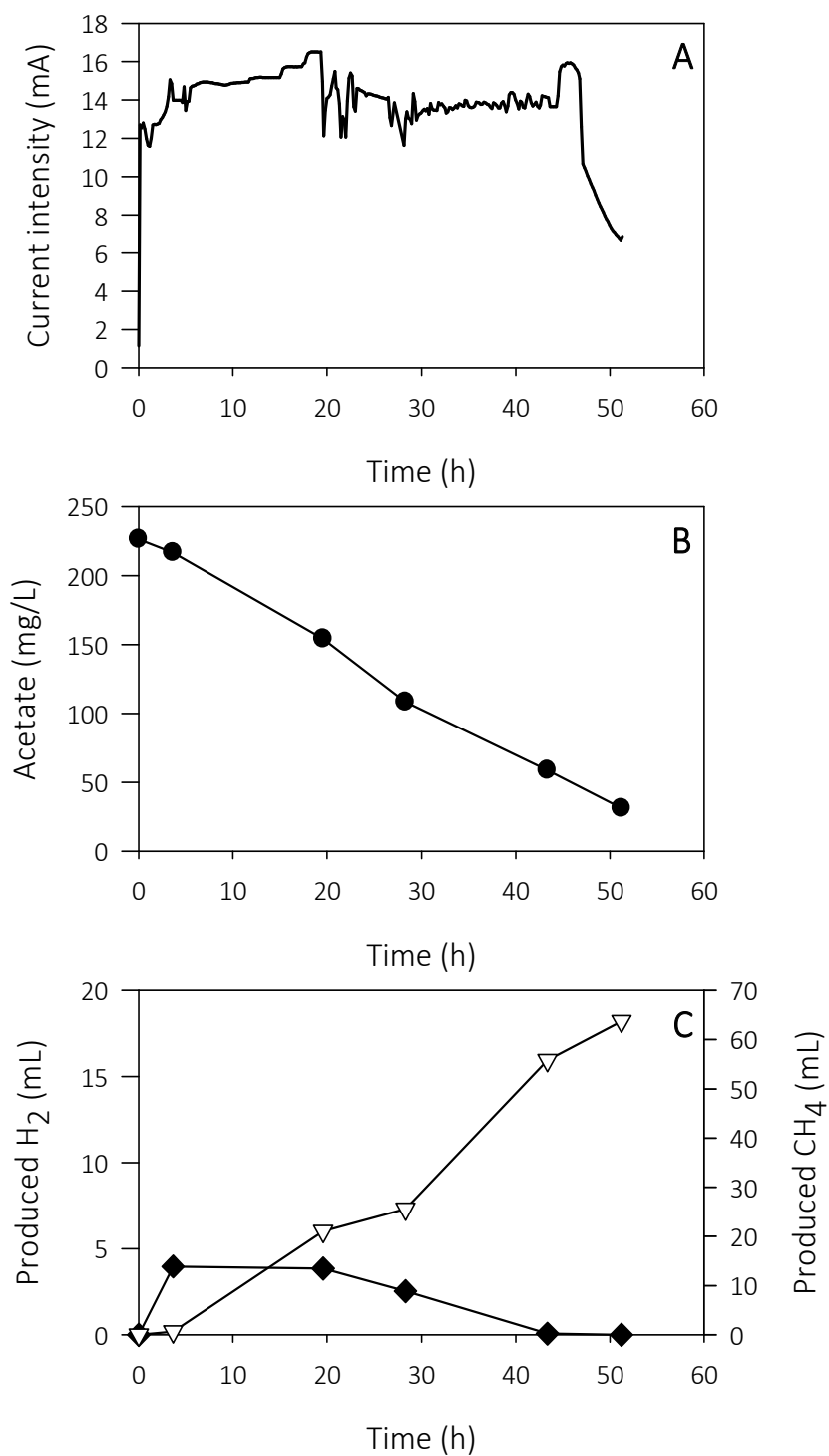
**Figure 4.5** Methanogenic activity vs time represented as the ratio  $H_2/H_2+CH_4$  at different weeks of operation. Week 9 (●), week 10 (×), week 16 (○), week 19 (△), week 29 (◆) and week 34 (▼) of operation. Concentration of BES: 90 mM (solid), 120 mM (dashed) and 50 mM (dash-dotted).

Figure 4.6 shows an example of the monitoring of a cycle (week 34) where methanogenic activity was significant. As it can be observed the cycle lasted approximately 50 hours, during which acetate concentration was decreasing (Figure 4.6B). Regarding gas production, hydrogen reached a maximum volume between hours 3 and 4 of monitoring



and then it started decreasing. In contrast, methane production was increasing during all the cycle.

The CE of the cell was 74.5 %, whereas the  $r_{\text{CAT}}$  if only comparing the coulombs recovered as hydrogen to those recovered as current intensity was 0. A much more realistic  $r_{\text{CAT}}$  value of 94.5% was calculated by computing methane into the balance, assuming that all methane produced came from hydrogen [86] and transforming moles of methane into moles of hydrogen by considering a  $Y_{\text{H}_2}^{\text{MET}}$  of  $0.1 \text{ mol e}^- \text{ biomass mol}^{-1} \text{ e}^- \text{ substrate}$  (equations 4.11 and 4.15). Acetate-driven methanogenesis could be discarded since it would have resulted in a much lower CE. These results show that when methanogenesis became important,  $\text{H}_2$ -recycling, if still occurring, lost importance since only the 5.5 % of the coulombs recovered as current intensity were not subsequently recovered as hydrogen or methane.



**Figure 4.6** Monitoring of the MEC with the presence of methanogens (A) Current intensity, (B) Acetate concentration and (C) Gas production: H<sub>2</sub> (◆) and CH<sub>4</sub> (▽). Note the different scales in (C).

As previously stated, the electron equivalent balances can also be used to describe the behaviour of the cell under methanogenesis conditions. In the presented case, the calculated CE suggested that H<sub>2</sub>-recycling was not occurring, thus C<sub>H</sub>, C<sub>H'</sub> and C<sub>H<sub>2</sub>\_r</sub> could be neglected. Therefore, the previous system of equations (equations 4.1, 4.2, 4.4, 4.5, 4.6 and 4.7) could be reduced to only three linear equations:

$$C_{Cl} = C_{Ac} - C_{Ac}^{ARB} \quad (4.22)$$

$$C_{Cl} = C_{H_2} + C_{CH_4} \quad (4.23)$$

$$C_{Ac}^{ARB} = \frac{100 - CE}{100} \cdot C_{Ac} \quad (4.24)$$

Note that CE<sub>A1</sub> was replaced by CE in equation 4.24 since CE did not need to be corrected by H<sub>2</sub>-recycling. According to the measurements/calculations, C<sub>Ac</sub> was 3378 C, C<sub>Cl</sub> was 2518 C, C<sub>H<sub>2</sub></sub> was 0 and C<sub>CH<sub>4</sub></sub> was 2379 C. Substituting these values into equations 4.22, 4.23 and 4.24 it was obtained:

$$-860 = -C_{Ac}^{ARB} \quad (4.25)$$

$$2518 = 2379 \quad (4.26)$$

$$C_{Ac}^{ARB} = \frac{100 - CE}{100} \cdot 3378 \quad (4.27)$$

As it can be observed, to solve the system C<sub>H<sub>2</sub>\_L</sub> had to be included in equation 4.26 as follows:

$$2518 = 2379 + C_{H_2\_L} \quad (4.28)$$

However, as deduced from equation 4.28, the value of C<sub>H<sub>2</sub>\_L</sub> was very low and can be assumed as experimental error. Table 4.4 summarizes the results of the CE, r<sub>CAT</sub> and electron equivalent balances calculations. The use of electron equivalent balances gives similar information to that provided by CE and r<sub>CAT</sub>, but returns the values of C<sub>Ac</sub><sup>ARB</sup> and C<sub>H<sub>2</sub>\_L</sub> in terms of coulombs.

**Table 4.4** Summary of the results in a cycle with methanogenic activity.

Parameter	Value
CE	74.5 %
$r_{\text{CAT}}$	0 %
$r_{\text{CAT}}$ (considering $\text{CH}_4$ )	94.5 %
$C_{\text{Cl}}$	2518 C
$C_{\text{Ac}}$	3378 C
$C_{\text{H}_2}$	0 C
$C_{\text{CH}_4}$	2379 C
$C_{\text{H}}$	0 C
$C_{\text{H}}'$	0 C
$C_{\text{H}_2_r}$	0 C
$C_{\text{Ac}}^{\text{ARB}}$	860 C
$C_{\text{H}_2}^{\text{HOMO}}$	0 C
$C_{\text{H}_2}^{\text{ARB}}$	0 C
$C_{\text{H}_2_L}$	139 C
$f_{\text{Cl}_{\text{Ac}}}$	100 %
$f_{\text{Cl}_{\text{H}_2}}$	0 C

The results so far suggest that  $\text{H}_2$ -recycling took place when the methanogenic activity was not important. Moreover, the CE evolution showed that CE was higher than 100 % when methanogens were not dominant. CE decrease to values around 75 % was proportional to the methanogenic activity increase. Results could also suggest that CE was decreasing as a consequence of acetate consumption by methanogens. However, this was ruled out taking into account results in the literature and our own results in the CE and  $r_{\text{CAT}}$  calculations.

The energy recovery of the cell under this scenario where methanogenesis emerged was also assessed by calculating  $r_{\text{E}}$  and  $r_{\text{E+S}}$  using equations 3.10 and 3.12 for methane as fuel. These values were compared to the theoretical values if hydrogen would not have been consumed by hydrogenotrophic methanogens, but recovered.

Practically all the invested electrical energy was recovered as methane ( $r_E$  of 95.0 %), although only about 30-40 % of the methane energy can be later converted into electricity by means of  $\text{CH}_4$ -driven engine-generators [6]. The energy recovery when the energy content of the substrate was considered ( $r_{E+S}$ ) decreased to 38.5 %. In the theoretical case where hydrogen could be recovered,  $r_E$  and  $r_{E+S}$  would be 135.6 % and 55.0 %, respectively. As expected, the energy recovery is more positive with hydrogen as fuel. However, the results evidence that methanogenesis is not such an unfavourable situation as  $\text{H}_2$ -recycling in terms of energy efficiency.

In fact, methane production in single-chamber membraneless MEC has been proposed as an alternative to hydrogen, since it is very difficult to obtain pure hydrogen and at the same time methane may offer some advantages over hydrogen [122]. Clauwaert and Verstraete [56] claimed that methane production in MEC would be more robust than hydrogen production and that the capital costs would be lower, since ion exchange membranes would not be required. Cheng et al. [117] highlighted that hydrogen storage can be problematic, whereas the transport and storage of methane involve mature technologies. Finally, Van Eerten-Jansen et al. [123] stated that methane production in MEC would have additional environmental benefits, since  $\text{CO}_2$  could be converted into additional fuel. Taking advantage of this latter, a new system coupling an anaerobic digester and an MEC has already been proposed for biogas upgrading by in situ converting  $\text{CO}_2$  into additional  $\text{CH}_4$  [124].

However, if hydrogen production remains the objective, the most feasible strategy to avoid hydrogen scavengers would be preventing hydrogen to be available for the microorganisms. Some options would be the use of membranes, strategies such as hydrogen stripping [87] or using reactors with architectures for a fast hydrogen separation in order to make hydrogen unavailable for these microorganisms [80]. On the other hand, other possible strategies based on the selective inhibition of methanogens would not be useful in a system with these characteristics, since  $\text{H}_2$ -recycling would not be avoided.

## 4.5 Conclusions

In membrane-less single-chamber MEC, the presence of hydrogen scavengers is a significant hurdle in view of its real application. Under these conditions, the classical indexes CE and  $r_{\text{CAT}}$  calculated to estimate its performance are no longer valid.

When methanogens are present,  $r_{\text{CAT}}$  should be calculated estimating the amount of hydrogen converted to methane.

When methanogens are selectively inhibited,  $\text{H}_2$ -recycling (due to homoacetogenic bacteria or due to direct hydrogen oxidation) is very likely to occur, causing large deviations in the estimated CE and  $r_{\text{CAT}}$  values. A different approach based on electron equivalent balances is presented in this work which, through a better understanding of the process occurring in the cell, results in the calculation of two new parameters,  $f_{\text{Cl}_{\text{Ac}}}$  and  $f_{\text{Cl}_{\text{H}_2}}$ , which are much more realistic indicators of the real cell performance.

Two experimental studies under different scenarios (proliferation of homoacetogens or methanogens) were presented. The proposed approach based on balances was successfully applied and under  $\text{H}_2$ -recycling conditions the estimation of the MEC performance was much more accurate.

Moreover, electron balances showed that  $\text{H}_2$ -recycling could be an issue much more important than methane generation, since the  $\text{H}_2$ -acetate loop increases the operating costs and makes infeasible the production of hydrogen in MEC.

# CHAPTER 5

---

Performance of microbial electrolysis cells  
with non-buffered and low-conductivity  
media





Microbial electrolysis cells have given successful results in lab-scale experiments with well buffered media and synthetically-increased conductivity because operational problems are avoided and the internal resistance of the cell is reduced. This is particularly important in two-chamber configuration where membranes cause potential losses associated to the pH gradients across them. However, domestic and many industrial wastewaters have a limited buffer capacity and low conductivity. In this chapter, the performance of an MEC with a culture medium similar to real wastewaters, in terms of buffer capacity and conductivity, was assessed in both single-chamber and two-chamber configurations and compared to that of a well-buffered cell. Single-chamber MEC tests demonstrated that the lack of buffer affected both the anodic and cathodic overpotentials, being the latter significantly higher. In two-chamber configuration, the non-buffered cell failed as a result of a high pH drop in the anode, which harmed the anodic biofilm. The conductivity increase did not improve significantly any configuration tested.

## 5.1 Introduction

At the current state of research, most studies in BES have been conducted with high buffer concentrations, including phosphate and bicarbonate [125]. The use of buffers in BES helps preventing operational problems such as proton-transport limitations inside the biofilm [126,127] and provides conductivity to the culture medium. This, in turn, reduces the internal resistance of the cells and therefore, increases the attainable power output in MFC or reduces the applied voltage requirements in MEC.

The use of high buffer concentrations is, however, unrealistic. Real wastewaters have a relatively low buffer capacity (the equivalent to 1 to 4 mM phosphate buffer) in addition to lower conductivities (around 1 mS/cm) than those used in most BES lab-scale studies [128,129].

Chapter 4 concluded that, in single-chamber MEC, the hydrogen produced was, in turn, consumed by hydrogenotrophic methanogens or homoacetogens [82,130]. Therefore, many MEC studies worked in two-chamber configuration since membranes prevent

hydrogen diffusion to the anode. Moreover, membranes are required for obtaining high-purity hydrogen. Otherwise, hydrogen would be contaminated with the gaseous products from the metabolic activity in the anode (e.g. CO<sub>2</sub>, CH<sub>4</sub>, or H<sub>2</sub>S) [88]. On the drawback side, membranes are expensive, increase the internal resistance of the cells leading to lower current densities and contribute to potential losses due to pH gradients across them [88], which are very detrimental for the MEC operation.

Besides electrons, protons are also produced in the anode during the biodegradation of organic matter. Thus, the transport of electrons from the anode to the cathode needs to be balanced to meet electroneutrality. Ideally, in a two-chamber MEC, protons and hydroxyls would be responsible for maintaining electroneutrality in the system. Ideally, if a cation exchange membrane (CEM) is used, protons (from anodic substrate oxidation) cross the permeable membrane and react in the cathode. In contrast, hydroxyls formed (as a consequence of the cathodic reaction) diffuse to the anode to compensate charges when an anion exchange membrane (AEM) is used. However, in reality, electroneutrality is mostly reached by the transport of ions other than protons and hydroxyls (e.g. Na<sup>+</sup>, K<sup>+</sup>, NH<sub>4</sub><sup>+</sup>, Cl<sup>-</sup> or S<sup>2-</sup>) as they are present in a much higher concentration [131]. The accumulation of protons and hydroxyls leads to a pH drop in the anodic chamber and a pH increase in the cathodic chamber [131,132]. Both the cathodic pH rise and the anodic pH drop lead to a power decrease in MFC or in energetic requirements increase in MEC, since both theoretical electrode potentials are pH-dependent. For instance, every pH unit difference between the anodic and the cathodic chambers in MEC leads to an additional energetic requirement of about 0.13 kWh/m<sup>3</sup> H<sub>2</sub> (0.059 V) [32].

Hence, under two-chamber configuration, buffers become even more important since they dampen the pH changes caused by the presence of an ion exchange membrane and therefore, prevent, to some extent, potential losses [131,132].

In this sense, from the stoichiometry of reaction 1 in Chapter 1, it can be deduced that 8 mols of protons are produced for each mole of acetate consumed, thus causing acidification of the anodic chamber. In the same reaction, 1 mol of buffer is produced as bicarbonate, which contributes to reduce the pH drop. However, 7 additional mols of buffer would be required to maintain a neutral pH in the anodic chamber [133].

So far, several studies have been conducted with non-buffered catholytes, in which the performance of saline solutions [134-136] or acids such as sulphuric and hydrochloric [137] were evaluated as catholytes and the performance of different cathode materials at neutral and alkaline pHs was assessed [92]. However, there is very little research on non-buffered anodes, although pH changes would have a significant impact on the anode operation as it is a biological system.

In this framework, Sleutels et al. [127] studied the effect of buffer concentration on MEC operation obtaining higher current intensities and coulombic efficiencies for the highest buffer concentration. The performance of both AEM and CEM in a continuous flow two-chamber MEC with a low PBS concentration (10 mM) was also evaluated in terms of chemical efficiency and internal resistance and in both cases AEM outperformed CEM [138,139].

In a further study, Rozendal et al. [140] evaluated the effect of different membranes on ion transport to that same PBS concentration and concluded that bipolar membranes could retard the increase of pH in the cathodic chamber. All these works showed how preventing pH changes in the cell can enhance its performance.

## 5.2 Objectives

A full understanding of the effect of buffer/conductivity in both single-chamber and two-chamber MEC will be very helpful in view of posterior design of practical bioelectrochemical applications. Moreover, the advantages of choosing anion or cation exchange membranes in two-chamber configuration under these non-ideal conditions should also be experimentally assessed and discussed.

Therefore, the aim of this chapter is the systematic performance comparison of an MEC mimicking real conditions in terms of buffer capacity and conductivity with the same MEC working with a medium with higher buffer capacity and higher conductivity. Three different MEC configurations were compared: i) single-chamber, ii) two-chamber with AEM and iii) two-chamber with CEM resulting in a wide matrix of experimental results.

## 5.3 Materials and Methods

### 5.3.1 Reactors description and medium composition

The same two-chamber small-scale MEC (SS-MEC, see Materials and Methods in Chapter 3) were used (with or without membrane) to maintain the distance between the electrodes at 6 cm regardless of the cell configuration. The performance of two different membranes, an AEM and a CEM, was evaluated. Three different MEC were used: BF (buffered), HC (high conductivity) and LC (low conductivity). The medium composition was different for each cell. For BF the synthetic medium described in Chapter 3 (100 mM PBS) was used. The initial pH and conductivity of the medium was 7.5 and 13 mS/cm. In HC, in contrast, the same medium was used but PBS was not added. NaOH and NaCl were used to adjust the initial pH and conductivity, respectively, to the same values to that in BF. In LC neither PBS nor NaCl was added, so only NaOH was used to adjust the initial pH at 7.5. The synthetic medium without PBS provided already a conductivity of 4 mS/cm to LC. This value was slightly higher than the conductivity of real wastewaters reported in Rozendal et al. [128] but, in any case, the differences between low- and high-conductivity cases could be likewise observed.

The methanogenic inhibitor 2-bromoethanesulfonate was used at a concentration of 50 mM according to the work of Parameswaran et al. [82] and acetate was added as substrate with an initial concentration of 1 g/L in all cases. The previous media for each cell were also used in the cathodic chamber when working in two-chamber configuration, but no acetate was added.

Anodes were inoculated in three different small-scale air-cathode MFC (SSAC-MFC) (see Materials and Methods in Chapter 3): MFC-1, MFC-2 and MFC-3. The same synthetic medium with PBS 100 mM was used for the three cells. The anodes worked in MFC mode with an external resistance of 1000  $\Omega$  for approximately a month before being transferred to MEC.

### 5.3.2 Electrochemical analyses

The MFC performance was assessed by means of polarization curves. The overpotentials of both anode and cathode in MEC were measured with LSV and the ohmic resistance of

the cell by means of EIS (see Materials and Methods in Chapter 3). Culture medium was renewed previous to LSV and EIS experiments.

### 5.3.3 Batch experiments

For each MEC, experiments were performed in three different configurations: (i) without membrane (WM), (ii) with AEM and (iii) with CEM. The applied voltage was 1.0 V.

In all experiments, current intensity was monitored and acetate and hydrogen were analysed (see Materials and Methods in Chapter 3). Moreover, routine pH and conductivity measurements were done at the initial and the final times of a batch experiment. The experiments conducted are summarized in Table 5.1.

**Table 5.1** Summary of the experimental conditions of batch experiments E1 to E9.

Experiment	MEC	Buffer	Conductivity (mS/cm)	IEM	Applied potential (V)	pH control
E1	BF	Yes	13	No	1.0	No
E2	BF	Yes	13	AEM	1.0	No
E3	BF	Yes	13	CEM	1.0	No
E4	HC	No	13	No	1.0	No
E5	HC	No	13	AEM	1.0	No
E6	HC	No	13	CEM	1.0	No
E7	LC	No	4	No	1.0	No
E8	LC	No	4	AEM	1.0	No
E9	LC	No	4	CEM	1.0	No

## 5.4 Results and Discussion

The results in this chapter are organized in different sections. The inoculation of the anodes and their operation in MFC mode will be firstly assessed. Then, the current intensity profiles of the three cells in each configuration will be discussed. Finally, the main limitations, in terms of potential losses, of both single-chamber and two-chamber will be estimated and the performance of each membrane will be detailed.

#### 5.4.1 Inoculation and MFC operation with buffered medium

The enrichment of the anode in ARB was assessed by monitoring the current intensity in a set of three identical MFC working with the conventional culture medium. As observed in Figure 5.1, despite the initial differences in current intensity, MFC-1, MFC-2 and MFC-3 ended up performing very similar. After only 13 days the three MFC reached a current intensity close to 0.5 mA. Moreover, the CE was 24-25 % in all cases.

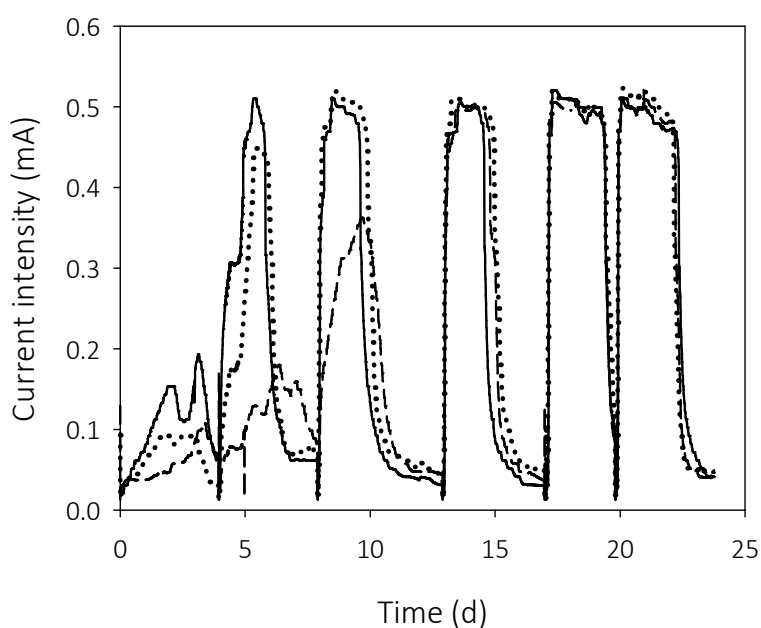


**Figure 5.1** Current intensity profiles of the MFC during inoculation. MFC-1 (solid), MFC-2 (dashed) and MFC-3 (dotted).

After 25 days operating in MFC mode, polarization and power curves were recorded in order to assess the performance of the anodes of MFC-1, MFC-2 and MFC-3 (Figure 5.2). The performance of the three MFC was very similar up to 0.35 V (Figure 5.2A), as expected considering the previous current intensity profiles. From this point, both the cell voltage and the current intensity decreased in MFC-1 and MFC-2, thus limiting the observed current intensity to 1.6 mA. This simultaneous decrease of the cell voltage and the current intensity at reduced external resistances (named overshoot) was already reported in power and polarization curves [141-145] and can result in underestimation of MFC performance at high current intensities. However, each study attributed it to a different cause, from mass transport limitations, ionic depletion or microbial exhaustion

to insufficient acclimation time for bacteria to a new resistance or voltage. Overshoot was also observed in MFC-3 at a potential of 0.25 mV and a current intensity of 2.5 mA. The same trend could be observed on power curves and therefore the maximum power of MFC-3 (640  $\mu$ W) was higher than that of MFC-1 and MFC-2 (550  $\mu$ W).

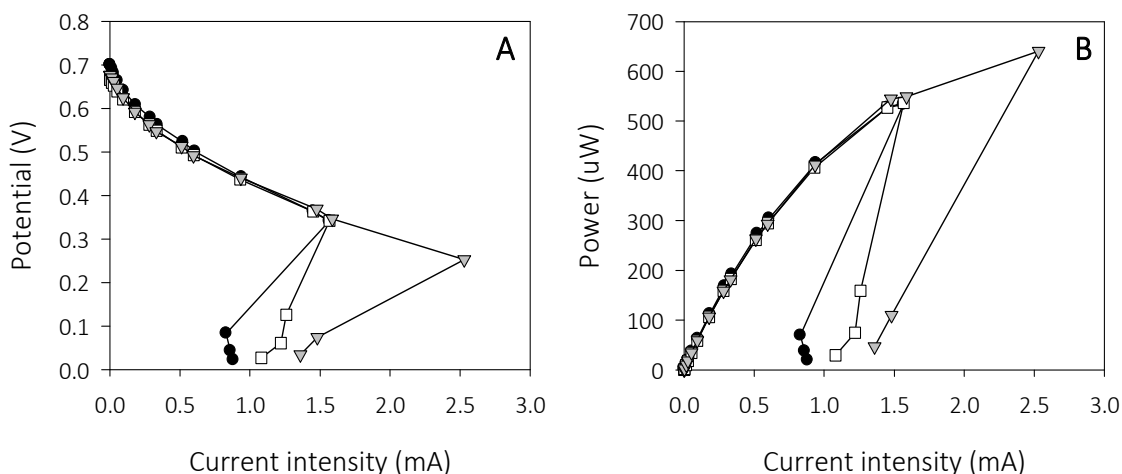


**Figure 5.2** Performance assessment of the MFC (A) Polarization curves and (B) power curves. MFC-1 (●), MFC-2 (□) and MFC-3 (▼).

In spite of these little differences, it was considered that the cells had the same performance and anodes were transferred to MEC. The anode of MFC-3, which slightly outperformed the other two, was transferred to MEC LC (low conductivity). The anode of MFC-2 to MEC HC (high-conductivity) and finally, the anode of MFC-1 to MEC BF (buffered). Then, if LC failed (LC presents *a priori* the most unfavourable conditions), it could not be attributed to the inoculation step.

MEC worked in single-chamber configuration for several cycles prior to any experiment with ion exchange membranes in order to acclimate the anodes to MEC operation and to the new culture media in the case of HC and LC.

Figure 5.3 presents the current intensity response of BF, HC and LC in single chamber configuration. After 11 days of operation, BF already reached current intensities close to 5 mA. HC, meanwhile, reached lower current intensities but from the second cycle onwards, the response of the cell was unvarying. From day 40 on, the initial acetate concentration was increased resulting in higher current intensities at the end of the

cycles. Finally, in the case of LC, it was not until day 40 that the current intensity developed a growing trend.

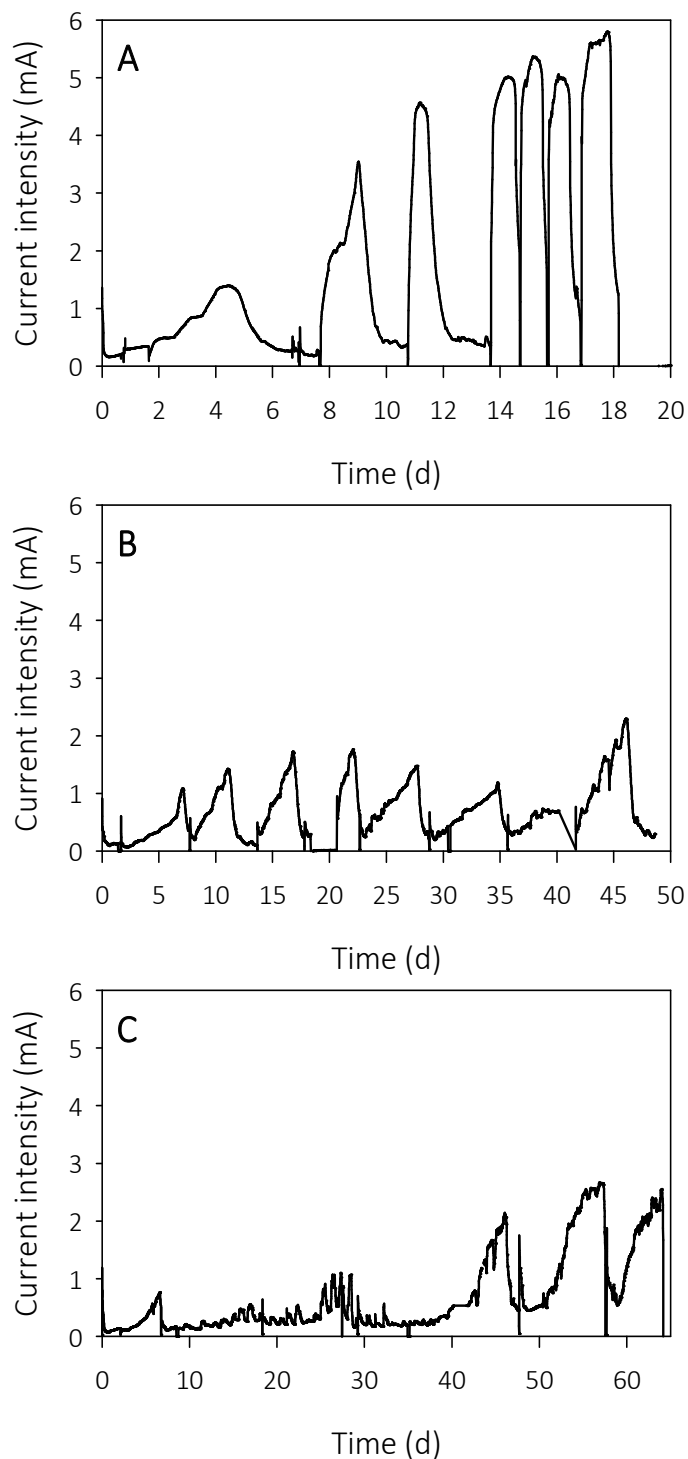


**Figure 5.3** Current intensity profiles after transferring the anodes to MEC: (A) buffered (BF), (B) high conductivity (HC) and (C) low conductivity (LC).



### 5.4.2 Current intensity performance in MEC

The conventional current intensity profiles of the MEC BF (buffered), HC (high conductivity) and LC (low conductivity) working with the three different configurations are presented in Figure 5.4. Figure 5.4A shows a plateau (around 6.1 mA) rapidly reached when no membrane was used in BF (E1). The initial current intensity was significantly lower when an AEM separated the anodic and cathodic chambers due to an increase of the internal cell resistance (E2). Moreover, the current intensity showed a decreasing trend throughout the batch cycle. On the other hand, the use of a CEM (E3) resulted in an initial current intensity near to that obtained without membrane, although the current intensity decreased even more sharply throughout the batch cycle than in E2. The initial higher current intensity achieved with the CEM was in accordance with the results in Sotres et al. [146], where higher current and power densities were obtained in two-chamber MFC using a CEM (Nafion-117) rather than an AEM (AMI-7001).

The current intensity profiles of HC and LC in Figures 5.4B and 5.4C when working without membrane (E4 and E7) showed a similar trend, observing an increased current intensity throughout the cycle without reaching a plateau. The current intensity increase in HC was higher (188 % for HC whereas only 88 % for LC) and thus, a higher current intensity was reached at the end of the cycle. The most significant outcome of Figure 5.4 is that the use of membranes, both AEM and CEM, in combination with a non-buffered medium (E5, E6, E8 and E9) led to a failed MEC, since the current intensity of HC and LC decreased sharply to 0. In addition, the anodes were severely damaged and needed several cycles operating without membrane to recover. Therefore, the use of PBS was demonstrated as essential for a proper operation of a two-chamber MEC working in batch mode and hence establishes an important limitation for treating wastewaters with low buffer capacity. Higher conductivities, meanwhile, slightly improved the operation in non-buffered single-chamber MEC, but in two-chamber configuration its effect was not relevant due to the low achieved intensities, which minimized the ohmic potential losses.

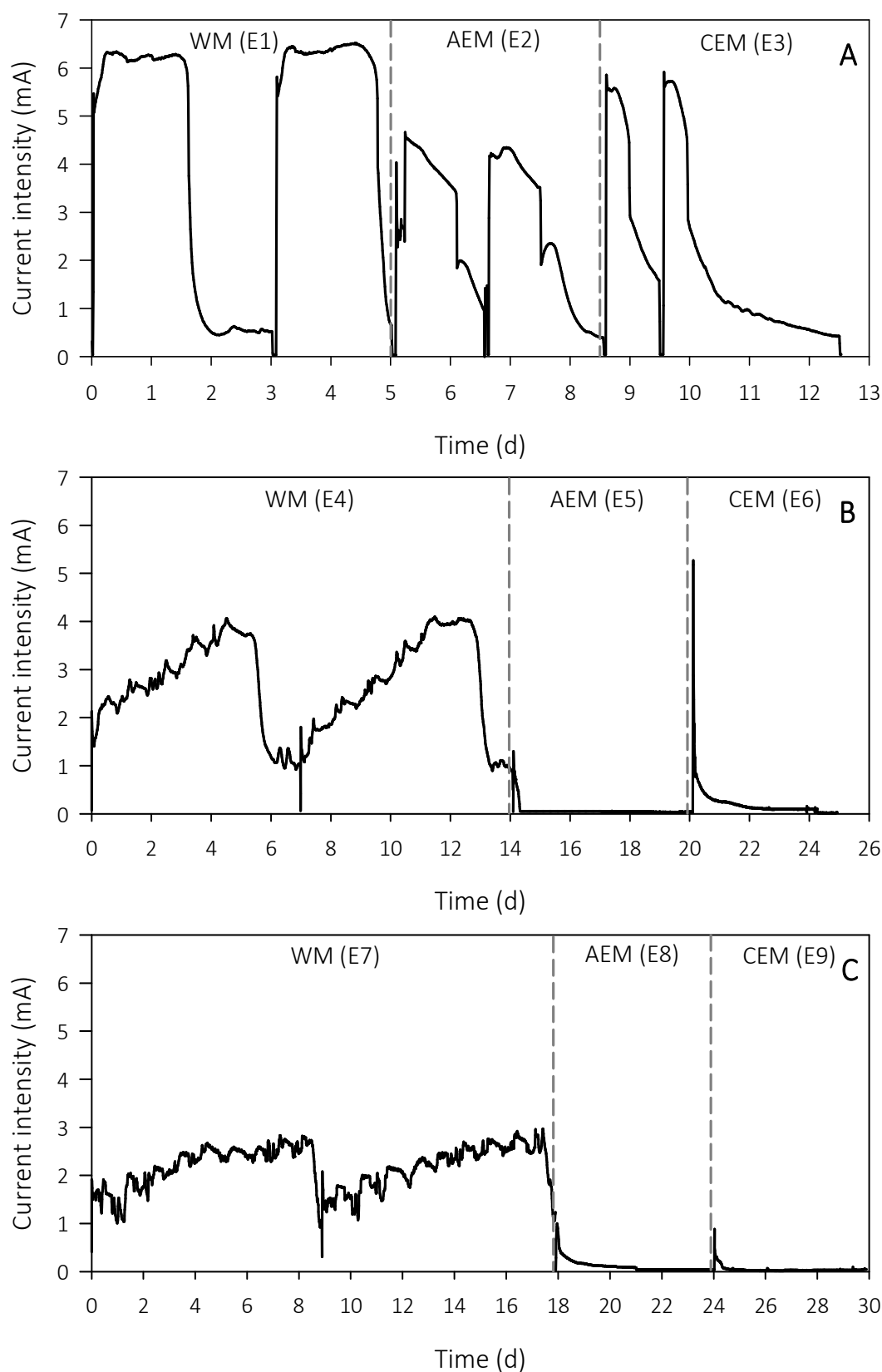


**Figure 5.4** Current intensity profiles of (A) buffered (BF), (B) high conductivity (HC) and (C) low conductivity (LC). MEC without membrane (WM), with an anion exchange membrane (AEM), and with a cation exchange membrane (CEM).

### 5.4.3 Analysis of single-chamber operation

LSV were recorded to assess the MEC performance when working in single-chamber configuration and for each culture medium (E1, E4 and E7). The electrode potentials were measured during LSV experiments to determine the main limitation in each case [88]. The highest current intensity was obtained in BF with a value close to 6.1 mA when 1 V was applied. Both HC and LC only reached a current intensity close to 2 and 1 mA, respectively, showing the relevance of buffer presence (Figure 5.5A).

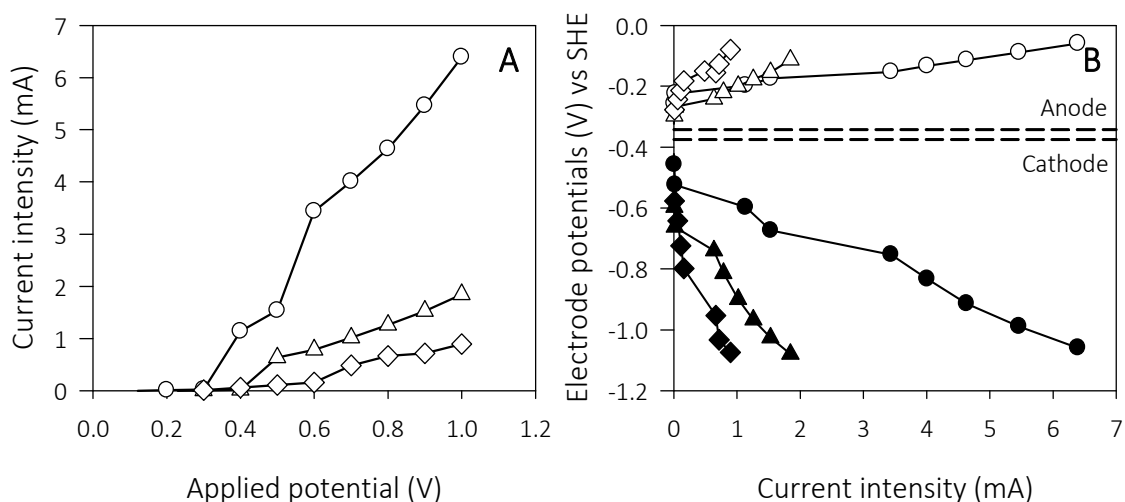


**Figure 5.5** Linear sweep voltammetry of the MEC in single-chamber configuration. BF (○), HC (△) and LC (◇). (A) Current intensity profiles and (B) Electrode potentials: anode potential (open symbols) and cathode potentials (filled symbols). Dashed lines indicate the theoretical electrode potentials under initial batch conditions (acetate concentration =  $1.69 \cdot 10^{-2}$  M, hydrogen partial pressure = 0.01 atm and pH = 7.5).

The electrode potentials during the LSV are presented in Figure 5.5B together with the theoretical electrode potentials calculated by means of the Nernst equation at the initial cycle conditions (equations 1.4 and 1.7 in Chapter 1). The difference between the measured and the theoretical electrode potential is the so-called overpotential, i.e. the voltage losses of each electrode. The highest overpotentials were observed in the cathode, which means that most of the applied cell voltage was lost in the cathode and therefore, there was more room for improvement in the cathode than in the anode. Theoretically, by reducing the cathodic overpotential, the same current intensity could be obtained with lower applied potentials, or higher current intensities could be achieved

by maintaining the same applied potential. In the case of BF, the overpotentials for the highest current intensity (6.4 mA at 1.0 V of applied voltage) were 0.28 V and 0.68 V for the anode and the cathode, respectively. Similar values were obtained for HC and LC when 1.0 V was applied, as observed in Figure 5.6, which displays the electrode overpotentials as a function of the applied potential. However, the achieved current densities were 3-fold and 6-fold lower, respectively. Returning to Figure 5.5B and for a given current intensity, the differences between the overpotentials in BF and HC and LC were more significant in the cathode, indicating that at low current densities the performance of the cathode was more affected by the lack of buffer than that of the anode. The cathodic overpotential for LC had a similar trend to that in HC but with higher values.

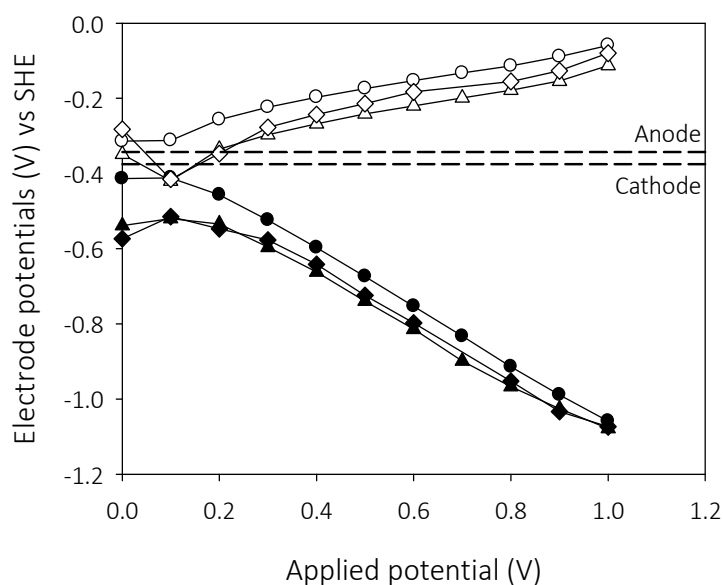


**Figure 5.6** Electrode potentials vs. applied cell potential of MEC in single-chamber configuration. BF (○), HC (△) and LC (◇). Anode potential (open symbols) and cathode potentials (filled symbols). Dashed lines indicate the theoretical electrode potentials under initial batch conditions.

In summary, the major potential losses in single-chamber cells within the presented current intensity range were located in the cathode regardless of PBS presence. For instance, the cathodic overpotential was 71 %, 75% and 73% of the total voltage losses at the electrodes at an applied voltage of 1.0 V for BF, HC and LC, respectively. For a given current intensity, however, these potential losses became more significant without PBS.

Moreover, PBS played a more important role than conductivity since overpotentials differed more between buffered and non-buffered cells than between high-conductivity and low-conductivity cells with the rest of conditions remaining constant.

The current intensity in HC and LC was quite low, since LSV were recorded after renewal of the culture medium. Figure 5.4 shows that current intensity in HC and LC increased over time, indicating that either the overpotential of the anode or the cathode decreased throughout the batch cycle. Therefore, the results obtained in LSV corresponded to the initial time of these cycles when the current intensity was still low. E7 was repeated in a cell of similar characteristics to MEC LC by monitoring the individual electrode potentials to gain insight on this fact. The results showed that, under single-chamber conditions, the anodic potential decreased during the batch cycle (from +0.31 to -0.14 V vs SHE). This means that the anodic overpotential decreased, since the difference between the real and the theoretical anodic potential became lower. Therefore, the increase of the overall performance of the non-buffered cells was caused by an improved performance of the anode (Figure 5.7), so that the cathodic overpotential became even more important throughout the batch cycle when compared to the anodic overpotential.

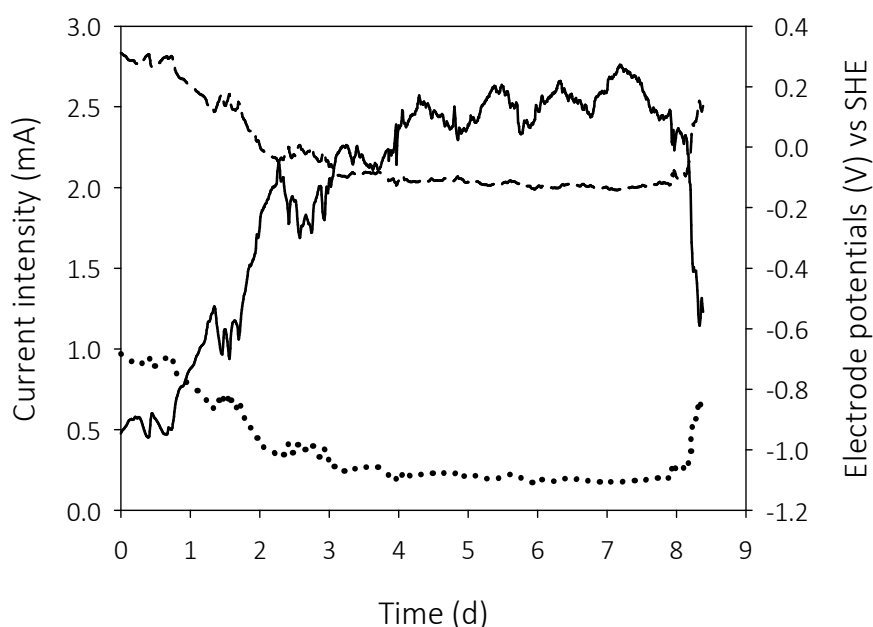


**Figure 5.7** Current intensity profile and electrode potentials of LC in single-chamber configuration using the same conditions as in E7. Current intensity (solid), anodic potential (dashed) and cathodic potential (dotted).

#### 5.4.4 Experimental assessment of ion exchange membranes inclusion

The effect of including a membrane in MEC performance was assessed from two different points of view. On the one hand, its contribution to the internal resistance of the cell and, on the other hand, the pH gradient across them.

Figure 5.8 presents the Nyquist diagrams of BF without membrane, with an AEM and with a CEM. The Nyquist plots described a partial semicircle continued by a linear region at very low frequencies. The ohmic resistance was calculated as the portion in the high-frequency range, i.e. the intercept of the semicircle with the real axis [147] (see Materials and Methods in Chapter 3).

The contribution of each membrane to the total ohmic resistance can be estimated by comparing the ohmic resistance of the cell with and without membrane. The ohmic resistance of the MEC working with CEM was very similar to that without membrane, which means that the resistance of CEM was very low ( $1 \Omega$ ). These results are in agreement with those in Rozendal, et al. [1] in which the ohmic resistance of the same type of membrane (Nafion N-117) was estimated to be  $2.2 \Omega$ . In that study, it is claimed that this resistance is too high for practical applications. Hence, in full-scale systems in which high current intensities would be expected, the ohmic losses related to the membrane would become important. The ohmic resistance of the AEM was much higher ( $14 \Omega$ ), in agreement with the slightly lower initial current intensity observed in E2 (Figure 5.4). Differences in performance between these two membranes will become more apparent in larger-scale MEC in which, as previously stated, the ohmic losses will play a more important role.

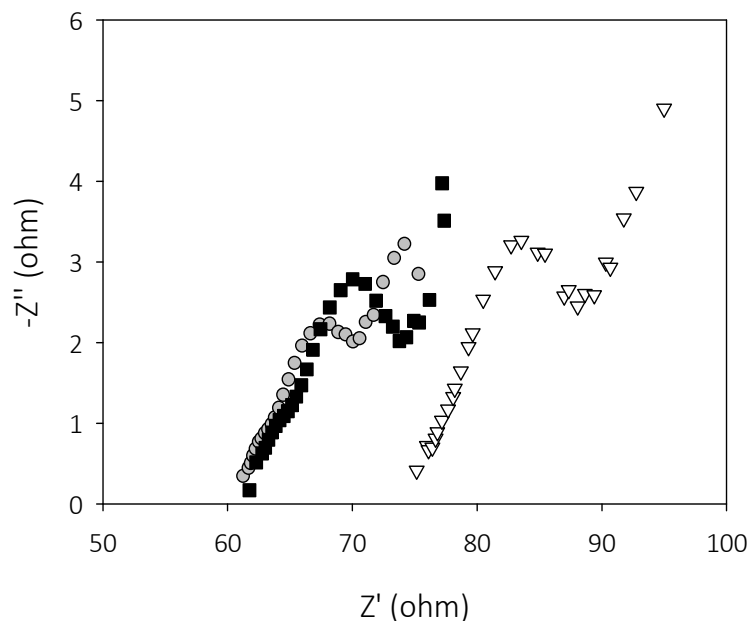


**Figure 5.8** Nyquist diagrams of BF at an applied voltage of 1.0 V without membrane (●), with an AEM (▽) and with a CEM (■).

Regarding pH, Figure 5.9A shows the conventional pH profiles of a cell with similar characteristics to MEC BF when working in two-chamber configuration with an initial pH of 7.5 and using the same conditions as in E2 (AEM) and E3 (CEM). Membrane inclusion resulted in a decrease of the anodic pH during the cycle and an increase of the cathodic pH. Both membranes provided very similar MEC performance with respect to pH trends as already reported by Rozendal et al. [140].

The cathodic chamber reached a slightly higher pH at the end of the cycle with an AEM (pH = 11.0) compared to a CEM (pH = 10.5) which, in turn, had a steeper growing trend at the beginning, probably as a result of the higher initial current intensity. Similarly, the pH in the anodic chamber at the end of the cycle was only slightly lower with the AEM but in both cases (i.e. AEM and CEM), the pH decreased almost linearly and practically at the same rate.

Both the anodic pH drop and the cathodic pH increase caused a decrease in current intensity (Figure 5.4) when compared to the single-chamber scenario.

Besides the effect that the pH changes could have on the operation of the electrodes (discussed below), the anodic pH decrease and the cathodic pH increase had a

detrimental effect on the system thermodynamics. Figure 5.9B displays the evolution of the theoretical anodic and cathodic potentials calculated by means of the Nernst equation (equations 1.4 and 1.7 in Chapter 1) according to the pH profiles in Figure 5.9A for a temperature of 298 K. Acetate concentration and hydrogen partial pressure were assumed to remain constant over time at their initial values ( $1.69 \cdot 10^{-2}$  M and 0.01 atm, respectively) in order to simplify calculations.

As observed, the higher the cathodic pH, the lower the theoretical potential of hydrogen formation, while the lower the anodic pH, the higher the potential of acetate oxidation. Thus, taking into account that the minimum theoretical applied potential to drive the reactions, i.e. the electromotive force,  $E_{emf}$ , (see General Introduction in Chapter 1), can be calculated as the difference between the theoretical potential of anodic and cathodic reactions, it can be seen that the energetic requirements according only thermodynamics increased along the experiments: from 0.05 V to 0.37 V for AEM and from 0.05 V to 0.31 V for CEM. This increase would be even higher if acetate concentration and hydrogen partial pressure profiles were considered. An increasing applied potential (linked to pH variations) should have been applied to maintain a constant current intensity in those cycles with membrane.

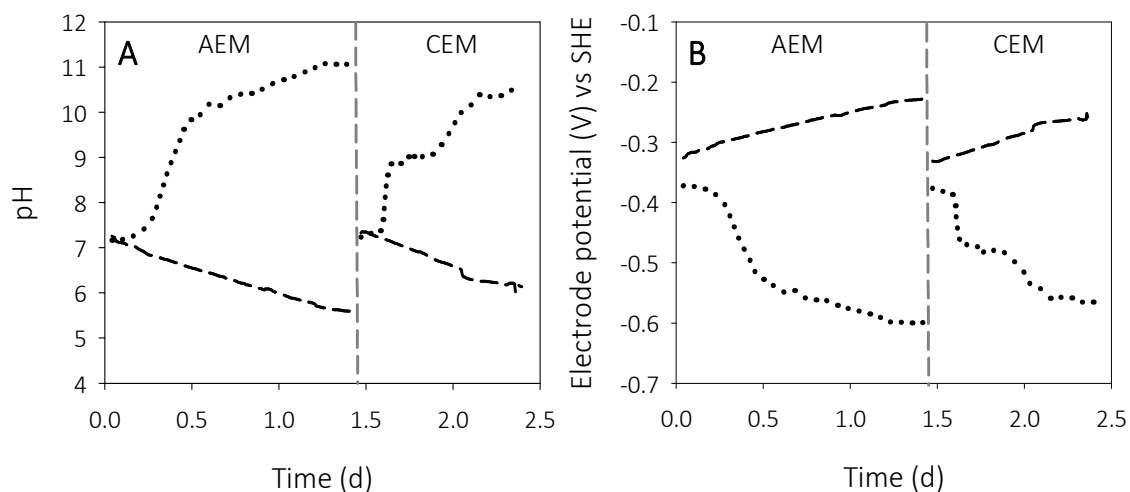


**Figure 5.9** Two-chamber MEC BF with an AEM and a CEM using the same conditions as in experiments E2 and E3. (A) pH evolution and (B) theoretical anodic and cathodic potentials at the corresponding pH by assuming an acetate concentration of  $1.69 \cdot 10^{-2}$  M and a hydrogen partial pressure of 0.01 atm. Anode (dashed) and cathode (dotted).



#### 5.4.5 Analysis of two-chamber operation

The previous results showed that single-chamber MEC were mainly limited by the cathode overpotential, thus much of the energy requirements are due to the cathodic reaction. However, these results cannot be extrapolated to a two-chamber configuration since both the anodic and the cathodic chamber experienced detrimental pH changes (Figure 5.9). Additional LSV in the two-chamber BF (with AEM) at the best and worst case scenarios (i.e. initial and final pH, respectively) were recorded to gain more knowledge from the system. Electrode potentials were measured to monitor the anodic and cathodic overpotential under each pH condition. Figure 5.10A shows the current-voltage profiles of BF: (i) without membrane, (ii) with membrane at pHs of 7.5 and (iii) with membrane at final pHs (i.e. 6 at the anode and 11.0 at the cathode). As it can be observed, the presence of the membrane slightly reduced the current intensity (25 % at 1.0 V of applied voltage), due to the contribution of membrane to potential losses. However, the trend of the current intensity at the initial pHs was very similar to that without membrane. The current intensity at the final pHs was much lower (a reduction of 80 % at 1.0 V of applied voltage), reaching values of only 1.3 mA at an applied voltage of 1.0 V. These results indicate that at such current intensities the membrane effect on the pH change was more important than the internal resistance increase.

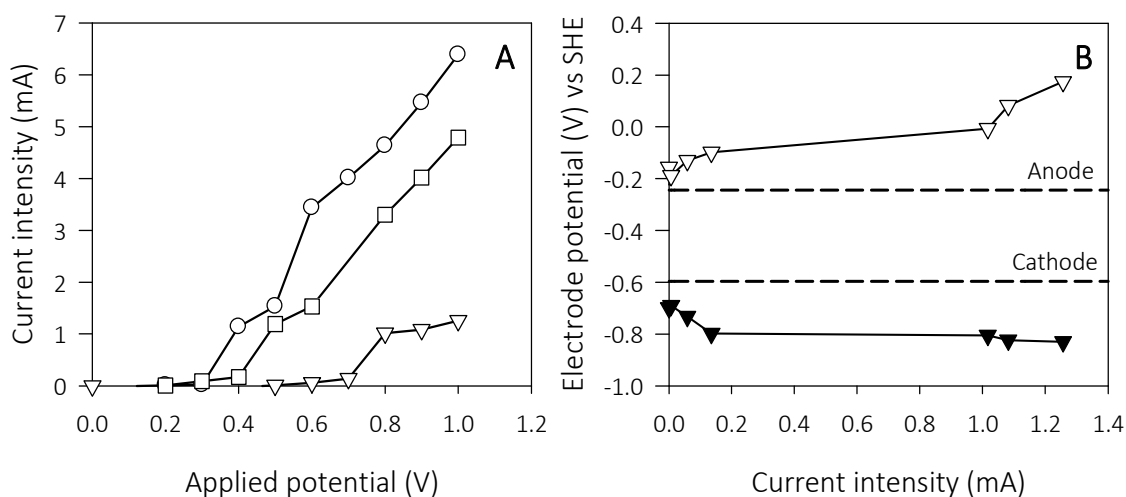


**Figure 5.10** Linear sweep voltammetry of BF without membrane (○), and with an AEM at the initial (□) and final pHs (▽) of a batch experiment (A) Current intensity profiles and (B) Electrode potentials at final pHs: anode potential (open symbols) and cathode potentials (filled symbols). Dashed lines indicate the theoretical electrode potentials under pH final conditions and an acetate concentration of  $1.69 \cdot 10^{-2}$  M and a hydrogen partial pressure of 0.01 atm.

The electrode overpotentials in two-chamber configuration at initial pHs were practically the same as without membrane (results not shown). Figure 5.10B only shows the electrode potentials at the final pHs together with the theoretical electrode potentials. The difference between the theoretical electrode potentials was higher than in Figure 5.5B, indicating that the minimum applied potential to drive the reaction was higher at this worst case scenario, as previously discussed. The major overpotential was in the anode, since a major increase was already observed from low current intensities (an overpotential of 0.42 V was reached at only 1.3 mA, whereas for the cathode it was 0.23 V). Thus, the anodic pH decrease due to the membrane influenced more than the cathodic pH increase. Anodic processes are biological thus, more sensible to pH changes. A near-neutral pH is required for the anode and thus, a decrease of anodic pH would lead to a severe loss of biological activity. Gil et al. [132] reported that a pH below 6 can inhibit current generation by ARB. This can explain HC and LC failure under two-chamber configuration, since anodic pH had probably dropped below values of 6 despite the lower current intensities.

Both the decrease in the anodic pH and the increase in the cathodic pH could be to a certain extent softened if working in continuous mode. However, in the best case, the scenario would be similar to the one observed in single-chamber configuration, in which MEC still performed worse than with buffered medium. Therefore, it is necessary to find strategies to improve the energy efficiency of MEC under these conditions.

#### 5.4.6 Summary of the experimental results

Figure 5.11 presents CE,  $r_{\text{CAT}}$ , energy efficiencies and hydrogen production of the experiments of Table 5.1. Note that hydrogen production was normalized to the volume of the anodic chamber, which in single-chamber configuration accounts for 60 mL and in two-chamber configuration for 30 mL.

The buffered experiments (E1, E2 and E3) resulted in CE and  $r_{\text{CAT}}$  very close to 100 %. However, the energy efficiencies decreased when a membrane was placed to separate both chambers, being  $r_s$  140%, 135% and 113%,  $r_E$  182 %, 130 % and 141 % and  $r_{E+S}$  79 %, 66 % and 63 % for E1, E2 and E3, respectively. Therefore, from an energetic point of view, both types of membranes gave fairly similar results. This may seem surprising since the ohmic resistance of the cell was higher for AEM than for CEM and the increase of the energetic requirements was slightly higher for AEM. However, the anodic overpotential increase (linked to anodic pH decrease) caused a decrease in the current intensity of the cell, which in turn minimized the ohmic losses and the differences between AEM and CEM. Similarly, differences between the theoretical required potentials in each case lost importance because of the high anode overpotential.

Hydrogen production was  $1.1 \text{ m}^3\text{m}^{-3}\text{d}^{-1}$  when BF worked without membrane. It decreased to 0.78 and  $0.50 \text{ m}^3\text{m}^{-3}\text{d}^{-1}$  when working with an AEM and a CEM, respectively.

Results of E4, in which HC worked in single-chamber configuration, showed a CE close to 100 % and a  $r_{\text{CAT}}$  of 84 %. Energy efficiencies were lower than in E1, being  $r_s$  112 %,  $r_E$  128 % and  $r_{E+S}$  60 %. In E5 and E6, in which HC worked in two-chamber configuration, CE was between 22 and 26 %, a value much lower than in E4. Both the  $r_{\text{CAT}}$  and the energy recoveries were 0 %, since hydrogen was not recovered at all. The experiment of LC in single-chamber configuration, E6, had the highest CE, probably as a consequence of the long duration of the cycles, which may have favoured the proliferation of

homoacetogens. In this sense,  $r_{\text{CAT}}$  was also low (63.3 %), resulting in low energy efficiencies as well. When a membrane was placed in LC (E7 and E8) CE decreased and a  $r_{\text{CAT}}$  of 0 % led to energy efficiencies of 0 %. Low CE in long cycles (E5, E6 and E8) could be attributed to some oxygen leakage in the cell, which is negligible in conventional cycles with high MEC performance.

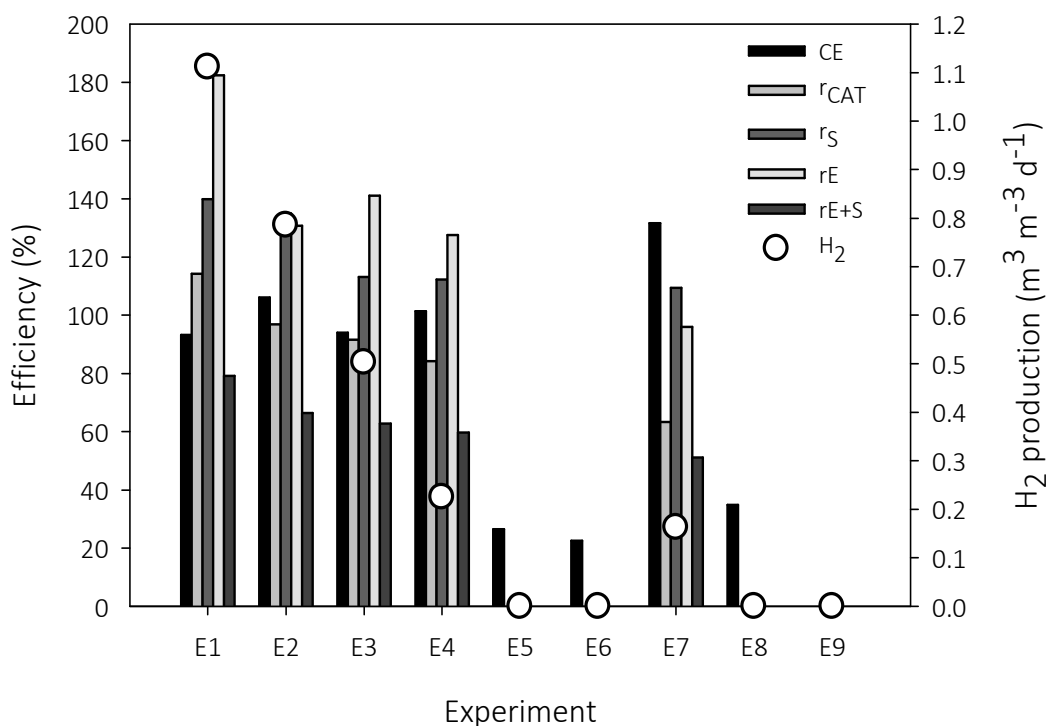


**Figure 5.11** Coulombic efficiency (CE), cathodic gas recovery ( $r_{\text{CAT}}$ ), energy efficiencies ( $r_{\text{S}}$ ,  $r_{\text{E}}$ ,  $r_{\text{S+E}}$ ) (bars) and hydrogen production (circles). Note that CE for E9 is not plotted due to problems with the analysis.

## 5.5 Conclusions

The results in this chapter evidenced that buffered media were essential for the proper operation of single-chamber MEC in batch mode, since the electrode overpotentials in non-buffered cells increased, particularly in the cathode. Experiments with single-chamber MEC with non-buffered media showed similar results between them, regardless of the conductivity. In these experiments, current intensity followed an increasing trend throughout the cycle, though it reached lower values than the buffered system. Conductivity, however, would play a major role in larger cells, where ohmic potential losses would become more important due to the higher current intensities.

The use of buffer became even more critical when working in two-chamber configuration, because it softened pH changes. Nevertheless, the pH of the anodic chamber of the buffered system decreased to values close to 6 at the end of the cycle, regardless of the membrane used. At such low pH, the current intensity was lower and the anode overpotential was very high. Non-buffered MEC did not work at all in two-chamber configuration, since in this case the pH drop in the anodic chamber would have been even higher. Higher conductivities did not improve the operation.



# CHAPTER 6

---

Enhanced performance of two-chamber microbial electrolysis cells using a pH control strategy

Part of the content of this chapter was published as:

Ruiz, Y., Baeza, J.A. and Guisasola, A. (2015) Enhanced Performance of Bioelectrochemical Hydrogen Production using a pH Control Strategy. *ChemSusChem* 8(2), 389-397.





The use of membranes in microbial electrolysis cells (MEC) is required to obtain high-purity hydrogen and to avoid the consumption of hydrogen by undesired microorganisms. However, as observed in Chapter 5, its utilization results in i) pH gradients across the membrane, ii) higher ohmic losses and iii) reduced MEC efficiency. A pH control approach to enhance the performance of two-chamber MEC is presented in this chapter as a proof of concept. Several pH-controlled and non-controlled scenarios were evaluated, which evidenced that the pH control was very beneficial for the MEC performance. On the one hand, the ARB activity remained constant by controlling the anodic pH at a near-neutral pH, thus largely avoiding the decrease of current intensity throughout a cycle. On the other hand, controlling the cathodic pH at a low value allowed hydrogen production at very low applied potentials thus, increasing the energy efficiency in relation to the electrical input. The presented pH control strategy was firstly tested and optimized in a well-buffered MEC and then implemented in non-buffered cells. The use of an acid effluent of the dairy industry was tested as catholyte with fairly positive results.

## 6.1 Introduction

Chapter 4 evidenced that hydrogen production in a single-chamber MEC was not feasible in the long-term, since other microorganisms such as homoacetogenic bacteria or hydrogenotrophic methanogens consumed hydrogen, thus hindering its recovery. The operation of an MEC with non-buffered medium and low conductivity was assessed in Chapter 5 for both single and two-chamber configurations. The performance of the non-buffered MEC in single-chamber configuration was lower than that of the well-buffered cell. However, hydrogen recovery in single chamber was high and therefore, the energy efficiency was relatively high. However, in two-chamber configuration, which seems more appropriate if the final goal is hydrogen production, MEC failed as a consequence of the pH gradients. Conductivity had a minor effect on the MEC performance since the achieved current intensities were low in small-scale cells and thus, ohmic losses were not important.

Several studies have tried to minimize the efficiency decrease caused by pH gradients across the membrane, because *a priori* the use of a buffer is neither economically nor environmentally feasible. For example, carbon dioxide addition to the cathode of an MFC was reported [148,149]. Carbon dioxide reacts with hydroxyls to form carbonate species, which in turn, are transported to the anodic chamber through an ion exchange membrane, thus sustaining the cathodic pH, while softening the anodic pH decrease.

In Freguia et al. [150], the cathodic compartment of an MFC was fed with the anodic effluent to minimize the cathodic pH rise. Qu et al. [151] operated a microbial desalination cell with recirculation of the solutions between the anode and the cathode to avoid pH imbalances that could inhibit bacterial activity. Sleutels et al. [133] operated an MEC with three compartments, which provided conductivity and alkalinity to the anode and thus reduced buffer requirements.

Erable et al. [152] designed a two-chamber air-cathode MFC that allowed the adjustment of the cathodic pH at a low value by adding concentrated HCl, obtaining current intensities 2.5-fold higher than those obtained in a traditional air-cathode MFC. Zhuang et al. [153] followed a similar strategy to improve the performance of an MFC by maintaining a high pH in the anolyte and a low pH in the catholyte through NaOH and HCl dosage. However, to the best of our knowledge, pH control approaches have been never tested in MEC for hydrogen production.

As already stated in Chapter 5, the use of saline catholytes has already been reported [134-136] and, in some cases, in combination with carbon dioxide sparging. However, in none of them the catholyte was a real industrial effluent. Cheese brine from the dairy industry presents pH and conductivity characteristics that makes it *a priori* a suitable catholyte for MEC. Cheese brine is used during the salting process for cheese flavouring and regulating the growth of microorganisms to slow microbial conversion of lactose into lactic acid and to protect cheese from undesirable microorganisms. Cheese salting also contributes to the formation of the rind of the cheese. Cheeses are immersed in a brine bath for a variable period of time and periodically turned over. Brine used in this process consist of a 19 % NaCl solution with the pH adjusted with lactic acid to the pH of the cheese. The brine is reused several times after a microfiltration process. However, when

it cannot be reused, it becomes a waste to be treated due to its high conductivity and low pH, which implies an additional cost for the dairy industry. In some regions of United States, brine is already being used along with rock salt to prevent freezing of roads.

## 6.2 Objectives

The objective of this study is to demonstrate as a proof-of-concept a pH control strategy for a better performance of a two-chamber MEC, both in non-buffered and well-buffered cells. Moreover, the benefits of working at a low pH at the cathode will be assessed by following two different strategies: (i) by increasing the current intensity by maintaining a high applied potential (1.0 V) to boost hydrogen production and (ii) by maintaining the same hydrogen production by significantly reducing the applied potential. Finally, the performance of cheese brine as catholyte will be evaluated as a possible strategy to improve the energy recovery of two-chamber MEC using an industrial effluent with low pH.

## 6.3 Materials and Methods

### 6.3.1 Reactor description and medium composition

Two-chamber small-scale MEC (SS-MEC, see materials and Methods in Chapter 3) with AEM were used to conduct the experiments. A glass tube was also provided to the anodic chamber to allow the increase of reactor volume when pH was controlled. AEM was chosen since cathodic pH in some experiments was controlled at low values such as 2.0 and, if a CEM was used, protons could have crossed to the anodic chamber resulting in an increase of pH control requirements. For example, if the pH of the anodic and the cathodic chambers was 7.5 and 2.0, respectively, the concentration gradients of protons would be 0.01 M and the gradient of hydroxyls  $3.2 \cdot 10^{-7}$  M. Therefore, diffusion of protons would be favoured with respect to hydroxyls. Thus, an AEM was more indicated in this scenario.

The cells and media described in Chapter 5 were used: BF (buffered), HC (high conductivity) and LC (low conductivity). Acetate was used as substrate at an initial concentration of 1.5 g/L.

In one of the experiments, the catholyte of MEC BF was replaced by cheese brine from the dairy industry (Planta de Tecnologia dels Aliments, Universitat Autònoma de Barcelona), which had an initial pH and conductivity of around 3.75 and 120 mS/cm, respectively.

### 6.3.2 Batch experiments and pH control

Current intensity was monitored and acetate and hydrogen were analysed in all the experiments (see Materials and Methods in Chapter 3). The applied voltage was 1.0 V unless otherwise specified. Monitoring of the electrode potentials was required in some of the experiments, thus, an Ag/AgCl reference electrode was placed in both the anodic and the cathodic chambers.

The pH in the anodic and the cathodic chambers was monitored on-line in all batch experiments using two pH probes (Crison pH electrode 5233) connected to a pH meter (Crison MultiMeter 44). Moreover, in most experiments, pH was controlled with acid dosage to the cathodic chamber and base dosage to the anodic chamber by using an automatic burette (Crison MultiBurette 2S) as shown in Figure 6.1. The pH controller actuated in MEC as an on/off controller and was programmed in a PC by using LabWindows CVI (2014) software. HCl and NaOH stock solutions had a concentration of 1-3 M, which depended on the specific requirements of each experiment and took into account that the total added volume of acid or base should not be higher than the 10% of the reactor volume. All experiments in which pH control was implemented were performed with orbital agitation at 100 rpm (DOS-20L ELMY Sky Line digital orbital shaker) to ensure liquid homogeneity. During these experiments the acid/base dosage was monitored. Conductivity was measured at the beginning and at the end of each batch experiment.

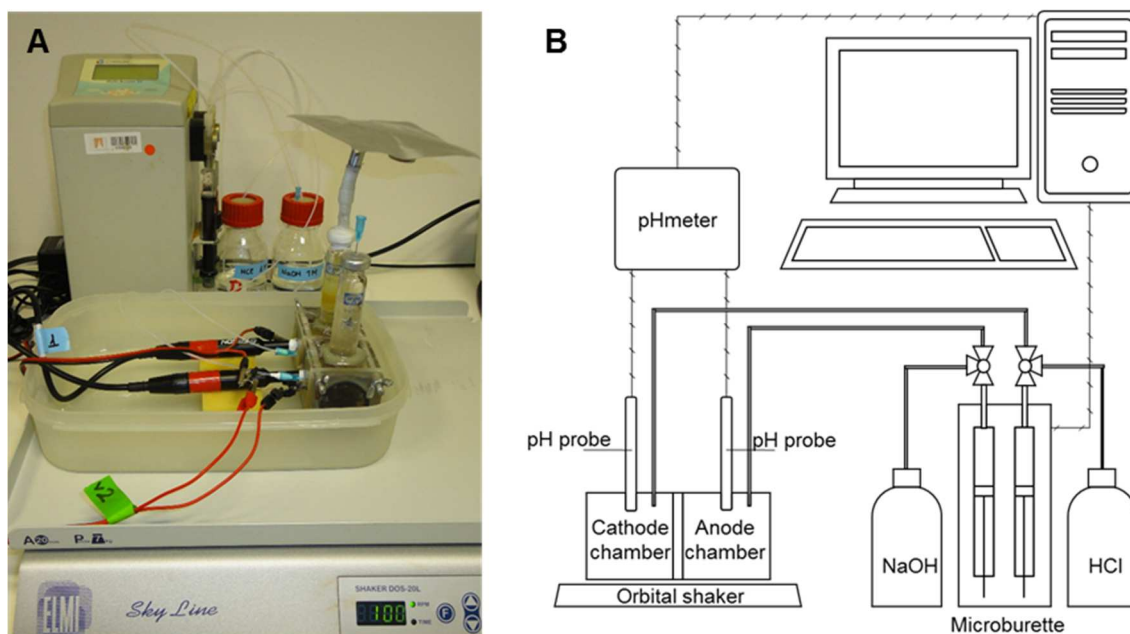


**Figure 6.1** (A) Image and (B) Schematics of the experimental setup.

All the experiments conducted in this chapter are summarized in Table 6.1. In the first part of this chapter the pH control strategy was first tested in BF, which include: (i) an experiment without pH control (E1), (ii) batch experiments with pH control only in the cathodic (E2) or in the anodic chamber (E3), (iii) a set of experiments in which the cathodic pH was controlled at different values (E4, E5, E6 and E7) and (iv) a batch experiment with a low cathodic pH (2.0) and low applied potential (0.2 V) (E8). In the second part, the best conditions obtained with BF were tested in HC (E9) and LC (E10). In the latter part, the performance of BF was evaluated with cheese brine as catholyte by setting the anode potential at -0.2 V vs SHE (E11). Note that E1 was conducted under the same conditions as E2 in Chapter 5, but it was also repeated in this chapter for a better comparison of the results.

**Table 6.1** Summary of the experimental conditions of batch experiments E1 to E11.

Experiment	MEC	Cathode chamber pH control	Anode chamber pH control	Applied potential (V)	Agitation
E1	BF	Not controlled	Not controlled	1.0	No
E2	BF	7.5	Not controlled	1.0	Yes
E3	BF	Not controlled	7.5	1.0	Yes
E4	BF	7.5	7.5	1.0	Yes
E5	BF	2	7.5	1.0	Yes
E6	BF	5	7.5	1.0	Yes
E7	BF	12.5	7.5	1.0	Yes
E8	BF	2	7.5	0.2	Yes
E9	HC	2	7.5	0.2	Yes
E10	LC	2	7.5	0.2	Yes
E11	BF/ brine	Not controlled	7.5	Anode at -0.2 V vs SHE	Yes

### 6.3.3 Electrochemical analyses

Cyclic voltammetry (CV) was recorded in two electrode configuration from 0 to 1.2 V at 0.1 mV/s. During the experiment, pH was controlled in both chambers with the same set points as in E5 and E8 and with orbital agitation at 100 rpm. Electrochemical impedance spectroscopy (EIS) measurements were performed using a two-electrode configuration to estimate the ohmic resistance under different conditions of conductivity due to acid/base dosage. Chronoamperometry (CA) was used to poise the anode at a potential of -0.2 V vs SHE in the experiment with brine as catholyte. The cell applied potential was monitored with a 3-Divider cable. The anode working potential was previously determined by means of a LSV.

### 6.3.4 Calculations

The theoretical and experimental proton production ( $HP_{\text{theo}}$  and  $HP_{\text{exp}}$ , respectively) were calculated for each chamber when pH was controlled.  $HP_{\text{theo}}$  was estimated from the

measured current intensity and the stoichiometry either of the anodic (equation 6.1) or the cathodic (equation 6.2) reactions according to Table 1.2 in Chapter 1.

$$HP_{\text{theo}} = \frac{\int_{t_0}^{t_F} I dt a_{\text{Ac}^-}}{F b_{\text{Ac}^-}} \quad (6.1)$$

$$HP_{\text{theo}} = \frac{\int_{t_0}^{t_F} I dt a_{\text{H}_2}}{F b_{\text{H}_2}} \quad (6.2)$$

where  $t_0$  and  $t_F$  (s) are initial and final time,  $I$  (A) is the current intensity,  $a_{\text{Ac}^-}$  is the number of protons produced per mole of acetate ( $9 \text{ mol H}^+ \text{ mol}^{-1} \text{ acetate}$ ),  $a_{\text{H}_2}$  is the number of protons consumed (or hydroxyls produced) per mole of hydrogen ( $2 \text{ mol H}^+ \text{ mol}^{-1} \text{ H}_2$ ),  $F$  is the Faraday's constant ( $96485 \text{ C/mol e}^-$ ),  $b_{\text{Ac}^-}$  is the moles of electrons transferred per mole of acetate ( $8 \text{ mol e}^- \text{ mol}^{-1} \text{ Ac}^-$ ) and  $b_{\text{H}_2}$  is the moles of electrons transferred per mole of hydrogen ( $2 \text{ mol e}^- \text{ mol}^{-1} \text{ H}_2$ ).

The  $HP_{\text{exp}}$  in each chamber was measured indirectly by titrimetry by monitoring the acid and base dosage profiles required to maintain the pH constant (equation 6.3) [154].

$$HP_{\text{exp}} = C_{\text{BASE}} \cdot V_{\text{BASE}} - C_{\text{ACID}} \cdot V_{\text{ACID}} \quad (6.3)$$

where  $V_{\text{BASE}}$  and  $V_{\text{ACID}}$  (L) are the accumulated base and acid dosage for a given time and  $C_{\text{BASE}}$  and  $C_{\text{ACID}}$  are the base and acid concentrations ( $\text{mol L}^{-1}$ ).  $HP_{\text{theo}}$  and  $HP_{\text{exp}}$  took positive values for the anodic chamber as protons were produced and pH was controlled by only adding base. Conversely, they took negative values for the cathodic chamber, where protons were consumed and the pH was controlled by adding acid. Determination of HP by titrimetry was already reported in Freguia et al. [155] to close proton balances in the anodic compartment of MFC fed with acetate and glucose.

## 6.4 Results and Discussion

### 6.4.1 Experiments with well-buffered medium

#### 6.4.1.1 Enhanced performance of the two-chamber MEC with pH control implementation

As discussed in Chapter 5, the presence of a membrane in two-chamber MEC leads to pH changes in both the anodic and the cathodic chambers. In this context, a pH control strategy was designed in order to minimize the detrimental effect of these pH changes in the cell performance. The first experiment, E1 (Table 6.1), was conducted without pH

control to be used as a reference operation. Then, pH control was only implemented in one of the chambers (E2 and E3), so that the effect of controlling the anodic and the cathodic pH could be studied separately. After that, pH control was applied to both chambers simultaneously (E4).

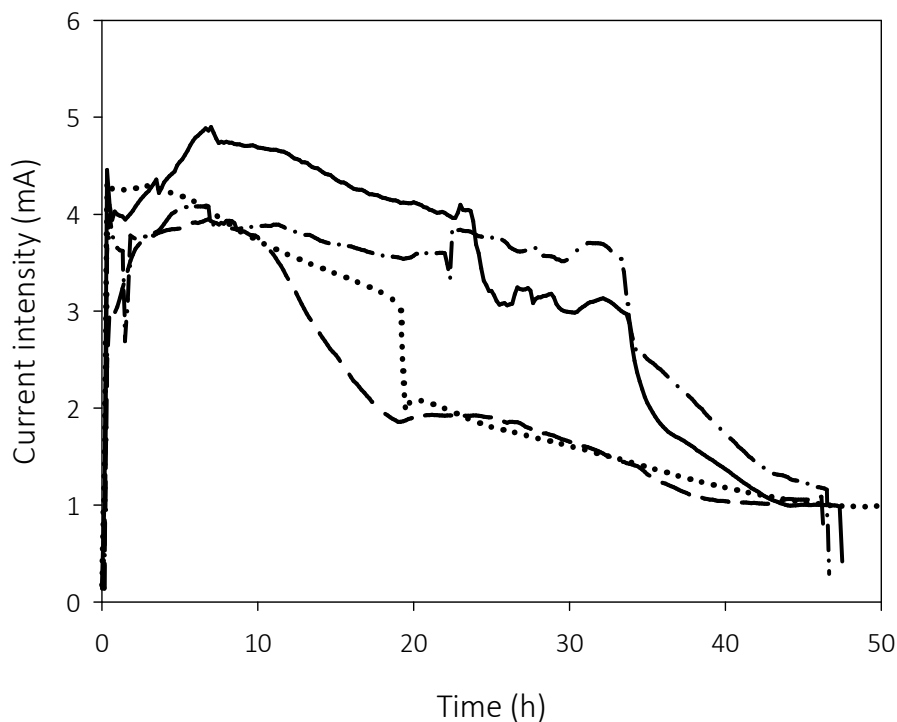


**Figure 6.2** Current intensity profiles of the two-chamber MEC in E1 (pH not controlled, dotted), E2 (cathode at pH 7.5, dashed), E3 (anode at pH 7.5, dash-dotted) and E4 (cathode and anode at pH 7.5, solid).

Figure 6.2 shows the current intensity profiles of these experiments with different pH control strategies. The current intensity in E1 decreased along the cycle due to the lack of pH control as already discussed in Chapter 5. Control of the cathodic pH at 7.5 (E2) did not prevent the decrease in current intensity and a similar profile to that in E1 was obtained. The decrease in current intensity was even sharper in E2. This could be caused by an increased transport of anions other than hydroxyls to meet the electroneutrality condition as the hydroxyl concentration is very low at near neutral pH (7.5) compared to other anions present in the medium (e.g.  $\text{Cl}^-$ ,  $\text{S}^{2-}$ ). However, when cathodic pH reached values close to 12 (non-controlled pH, E1), hydroxyl concentration increased more than four orders of magnitude with respect to neutrality. This could favor hydroxyl transfer



through the AEM and, then, soften the anodic pH decrease. This observation has already been discussed and experimentally corroborated by Ahn and Logan [134].

When the anodic pH was controlled at 7.5 (E3), current intensity remained practically constant around 3.8 mA, despite minor fluctuations, until substrate was depleted (33 h). The area under the curve time-intensity was much higher in E3 than that in E1 and E2, which suggests a higher ARB activity during the whole batch cycle. Therefore, as expected, the anodic pH decrease were more critical to the MEC performance since they result in not only an increase in the energetic requirements, but also in a loss of ARB activity. This was also observed in Chapter 5, where the anodic overpotential increased significantly more than the cathodic overpotential as a result of pH changes.

The implementation of anodic and cathodic pH control at 7.5 (E4) showed a current intensity profile very similar to that obtained in E3. This suggests that when the anodic pH is controlled, control of the cathodic pH at 7.5 is not that crucial. A similar effect in relation to the initial pH was observed in Ribot-Llobet et al. [92], where the performance of an MEC with a platinum cathode was independent of the initial cathodic pH in a range of 7-12. Zhuang et al. [153] assessed the effect of the cathodic pH on the open circuit voltages in a two-chamber MFC. The cathode potential decreased linearly with a slope of -59mV/pH from pH 1 to pH 6, whereas the decrease was much lower for pH values above 6, which was attributed to proton-transport limitations. Therefore, either limitations in transport of protons from the bulk solution to the cathode surface or hydroxyls from the cathode surface to the bulk solution might have caused that the same local pH at the cathode surface was attained regardless of the bulk pH. Thus, working at either pH 7.5 or 12 in the cathodic compartment would have had a minor impact in the overall MEC performance.

Figure 6.3 summarizes the results in terms of efficiency and hydrogen production for E1 to E8. Note that hydrogen production was normalized to the volume of the anodic chamber. Results in E1 and E2 were very similar in accordance to the intensity profiles. Both CE and  $r_{\text{CAT}}$  took values close to 100 %, whereas the values of  $r_{\text{S}}$ ,  $r_{\text{E}}$ , and  $r_{\text{E+S}}$  were 118%, 126% and 61% for E1, and 104%, 141 % and 60 % for E2. Hydrogen production was almost the same in both cases ( $0.77 \text{ m}^3\text{m}^{-3}\text{d}^{-1}$  for E1 and  $0.74 \text{ m}^3\text{m}^{-3}\text{d}^{-1}$  for E2).

Efficiency values in E4 were not higher than in E1 and E2. However, pH control allowed maintaining the biomass active throughout the batch cycle, so that hydrogen production was higher ( $0.88 \text{ m}^3 \text{ m}^{-3} \text{ d}^{-1}$ ). Furthermore, the acetate removal efficiency in E4 was higher (91%) than in the previous cases (69% for E1 and 70% for E2).

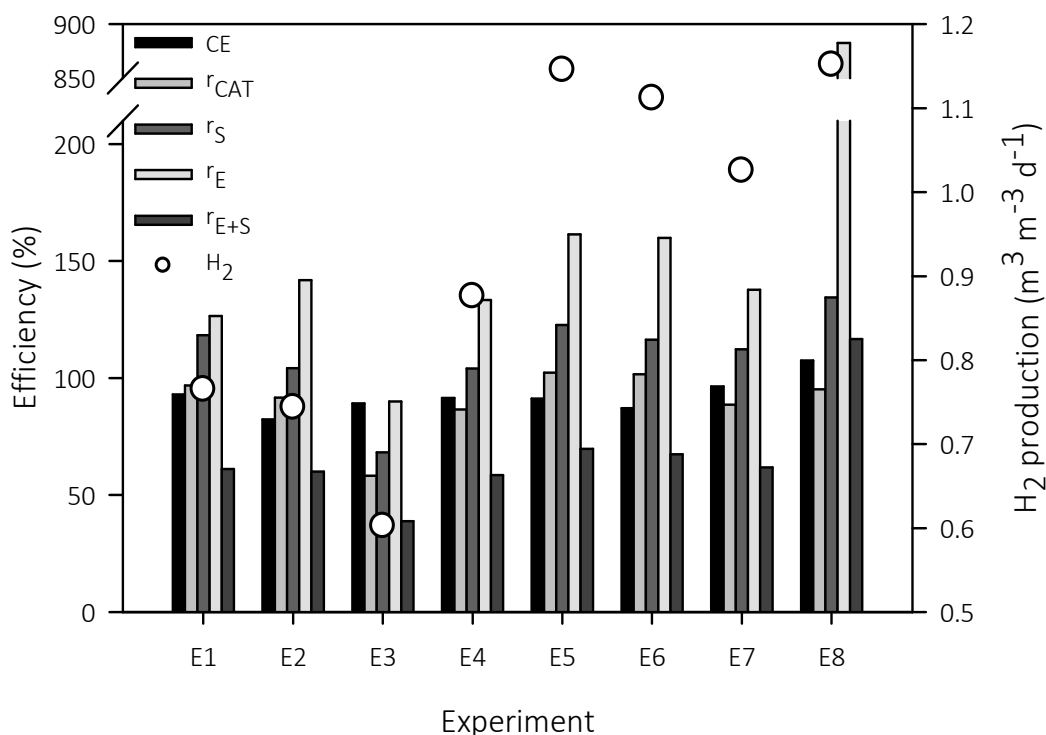


**Figure 6.3** Coulombic efficiency (CE), cathodic gas recovery ( $r_{\text{CAT}}$ ), energy efficiencies ( $r_{\text{S}}$ ,  $r_{\text{E}}$ ,  $r_{\text{S+E}}$ ) (bars) and hydrogen production (circles) for experiments conducted in this study.

Figure 6.4 shows the pH profiles of E1, E2, E3 and E4. As observed, the anodic pH in E1 decreased almost linearly to a value of 6, whereas the cathodic pH increased rapidly from 7.5 to 10.8 in the first 10 hours of experiment. When only the pH of the cathodic chamber was controlled (E2), the anodic pH decreased down to a value of 5.8. Meanwhile, when only the anodic pH was controlled (E3), the pH in the cathodic chamber increased to 11.8, which is a parallel trend to that in E1. In E4, the pH of both the anodic and the cathodic chambers remained practically constant during the whole experiment because of the pH control.

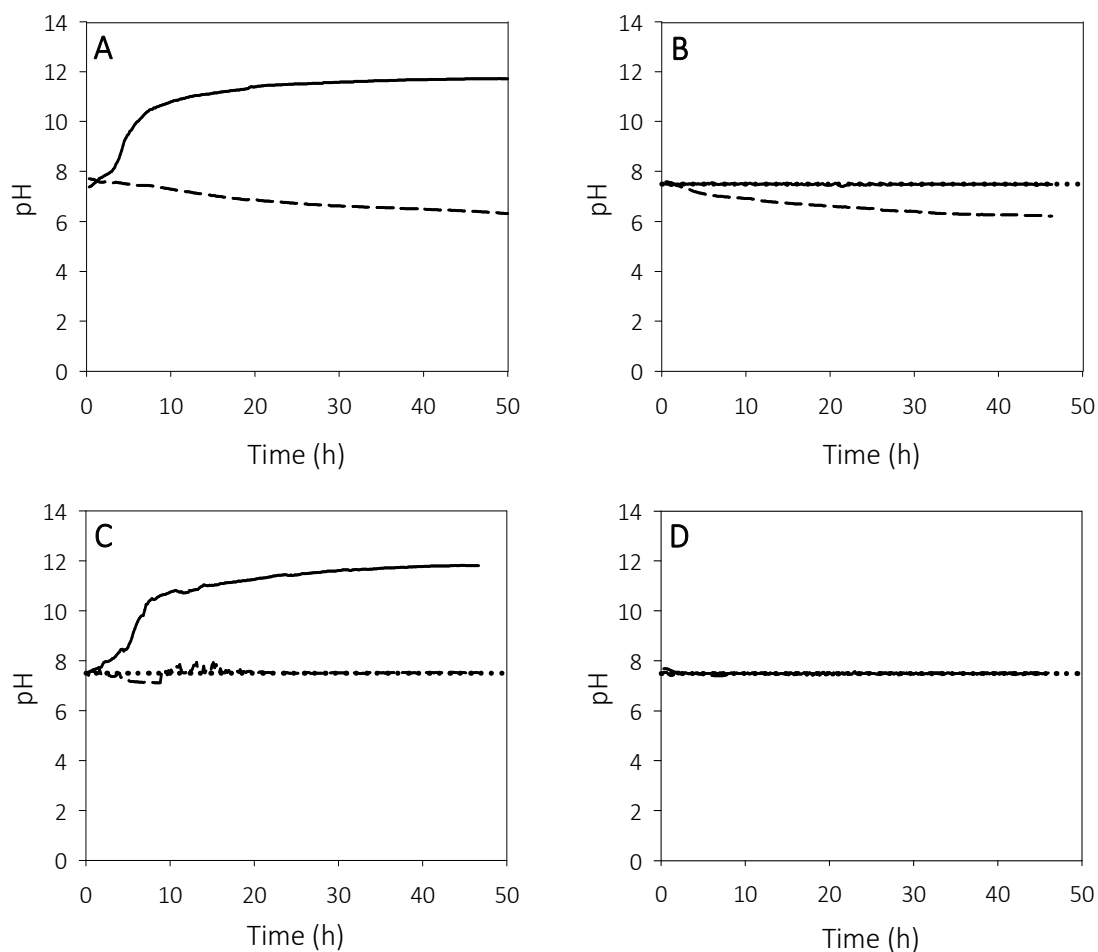


**Figure 6.4** pH profiles of (A) E1 (pH not controlled) (B) E2 (cathode at pH 7.5), (C) E3 (anode at pH 7.5) and (D) E4 (cathode and anode at pH 7.5). Cathodic pH (solid), anodic pH (dashed) and setpoint (dotted).

The proton production (HP) was calculated when pH control was activated. The theoretical proton production ( $HP_{\text{theo}}$ ) was estimated from the measured current intensity (equations 7.1 and 7.2), whereas the experimental proton production ( $HP_{\text{exp}}$ ) was measured indirectly by titrimetry i.e. by the numerical analysis of the dosage profile of the acid/base required to maintain pH constant (equation 6.3). Figure 6.5 shows  $HP_{\text{theo}}$  and  $HP_{\text{exp}}$  when pH was maintained at 7.5 in the cathodic (E2), anodic (E3), or both anodic and cathodic chambers (E4). The value of  $HP_{\text{theo}}$  successfully matched that of  $HP_{\text{exp}}$ , which may open a wide range of different possibilities in pH-controlled MEC. Titrimetric measurements are simply implementable on-line measurements that provide real-time information [154], which can be used as an indirect measure of acetate consumption and/or hydrogen production in two-chamber MEC and as a new variable for modelling or

control purposes. Note that HP in the cathodic chamber in E2 was slightly lower than that in E4, as a consequence of the lower intensity in E2 from time 10 h, so that the pH control requirements decrease up to this point. Conversely, HP in the anodic chamber in E3 and E4 was almost identical, as a result of a very similar current intensity profile.

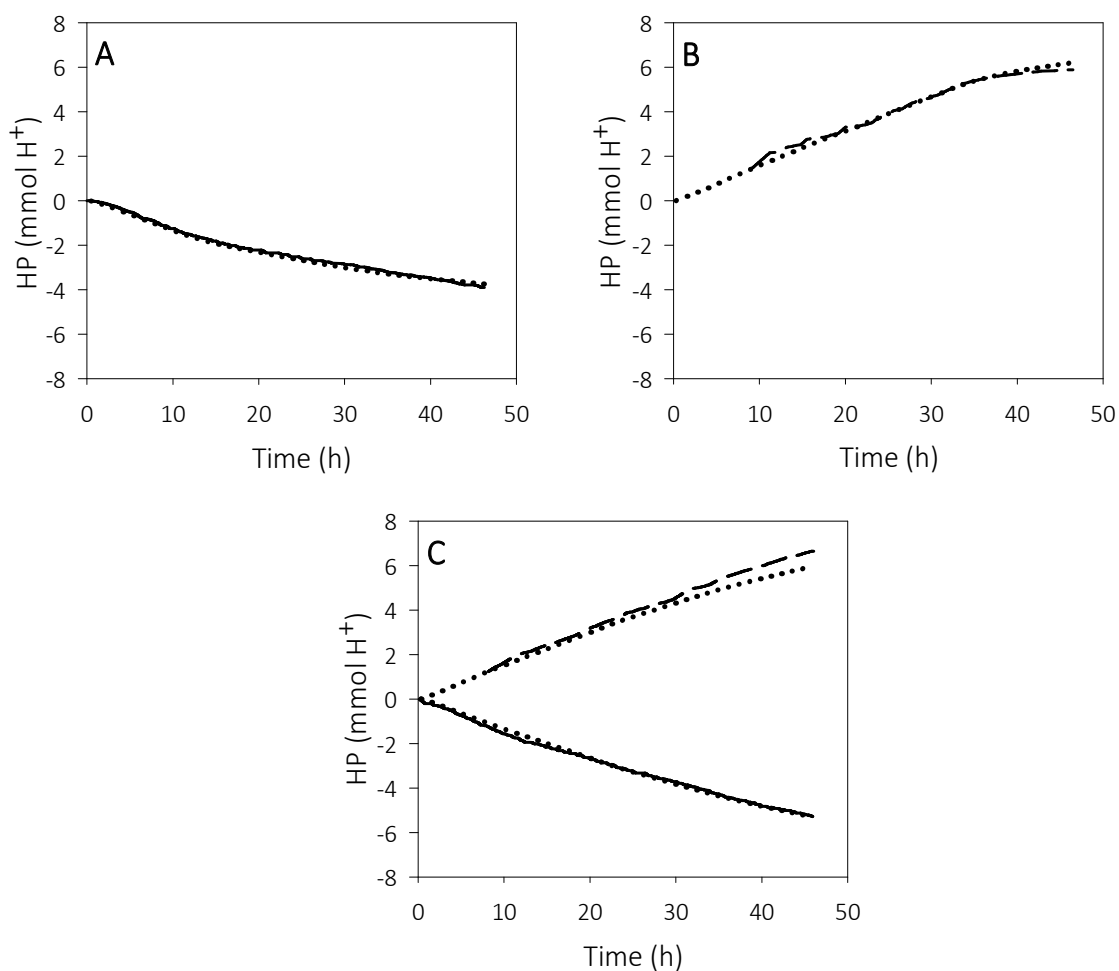


**Figure 6.5** Theoretical and experimental proton production (HP) in (A) E2 (cathode at pH 7.5), (B) E3 (anode at pH 7.5) and (C) E4 (cathode and anode at pH 7.5). Cathodic  $HP_{exp}$  (solid), anodic  $HP_{exp}$  (dashed) and  $HP_{theo}$  (dotted). Positive HP (proton production) correspond to the anodic chamber and negative HP (proton consumption) to the cathodic chamber.

#### 6.4.1.2 Effect of the cathodic pH on the two-chamber MEC performance

Once the pH of the anodic chamber was controlled, the goal was to find the optimal cathodic pH to optimize the MEC operation. An increase of the cathodic pH increases the energetic requirements for hydrogen production as the reduction reaction in the cathode

becomes thermodynamically less favorable. Thus, a low cathodic pH should entail a more thermodynamically favorable overall process and thus, high current intensities.

Figure 6.6 shows the current intensity profiles when the pH of the anodic chamber was set to 7.5 and the pH of the cathodic chamber was set to 2.0 (E5), 5.0 (E6), 7.5 (E4) or 12.5 (E7). Under these conditions, the initial theoretical minimum applied potential to drive the reactions (calculated at the initial concentration and partial pressure values as in Chapter 5) were 0.28 V for E5, 0.11 V for E6, -0.035 V for E4 and -0.33 V for E7. The positive values for E5 and E6 indicate that theoretically the application of an electric potential would not be required if only thermodynamics was considered.

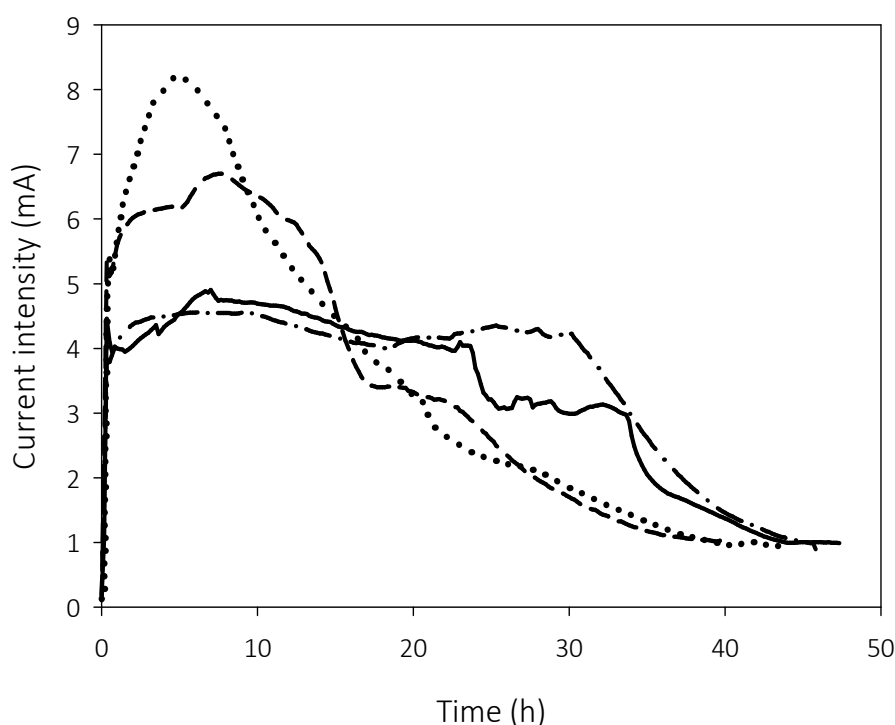


**Figure 6.6** Current intensity profiles of the two-chamber MEC in E5 (cathode at pH 2.0, dotted), E6 (cathode at pH 5.0, dashed), E4 (cathode at pH 7.5, solid) and E7 (cathode at pH 12.5, dash-dotted). The anodic chamber was controlled at pH 7.5.

The highest current intensity, approximately 8 mA, was obtained in E5 in agreement with the theoretical foundations of electrochemistry. In E6, current intensity reached a value of 6.7 mA, whereas in E4 and E7, current intensity reached values close to 4.5 mA. CE (Figure 6.3) was similar in all cases with values that ranged between 87 and 96%.  $r_{CAT}$  was also high and 102 and 101% was obtained for E5 and E6, respectively and 86 and 88% for

E4 and E7, respectively. As a general trend, the lower the cathodic pH, the higher the values of  $r_S$ ,  $r_E$  and  $r_{S+E}$ . However, the overall MEC performance was very similar in all cases and, after the 48-hour cycle, the benefits of working at low pH in the cathodic chamber were not readily apparent. Nevertheless, the hydrogen production rate in E5 and E6 was very high in the first hours of operation according to the current peaks and then decreased (at 5 h and 7.5 h, respectively). This decrease could not be caused by acetate depletion as the CE calculated by integration of the current intensity from 0 h to 5 h (E5) and from 0 h to 7.5 h (E6) would have been 19.3 % for E5 and 25.4 % for E6. These values are unrealistic for these systems as high CE is usually reached (see, for example, experiments E1 to E4). Moreover, this sudden intensity decrease was also observed in experiments with two-fold the initial acetate concentration (results not shown).

The pH profiles for E5, E6 and E7 are presented in Figure 6.7. Current intensity decrease in E5 and E6 was not caused by a pH control failure, as the pH remained close to the setpoint all the time.

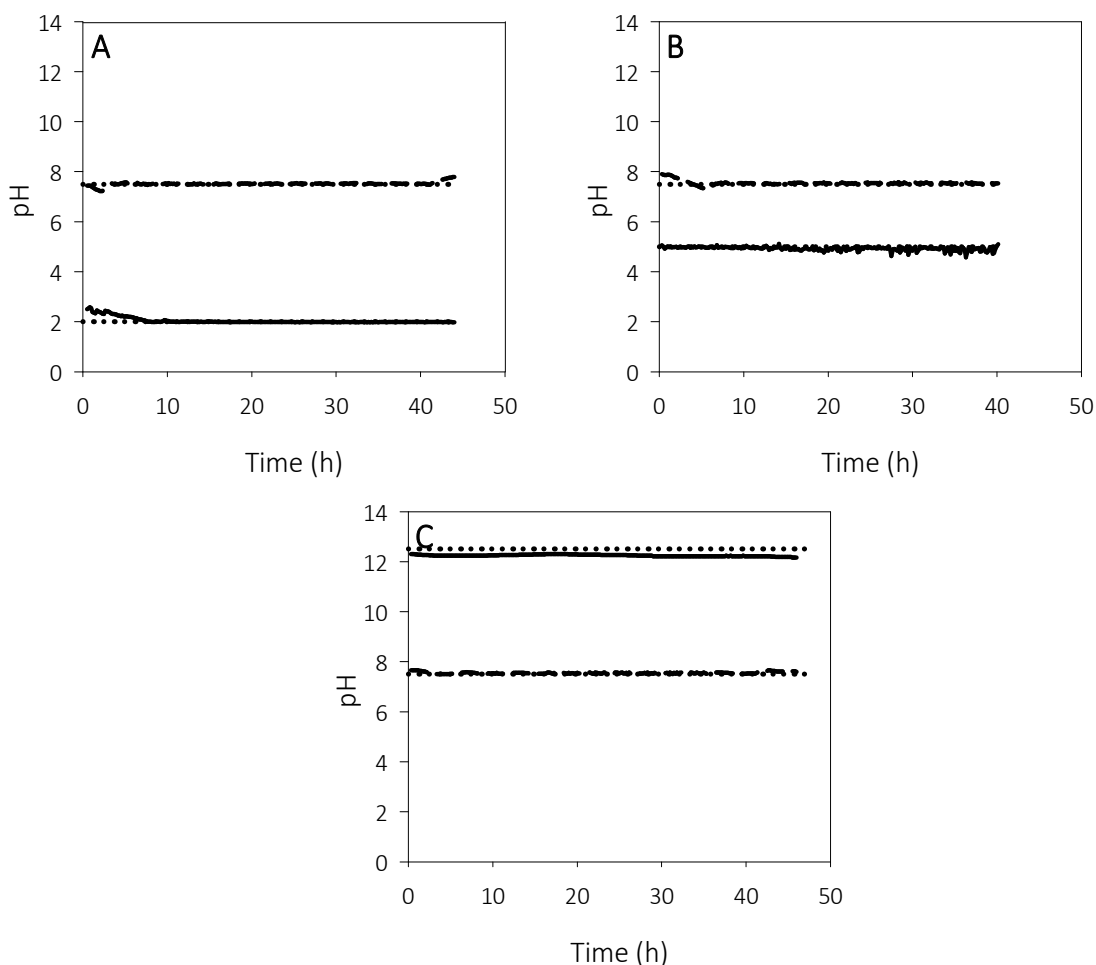


**Figure 6.7** pH profiles of (A) E5 (cathode at pH 2.0), (B) E6 (cathode at pH 5.0) and (C) E7 (cathode at pH 12.5). Cathodic pH (solid), anodic pH (dashed) and setpoint (dotted).

For E7 (cathodic pH of 12.5), controlling cathodic pH was not required because pH did not change during the experiment and therefore, the cathodic  $HP_{exp}$  was 0. In this experiment,  $HP_{exp}$  in both the anodic and the cathodic chambers was much lower than  $HP_{theo}$ , in agreement with the fact that hydroxyls crossed the anionic membrane instead of other anions to meet the electroneutrality condition. This transfer contributed to counteract the anodic pH decrease [134] (Figure 6.8). On the other hand,  $HP_{theo}$  matched  $HP_{exp}$  in E5 and E6, where the pH of the cathodic chamber was controlled at a low value.

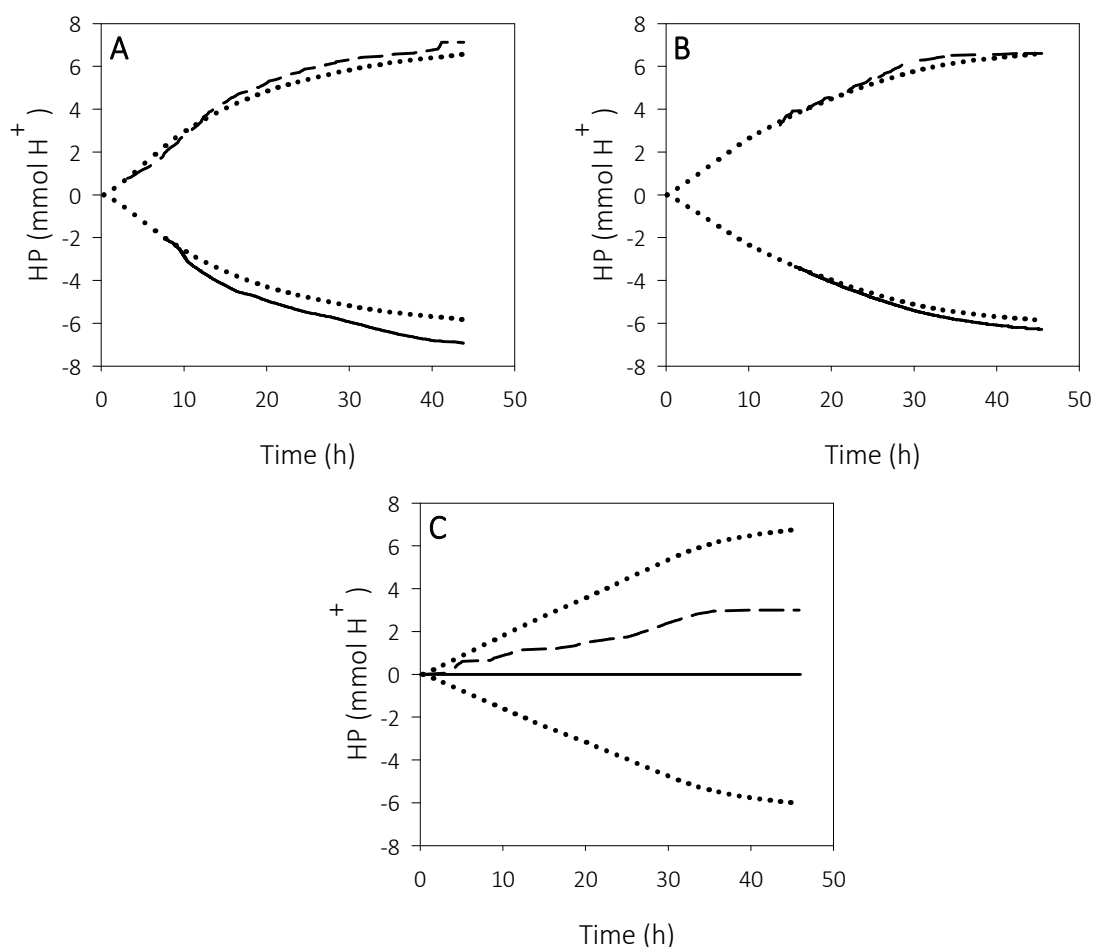


**Figure 6.8** Theoretical and experimental proton production (HP) in (A) E5 (cathode at pH 2.0), (B) E6 (cathode at pH 5.0) and (C) E7 (cathode at pH 12.5). Cathodic  $HP_{\text{exp}}$  (solid), anodic  $HP_{\text{exp}}$  (dashed) and  $HP_{\text{theo}}$  (dotted). Positive HP (proton production) correspond to the anodic chamber and negative HP (proton consumption) to the cathodic chamber.

#### 6.4.1.3 Operational problems with high current intensities

E5 was repeated using in a cell with similar characteristics to BF, but monitoring anodic and cathodic potentials to investigate the causes of the decrease of current intensity in E5 and E6. Electrode potentials should theoretically move to more negative values if the decrease in current intensity was caused by cathodic operational problems (e.g. an increase of pH at the surface of the cathode) as the cathodic concentration losses would be higher at this higher pH. On the other hand, electrode potentials should move to more positive values if the current intensity decreased as a consequence of anodic operational problems at the anode, as the anode overpotential would be higher. Figure 6.9A shows the current intensity profile as well as the electrode potential profiles of the



aforementioned experiment (applied voltage of 1.0 V, anodic pH of 7.5 and cathodic pH of 2.0). The initial potentials of the anode and the cathode were 128 mV and -750 mV vs SHE, respectively. The electrode potentials increased along the cycle and reached 730 mV (anode) and -253 mV (cathode) after 48 h. Thus, the cause of the decrease in current intensity was located in the anode. One of the possible causes of the decrease in the anodic performance could be the accumulation of protons inside the biofilm [126] at such high current intensities, which could not have been transported out of the biofilm despite the use of a high buffer concentration.

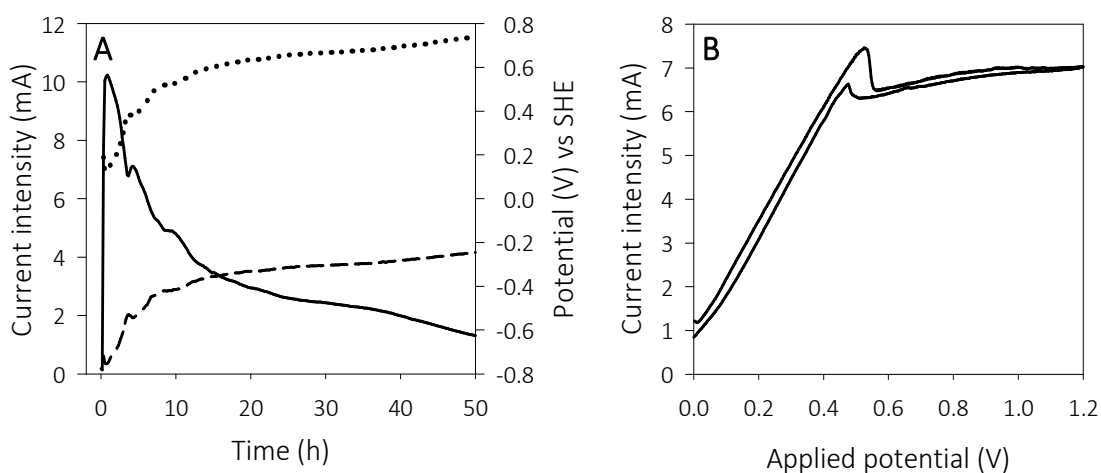
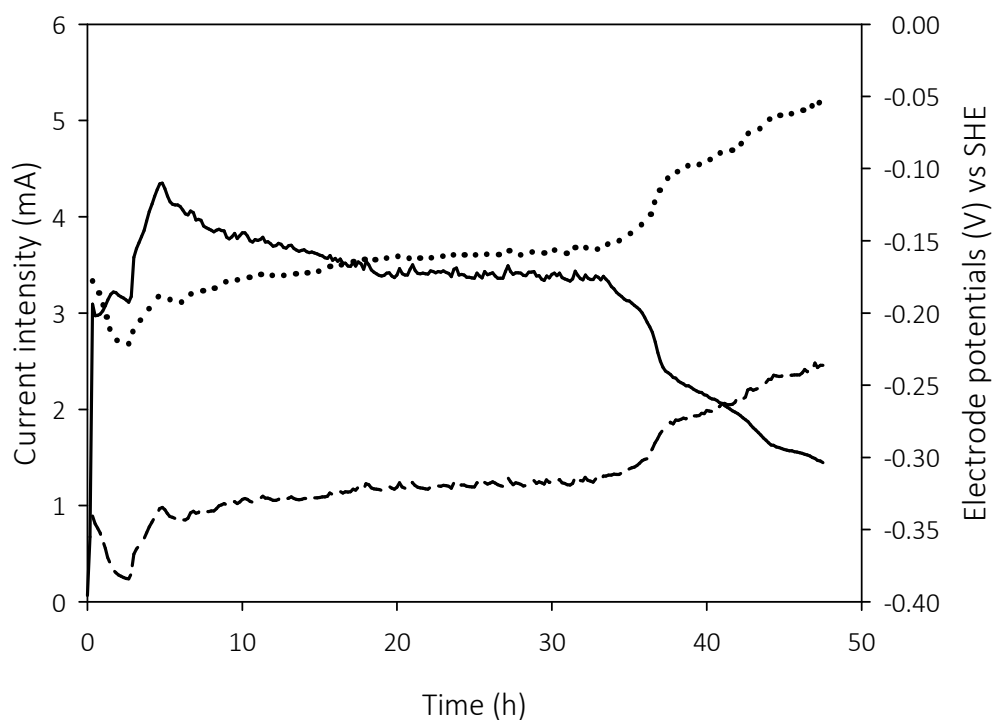


**Figure 6.9** (A) Monitoring of current intensity (solid), anode potential (dotted), and cathode potential (dashed) in a replicate of E5 with pH 7.5 in the anodic chamber and pH 2.0 in the cathodic chamber. (B) CV recorded under the same conditions as in E5.

Thus, an important outcome of this work is the experimental observation that a decreased cathodic pH improves MEC operation but could lead to practical failures. Although this study was aimed to enhance the performance of two-chamber MEC by means of pH control, alternative operational conditions with reduced applied voltage were evaluated. Figure 6.9B shows a CV performed in a cell with the anodic and cathodic pH controlled at 7.5 and 2.0, respectively. It can be seen that the application of a cell voltage of only 0.2 V led to a current intensity close to that in E3, E4 and E7, in which the stability of the MEC, in terms of microbiological activity, was ensured during a whole cycle. Thus, E8, aimed to reduce the applied potential, was performed by applying a voltage of only 0.2 V.

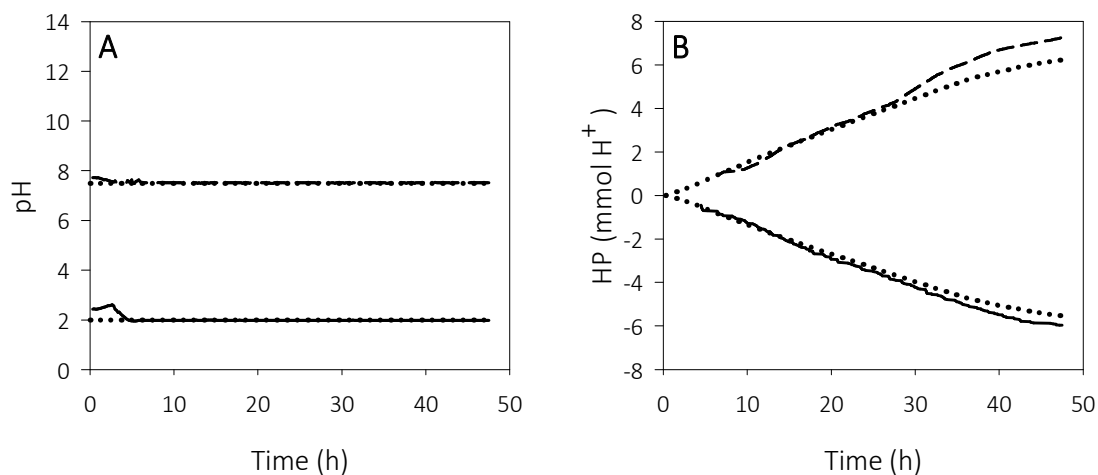
#### 6.4.1.4 Hydrogen production with very low applied voltage

Figure 6.10 shows the current intensity profile of E8. The current intensity remained between 3.5 and 4 mA during the whole batch experiment until substrate was depleted. This current intensity was only slightly lower than in E3, E4 and E7. The electrode potentials, meanwhile, did not increase as in E5 and remained fairly stable during most of the experiment.



**Figure 6.10** Current intensity (solid), cathode potential (dashed) and anode potential (dotted) of E8 with pH 7.5 in the anodic chamber and pH 2.0 in the cathodic chamber. The applied potential was 0.2 V.

Figure 6.11 displays the pH profiles of E8 and  $HP_{\text{theo}}$  and  $HP_{\text{exp}}$  when the anodic pH was maintained at 7.5 and the cathodic pH at 2.0. As in the previous experiments, the pH of both chambers was kept close to the setpoint and  $HP_{\text{theo}}$  and  $HP_{\text{exp}}$  successfully matched.



**Figure 6.11** E8 (A) pH profiles. Cathodic pH (solid), anodic pH (dashed) and setpoint (dotted) (B) Theoretical and experimental proton production. Cathodic HP<sub>exp</sub> (solid), anodic HP<sub>exp</sub> (dashed) and HP<sub>theo</sub> (dotted). Positive HP (proton production) correspond to the anodic chamber and negative HP (proton consumption) to the cathodic chamber.

Finally, both the CE and  $r_{\text{CAT}}$  were very high and reached values close to 100 %. A very significant increase was observed in the energy efficiencies, especially in those that consider the electrical energy input. Hence, taking the highest values obtained so far (E5) as reference,  $r_s$  increased from 122 % to 134 %,  $r_E$  from 162 % to 883 % and  $r_{s+E}$  from 70 % to 117 % (Figure 6.3).

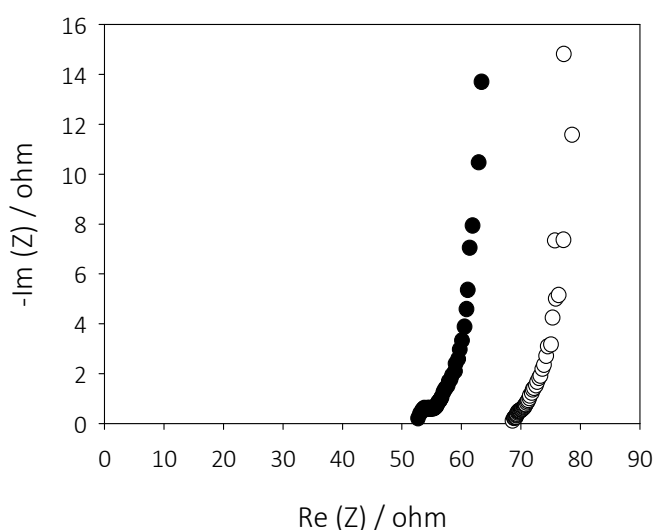
#### 6.4.1.5 Effect of conductivity on MEC performance

Finally, an additional experiment was designed to discard the relevance of the conductivity increase caused by HCl / NaOH dosages on the cell performance. The initial conductivity of the anolyte was 14 mS/cm in all experiments, whereas the conductivity of the catholyte ranged between 14-19 mS/cm, which depended on the amount of HCl or NaOH used to adjust the initial pH. During the experiments with controlled pH, the highest measured final conductivities were between 20-24 mS/cm in both the anodic and cathodic chambers.

An additional experiment with pH control at 7.5 in both chambers and an initial conductivity of 24 mS/cm was conducted (results not shown) without any significant improvement with respect to E4. Then, it was confirmed that these conductivity changes did not play a significant role in the observed performance enhancement. This was also

supported by the current intensity plateau reached in most of the experiments (E3, E4, E7 and E8). A significant effect of increasing the conductivity would have probably resulted in an increase of the current intensity throughout the batch cycle.

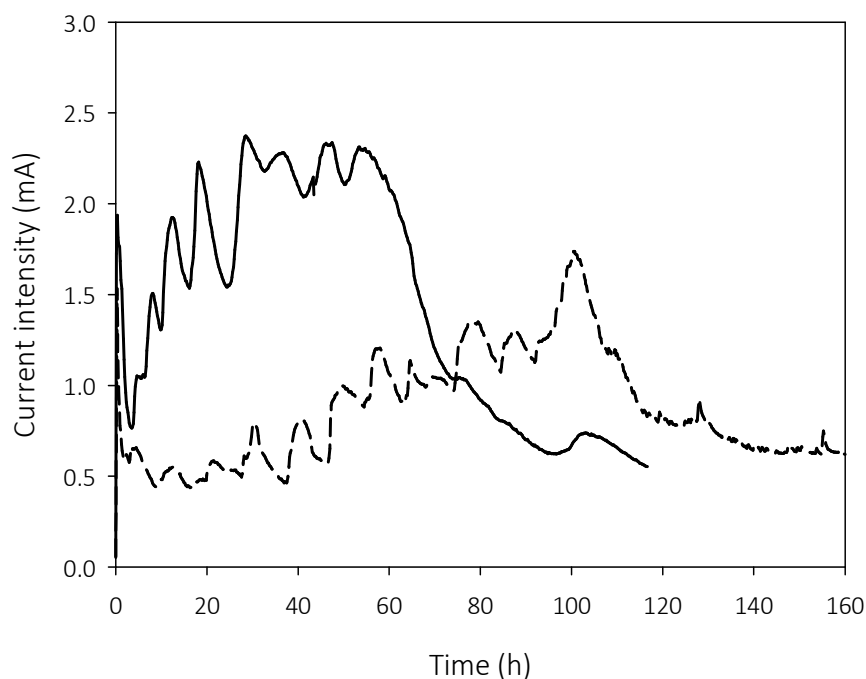
With regard to the different initial cathodic conductivities caused by the different initial cathodic pH values, impedance measurements showed that the difference in ohmic resistance with a conductivity of 14 mS/cm (pH 7.5) and 19 mS/cm (pH 12.5) was approximately 15  $\Omega$ . For usual operation at 4 mA, this would mean a potential loss of only 60 mV which was only 6 % of the total potential applied (1 V), thus it was assumed that this effect was minimal.



**Figure 6.12** Nyquist diagrams of BF with different conductivities in the cathodic chamber: 14 ms/cm (○) and 19 ms/cm (●).

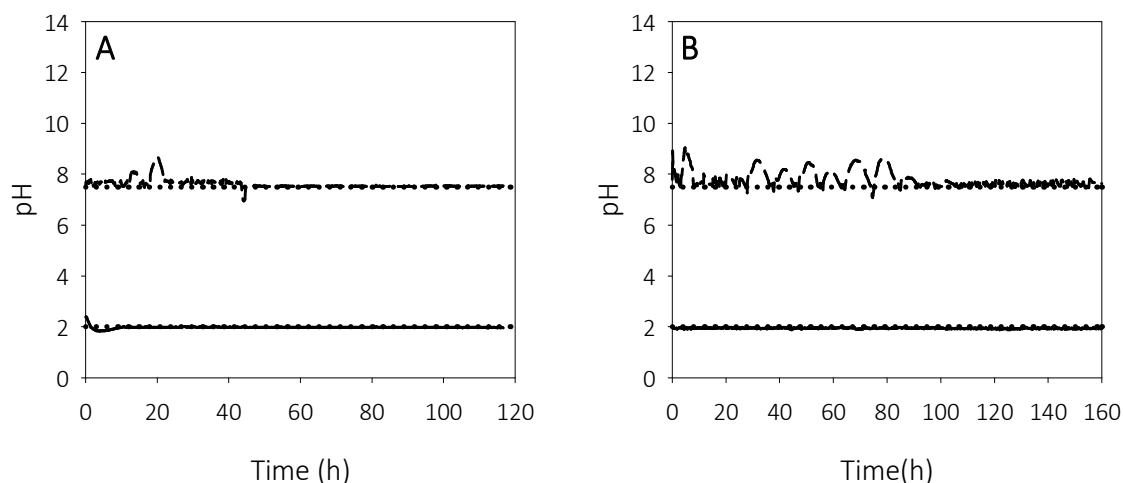
#### 6.4.2 Experiments with non-buffered medium

The pH-control approach was also implemented in the non-buffered cells with the aim of improving their performance and energy recovery. The best conditions obtained for BF scenario (anodic pH of 7.5 and low cathodic pH, i.e. 2.0) were tested in both HC (E9) and LC (E10). Again, Only 0.2 V were applied, since at these pH conditions the overall process was more favourable thermodynamically.



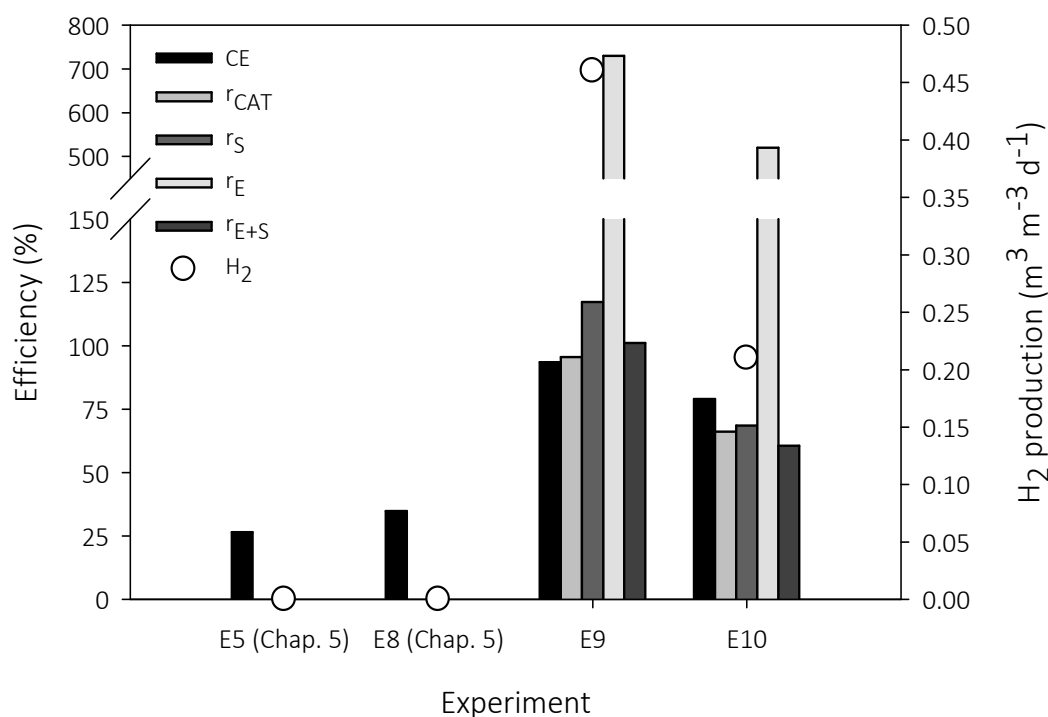
**Figure 6.13** Current intensity profiles of HC in E9 (solid) and LC in E10 (dashed). The cathodic pH was controlled at 7.5, the anodic pH at 2.0 and the applied voltage was 0.2V.

Figure 6.13 shows the current intensity profiles of E9 and E10. The pH control strategy led to successful results in the non-buffered cells: as already discussed in Chapter 5, the current intensity of HC working with an AEM was very close to 0 mA, whereas the pH control led to a current intensity higher than 2 mA. Similarly, the current intensity in LC increased more slowly, although it finally reached values close to 1.5 mA. The oscillations in current intensity for both HC and LC were probably caused by small changes in pH, since controlling the pH at a specific value with non-buffered cells was a complex task (Figure 6.14).



**Figure 6.14** pH profiles of (A) E9 and (B) E10 where the anodic pH of HC and LC was controlled at 7.5 and the cathodic pH at 2.0. The applied voltage was 0.2 V. Cathodic pH (solid), anodic pH (dashed) and setpoint (dotted).

The hydrogen production and the efficiencies in E9 and E10 are presented in Figure 6.15. For an easier comparison, the results of the analogous experiments without pH control (E5 for HC and E8 for LC) from Chapter 5 are also displayed. In E9, hydrogen production was  $0.46 \text{ m}^3\text{m}^{-3}\text{d}^{-1}$ . Both CE and  $r_{\text{CAT}}$  had values close to 100 %, leading to  $r_{\text{S}}$ ,  $r_{\text{E}}$  and  $r_{\text{E+S}}$  of 117 %, 730 % and 101 %, respectively. In E10, meanwhile, hydrogen production was  $0.21 \text{ m}^3\text{m}^{-3}\text{d}^{-1}$  and CE and  $r_{\text{CAT}}$  were 79 % and 76 %, respectively. Thus,  $r_{\text{S}}$  was 69 %,  $r_{\text{E}}$  was 520 % and  $r_{\text{E+S}}$  was 61 %. Although these values are slightly lower than the obtained in the buffered cells, these results represent a great improvement over the experiments in Chapter 5, in which the CE was very low, no hydrogen was recovered and as a result, the energy efficiencies were 0.



**Figure 6.15** Coulombic efficiency (CE), cathodic gas recovery ( $r_{CAT}$ ), energy efficiencies ( $r_S$ ,  $r_E$ ,  $r_{E+S}$ ) (bars) and hydrogen production (circles) for E9 and E10.

### 6.4.3 Assessment of the performance of cheese brine as catholyte

The addition of chemicals for pH control may not be in most cases a sustainable full-scale solution for the pH gradients across the membrane. However, the previous experiments have shown that the energy efficiency of the cells could significantly increase by maintaining the anodic pH constant (which can be achieved with a continuous mode operation, despite the lack of buffer in the medium) and by working at an acid pH at the cathode. Thereby, the use of cheese brine as an alternative catholyte was tested. Cheese brine is an effluent of the dairy industry and its high conductivity and particularly its low pH make it *a priori* an ideal catholyte for MEC.

The anodic pH was controlled at 7.5 when working with cheese brine as catholyte, since high alkalinity is required in the anodic chamber when using saline catholytes [136]. The operational procedure followed in this case was a bit different: current intensity was maintained constant throughout the experiment by working at a set anode potential instead of applying a cell voltage. In this manner, the advantages of using cheese brine on the applied cell potential requirements could be evaluated.

Figure 6.16 displays a LSV recorded in BF with the anodic pH controlled at 7.5 and cheese brine as catholyte. As observed, an anode potential of -0.2 V vs SHE was required for obtaining a current intensity of around 4 mA as in E8. Thus, this value was selected as anode potential during E11.

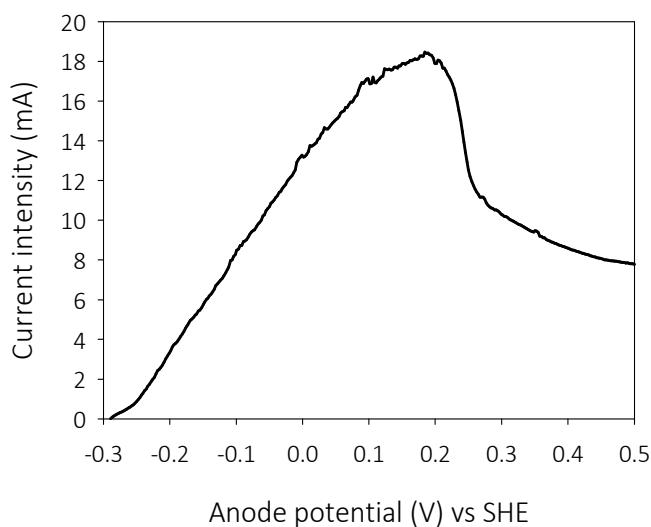


**Figure 6.16** LSV recorded in BF with the anodic pH controlled at 7.5 and cheese brine as catholyte.

Figure 6.17A shows the current intensity profile of BF in E11. The current intensity remained practically constant during the whole batch cycle as a consequence of having controlled the anodic pH. So, the performance remained practically the same for a given anode potential. The cell applied potential, however, increased from 0.48 to 0.64 V during the first hours of experiment in agreement with the pH evolution in the cathodic chamber, which increased to 12 after only 8.5 hours of experiment (Figure 6.17B). From this moment on, the pH of the cathodic chamber remained unchanged and the cell applied potential only experienced small variations as a result of minor changes in the current intensity.

The energy efficiencies of BF with cheese brine as catholyte were:  $r_S$  136 %,  $r_E$  234 and  $r_{E+S}$  86 %. Both  $r_E$  and  $r_{E+S}$  were much lower than in E8 but these results represented a great improvement over those in E4, in which the pH of both the anode and the cathode was controlled at 7.5.



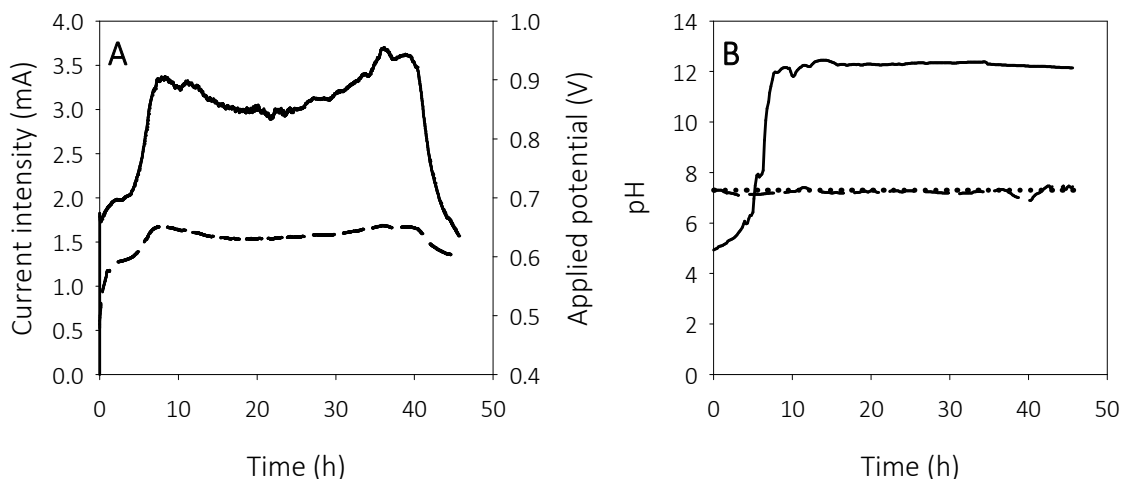


**Figure 6.17** (A) Monitoring of current intensity (solid) and cell applied potential (dashed) in E11 with pH 7.5 in the anodic chamber and cheese brine as catholyte (B) pH profiles of the experiments. Cathodic pH (solid), anodic pH (dashed) and setpoint (dotted).

The cell efficiency could even be improved by continuously circulating the catholyte and, thus, avoiding high cathodic pH variations. Moreover, the cell applied potential would remain lower by operating the cathodic chamber as a plug flow reactor (no mixing) and controlling the output pH at a near-neutral value. In this case, besides organic matter removal in the anodic chamber and hydrogen production, MEC would partially treat the cheese brine by adjusting the pH of the stream to an acceptable discharge range.

It should be noted that the high conductivity of the cheese brine would be an additional advantage over conventional catholytes in a full-scale reactor, where higher intensities would be achieved and thus, a reduction of the ohmic resistance would be a key factor. The use of a catalyst with high activity and stability in acidic environments would be also required. Currently, platinum is the best known HER catalyst, but both its scarcity and high cost limit its use for large scale applications. Among the non-noble-metal alternatives, stainless steel, nickel and nickel alloy catalysts have been proven as efficient cost-effective HER catalysts in either neutral or alkaline media [91,92,156], but they are not stable in acidic environments. Recently, the high activity of nanostructured nickel phosphide [157], cobalt phosphide [158], molybdenum sulfides [159,160] and molybdenum phosphosulfide [161] as catalysts for the HER in acidic electrolytes has been

reported, which together with this work opens up new possibilities of producing hydrogen at low applied voltages in MEC.

## 6.5 Conclusions

This work shows the possibility to obtain fairly high hydrogen production in an MEC with a very low applied potential (0.2 V) through a pH control strategy to control the anodic pH at a neutral level and the cathodic pH at an acid level. This strategy was tested with successful results in both well-buffered and non-buffered MEC.

In the case of the well-buffered MEC, hydrogen production at such low applied potential led to an increase of energy efficiency in relation to the electrical input ( $r_E$ ), the energy content of substrate ( $r_S$ ) and both the electrical input and the energy content of the substrate ( $r_{E+S}$ ) up to 883%, 135% and 117%, respectively. The intensity could have been doubled by applying a more conventional cell potential (around 1V) but it was also observed that high current intensities could be detrimental to the biological anode, which would thus reduce the effectiveness of the pH control. Moreover, when both the anodic and cathodic pH values were controlled at 7.5, hydrogen production increased by 14% when compared to a non-controlled two-chamber MEC with the same initial pHs.

The efficiencies of the non-buffered cells when applying 0.2 V were slightly lower than in the well-buffered cell, but still  $r_E$  was 730 % and 520 % for HC and LC, respectively, which opens the possibility to treat low-buffered wastewaters in two-chamber MEC.

Although pH control may not be feasible at full-scale, the outcome of this work is that MEC performance could be enhanced avoiding a large anodic pH decrease and/or when working with acid catholytes. In reference to the latter, the use of cheese brine of the dairy industry as catholyte, which had a low pH and high conductivity, was tested with positive results. Continuous feeding of this catholyte to avoid large increases in pH might further improve these results.

Furthermore, proton production was successfully described in MEC by means of titrimetry, which provided real-time information regarding substrate consumption and hydrogen production.

# CHAPTER 7

---

## Design, building and preliminary data from a novel pilot-scale microbial electrolysis cell

Part of the experiments in this chapter have been financed by the project VALTEC13-1-0140 granted by ACCIO (Generalitat de Catalunya).

**Part of the content of this chapter has been submitted to Bioelectrochemistry as:**

Ruiz, Y., Ribot-Llobet, E., Baeza, J.A. and Guisasola, A. Performance of bioelectrochemical systems after different starvation periods.



This chapter presents the design, building and preliminary tests in an MEC unit that will be part of a pilot-scale MEC to be constructed in the near future. Inoculation with anaerobic sludge by gradually increasing the applied cell potential was carried out successfully. Preliminary data from the first days of operation showed that only a small fraction of substrate was consumed for current intensity production, while some hydrogen was lost. Hence, some design modifications will be required.

The effect of starvation was also studied in this chapter. Preliminary experiments aiming at understanding the performance of an MEC when subjected to different starvation periods show that it could resist starvation up to 10 days without any significant decrease in their performance when endogenous consumption was enabled by applying an external voltage. By contrast, starvation periods longer than 5 days when the flow of electrons from the anode to the cathode was not permitted thereby avoiding endogenous consumption, led to a reversible decrease in the cell performance.

## 7.1 Introduction

Results in Chapter 4 evidenced that single-chamber MEC was not suitable for hydrogen production, since output gas will be mainly methane rather than hydrogen in the long-term. Hence, a two-chamber MEC was proposed for the scale-up from lab- to pilot-scale. Regarding the influent, the group acquired a background in parallel to this thesis on lab-scale MEC with different complex carbon sources [22] and even with real industry effluents. This expertise was summarised in the project VALTEC13-1-0140 granted by ACCIO (Generalitat de Catalunya) where a pilot-scale MEC will be constructed for energetic wastewater valorisation.

Building a pilot-scale MEC for real wastewater treatment is not a straightforward issue and there are very few studies reported. Cusick et al. [26] operated a 1000 L pilot-scale membraneless MEC with winery wastewater for 100 days. Inoculation of such a large reactor and hydrogen recovery were the two biggest challenges to face. Moreover, biogas was mainly composed of methane (up to 86 %), since under this configuration

hydrogen was consumed by hydrogenotrophic methanogens. Heidrich et al. [70] operated a 120 L pilot-scale MEC consisting of six two-chamber MEC cassettes fed with domestic wastewater for over three months. This configuration allowed recovering hydrogen rather than methane. Because of some hydrogen losses, whole energy recovery was not achieved. Nevertheless, MEC operation outperformed the activated sludge process in terms of energy requirements. Moreover, the authors claimed that, with further design improvements, energy neutral or even positive wastewater treatment could be obtained with this technology. The long-term operation of the same pilot-scale MEC was assessed for 12 months [162]. On the one side, low temperatures (1-5°C) did not show any significant effect on the biological activity of the anode. On the other side, 48.7 % of the electrical input could be recovered, while the 41.2 % of the theoretical produced hydrogen was measured. However, MEC performance deteriorated with time as a result of a build-up of inactive biomass on the anode and fouling of the membrane and wire connections.

Experiences with semi-pilot scale MEC have also been reported. Brown et al. [163] evaluated the effects of technical improvements on a 16 L scale reactor fed with filtered primary settled wastewater and treatment plant effluent amended with acetate in which a high COD removal was achieved. Escapa et al. [164] assessed the performance of two 3 L membrane-less MEC that would make up a pilot-scale MEC for domestic wastewater treatment. A high COD removal was achieved in batch operation but not in continuous mode. Moreover, the authors had to deal with hydrogen recycling and an inefficient cell design, which caused insufficient mixing, dead zones and preferable flow paths. Parameters such as applied voltage, hydraulic retention time and organic loading rate were also studied and optimized in a tubular MEC in view of the scale-up of the process [165,166].

All these works showed that MEC may become a viable technology for wastewater treatment but further efforts are needed to implement MEC at full-scale. When dealing with biological processes, one has to be aware of the need of maintaining bacterial activity. In this frame, starvation periods (i.e. periods in absence of substrate) may occur often in real systems due to technical plant stops and, therefore, in view of the scaling-up it will be very important to know i) how detrimental will be this period to the biomass

activity and ii) which are the best conditions for biomass maintenance in case starvation is unavoidable.

To the best of our knowledge, there is little information about starvation in both MFC and MEC. Oh and Logan [167] studied the relationship between starvation and voltage reversal in two MFC stacked together and concluded that starvation periods up to 25 hours were detrimental for the MFC performance. In contrast, Kaur et al. [168] evaluated starvation as strategy to avoid electron losses derived from methanogenesis and the results suggested that 12 days of starvation were not excessively harmful for ARB in MFC. Gao et al. [169] studied the syntrophy between biopolymer-accumulating bacteria and ARB both in MFC and MEC, which allowed current generation without the addition of an external substrate for several days. Moreover, the system recovered the initial current generation when external substrate was added.

## 7.2 Objectives

The aim of this chapter is to conduct the first tests with an MEC prototype based on the cassette configuration, the basis of a pilot-scale MEC (PS-MEC). This first MEC prototype will be fed with synthetic wastewater during start up and discontinuous operation providing useful information for the pilot-plant to be constructed in the near future. Moreover, some studies will be conducted at lab scale to shed light on MEC starvation processes under different operating conditions, which will be very useful when working with the PS-MEC. The application or not of an electrical voltage was studied in order to know which condition was better to maintain ARB activity and where was the limit of starvation time for each case.

## 7.3 Materials and Methods

### 7.3.1 Reactors description and medium composition

For the start-up of the pilot-scale MEC (PS-MEC) prototype, the usual culture medium mixed with anaerobic sludge was used. Under daily operation, the medium was used alone with acetate and glucose as substrate. The catholyte was a saline solution which was not renewed throughout the experiments. The applied cell potential was gradually increased during the inoculation period.

For starvation experiments, two small-scale MEC (SS-MEC) were used (see Materials and Methods in Chapter 3). MEC worked for 15 days under pseudo steady-state conditions prior to the experiments. Under feast conditions, MEC had a constant applied voltage of 0.8 V and an initial acetate concentration of 1.5 g/L. A 50 mM 2-bromoethanesulfonate concentration was used to selectively inhibit methanogenic activity. Starvation tests in MEC included tests with applied voltage ( $MEC_{AV}$ ) and without it ( $MEC_{WV}$ ). During the starvation periods in  $MEC_{WV}$ , the experimental setup remained unchanged but the power supply was disconnected. Cells were filled with medium without acetate at the end of a batch cycle and before each starvation period to ensure fully starvation conditions. The medium was replaced with fresh medium with substrate after each starvation period. Cycles after starvation periods were monitored to evaluate the potential detrimental effects of each starvation period on the cell performance. MEC were sparged with nitrogen for 10 minutes after replacing the medium to guarantee anaerobic conditions.

### 7.3.2 Batch experiments

The experimental monitored data in the experiments with PS-MEC prototype comprised acetate and glucose concentration, hydrogen production, current intensity, anodic potential and pH monitoring. Regarding the starvation experiments, current intensity was monitored and acetate and hydrogen were analysed (see Materials and Methods in Chapter 3).

## 7.4 Results and Discussion

### 7.4.1 Reactor design

The PS-MEC under development was a two-chamber MEC derived from the cassette configuration presented in Heidrich et al. [70]. The preliminary experiments were conducted with only one cassette as a prototype of the full pilot plant, which will be constructed in the near future.

The cassette (Figure 7.1) consisted of a central PVC frame (3 cm length x 36 cm width x 46 cm height) with an internal cathode section of 3.7 L. The cathode was pressed stainless steel wool inside this section. A titanium wire was wound into the stainless steel wool and then brought to outside for its electrical connection. The central frame was provided with



an olive fitting at the top, where a 0.5 L gas sample bag with a twist type valve (Cali-5-Bond, Ritter) was connected by means of a flexible PTFE tube and with two additional ports, which allowed the catholyte circulation if required.

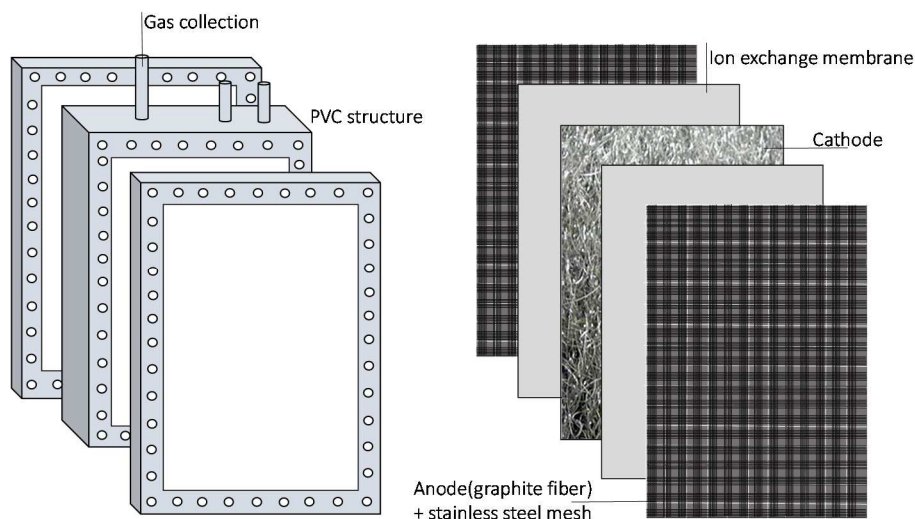


**Figure 7.1** Schematic diagram of the MEC prototype.

The cathode was separated from the anodes using an AEM on both sides (AMI-7001, Membranes International INC). The anodes consisted of a stainless steel mesh (used as current collector) wrapped with graphite fibers (fibers of 7.2  $\mu\text{m}$  diameter; PANEX<sup>®</sup>33 160 K, ZOLTEK) thermally treated to enhance biomass adhesion. As before, titanium wires were wound into the stainless steel mesh and then brought to outside for its electrical connection. The anodes were placed next to the membranes on both sides of the cathode. Both the membranes and the anodes were sandwiched between the central frame and a lateral PVC frame (1 cm length x 36 cm width x 46 cm height). Pieces were kept together by tightening wing nuts onto bolts through five mm holes in the PVC frames. The first tests with the prototype were conducted by placing the cassette in a reservoir of 40 litres, where culture medium was added in batch mode. The anodes, in the outermost layer of the cassette, were in contact with the medium, so that ARB could consume the substrate. An Ag/AgCl reference electrode (+210 mV vs SHE, Crison reference electrode 5240) was used to monitor the anode potential and a pH probe (Crison pH electrode 5233) to monitor the anodic pH.

Porexpan balls were placed in the uppermost layer of the reactor to reduce entry of atmospheric oxygen. Moreover, periodic nitrogen sparging (10 seconds every 3 minutes) was conducted by means of a circular diffuser placed at the bottom of the reservoir, which ensured removal of dissolved oxygen and good mixing. Nitrogen sparging periods were programmed in Labwindows CVI 2014, which sent the signal to an electrovalve connected to the system. The nitrogen flow rate supplied was not monitored.

The PS-MEC to be constructed will consist of 10 cassettes placed vertically in a stainless steel tank. Wastewater will circulate through the cell in an S-like flow as in [70].

This design was the result of some modifications made in a preliminary prototype, in which corrosion problems evolved due to electrical contact between the stainless steel mesh used as current collector and the bolts used to maintain all pieces together. Evidence of corrosion was observed from day 6 of operation (Figure 7.2), when the cell operated with an applied voltage of 0.8 V and a sudden increase in current intensity to values close to 60 mA occurred. This increase was independent from substrate oxidation since there had not been sufficient time for biofilm development. Moreover, the anode potential decreased to a value more negative despite the higher current intensity, indicating that a different reaction was occurring.

Once the problem was fixed by avoiding contact between the current collector and the bolts, additional tests were conducted to ensure that current intensity would be produced only as a result of substrate oxidation. Hence, when substrate was not added, current intensity remained at very low values (results not shown).

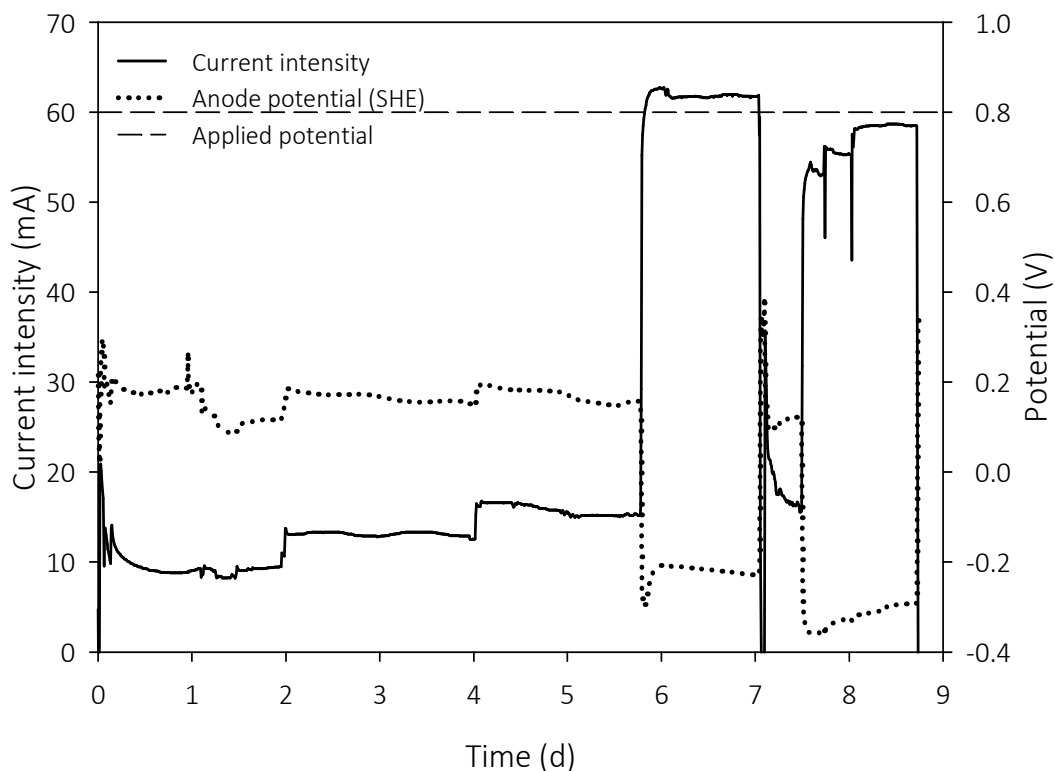


**Figure 7.2** Current intensity, anode potential and applied potential before cell design modifications in the preliminary prototype.

#### 7.4.2 Reactor inoculation with anaerobic sludge

Anaerobic sludge was used as inoculum for the PS-MEC since, as stated in Materials and Methods in Chapter 3, it is easily available and contains electrochemically active strains of bacteria [93]. Moreover, there was no reactor with an ARB-enriched biomass capable of providing the sufficient amount of inoculum. Culture medium was mixed with 3.5 L of anaerobic sludge and the cell was placed horizontally in the reservoir to enhance biomass adhesion. Figure 7.3 shows the PS-MEC performance during the inoculation period (cycles 1-3). The cell applied potential was gradually increased as in Heidrich et al. [70] to ensure that the anodic potential did not reach values higher than 0.20 V vs SHE, since very positive anodic potentials were reported as unfavourable conditions for biomass growth [170].

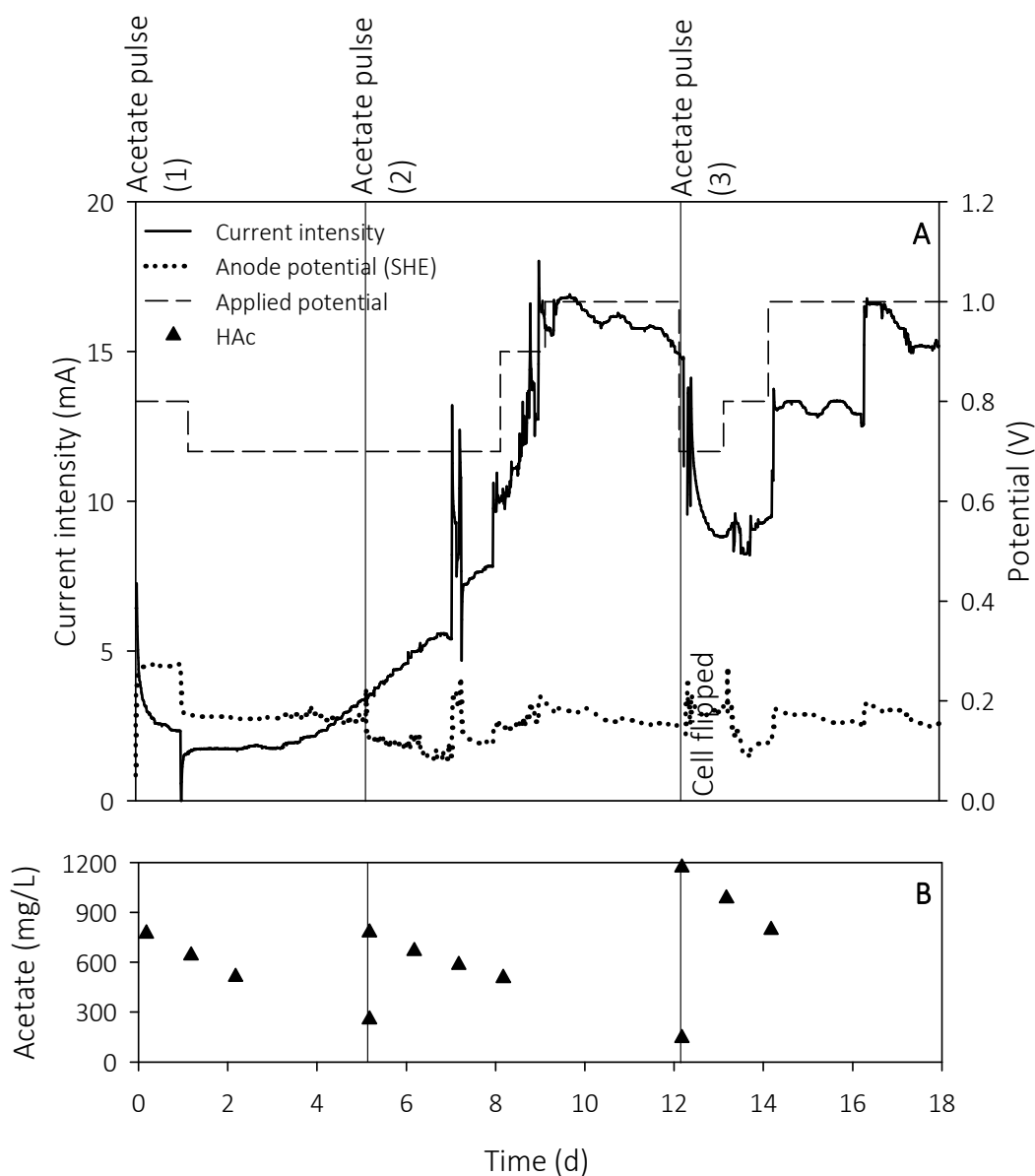


**Figure 7.3** (A) Current intensity, anode potential, applied potential and (B) acetate concentration profiles during inoculation of MEC with anaerobic sludge, cycles 1-3.

The initial applied cell potential was 0.8 V. However, on day 1 it was lowered to 0.7 V to decrease the anode potential. From day 1 to 8 the current intensity increased from 1.5 to 8 mA and at the same time the anode potential decreased from 0.17 to 0.12 V vs SHE, indicating a decrease in the anode overpotential, and thus that the anode was being inoculated. At day 8, the applied voltage was increased to 0.9 V and, one day later, to 1.0 V, reaching a current intensity close to 17 mA. The anode potential, meanwhile, followed a downward trend. On day 12, the reactor was turned over to promote inoculation of the anode on the reverse side. A decrease in current intensity was then observed, probably

due to air-exposition while turning over the cell. The applied potential was decreased again to 0.7 V and then gradually increased to 1.0 V. On day 16, a current intensity of 17 mA was again achieved. The pH inside the reservoir (which operated as anodic chamber) did not decrease despite being working in two-chamber configuration, as a result of both a large liquid volume and buffer addition. Moreover, it slightly increased during some periods probably due to carbon dioxide stripping by nitrogen sparging. During this first inoculation process no hydrogen was detected in the gas bag.

**Table 7.1** Summary of the efficiencies in batch cycles 1 to 10.

Batch cycle	Days	CE (%)	H <sub>2</sub> (m <sup>3</sup> m <sup>-3</sup> d <sup>-1</sup> )	r <sub>CAT</sub> (%)	r <sub>E</sub> (%)	r <sub>E+S</sub> (%)
1	0-5	0.12	0	0	0	0
2	5-12	2.1	0	0	0	0
3	12-18	--	0	0	0	0
4	18-28	4.5	0	0	0	0
5	28-39	6.9	0	0	0	0
6	39-54	10	0.003	31	54	4
7	54-64	19	0.005	49	72	8
8	64-76	11	0.003	22	37	3
9	76-93	23	0.001	10	15	2
10	93-109	14	0.006	55	85	9

Table 7.1 shows the results of each batch cycle in terms of CE, r<sub>CAT</sub>, r<sub>E</sub>, r<sub>E+S</sub> and hydrogen production. During the first three cycles, the CE was only 0.12 and 2 % (for the third batch cycle it could not be calculated) indicating that practically all substrate was consumed by microorganisms other than ARB. Oxygen could have diffused into the anodic chamber in spite of the periodical nitrogen sparging and the insulation layer of porexpan balls, thus promoting aerobic COD consumption. In fact, the presence of a biofilm in the uppermost layer of water was visually detected. Moreover, acetate consumption by acetoclastic methanogens must have played a very important role, since anaerobic sludge was mixed

with the culture medium and chemical inhibitors to suppress methanogenic activity were not used. However, methane production could not be measured in the anodic chamber due to configuration restrictions. The energy efficiency ( $r_E$  and  $r_{E+S}$ ) was 0, since no hydrogen was recovered at all.

### 7.4.3 Reactor operation with acetate as substrate

Figure 7.4 displays the MEC performance from days 18 to 64 (cycles 4-7), once anaerobic sludge was removed and the cell was placed vertically. After medium renewal on day 18 the current intensity decreased to 10 mA, although it followed an upward trend. The anode potential followed the opposite trend as expected for an anode, which is still being inoculated. The applied potential was kept at 1.0 V.

On day 32, hydrogen was measured for the first time, although in very low quantities. Seven days later, the medium was again renewed and the applied voltage was increased to 1.5 V, since the anode potential had been remaining low. From this moment onwards, the current intensity increased to a value between 50 and 60 mA and a plateau was achieved. The anode potential remained at a value close to -0.2 V vs SHE, which suggested good anode performance.

This was the first cycle in which the anode was considered to be inoculated. Then, the start-up of the cell lasted about 39 days, a period quite similar to that reported for a pilot-scale MEC [26,70]. In these other studies, the start-up was reported to be a key step in the MEC performance and was carried out from winery wastewater and domestic wastewater. However, in both cases wastewater was amended with acetate due to low COD values and, in Cusick et al. [26] the addition of buffer to maintain the pH above 6 as well as controlling the temperature at 31°C were also required. Operation was moved to continuous mode after 20-30 days in both studies. Thus, the use of anaerobic sludge seemed a good strategy for the whole plant inoculation. Moreover, transfer from this reactor could be also a good option to reduce the start-up when inoculating the whole plant.

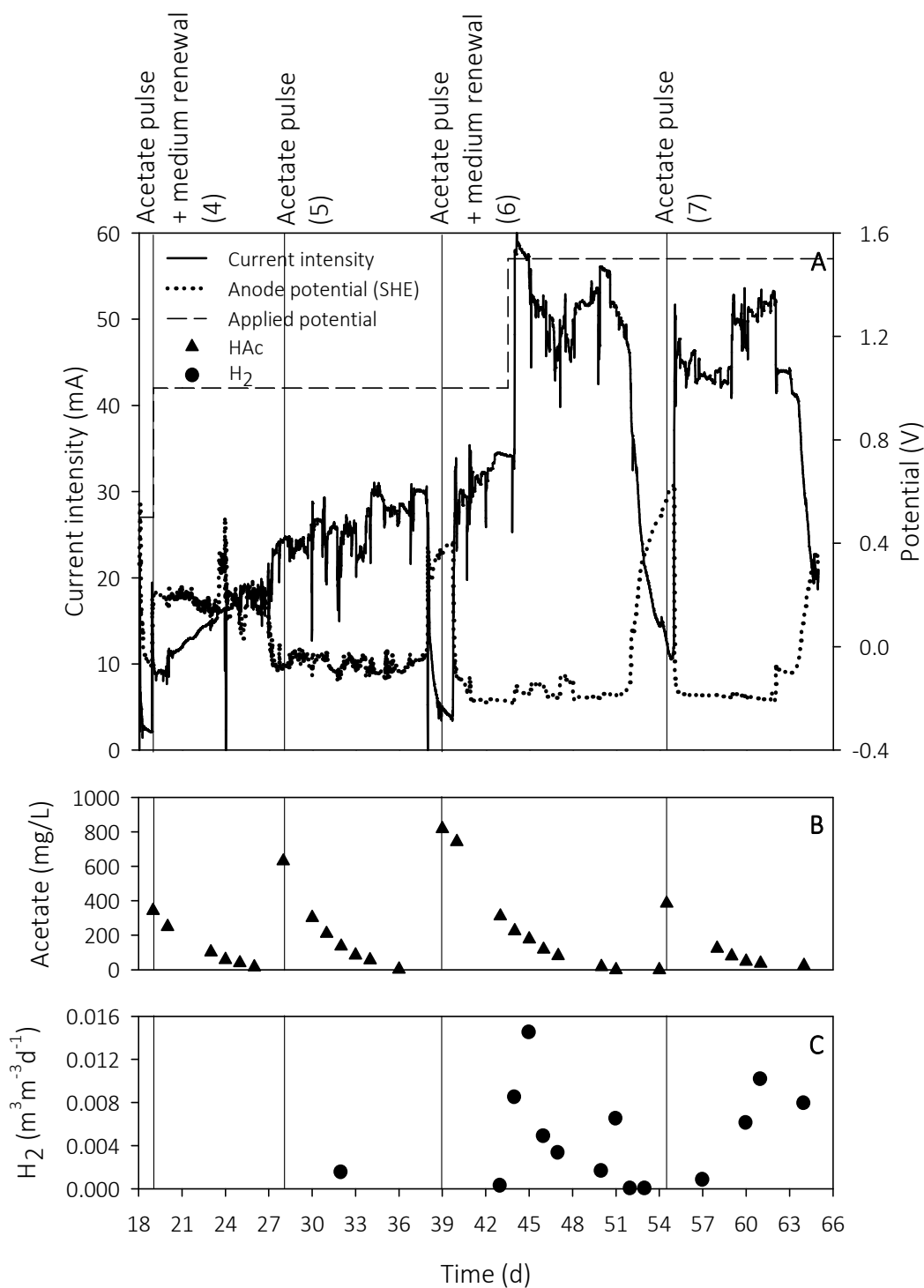


**Figure 7.4** (A) Current intensity, anode potential, applied potential, (B) acetate concentration and (C) hydrogen production rate profiles of MEC with acetate with substrate, cycles 4-7.

During the two last cycles (6 and 7) hydrogen could be regularly measured, although hydrogen production rate was highly variable. A peak could be observed on day 45, when  $0.014 \text{ m}^3\text{m}^{-3}\text{d}^{-1}$  were produced. Measuring variable hydrogen production rates could be attributed to hydrogen leakages or some hydrogen trapped in the stainless steel wool. Previous lab scale experiment showed that hydrogen bubbles were easily got trapped in the stainless steel wool, thus preventing its recovery in the gas bag. The average hydrogen production rate was  $0.003 \text{ m}^3\text{m}^{-3}\text{d}^{-1}$  and  $0.005 \text{ m}^3\text{m}^{-3}\text{d}^{-1}$  for cycles 6 and 7, respectively, which corresponded to a  $r_{\text{CAT}}$  of 31 and 49 % (Table 7.1). The CE, meanwhile, followed an increasing trend from 4.5 % to 19 %, probably as a result of the anodic enrichment with ARB.

The value of  $r_{\text{E}}$  with such a hydrogen recovery was 0 % for cycles 4 and 5 and 54 % and 72 % for cycles 6 and 7, respectively. In the case of  $r_{\text{E+S}}$ , the results were much lower: 0 % for cycles 4 and 5, 4 % for cycle 6 and 8 % for cycle 7, which indicated that only very little energy from that contained in the wastewater was recovered as hydrogen. If all hydrogen according to the measured current intensity had been recovered, the average hydrogen production rate would have been  $0.009 \text{ m}^3\text{m}^{-3}\text{d}^{-1}$  and  $0.011 \text{ m}^3\text{m}^{-3}\text{d}^{-1}$  in cycles 6 and 7, respectively, resulting in values of  $r_{\text{E}}$  and  $r_{\text{E+S}}$  of 172 % and 13 % for cycle 6 and 155 % and 17 % for cycle 7. These results suggested that the electrical energy invested in hydrogen production could be recovered with a better hydrogen collection system, but still, only a little fraction of the energy contained in the substrate would have been recovered.

Current intensity in this reactor was much lower than expected from mere extrapolation of the lab-scale results. In a lab-scale two-chamber MEC of 60 mL with a cathodic surface area of  $7 \text{ cm}^2$  and an applied voltage of 1.0 V, an initial current intensity of 4.5 mA was achieved (Experiment E2 in Chapter 5). Thus, extrapolation of this value for a reactor volume of 40 L and a cathodic surface area (projected area) of  $2310 \text{ cm}^2$  resulted in a current intensity of 3000 mA and 1485 mA, respectively. The cathodic surface area has been used rather than the anodic one, because of the overpotentials in the cathode being higher than in the anode. However, it has to be noted that a Pt-based cathode was used in lab-scale cells and that large reactors entail higher overpotentials.



#### 7.4.4 Reactor operation with glucose as substrate

From day 64 to 100 (cycles 8-10), PS-MEC was fed with glucose to conduct tests with a carbon source more complex than acetate (Figure 7.5). Glucose consumption has been reported to occur either by direct anodic oxidation by pure cultures [13] (reaction 1 in Table 7.2) or by fermenters by producing reduced byproducts such as hydrogen, lactate, ethanol, acetate, propionate, and butyrate [171] (reactions 2-6 in Table 7.2).

**Table 7.2** Glucose consumption pathways in bioelectrochemical systems [171].

Reaction	Stoichiometry
1. Glucose oxidation	Glucose + 6H <sub>2</sub> O → 6CO <sub>2</sub> + 24H <sup>+</sup> + 24e <sup>-</sup>
2. Homolactic fermentation	Glucose → 2lactate <sup>-</sup> + 2H <sup>+</sup>
3. Alcoholic fermentation	Glucose → 2ethanol + 2CO <sub>2</sub>
4. Acetogenesis fermentation	Glucose + 2H <sub>2</sub> O → 2acetate <sup>-</sup> + 2CO <sub>2</sub> + 4H <sub>2</sub> + 2H <sup>+</sup>
5. Mixed acid fermentation	Glucose → acetate <sup>-</sup> + propionate <sup>-</sup> + CO <sub>2</sub> + H <sub>2</sub> + 2H <sup>+</sup>
6. Butyric fermentation	Glucose → butyrate <sup>-</sup> + 2CO <sub>2</sub> + 2H <sub>2</sub> + H <sup>+</sup>

In cycle 8, the medium was renewed and PS-MEC was fed with both acetate and glucose. Moreover, PBS concentration was halved to move gradually from the ideal lab conditions to a more realistic situation. In the two following cycles, PS-MEC was only fed with glucose and, as observed, it was consumed in the first days of the batch cycle, while acetate concentration experienced an initial increase due to glucose degradation and a subsequent decrease due to its consumption by ARB. According to these results, acetogenesis (reaction 4 in Table 7.2) was the fermentation pathway more likely to occur as acetate was the only by-product accumulated in the reactor. Both the open reactor and regular nitrogen sparging could have probably prevented current intensity generation from fermentative hydrogen oxidation.

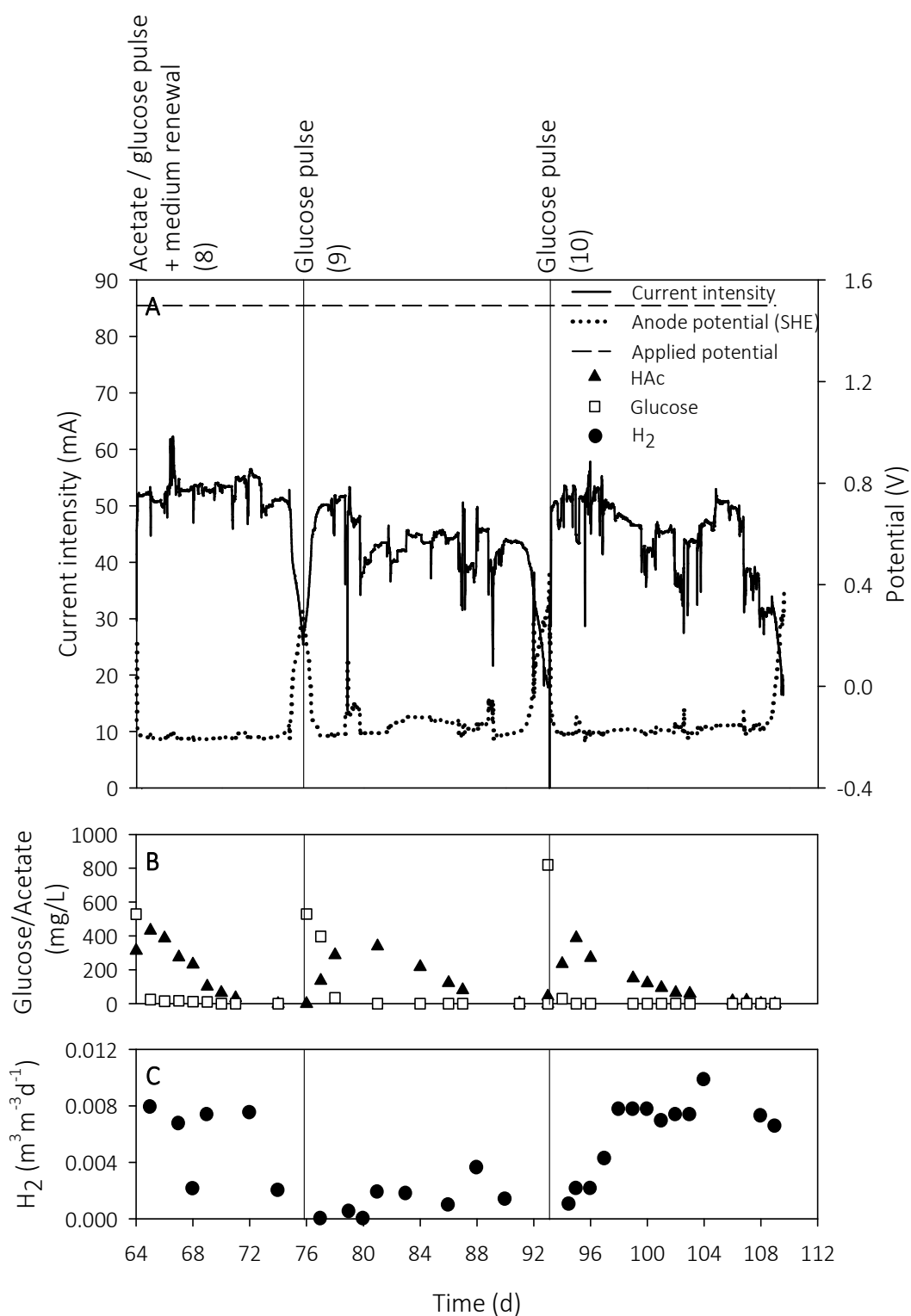


**Figure 7.5** (A) Current intensity, anode potential, applied potential, (B) acetate and glucose concentration and (C) hydrogen production rate profiles of MEC after changing the carbon source, cycles 8-10.

The predominance of acetogenesis was numerically assessed by means of mass and electron balances for cycle 10. A theoretical acetate concentration was calculated from the total initial amount of glucose at day 93 (32.8 g at 0.82 g/L) by considering the stoichiometry of reaction 4 in Table 7.2 (equation 7.1).

$$C_{Ac^-}^{th} = \frac{C_{glucose}}{M_{glucose}} \cdot 2 \cdot M_{Ac^-} \quad (7.1)$$

where  $C_{Ac^-}^{th}$  (mg L<sup>-1</sup>) is the theoretical acetate concentration resulting from the fermentation of glucose,  $C_{glucose}$  (mg L<sup>-1</sup>) is the initial glucose concentration and  $M_{glucose}$  and  $M_{acetate}$  are the molecular weight of glucose (180.1 g L<sup>-1</sup>) and acetate (59 g L<sup>-1</sup>), respectively.

This value was then compared to the maximum acetate concentration measured on day 95 (0.39 mg L<sup>-1</sup>). However, previously,  $C_{Ac^-}^{th}$  was corrected by taking into account the fraction of acetate consumed by ARB for current generation and microorganisms other than ARB from days 93 to 95 (equation 7.2). For the calculation of the acetate consumed by aerobic bacteria or methanogens, the CE of cycle 7 was used as reference.

$$C_{Ac^-}^{th'} = C_{Ac^-}^{th} - \left( \frac{\int_{t_0}^{t_F} I dt M_{Ac^-}}{F b_{Ac^-} V_L} \cdot \frac{100}{CE_7} \right) \quad (7.2)$$

where  $C_{Ac^-}^{th'}$  (mg L<sup>-1</sup>) is the corrected theoretical acetate concentration,  $t_0$  and  $t_F$  are days 93 and 95, respectively,  $b_{Ac^-}$  is the number of e<sup>-</sup> transferred per mole of acetate (8 mols e<sup>-</sup> mol<sup>-1</sup>Ac<sup>-</sup>),  $V_L$  is the volume of liquid in the reactor (40 L) and  $CE_7$  is the coulombic efficiency of the batch cycle 7 (19 %).

$$\% \text{ Error} = \frac{C_{Ac^-}^{th'} - C_{Ac^-}^{exp}}{C_{Ac^-}^{th'}} \cdot 100 \quad (7.3)$$

where  $C_{Ac^-}^{exp}$  (mg L<sup>-1</sup>) is the experimentally measured acetate concentration on day 95. The results obtained from equation 7.3 show an error lower than 15 %, that is a relative low value both considering that a fraction of glucose may have been used for biomass growth and the CE was taken from another batch cycle. Therefore, numerical calculations supports that only acetogenesis was occurring in the reactor.

Current intensity remained at values between 50-60 mA, as in those cycles with acetate as substrate. The anode potential, which was -0.2 V vs SHE during the current intensity plateaus, also shown a similar trend to that observed with acetate. CE ranged between 12 and 23 % in cycles 8-10, whereas  $r_{\text{CAT}}$  between 10 and 55 %, since high variability in hydrogen production rate was again observed, although in cycle 10 it seemed to finally stabilize. The average hydrogen production was 0.003, 0.001 and 0.006  $\text{m}^3\text{m}^{-3}\text{d}^{-1}$  for cycles 8, 9 and 10, respectively (Table 7.1). As a consequence of the different hydrogen recoveries, the energy efficiencies took very different values from one cycle to the other. The highest values were obtained in cycle 10, in which 85 % of the energy invested in hydrogen production ( $r_E$ ) could be recovered as hydrogen, although  $r_{E+S}$  was still far from desirable values (9 %). In the case hydrogen had completely been recovered, the average hydrogen production rate would have been 0.014  $\text{m}^3\text{m}^{-3}\text{d}^{-1}$  for cycle 8 and 0.012  $\text{m}^3\text{m}^{-3}\text{d}^{-1}$  for cycles 9 and 10. The values of  $r_E$  would have ranged between 151 and 168 %, which are fairly good results taking into account the reactor size.

#### 7.4.5 Comparison with other works

Table 7.3 compares the results obtained in this work with the results reported on similar studies. This study is the only one conducted with synthetic wastewater, since these were the first tests with this configuration. Similarly, reactor operation in all other studies was moved to continuous mode after a period in batch mode. However, this comparison will allow drawing conclusions despite the operational differences. First, it draws attention that the applied voltage in this work was the highest one and was even above the theoretical standard potential for water electrolysis. Current intensity was monitored through the measurement of the voltage across an external resistance of 12  $\Omega$ , so, in those cycles with a current intensity around 50 mA, the potential difference between the anode and the cathode was only 0.9 V, which was similar to the other values in Table 7.3. A resistor of 0.01  $\Omega$  was used in Cusick et al. [26] and of 0.1  $\Omega$  in both Heidrich et al. [70,162], thus minimizing voltage losses across the resistor. A lower external resistance must be used for monitoring of the current intensity in following tests to avoid differences between the formal and the real applied potential.

CE in this study was higher than that in Heidrich et al. [162], probably due to more complex carbon sources in this latter. In contrast, the average CE was higher in Heidrich et al. [70] than in this work. In that study, the pilot-plant operated for 3 months and the plant had probably a more optimized ratio between reactor volume and electrode surface. In fact, in our study batch cycles were very long and in some cases they lasted up to 17 days, which could have promoted substrate consumption by microorganisms other than ARB. Thus, a more appropriate design regarding the ratio between reactor volume and electrode surface will be required when constructing the whole plant. This would affect the anode pH, which could no longer be maintained and would decrease. However, continuous flow circulation of wastewater would soften the pH drop.

CE was also higher in Escapa et al. [164] and Gil-Carrera et al. [166], but in both cases problems related to hydrogen recycling were observed.

The average  $r_{\text{CAT}}$  was low in this study, since as previously stated some hydrogen was trapped in the stainless steel wool. Some design modifications will be required for improvements in this area. However,  $r_{\text{CAT}}$  was even lower in Escapa et al. [164] both in batch and continuous operation mostly due to the hydrogen recycling phenomenon, which evidenced that the use of membranes to separate the anode and the cathode are essential for producing hydrogen in MEC.

The highest hydrogen production rates were measured in single-chamber MEC [26,166], since potential losses in this configuration are lower. However, in Cusick et al. [26] part of the hydrogen was produced from sugar fermentation and in the long-term hydrogen was consumed by hydrogenotrophic methanogens.

**Table 7.3** Comparison of this work with other studies dealing with pilot-scale or semi-pilot MEC

Study	Operation mode	Carbon source	Reactor volume (L)	Applied voltage (V)	CE (%)	$r_{\text{CAT}}$ (%)	$\text{H}_2$ ( $\text{m}^3 \text{m}^{-3} \text{d}^{-1}$ )
Cusick et al. [26]	Continuous	winery WW	1000	0.9	--	--	0.07
Heidrich et al. [70]	Continuous	domestic WW	120	1.1	29 <sup>1</sup>	55	0.015
Heidrich et al. [162]	Continuous	domestic WW	120	1.1	3.9 <sup>1</sup>	41.2	0.005-0.009
Escapa et al. [164]	Batch/ continuous	domestic WW	3	0.7	> 100	7.5 / 0 <sup>2</sup>	0.01 / 0 <sup>2</sup>
Gil-Carrera et al. [166] <sup>3</sup>	Continuous	domestic WW	2+2	1.0	10.6 / 44.8	24.3 / 54.7	0.045
This study <sup>4</sup>	Batch	glucose	40	1.5	16	29	0.004

<sup>1</sup> CE has been calculated from the data presented in the specific publication.

<sup>2</sup> Parameters have been calculated as the average of the set of *data* presented in the specific publication.

<sup>3</sup> The study was conducted with two reactors hydraulically connected in series. CE and  $r_{\text{CAT}}$  values are presented for both reactors separately.

<sup>4</sup> Average values in those batch cycles with glucose as substrate.

#### 7.4.6 Performance of MEC after different starvation periods

The effect of starvation processes in MEC was studied in parallel to the pilot-plant build-up. Starvation processes can occur in real systems due to technical stops. Therefore, it is interesting to study the resistance of ARB to starvation periods in view of the scaling-up of this technology.

The effect of starvation periods was tested in MEC aiming at hydrogen production following two different strategies: (i) maintaining an applied voltage of 0.8 V ( $\text{MEC}_{\text{AV}}$ ) and (ii) without any applied voltage ( $\text{MEC}_{\text{WV}}$ ) during the starvation periods. The experimental current intensity and anode potential profiles during starvation tests in  $\text{MEC}_{\text{AV}}$  are shown in Figure 7.6.

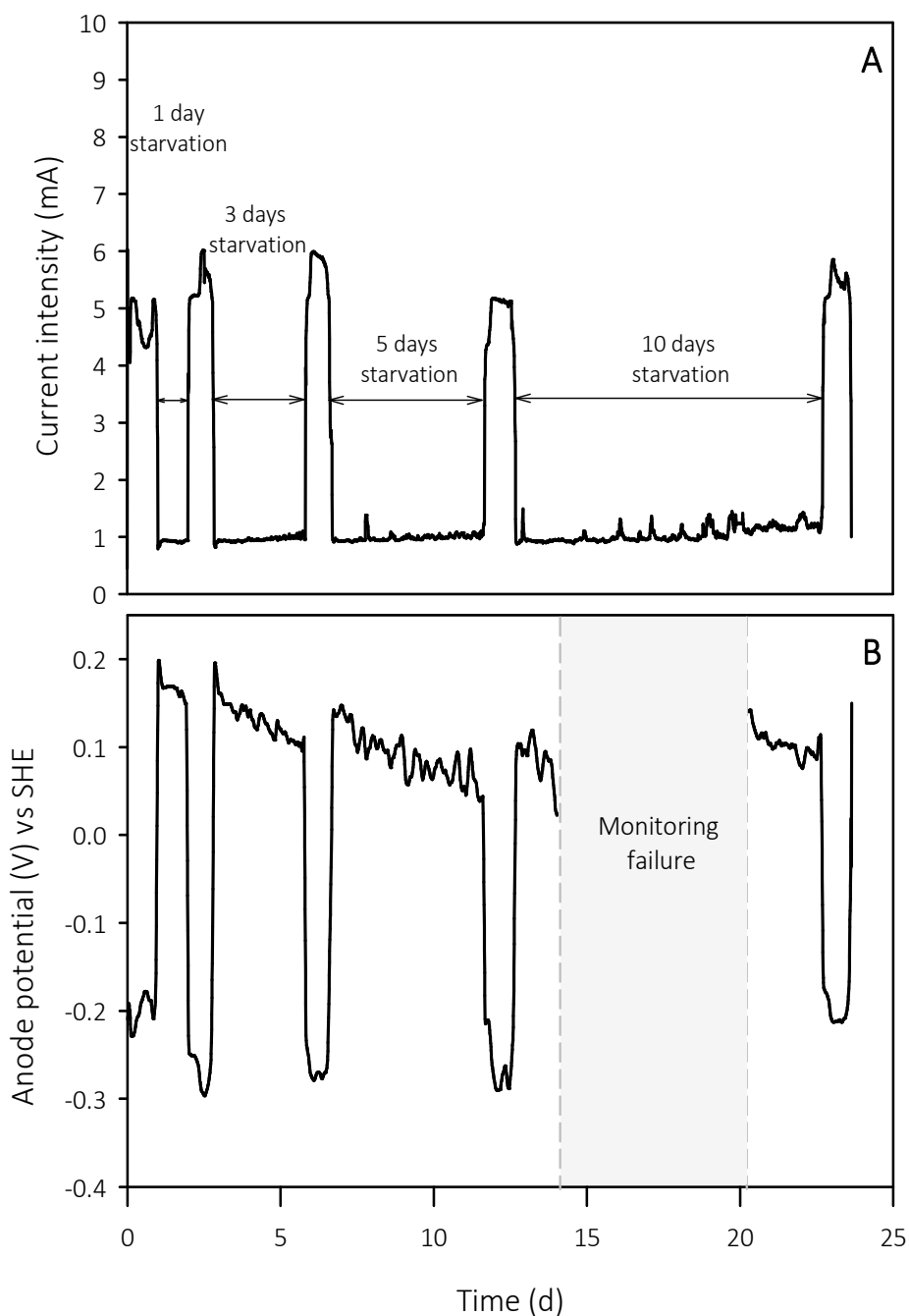


**Figure 7.6** Evaluating starvation in MEC with an applied voltage of 0.8 V ( $MEC_{AV}$ ) (A) Current intensity and (B) anode potential. Note that from days 14 to 20 the anode potential could not be monitored.

The cell performance remained practically constant even after a starvation period of 10 days, since the maximum current intensity was very similar after 1, 3, 5 and 10 days of starvation (ranging between 5 and 6 mA). Moreover, during the starvation periods, the current intensity remained positive indicating that electrons were flowing from the anode

to the cathode regardless of the lack of substrate in the medium. The anode potential had a value between  $-0.20$  and  $-0.28$  V vs SHE during conventional operation, which indicated a good performance of the anode. However, during the starvation periods it took positive values ranging between  $0.02$  and  $0.18$  V vs SHE. Anode potential profiles remained almost constant as well after 1, 3, 5 and 10 days under starvation conditions (Figure 7.6B).

The common MEC performance indexes obtained in all the tested cycles are displayed in Figure 7.7. The CE was practically the same in all batch cycles, being the highest value 88 % after 1 day and the lowest value 77 % after 5 days of starvation. Hydrogen was almost fully recovered, since  $r_{\text{CAT}}$  was practically 100 % in all cases. No significant differences were found in energy efficiencies, since  $r_{\text{S}}$ ,  $r_{\text{E}}$  and  $r_{\text{S+E}}$  were in narrow ranges between 107 and 121 %, 164 and 177 %, and 64 and 70 %, respectively. The differences in hydrogen production were also minimal, since the lowest and the highest hydrogen production were  $1.2$  and  $1.3$   $\text{m}^3/\text{m}^3\cdot\text{d}$ , suggesting again that starvation periods up to 10 days with an applied voltage of  $0.8$  V did not affect the MEC performance.

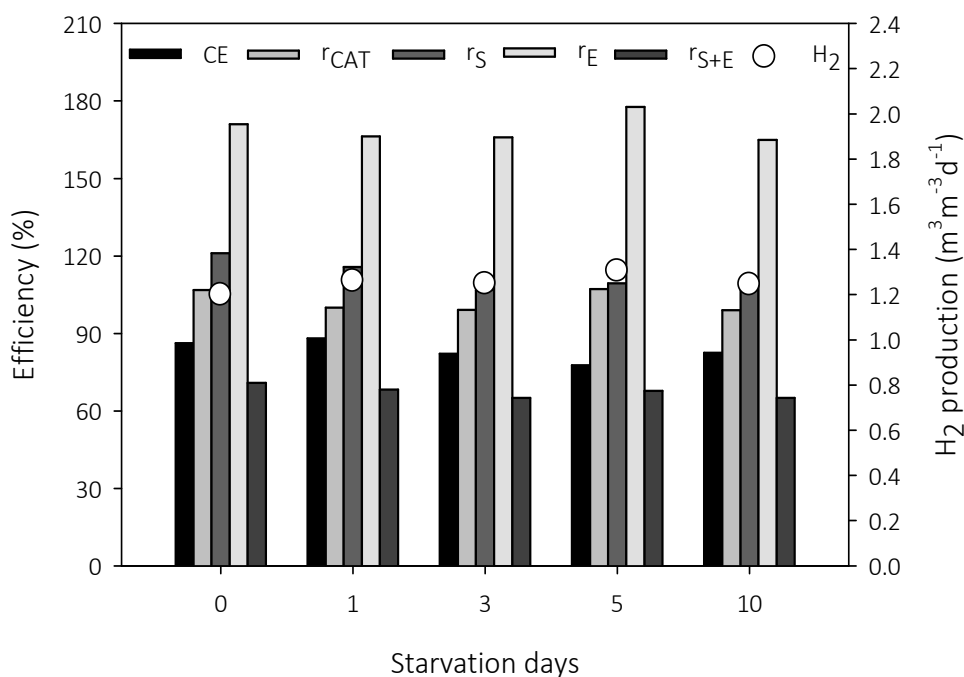


**Figure 7.7** Coulombic efficiency (CE), cathodic gas recovery ( $r_{\text{CAT}}$ ), energy efficiencies ( $r_{\text{E}}$  and  $r_{\text{S+E}}$ ) and hydrogen production after different starvation periods at an applied voltage of  $0.8$  V ( $\text{MEC}_{\text{AV}}$ ).



The results obtained with the starvation tests without any applied voltage ( $MEC_{WV}$ ) are shown in Figure 7.8. The current intensity profile of  $MEC_{WV}$  during the starvation periods showed a lower performance after 10 days of starvation while 1, 3 and 5 days of starvation did not seem to have a significant effect on the cell performance. The maximum current intensity only ranged between 6 and 7.5 mA for the initial and the 3 subsequent cycles (after 1, 3 and 5 days of starvation), whereas after 10 days of starvation it decreased to 3.5 mA and the duration of the cycle increased from 1 to 3 days. Two additional batch cycles (R2 and R3) were monitored after the 10 days starvation cycle (R1) and the current intensity practically recovered its initial value.

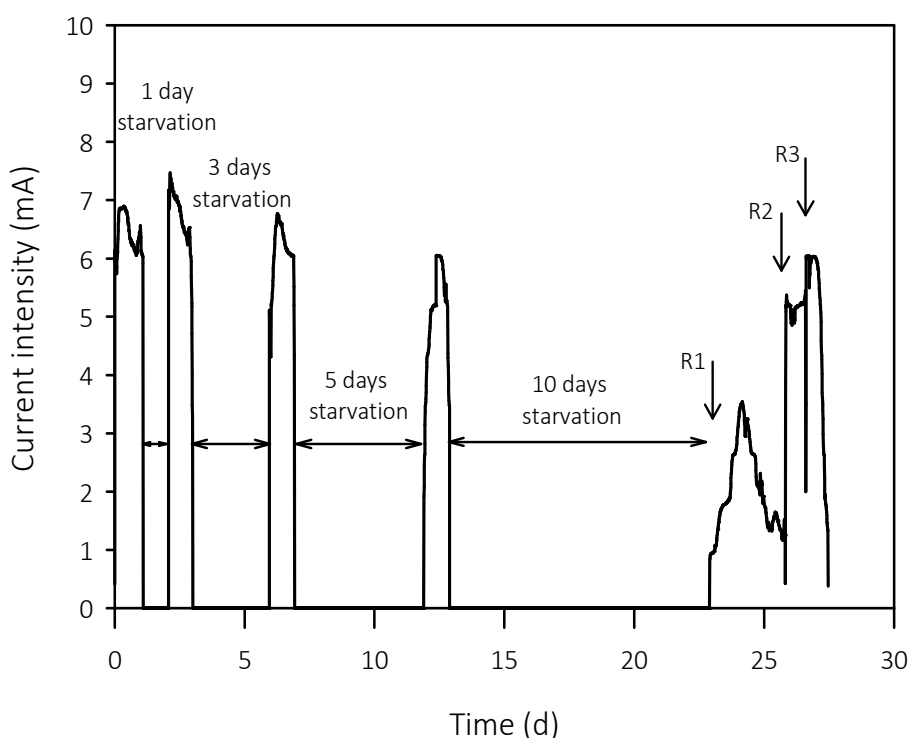


**Figure 7.8** Evaluating starvation in MEC without any applied voltage ( $MEC_{WV}$ ).

The efficiencies and hydrogen production of  $MEC_{WV}$  are shown in Figure 7.9. The CE decreased as the starvation periods increased, being initially 89 % and 40 % after 10 days of starvation. The  $r_{CAT}$  remained close to 100 % after 1, 3 and 5 days of starvation, but significantly decreased to 63 % after 10 days of starvation. Following a similar trend,  $r_S$ ,  $r_E$  and  $r_{S+E}$  remained between 79 and 107 %, 160 and 172 %, and 52 and 64 % even after 5 days of starvation, but after 10 days without substrate they were 33 %, 65 % and 22 %, respectively.

As previously stated, two additional batch cycles were monitored after the 10-days starvation period. The previous performance indexes were also calculated and CE increased to 65 and 102 %,  $r_{\text{CAT}}$  to 77 and 91 %,  $r_{\text{S}}$  to 67 and 123 %,  $r_{\text{E}}$  to 127 and 150 % and  $r_{\text{E+S}}$  to 44 and 68 %, for R2 and R3 respectively, thus, practically recovering the values previous to any starvation period.

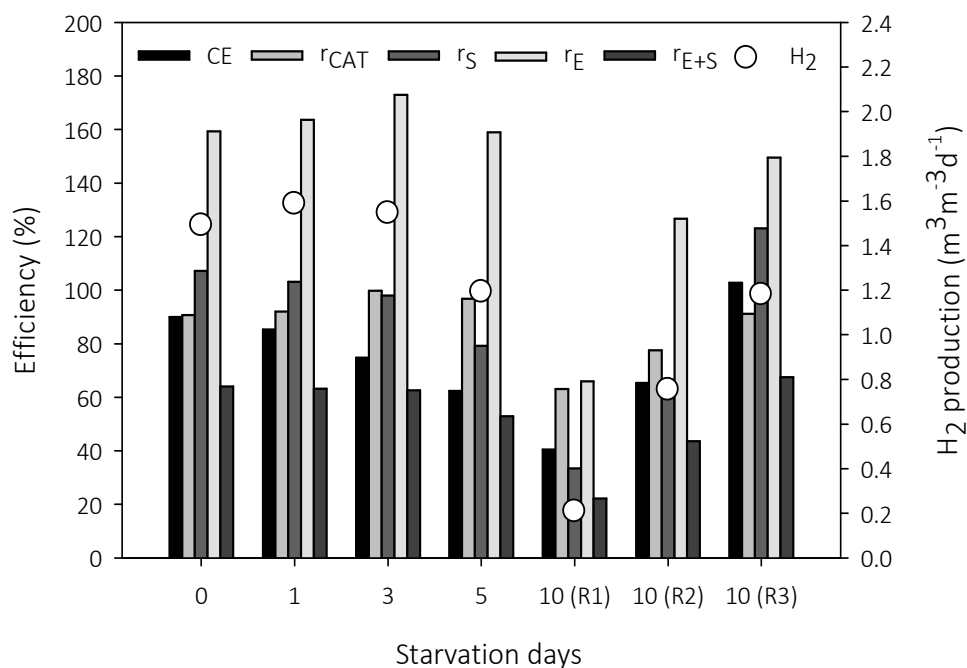


**Figure 7.9** Coulombic efficiency (CE), cathodic gas recovery ( $r_{\text{CAT}}$ ), energy efficiencies ( $r_{\text{E}}$  and  $r_{\text{S+E}}$ ) and hydrogen production after different starvation periods without any applied voltage ( $\text{MEC}_{\text{WV}}$ ).

The results showed that starvation periods up to 10 days did not have any significant effect on MEC performance as long as the applied voltage was maintained. In contrast, when no voltage was applied 10 days without substrate led to a decrease of the MEC performance, although this negative effect was reversible.

SS-MEC are usually operated under batch mode and, as such, subjected under alternating feast and starvation conditions. Biomass can easily adapt to this scenario by using storage polymers as carbon and energy source under famine conditions. This observation has been already detailed in conventional activated sludge systems [172]. Hence, under alternating feast and starvation conditions, the population selected is able to survive

under substrate limitation by accumulating substrate as a polymer inside of the bacterial cell under high substrate concentrations, and consumed it under starvation conditions. According to the literature this could be accomplished either by only ARB [155] or by a syntrophic consortium [169]. This endogenous behaviour can explain the observed current intensity under the starvation periods with an applied voltage. These results agree with those obtained in Gao et al. [169], where an MEC operating with a fixed anode potential of -0.4 vs Ag/AgCl (-0.19 vs SHE) recovered its initial current intensity after 4 days without substrate. High resistance to starvation has also been reported in MFC. In Kaur et al. [168] the performance of an acetate-fed MFC was only slightly affected by 12 days without substrate. Moreover, Chang et al. [173] showed that an MFC usually fed with glucose and glutamic acid could recover its initial current intensity after 12 days of starvation.

On the other hand, MEC without any applied voltage during starvation periods lost part of its activity after 10 days, as accumulated substrate could not be used, as the MEC overall process is thermodynamically unfavourable and electrons did not flow spontaneously from the anode to the cathode. Hence, for starvation periods longer than 5 days the best alternative is maintaining an applied voltage.

## 7.5 Conclusions

Preliminary tests with a unit that would be a part of a pilot-scale MEC allowed drawing helpful information in view of the imminent construction of the whole pilot plant. In this context, corrosion problems producing a current intensity independent from COD consumption could be detected and solved.

Inoculation from anaerobic sludge by gradually increasing the applied potential appeared to be a good strategy for the start-up of MEC. The same strategy could be followed when starting up the whole plant, although this reactor could probably provide an ARB-enriched inoculum for the rest of units.

Substrate consumption by anaerobic microorganisms other than ARB will be unavoidable, especially when working with real wastewater, thus a low CE is expected. However, it could be increased to some extent by reducing the batch cycles (or the hydraulic

retention time) by optimizing the ratio between the reactor volume and the electrode area.

Hydrogen recovery needs to be improved. Highly variable hydrogen production rates have been obtained probably as a result of some hydrogen trapped in the cathode. If all the hydrogen had been recovered, the energy balance regarding the electrical input would have been positive, so improvements on this point will be critical for MEC technology to be feasible at full-scale. However, further studies need to be performed with the real wastewater to be treated as MEC performance will depend largely on this.

MEC with an applied voltage of 0.8 V during starvation periods displayed a high resistance to starvation, probably due to the consumption of the accumulated substrate as polymer inside the bacterial cell. In this sense, bacterial activity in MEC was not affected by a period up to 10 days without substrate. Nevertheless, when the accumulated substrate could not be consumed by ARB during starvation periods, i.e. when no voltage was applied in MEC, the performance after starvation periods drastically decreased. Starvation periods longer than 5 days produced a negative effect on the cells performance, although it was recovered after one or two cycles with substrate. Thus, the utilization of the accumulated substrate has to be enabled by applying a voltage in MEC for long starvation periods.

# CHAPTER 8

---

General conclusions and future work



The main objective of this thesis was to understand the basics of microbial electrolysis cells with the aim of proposing strategies in view of the scale-up of this technology.

This section summarizes the main achievements and conclusions that can be drawn from this thesis. Some future research directions will be also suggested, in order to further develop bioelectrochemical systems in different ways.

## 8.1 General conclusions

- Single-chamber configuration does not seem suitable for hydrogen production, because of hydrogen losses due to its consumption by microorganisms (hydrogen oxidizing ARB, homoacetogens or hydrogenotrophic methanogens).  
Hydrogen consumption by ARB or homoacetogens led to hydrogen recycling, a very unfavourable scenario, in which up to the 80.5% of current intensity came from hydrogen and only the 6.3% of the energy invested could be recovered. Hydrogen consumption by methanogens to produce methane was not such an unfavourable situation in terms of energy recovery (95.0%), which, however, was lower than that attained if hydrogen would not have been consumed but recovered (135.6%).
- Tests with media similar to wastewaters in terms of buffer capacity and conductivity showed a decrease in MEC performance compared to that with well-buffered medium. The detrimental effects of the lack of buffer in single-chamber configuration were more significant on the cathode than on the anode. However, the highest voltage losses were located in the anode when pH gradients were generated due to the presence of an ion exchange membrane in two-chamber configuration. The decrease of the anodic pH and the increase of the cathodic pH did not only negatively affect the thermodynamics of the process, but also caused a loss of biological activity, which in turn, led to a failed MEC when working with non-buffered media. Both AEM and CEM performed very similar with respect to the pH gradients, although the ohmic resistance of this latter was lower. However, the low current intensities achieved in such small reactors did not allow assessing

the effect of membranes and conductivity on the MEC performance in terms of ohmic losses.

- A pH control strategy enhanced the performance of a two-chamber MEC, either with well-buffered or non-buffered media. A fairly high hydrogen production could be obtained with a very low applied potential (0.2 V) by controlling the pH of the cathodic chamber at a low value (2.0). This strategy led to an increase of the energy efficiency with respect to the electrical input up to 883% and 730 % for the well-buffered and the non-buffered MEC, respectively.  
The use of acid effluents (such as cheese brine from the dairy industry) as catholyte could be a good alternative to increase the energy recovery in full-scale systems, where the pH control would be hardly implementable.
- Experiments with an MEC unit that will form part of a pilot-scale MEC provided helpful information for improving the design of the pilot plant. The anode was successfully inoculated from anaerobic sludge by gradually increasing the applied cell potential. Inoculation of the whole pilot-plant could be carried out either following the same strategy or using the effluent of this reactor as inoculum to reduce the start-up time. The batch cycle time (or the hydraulic retention time when operating in continuous mode) should be reduced to minimize substrate consumption by anaerobic microorganisms other than ARB. Optimizing the ratio between the reactor volume and the electrode area would be a good option to achieve it. Entrapment of hydrogen bubbles in the cathode needs to be avoided, since complete hydrogen recovery would lead to an offset of the electrical energy to produce it.
- Bacterial activity could be maintained during starvation periods up to 10 days as long as an electrical voltage was applied, so that the accumulated substrate as polymer inside the bacterial cell could be consumed. Hence, technical plant stops would not be an issue in real systems. However, the resistance to starvation periods decreased when no voltage was applied, since endogenous consumption was not enabled. Under these conditions starvation periods longer than 5 days



produced a negative effect on the cells performance, although it could be recovered after one or two cycles with substrate.

## 8.2 Future work

The results of this thesis suggest a variety of research directions for future work:

One of these directions is to finish the construction of the two-chamber pilot-scale MEC for hydrogen production and start operating it with real wastewaters in the anodic chamber. The use of continuously fed acid catholytes (such as cheese brine) to enhance the energy recovery at full-scale should be also examined. In this framework, research should be done in platinum-free cathode materials, which efficiently work at acid pH. Hydrogen storage is another important point that needs to be investigated. No matter how efficient hydrogen production in MEC may become if hydrogen storage systems are not.

Methane production in MEC provides an alternative to hydrogen production. Lower energy recoveries can be achieved, but in return the reactor design and operation would be simpler (single-chamber configuration). In this context, research could be conducted in biogas upgrading by coupling an anaerobic digester with an MEC.

Despite not being directly related to the results of this thesis, the knowledge acquired on BES can be used for starting the construction of a computational model. A sufficiently accurate model would allow to assess many different situations in a cost-effective way without performing experiments. Therefore, the design of a cell could be easily optimized.

Finally, BES could be employed for other purposes different from hydrogen/methane production. The research group has recently started with both microbial electrosynthesis of acetate from carbon dioxide and sulphate reduction in biocathodes.



---

## References



- [1] INE National Statistics Institute, 2012.
- [2] IDAE Instituto para la Diversificación y ahorro de la Energía, Estudio de Prospectiva: Consumo Energético en el sector del agua, 2010.
- [3] Ministry of Industry Energy and Tourism (Spain), La energía en España 2013, 2013.
- [4] E.S. Heidrich, T.P. Curtis, J. Dolfig, Determination of the Internal Chemical Energy of Wastewater, *Environ Sci Technol*, 45 (2011) 827-832.
- [5] I. Shizas, D. Bagley, Experimental Determination of Energy Content of Unknown Organics in Municipal Wastewater Streams, *Journal of Energy Engineering*, 130 (2004) 45-53.
- [6] P.L. McCarty, J. Bae, J. Kim, Domestic Wastewater Treatment as a Net Energy Producer—Can This be Achieved?, *Environ Sci Technol*, 45 (2011) 7100-7106.
- [7] D.R. Lovley, D.E. Holmes, K.P. Nevin, Dissimilatory Fe(III) and Mn(IV) Reduction, *Advances in Microbial Physiology*, Academic Press 2004, pp. 219-286.
- [8] B.E. Logan, Exoelectrogenic bacteria that power microbial fuel cells, *Nat Rev Micro*, 7 (2009) 375-381.
- [9] D.R. Bond, D.R. Lovley, Electricity Production by *Geobacter sulfurreducens* Attached to Electrodes, *Appl Environ Microb*, 69 (2003) 1548-1555.
- [10] D.R. Bond, D.E. Holmes, L.M. Tender, D.R. Lovley, Electrode-Reducing Microorganisms That Harvest Energy from Marine Sediments, *Science*, 295 (2002) 483-485.
- [11] O. Bretschger, A. Obraztsova, C.A. Sturm, I.S. Chang, Y.A. Gorby, S.B. Reed, D.E. Culley, C.L. Reardon, S. Barua, M.F. Romine, J. Zhou, A.S. Beliaev, R. Bouhenni, D. Saffarini, F. Mansfeld, B.-H. Kim, J.K. Fredrickson, K.H. Nealson, Current Production and Metal Oxide Reduction by *Shewanella oneidensis* MR-1 Wild Type and Mutants, *Appl Environ Microb*, 74 (2008) 553-553.
- [12] K. Rabaey, N. Boon, S.D. Siciliano, M. Verhaege, W. Verstraete, Biofuel Cells Select for Microbial Consortia That Self-Mediate Electron Transfer, *Appl Environ Microb*, 70 (2004) 5373-5382.

- [13] S.K. Chaudhuri, D.R. Lovley, Electricity generation by direct oxidation of glucose in mediatorless microbial fuel cells, *Nat Biotech*, 21 (2003) 1229-1232.
- [14] D.R. Bond, D.R. Lovley, Evidence for Involvement of an Electron Shuttle in Electricity Generation by *Geothrix fermentans*, *Appl Environ Microb*, 71 (2005) 2186-2189.
- [15] C.R. Myers, J.M. Myers, Localization of cytochromes to the outer membrane of anaerobically grown *Shewanella putrefaciens* MR-1, *J Bacteriol*, 174 (1992) 3429-3438.
- [16] G. Reguera, K.D. McCarthy, T. Mehta, J.S. Nicoll, M.T. Tuominen, D.R. Lovley, Extracellular electron transfer via microbial nanowires, *Nature*, 435 (2005) 1098-1101.
- [17] Y.A. Gorby, S. Yanina, J.S. McLean, K.M. Rosso, D. Moyles, A. Dohnalkova, T.J. Beveridge, I.S. Chang, B.H. Kim, K.S. Kim, D.E. Culley, S.B. Reed, M.F. Romine, D.A. Saffarini, E.A. Hill, L. Shi, D.A. Elias, D.W. Kennedy, G. Pinchuk, K. Watanabe, S.i. Ishii, B. Logan, K.H. Nealson, J.K. Fredrickson, Electrically conductive bacterial nanowires produced by *Shewanella oneidensis* strain MR-1 and other microorganisms, *Proceedings of the National Academy of Sciences*, 103 (2006) 11358-11363.
- [18] D.R. Lovley, Bug juice: harvesting electricity with microorganisms, *Nat Rev Micro*, 4 (2006) 497-508.
- [19] K.-J. Chae, M.-J. Choi, J.-W. Lee, K.-Y. Kim, I.S. Kim, Effect of different substrates on the performance, bacterial diversity, and bacterial viability in microbial fuel cells, *Bioresource Technol*, 100 (2009) 3518-3525.
- [20] A.K. Manohar, F. Mansfeld, The internal resistance of a microbial fuel cell and its dependence on cell design and operating conditions, *Electrochim Acta*, 54 (2009) 1664-1670.
- [21] J. Niessen, U. Schröder, F. Scholz, Exploiting complex carbohydrates for microbial electricity generation – a bacterial fuel cell operating on starch, *Electrochem Commun*, 6 (2004) 955-958.
- [22] N. Montpart, L. Rago, J.A. Baeza, A. Guisasola, Hydrogen production in single chamber microbial electrolysis cells with different complex substrates, *Water Res*, 68 (2015) 601-615.

- [23] T. Catal, K. Li, H. Bermek, H. Liu, Electricity production from twelve monosaccharides using microbial fuel cells, *J Power Sources*, 175 (2008) 196-200.
- [24] A. Bonmati, A. Sotres, Y. Mu, R. Rozendal, K. Rabaey, Oxalate degradation in a bioelectrochemical system: Reactor performance and microbial community characterization, *Bioresource Technol*, 143 (2013) 147-153.
- [25] Y. Feng, X. Wang, B. Logan, H. Lee, Brewery wastewater treatment using air-cathode microbial fuel cells, *Appl Microbiol Biot*, 78 (2008) 873-880.
- [26] R. Cusick, B. Bryan, D. Parker, M. Merrill, M. Mehanna, P. Kiely, G. Liu, B. Logan, Performance of a pilot-scale continuous flow microbial electrolysis cell fed winery wastewater, *Appl Microbiol Biot*, 89 (2011) 2053-2063.
- [27] S.A. Patil, V.P. Surakasi, S. Koul, S. Ijmulwar, A. Vivek, Y.S. Shouche, B.P. Kapadnis, Electricity generation using chocolate industry wastewater and its treatment in activated sludge based microbial fuel cell and analysis of developed microbial community in the anode chamber, *Bioresource Technol*, 100 (2009) 5132-5139.
- [28] L. Huang, B. Logan, Electricity generation and treatment of paper recycling wastewater using a microbial fuel cell, *Appl Microbiol Biot*, 80 (2008) 349-355.
- [29] N. Montpart, E. Ribot-Llobet, V.K. Garlapati, L. Rago, J.A. Baeza, A. Guisasola, Methanol opportunities for electricity and hydrogen production in bioelectrochemical systems, *Int J Hydrogen Energ*, 39 (2014) 770-777.
- [30] B.E. Logan, B. Hamelers, R.A. Rozendal, U. Schröder, J. Keller, S. Freguia, P. Aelterman, W. Verstraete, K. Rabaey, Microbial fuel cells: Methodology and technology, *Environ Sci Technol*, 40 (2006) 5181-5192.
- [31] R.A. Rozendal, Hydrogen Production through Biocatalyzed Electrolysis, Department of Environmental Technology, Wageningen University, 2007.
- [32] B.E. Logan, D. Call, S. Cheng, H.V.M. Hamelers, T.H.J.A. Sleutels, A.W. Jeremiasse, R.A. Rozendal, Microbial Electrolysis Cells for High Yield Hydrogen Gas Production from Organic Matter, *Environ Sci Technol*, 42 (2008) 8630-8640.

- [33] A.J. Bard, L.R. Faulkner, *Electrochemical Methods: Fundamentals and Applications*, 2nd ed., Wiley, New York, 2001.
- [34] S.C. Popat, D. Ki, B.E. Rittmann, C.I. Torres, Importance of  $\text{OH}^-$  Transport from Cathodes in Microbial Fuel Cells, *Chemosuschem*, 5 (2012) 1071-1079.
- [35] S. Freguia, K. Rabaey, Z. Yuan, J. Keller, Non-catalyzed cathodic oxygen reduction at graphite granules in microbial fuel cells, *Electrochim Acta*, 53 (2007) 598-603.
- [36] Z.H. Wang, C.Y. Wang, K.S. Chen, Two-phase flow and transport in the air cathode of proton exchange membrane fuel cells, *J Power Sources*, 94 (2001) 40-50.
- [37] C.I. Torres, A.K. Marcus, P. Parameswaran, B.E. Rittmann, Kinetic Experiments for Evaluating the Nernst–Monod Model for Anode-Respiring Bacteria (ARB) in a Biofilm Anode, *Environ Sci Technol*, 42 (2008) 6593-6597.
- [38] H.V.M. Hamelers, A. ter Heijne, N. Stein, R.A. Rozendal, C.J.N. Buisman, Butler–Volmer–Monod model for describing bio-anode polarization curves, *Bioresource Technol*, 102 (2011) 381-387.
- [39] C.I. Torres, *Microbial kinetics of anode-respiring bacteria*, Arizona State University, United States, 2009.
- [40] J. Wang, *Analytical Electrochemistry*, Wiley Chichester, England, 2000.
- [41] M.C. Potter, *Electrical Effects Accompanying the Decomposition of Organic Compounds*, 1911.
- [42] B. Cohen, The Bacteria Culture as an Electrical Half-Cell, *J Bacteriol*, 21 (1931) 18-19.
- [43] R.C. Bean, Y.H. Inami, P.R. Basford, M.H. Boyer, W.C. Shepherd, E.R. Walwick, Study of the fundamental principles of bio-electrochemistry, NASA Final technical report, Research Laboratories, Philco Corporation, 1964.
- [44] J.H. Canfield, B.H. Goldner, R. Lutwack, Utilization of human wastes as electrochemical fuels, NASA Technical report, Magma Corporation, Anaheim, CA, 1963.
- [45] G.E. Ellis, S. E.E., *Biochemical fuel cells*, Nasa Technical Report, The Marquardt Corporation, 1963.



- [46] R. Allen, H.P. Bennetto, Microbial fuel-cells, *Appl Biochem Biotechnol*, 39-40 (1993) 27-40.
- [47] B.H. Kim, D.H. Park, P.K. Shin, I.S. Chang, H.J. Kim, Anode, cathode, microbial catalyst, 1999.
- [48] H.J. Kim, M.S. Hyun, I.S. Chang, B.H. Kim, A microbial fuel cell type lactate biosensor using a metal-reducing bacterium, *Shewanella putrefaciens*, *J Microbiol Biotechnol*, 9 (1999) 365-367.
- [49] H. Liu, B.E. Logan, Electricity generation using an air-cathode single chamber microbial fuel cell in the presence and absence of a proton exchange membrane, *Environ Sci Technol*, 38 (2004) 4040-4046.
- [50] H. Liu, S. Grot, B.E. Logan, Electrochemically Assisted Microbial Production of Hydrogen from Acetate, *Environ Sci Technol*, 39 (2005) 4317-4320.
- [51] R.A. Rozendal, H.V.M. Hamelers, G.J.W. Euverink, S.J. Metz, C.J.N. Buisman, Principle and perspectives of hydrogen production through biocatalyzed electrolysis, *Int J Hydrogen Energ*, 31 (2006) 1632-1640.
- [52] C.J.N. Buisman, R.A. Rozendal, Bio-electrochemical process for producing hydrogen, 2005.
- [53] P. Clauwaert, K. Rabaey, P. Aelterman, L. De Schampelaire, T.H. Pham, P. Boeckx, N. Boon, W. Verstraete, Biological Denitrification in Microbial Fuel Cells, *Environ Sci Technol*, 41 (2007) 3354-3360.
- [54] D.P.B.T.B. Strik, H.V.M. Hamelers, J.F.H. Snel, C.J.N. Buisman, Green electricity production with living plants and bacteria in a fuel cell, *International Journal of Energy Research*, 32 (2008) 870-876.
- [55] D. Call, B.E. Logan, Hydrogen production in a single chamber microbial electrolysis cell lacking a membrane, *Environ Sci Technol*, 42 (2008) 3401-3406.
- [56] P. Clauwaert, W. Verstraete, Methanogenesis in membraneless microbial electrolysis cells, *Appl Microbiol Biot*, 82 (2009) 829-836.

- [57] X. Cao, X. Huang, P. Liang, K. Xiao, Y. Zhou, X. Zhang, B.E. Logan, A New Method for Water Desalination Using Microbial Desalination Cells, *Environ Sci Technol*, 43 (2009) 7148-7152.
- [58] Y. Mu, R.A. Rozendal, K. Rabaey, J. Keller, Nitrobenzene Removal in Bioelectrochemical Systems, *Environ Sci Technol*, 43 (2009) 8690-8695.
- [59] Y.F. Zhang, I. Angelidaki, Submersible Microbial Fuel Cell Sensor for Monitoring Microbial Activity and BOD in Groundwater: Focusing on Impact of Anodic Biofilm on Sensor Applicability, *Biotechnol Bioeng*, 108 (2011) 2339-2347.
- [60] Z.D. Liu, J. Liu, S.P. Zhang, X.H. Xing, Z.G. Su, Microbial fuel cell based biosensor for in situ monitoring of anaerobic digestion process, *Bioresource Technol*, 102 (2011) 10221-10229.
- [61] S. Patil, F. Harnisch, U. Schroder, Toxicity Response of Electroactive Microbial Biofilms-A Decisive Feature for Potential Biosensor and Power Source Applications, *Chemphyschem*, 11 (2010) 2834-2837.
- [62] N.E. Stein, H.M.V. Hamelers, G. van Straten, K.J. Keesman, On-line detection of toxic components using a microbial fuel cell-based biosensor, *J Process Contr*, 22 (2012) 1755-1761.
- [63] N.E. Stein, H.V.M. Hamelers, G. van Straten, K.J. Keesman, Effect of Toxic Components on Microbial Fuel Cell-Polarization Curves and Estimation of the Type of Toxic Inhibition, *Biosensors*, 2 (2012) 255-268.
- [64] Y.F. Zhang, I. Angelidaki, A simple and rapid method for monitoring dissolved oxygen in water with a submersible microbial fuel cell (SBMFC), *Biosens Bioelectron*, 38 (2012) 189-194.
- [65] A.W. Jeremiase, H.V.M. Hamelers, C.J.N. Buisman, Microbial electrolysis cell with a microbial biocathode, *Bioelectrochemistry*, 78 (2010) 39-43.
- [66] K.P. Nevin, T.L. Woodard, A.E. Franks, Z.M. Summers, D.R. Lovley, Microbial Electrosynthesis: Feeding Microbes Electricity To Convert Carbon Dioxide and Water to Multicarbon Extracellular Organic Compounds, *mBio*, 1 (2010).

- [67] K. Rabaey, S. Bützer, S. Brown, J. Keller, R.A. Rozendal, High Current Generation Coupled to Caustic Production Using a Lamellar Bioelectrochemical System, *Environ Sci Technol*, 44 (2010) 4315-4321.
- [68] M. Mehanna, P.D. Kiely, D.F. Call, B.E. Logan, Microbial Electrodialysis Cell for Simultaneous Water Desalination and Hydrogen Gas Production, *Environ Sci Technol*, 44 (2010) 9578-9583.
- [69] P.G. Dennis, F. Harnisch, Y.K. Yeoh, G.W. Tyson, K. Rabaey, Dynamics of cathode-associated microbial communities and metabolite profiles in a glycerol-fed bioelectrochemical system, *Appl Environ Microb*, (2013).
- [70] E.S. Heidrich, J. Dolfing, K. Scott, S.R. Edwards, C. Jones, T.P. Curtis, Production of hydrogen from domestic wastewater in a pilot-scale microbial electrolysis cell, *Appl Microbiol Biot*, 97 (2013) 6979-6989.
- [71] R.H. Perry, D.W. Green, *Perrys Chemical Engineers Handbook (7th Edition)*, Mc Graw Hill 1997.
- [72] T.H. Pham, K. Rabaey, P. Aelterman, P. Clauwaert, L. De Schampelaire, N. Boon, W. Verstraete, Microbial fuel cells in relation to conventional anaerobic digestion technology, *Eng Life Sci*, 6 (2006) 285-292.
- [73] I.E.A. IEA, *Hydrogen production and storage: R&D Priorities and Gaps*, Paris, France, 2006
- [74] H.S. Lee, W.F.J. Vermaas, B.E. Rittmann, Biological hydrogen production: prospects and challenges, *Trends Biotechnol*, 28 (2010) 262-271.
- [75] P.P. Edwards, V.L. Kuznetsov, W.I.F. David, N.P. Brandon, Hydrogen and fuel cells: Towards a sustainable energy future, *Energy Policy*, 36 (2008) 4356-4362.
- [76] Fuel Cell Technology Program, *Hydrogen Storage*, U.S. Department of Energy, (2011).
- [77] R.D. Cusick, P.D. Kiely, B.E. Logan, A monetary comparison of energy recovered from microbial fuel cells and microbial electrolysis cells fed winery or domestic wastewaters, *Int J Hydrogen Energ*, 35 (2010) 8855-8861.

- [78] F. Harnisch, F. Aulenta, U. Schröder, 6.49 - Microbial Fuel Cells and Bioelectrochemical Systems: Industrial and Environmental Biotechnologies Based on Extracellular Electron Transfer, in: M. Moo-Young (Ed.) *Comprehensive Biotechnology* (Second Edition), Academic Press, Burlington, 2011, pp. 643-659.
- [79] Y. Zhang, I. Angelidaki, Microbial electrolysis cells turning to be versatile technology: Recent advances and future challenges, *Water Res*, 56 (2014) 11-25.
- [80] H.S. Lee, C.I. Torres, P. Parameswaran, B.E. Rittmann, Fate of H<sub>2</sub> in an upflow single-chamber microbial electrolysis cell using a metal-catalyst-free cathode, *Environ Sci Technol*, 43 (2009) 7971-7976.
- [81] H.S. Lee, B.E. Rittmann, Significance of Biological Hydrogen Oxidation in a Continuous Single-Chamber Microbial Electrolysis Cell, *Environ Sci Technol*, 44 (2010) 948-954.
- [82] P. Parameswaran, C.I. Torres, H.S. Lee, B.E. Rittmann, R. Krajmalnik-Brown, Hydrogen consumption in microbial electrochemical systems (MXCs): The role of homo-acetogenic bacteria, *Bioresource Technol*, 102 (2011) 263-271.
- [83] K.-J. Chae, M.-J. Choi, K.-Y. Kim, F.F. Ajayi, W. Park, C.-W. Kim, I.S. Kim, Methanogenesis control by employing various environmental stress conditions in two-chambered microbial fuel cells, *Bioresource Technol*, 101 (2010) 5350-5357.
- [84] F.F. Ajayi, K.-Y. Kim, K.-J. Chae, M.-J. Choi, I.S. Kim, Effect of hydrodynamic force and prolonged oxygen exposure on the performance of anodic biofilm in microbial electrolysis cells, *Int J Hydrogen Energ*, 35 (2010) 3206-3213.
- [85] H. Hu, Y. Fan, H. Liu, Hydrogen production using single-chamber membrane-free microbial electrolysis cells, *Water Res*, 42 (2008) 4172-4178.
- [86] A. Wang, W. Liu, S. Cheng, D. Xing, J. Zhou, B.E. Logan, Source of methane and methods to control its formation in single chamber microbial electrolysis cells, *Int J Hydrogen Energ*, 34 (2009) 3653-3658.
- [87] B.S. Guri, F.M.L. Vega, J. Cirucci, P.N. Montpart, S.F.J. Lafuente, L.J.A. Baeza, C.A. Guisasola, Process for the methanogenesis inhibition in single chamber microbial electrolysis cells, EP274718 A1, 2014.

- [88] R.A. Rozendal, H.V.M. Hamelers, R.J. Molenkmp, J.N. Buisman, Performance of single chamber biocatalyzed electrolysis with different types of ion exchange membranes, *Water Res*, 41 (2007) 1984-1994.
- [89] A.W. Jeremiasse, H.V.M. Hamelers, M. Saakes, C.J.N. Buisman, Ni foam cathode enables high volumetric H<sub>2</sub> production in a microbial electrolysis cell, *Int J Hydrogen Energ*, 35 (2010) 12716-12723.
- [90] A.W. Jeremiasse, J. Bergsma, J.M. Kleijn, M. Saakes, C.J.N. Buisman, M. Cohen Stuart, H.V.M. Hamelers, Performance of metal alloys as hydrogen evolution reaction catalysts in a microbial electrolysis cell, *Int J Hydrogen Energ*, 36 (2011) 10482-10489.
- [91] P.A. Selembo, M.D. Merrill, B.E. Logan, The use of stainless steel and nickel alloys as low-cost cathodes in microbial electrolysis cells, *J Power Sources*, 190 (2009) 271-278.
- [92] E. Ribot-Llobet, J.Y. Nam, J.C. Tokash, A. Guisasola, B.E. Logan, Assessment of four different cathode materials at different initial pHs using unbuffered catholytes in microbial electrolysis cells, *Int J Hydrogen Energ*, 38 (2013) 2951-2956.
- [93] E. Ribot-Llobet, N. Montpart, Y. Ruiz-Franco, L. Rago, J. Lafuente, J.A. Baeza, A. Guisasola, Obtaining microbial communities with exoelectrogenic activity from anaerobic sludge using a simplified procedure, *J Chem Technol Biot*, 89 (2014) 1727-1732.
- [94] L. Rago, J. Guerrero, A. Guisasola, J.A. Baeza, Revealed 2-bromoethanesulfonate degradation in bioelectrochemical systems, *Bioelectrochemistry*, Under revision (2015).
- [95] L. Rago, Y. Ruiz, J.A. Baeza, A. Guisasola, P. Cortés, Microbial community analysis in a long-term membrane-less microbial electrolysis cell with hydrogen and methane production, *Bioelectrochemistry*, Under revision (2015).
- [96] B. Logan, S. Cheng, V. Watson, G. Estadt, Graphite fiber brush anodes for increased power production in air-cathode microbial fuel cells, *Environ Sci Technol*, 41 (2007) 3341-3346.
- [97] Y. Feng, Q. Yang, X. Wang, B.E. Logan, Treatment of carbon fiber brush anodes for improving power generation in air-cathode microbial fuel cells, *J Power Sources*, 195 (2010) 1841-1844.

- [98] J. Middaugh, S. Cheng, W. Liu, R. Wagner, How to Make Cathodes with a Diffusion Layer for Single-Chamber Microbial Fuel Cells, (2006) [http://www.engr.psu.edu/ce/enve/logan/bioenergy/pdf/Cathode\\_093008.pdf](http://www.engr.psu.edu/ce/enve/logan/bioenergy/pdf/Cathode_093008.pdf).
- [99] S. Cheng, H. Liu, B.E. Logan, Increased performance of single-chamber microbial fuel cells using an improved cathode structure, *Electrochem Commun*, 8 (2006) 489-494.
- [100] S. Cheng, H. Liu, B.E. Logan, Power densities using different cathode catalysts (Pt and CoTMPP) and polymer binders (Nafion and PTFE) in single chamber microbial fuel cells, *Environ Sci Technol*, 40 (2006) 364-369.
- [101] Z. Lu, G. Polizos, D.D. Macdonald, E. Manias, State of Water in Perfluorosulfonic Ionomer (Nafion 117) Proton Exchange Membranes, *J Electrochem Soc*, 155 (2008) B163-B171.
- [102] C. Dumas, A. Mollica, D. Féron, R. Basséguy, L. Etcheverry, A. Bergel, Marine microbial fuel cell: Use of stainless steel electrodes as anode and cathode materials, *Electrochim Acta*, 53 (2007) 468-473.
- [103] S.W. Hong, I.S. Chang, Y.S. Choi, T.H. Chung, Experimental evaluation of influential factors for electricity harvesting from sediment using microbial fuel cell, *Bioresour Technol*, 100 (2009) 3029-3035.
- [104] C.E. Reimers, L.M. Tender, S. Fertig, W. Wang, Harvesting Energy from the Marine Sediment–Water Interface, *Environ Sci Technol*, 35 (2001) 192-195.
- [105] J. Zhao, X.-F. Li, Y.-P. Ren, X.-H. Wang, C. Jian, Electricity generation from Taihu Lake cyanobacteria by sediment microbial fuel cells, *Journal of Chemical Technology & Biotechnology*, 87 (2012) 1567-1573.
- [106] Y. Ren, D. Pan, X. Li, F. Fu, Y. Zhao, X. Wang, Effect of polyaniline-graphene nanosheets modified cathode on the performance of sediment microbial fuel cell, *Journal of Chemical Technology & Biotechnology*, 88 (2013) 1946-1950.
- [107] J.R. Kim, B. Min, B.E. Logan, Evaluation of procedures to acclimate a microbial fuel cell for electricity production, *Appl Microbiol Biot*, 68 (2005) 23-30.

- [108] N.S. Malvankar, D.R. Lovley, Microbial nanowires for bioenergy applications, *Current Opinion in Biotechnology*, 27 (2014) 88-95.
- [109] A. Chidthaisong, R. Conrad, Specificity of chloroform, 2-bromoethanesulfonate and fluoroacetate to inhibit methanogenesis and other anaerobic processes in anoxic rice field soil, *Soil Biol Biochem*, 32 (2000) 977-988.
- [110] J.R. Ambler, B.E. Logan, Evaluation of stainless steel cathodes and a bicarbonate buffer for hydrogen production in microbial electrolysis cells using a new method for measuring gas production, *Int J Hydrogen Energ*, 36 (2011) 160-166.
- [111] K. Fricke, F. Harnisch, U. Schroder, On the use of cyclic voltammetry for the study of anodic electron transfer in microbial fuel cells, *Energ Environ Sci*, 1 (2008) 144-147.
- [112] D.K. Gosser, *Cyclic voltammetry: simulation and analysis of reaction mechanisms*, VCH1993.
- [113] Z. He, F. Mansfeld, Exploring the use of electrochemical impedance spectroscopy (EIS) in microbial fuel cell studies, *Energ Environ Sci*, 2 (2009) 215-219.
- [114] P. Parameswaran, C.I. Torres, H.S. Lee, R. Krajmalnik-Brown, B.E. Rittmann, Syntrophic Interactions Among Anode Respiring Bacteria (ARB) and Non-ARB in a Biofilm Anode: Electron Balances, *Biotechnol Bioeng*, 103 (2009) 513-523.
- [115] P. Parameswaran, C.I. Torres, D.W. Kang, B.E. Rittmann, R. Krajmalnik-Brown, The role of homoacetogenic bacteria as efficient hydrogen scavengers in microbial electrochemical cells (MXCs), *Water Sci Technol*, 65 (2012) 1-6.
- [116] H.S. Lee, P. Parameswaran, A. Kato-Marcus, C.I. Torres, B.E. Rittmann, Evaluation of energy-conversion efficiencies in microbial fuel cells (MFCs) utilizing fermentable and non-fermentable substrates, *Water Res*, 42 (2008) 1501-1510.
- [117] S.A. Cheng, D.F. Xing, D.F. Call, B.E. Logan, Direct Biological Conversion of Electrical Current into Methane by Electromethanogenesis, *Environ Sci Technol*, 43 (2009) 3953-3958.

- [118] M. Villano, F. Aulenta, C. Ciucci, T. Ferri, A. Giuliano, M. Majone, Bioelectrochemical reduction of CO<sub>2</sub> to CH<sub>4</sub> via direct and indirect extracellular electron transfer by a hydrogenophilic methanogenic culture, *Bioresource Technol*, 101 (2010) 3085-3090.
- [119] M. Siegert, M.D. Yates, D.F. Call, X.P. Zhu, A. Spormann, B.E. Logan, Comparison of Nonprecious Metal Cathode Materials for Methane Production by Electromethanogenesis, *Acs Sustain Chem Eng*, 2 (2014) 910-917.
- [120] T.H.J.A. Sleutels, L. Darus, H.V.M. Hamelers, C.J.N. Buisman, Effect of operational parameters on Coulombic efficiency in bioelectrochemical systems, *Bioresource Technol*, 102 (2011) 11172-11176.
- [121] E.M. Ungerfeld, S.R. Rust, D.R. Boone, Y. Liu, Effects of several inhibitors on pure cultures of ruminal methanogens, *J Appl Microbiol*, 97 (2004) 520-526.
- [122] A. Escapa, M.I. San Martin, A. Moran, Potential use of microbial electrolysis cells in domestic wastewater treatment plants for energy recovery, *Frontiers in Energy Research*, 2 (2014).
- [123] M.C.A.A. Van Eerten-Jansen, A.T. Heijne, C.J.N. Buisman, H.V.M. Hamelers, Microbial electrolysis cells for production of methane from CO<sub>2</sub>: long-term performance and perspectives, *International Journal of Energy Research*, 36 (2012) 809-819.
- [124] T. Bo, X. Zhu, L. Zhang, Y. Tao, X. He, D. Li, Z. Yan, A new upgraded biogas production process: Coupling microbial electrolysis cell and anaerobic digestion in single-chamber, barrel-shape stainless steel reactor, *Electrochem Commun*, 45 (2014) 67-70.
- [125] Y.Z. Fan, H.Q. Hu, H. Liu, Sustainable power generation in microbial fuel cells using bicarbonate buffer and proton transfer mechanisms, *Environ Sci Technol*, 41 (2007) 8154-8158.
- [126] C.I. Torres, A.K. Marcus, B.E. Rittmann, Proton transport inside the biofilm limits electrical current generation by anode-respiring bacteria, *Biotechnol Bioeng*, 100 (2008) 872-881.



- [127] T.H.J.A. Sleutels, R. Lodder, H.V.M. Hamelers, C.J.N. Buisman, Improved performance of porous bio-anodes in microbial electrolysis cells by enhancing mass and charge transport, *Int J Hydrogen Energ*, 34 (2009) 9655-9661.
- [128] R.A. Rozendal, H.V.M. Hamelers, K. Rabaey, J. Keller, C.J.N. Buisman, Towards practical implementation of bioelectrochemical wastewater treatment, *Trends Biotechnol*, 26 (2008) 450-459.
- [129] H. Liu, S.A. Cheng, B.E. Logan, Power generation in fed-batch microbial fuel cells as a function of ionic strength, temperature, and reactor configuration, *Environ Sci Technol*, 39 (2005) 5488-5493.
- [130] Y. Ruiz, J.A. Baeza, A. Guisasola, Revealing the proliferation of hydrogen scavengers in a single-chamber microbial electrolysis cell using electron balances, *Int J Hydrogen Energ*, 38 (2013) 15917-15927.
- [131] R.A. Rozendal, H.V.M. Hamelers, C.J.N. Buisman, Effects of membrane cation transport on pH and microbial fuel cell performance, *Environ Sci Technol*, 40 (2006) 5206-5211.
- [132] G.C. Gil, I.S. Chang, B.H. Kim, M. Kim, J.K. Jang, H.S. Park, H.J. Kim, Operational parameters affecting the performance of a mediator-less microbial fuel cell, *Biosens Bioelectron*, 18 (2003) 327-334.
- [133] T.H.J.A. Sleutels, H.V.M. Hamelers, C.J.N. Buisman, Reduction of pH Buffer Requirement in Bioelectrochemical Systems, *Environ Sci Technol*, 44 (2010) 8259-8263.
- [134] Y. Ahn, B.E. Logan, Saline catholytes as alternatives to phosphate buffers in microbial fuel cells, *Bioresource Technol*, 132 (2013) 436-439.
- [135] J.Y. Nam, B.E. Logan, Enhanced hydrogen generation using a saline catholyte in a two chamber microbial electrolysis cell, *Int J Hydrogen Energ*, 36 (2011) 15105-15110.
- [136] J.Y. Nam, B.E. Logan, Optimization of catholyte concentration and anolyte pHs in two chamber microbial electrolysis cells, *Int J Hydrogen Energ*, 37 (2012) 18622-18628.
- [137] S. Yossan, L. Xiao, P. Prasertsan, Z. He, Hydrogen production in microbial electrolysis cells: Choice of catholyte, *Int J Hydrogen Energ*, 38 (2013) 9619-9624.

- [138] T.H.J.A. Sleutels, H.V.M. Hamelers, R.A. Rozendal, C.J.N. Buisman, Ion transport resistance in Microbial Electrolysis Cells with anion and cation exchange membranes, *Int J Hydrogen Energ*, 34 (2009) 3612-3620.
- [139] T.H.J.A. Sleutels, A. Ter Heijne, C.J.N. Buisman, H.V.M. Hamelers, Steady-state performance and chemical efficiency of Microbial Electrolysis Cells, *Int J Hydrogen Energ*, 38 (2013) 7201-7208.
- [140] R.A. Rozendal, T.H.J.A. Sleutels, H.V.M. Hamelers, C.J.N. Buisman, Effect of the type of ion exchange membrane on performance, ion transport, and pH in biocatalyzed electrolysis of wastewater, *Water Sci Technol*, 57 (2008) 1757-1762.
- [141] P. Aelterman, K. Rabaey, H.T. Pham, N. Boon, W. Verstraete, Continuous electricity generation at high voltages and currents using stacked microbial fuel cells, *Environ Sci Technol*, 40 (2006) 3388-3394.
- [142] I. Ieropoulos, J. Winfield, J. Greenman, Effects of flow-rate, inoculum and time on the internal resistance of microbial fuel cells, *Bioresource Technol*, 101 (2010) 3520-3525.
- [143] V.J. Watson, B.E. Logan, Analysis of polarization methods for elimination of power overshoot in microbial fuel cells, *Electrochem Commun*, 13 (2011) 54-56.
- [144] Y.Y. Hong, D.F. Call, C.M. Werner, B.E. Logan, Adaptation to high current using low external resistances eliminates power overshoot in microbial fuel cells, *Biosens Bioelectron*, 28 (2011) 71-76.
- [145] X. Zhu, J.C. Tokash, Y. Hong, B.E. Logan, Controlling the occurrence of power overshoot by adapting microbial fuel cells to high anode potentials, *Bioelectrochemistry*, 90 (2013) 30-35.
- [146] A. Sotres, J. Díaz-Marcos, M. Guivernau, J. Illa, A. Magrí, F.X. Prenafeta-Boldú, A. Bonmatí, M. Viñas, Microbial community dynamics in two-chambered microbial fuel cells: effect of different ion exchange membranes, *Journal of Chemical Technology & Biotechnology*, (2014) n/a-n/a.

- [147] Z. He, N. Wagner, S.D. Minteer, L.T. Angenent, An upflow microbial fuel cell with an interior cathode: Assessment of the internal resistance by impedance Spectroscopy, *Environ Sci Technol*, 40 (2006) 5212-5217.
- [148] C.I. Torres, H.-S. Lee, B.E. Rittmann, Carbonate Species as OH<sup>-</sup> Carriers for Decreasing the pH Gradient between Cathode and Anode in Biological Fuel Cells, *Environ Sci Technol*, 42 (2008) 8773-8777.
- [149] J.J. Fornero, M. Rosenbaum, M.A. Cotta, L.T. Angenent, Carbon Dioxide Addition to Microbial Fuel Cell Cathodes Maintains Sustainable Catholyte pH and Improves Anolyte pH, Alkalinity, and Conductivity, *Environ Sci Technol*, 44 (2010) 2728-2734.
- [150] S. Freguia, K. Rabaey, Z.G. Yuan, J. Keller, Sequential anode-cathode configuration improves cathodic oxygen reduction and effluent quality of microbial fuel cells, *Water Res*, 42 (2008) 1387-1396.
- [151] Y. Qu, Y. Feng, X. Wang, J. Liu, J. Lv, W. He, B.E. Logan, Simultaneous water desalination and electricity generation in a microbial desalination cell with electrolyte recirculation for pH control, *Bioresource Technol*, 106 (2012) 89-94.
- [152] B. Erable, L. Etcheverry, A. Bergel, Increased power from a two-chamber microbial fuel cell with a low-pH air-cathode compartment, *Electrochem Commun*, 11 (2009) 619-622.
- [153] L. Zhuang, S.G. Zhou, Y.T. Li, Y. Yuan, Enhanced performance of air-cathode two-chamber microbial fuel cells with high-pH anode and low-pH cathode, *Bioresource Technol*, 101 (2010) 3514-3519.
- [154] A. Guisasola, M. Vargas, M. Marcelino, J. Lafuente, C. Casas, J.A. Baeza, On-line monitoring of the enhanced biological phosphorus removal process using respirometry and titrimetry, *Biochem Eng J*, 35 (2007) 371-379.
- [155] S. Freguia, K. Rabaey, Z.G. Yuan, J. Keller, Electron and carbon balances in microbial fuel cells reveal temporary bacterial storage behavior during electricity generation, *Environ Sci Technol*, 41 (2007) 2915-2921.

- [156] J. Zhang, M.D. Baro, E. Pellicer, J. Sort, Electrodeposition of magnetic, superhydrophobic, non-stick, two-phase Cu-Ni foam films and their enhanced performance for hydrogen evolution reaction in alkaline water media, *Nanoscale*, 6 (2014) 12490-12499.
- [157] E.J. Popczun, J.R. McKone, C.G. Read, A.J. Biacchi, A.M. Wiltrout, N.S. Lewis, R.E. Schaak, Nanostructured Nickel Phosphide as an Electrocatalyst for the Hydrogen Evolution Reaction, *J Am Chem Soc*, 135 (2013) 9267-9270.
- [158] E.J. Popczun, C.G. Read, C.W. Roske, N.S. Lewis, R.E. Schaak, Highly Active Electrocatalysis of the Hydrogen Evolution Reaction by Cobalt Phosphide Nanoparticles, *Angewandte Chemie International Edition*, 53 (2014) 5427-5430.
- [159] J. Kibsgaard, Z. Chen, B.N. Reinecke, T.F. Jaramillo, Engineering the surface structure of MoS<sub>2</sub> to preferentially expose active edge sites for electrocatalysis, *Nat Mater*, 11 (2012) 963-969.
- [160] H. Vrubel, D. Merki, X. Hu, Hydrogen evolution catalyzed by MoS<sub>3</sub> and MoS<sub>2</sub> particles, *Energ Environ Sci*, 5 (2012) 6136-6144.
- [161] J. Kibsgaard, T.F. Jaramillo, Molybdenum Phosphosulfide: An Active, Acid-Stable, Earth-Abundant Catalyst for the Hydrogen Evolution Reaction, *Angewandte Chemie International Edition*, 53 (2014) 14433-14437.
- [162] E.S. Heidrich, S.R. Edwards, J. Dolfig, S.E. Cotterill, T.P. Curtis, Performance of a pilot scale microbial electrolysis cell fed on domestic wastewater at ambient temperatures for a 12 month period, *Bioresource Technol*, 173 (2014) 87-95.
- [163] R.K. Brown, F. Harnisch, S. Wirth, H. Wahlandt, T. Dockhorn, N. Dichtl, U. Schroder, Evaluating the effects of scaling up on the performance of bioelectrochemical systems using a technical scale microbial electrolysis cell, *Bioresource Technol*, 163 (2014) 206-213.
- [164] A. Escapa, M.I. San-Martín, R. Mateos, A. Morán, Scaling-up of membraneless microbial electrolysis cells (MECs) for domestic wastewater treatment: Bottlenecks and limitations, *Bioresource Technol*, 180 (2015) 72-78.

- [165] L. Gil-Carrera, A. Escapa, B. Carracedo, A. Moran, X. Gomez, Performance of a semi-pilot tubular microbial electrolysis cell (MEC) under several hydraulic retention times and applied voltages, *Bioresource Technol*, 146 (2013) 63-69.
- [166] L. Gil-Carrera, A. Escapa, R. Moreno, A. Moran, Reduced energy consumption during low strength domestic wastewater treatment in a semi-pilot tubular microbial electrolysis cell, *J Environ Manage*, 122 (2013) 1-7.
- [167] S.E. Oh, B.E. Logan, Voltage reversal during microbial fuel cell stack operation, *J Power Sources*, 167 (2007) 11-17.
- [168] A. Kaur, H.C. Boghani, I. Michie, R.M. Dinsdale, A.J. Guwy, G.C. Premier, Inhibition of methane production in microbial fuel cells: Operating strategies which select electrogens over methanogens, *Bioresource Technol*, 173 (2014) 75-81.
- [169] Y. Gao, J. An, H. Ryu, H.-S. Lee, Microbial Fuel Cells as Discontinuous Portable Power Sources: Syntropic Interactions with Anode-Respiring Bacteria, *Chemosuschem*, 7 (2014) 1026-1029.
- [170] X. Zhu, M.D. Yates, M.C. Hatzell, H. Ananda Rao, P.E. Saikaly, B.E. Logan, Microbial Community Composition Is Unaffected by Anode Potential, *Environ Sci Technol*, 48 (2013) 1352-1358.
- [171] S. Freguia, K. Rabaey, Z. Yuan, J. Keller, Syntrophic Processes Drive the Conversion of Glucose in Microbial Fuel Cell Anodes, *Environ Sci Technol*, 42 (2008) 7937-7943.
- [172] G. Sin, A. Guisasola, D.J.W. De Pauw, J.A. Baeza, J. Carrera, P.A. Vanrolleghem, A new approach for modelling simultaneous storage and growth processes for activated sludge systems under aerobic conditions, *Biotechnol Bioeng*, 92 (2005) 600-613.
- [173] I.S. Chang, J.K. Jang, G.C. Gil, M. Kim, H.J. Kim, B.W. Cho, B.H. Kim, Continuous determination of biochemical oxygen demand using microbial fuel cell type biosensor, *Biosens Bioelectron*, 19 (2004) 607-613.



## Chapter 1

**Figure 1.1** Schematic diagram of (A) microbial fuel cell (MFC) and (B) microbial electrolysis cell (MEC) aiming at hydrogen production.

**Figure 1.2** Extracellular electron transfer for ARB (A) Direct transfer by direct contact or through a conductive biofilm matrix (B) Direct transfer by conductive pili and (C) Indirect transfer by means of electron shuttles.

**Figure 1.3** Electron flow according to electrodes potentials. Arrows indicate the direction of electron flow, which is spontaneous only from lower to higher potentials.

**Figure 1.4** Effect of pH on the (A) theoretical reduction potential of the cathode ( $E_{\text{cathode}}^{\text{eq}}$ ) and (B) cell electromotive force ( $E_{\text{emf}}$ ). For spontaneous processes,  $E_{\text{emf}}$  is above the dashed line, whereas for non-spontaneous processes  $E_{\text{emf}}$  is below. MFC (●) and MEC (○). For the  $E_{\text{emf}}$  calculation, biological standard conditions (pH of 7) were assumed for the anode (adapted from Rozendal [31]).

**Figure 1.5** Schematic representation of the experimental setup when using a potentiostat. RE: reference electrode, WE: working electrode, AE: auxiliary electrode, V: voltmeter, A: ammeter. The voltage between the WE and the RE is measured and controlled by modifying the applied voltage between the WE and the AE. The response of the system in terms of current intensity is measured between both the WE and the AE.

## Chapter 3

**Figure 3.1** (A) Schematic diagram and (B) image of the CC-MEC.

**Figure 3.2** (A) Schematic diagram and (B) image of the SSAC-MFC.

**Figure 3.3** (A) Schematic diagram and (B) image of the SS-MEC.

**Figure 3.4** (A) Schematic diagram and (B) image of the two-chamber SS-MEC.

**Figure 3.5** (A) Schematic diagram and (B) image of the Sed-MFC.

**Figure 3.6** (A) Schematic diagram and (B) image of the AC-MFC.

**Figure 3.7** Example of a polarization curve (A) and a power curve (B) in an MFC.

**Figure 3.8** (A) Potential waveform (B) current-time and (C) current-potential representations for a CV experiment.

**Figure 3.9** Example of impedance measurement of the cathode of an MEC (A) Nyquist plot and (B) Bode plot: logarithm of impedance modulus (●) and phase angle (□).

## Chapter 4

**Figure 4.1** Acetate concentration versus time in the MEC without applied voltage.

**Figure 4.2** Reaction pathways and parameters of electron equivalent balances in an acetate-fed single-chamber MEC.

**Figure 4.3** Batch experiment with the addition of sodium bicarbonate and H<sub>2</sub> sparging (A) Acetate concentration and (B) Current intensity over time. Current intensity is shown from time 5 hours due to monitoring problems.

**Figure 4.4** Monitoring of the MEC with H<sub>2</sub>-recycling (A) Current intensity under conventional operation (solid) and with N<sub>2</sub> sparging (experiment A1) (dashed), (B) Acetate concentration under conventional operation (●), with N<sub>2</sub> sparging (experiment A1) (△) and with N<sub>2</sub> sparging and no applied voltage (experiment A2) (□) and (C) Gas production under conventional operation: H<sub>2</sub> (◆) and CH<sub>4</sub> (▽).

**Figure 4.5** Methanogenic activity vs time represented as the ratio H<sub>2</sub>/H<sub>2</sub>+CH<sub>4</sub> at different weeks of operation. Week 9 (●), week 10 (×), week 16 (○), week 19 (△), week 29 (◆) and week 34 (▼) of operation. Concentration of BES: 90 mM (solid), 120 mM (dashed) and 50 mM (dash-dotted).

**Figure 4.6** Monitoring of the MEC with the presence of methanogens (A) Current intensity, (B) Acetate concentration and (C) Gas production: H<sub>2</sub> (◆) and CH<sub>4</sub> (▽). Note the different scales in (C).



## Chapter 5

**Figure 5.1** Current intensity profiles of the MFC during inoculation. MFC-1 (solid), MFC-2 (dashed) and MFC-3 (dotted).

**Figure 5.2** Performance assessment of the MFC (A) Polarization curves and (B) power curves. MFC-1 (●), MFC-2 (□) and MFC-3 (▼).

**Figure 5.3** Current intensity profiles after transferring the anodes to MEC: (A) buffered (BF), (B) high conductivity (HC) and (C) low conductivity (LC).

**Figure 5.4** Current intensity profiles of (A) buffered (BF), (B) high conductivity (HC) and (C) low conductivity (LC). MEC without membrane (WM), with an anion exchange membrane (AEM), and with a cation exchange membrane (CEM).

**Figure 5.5** Linear sweep voltammetry of the MEC in single-chamber configuration. BF (○), HC (△) and LC (◇). (A) Current intensity profiles and (B) Electrode potentials: anode potential (open symbols) and cathode potentials (filled symbols). Dashed lines indicate the theoretical electrode potentials under initial batch conditions (acetate concentration =  $1.69 \cdot 10^{-2}$  M, hydrogen partial pressure = 0.01 atm and pH = 7.5).

**Figure 5.6** Electrode potentials vs. applied cell potential of MEC in single-chamber configuration. BF (○), HC (△) and LC (◇). Anode potential (open symbols) and cathode potentials (filled symbols). Dashed lines indicate the theoretical electrode potentials under initial batch conditions.

**Figure 5.7** Current intensity profile and electrode potentials of LC in single-chamber configuration using the same conditions as in E7. Current intensity (solid), anodic potential (dashed) and cathodic potential (dotted).

**Figure 5.8** Nyquist diagrams of BF at an applied voltage of 1.0 V without membrane (●), with an AEM (▽) and with a CEM (■).

**Figure 5.9** Two-chamber MEC BF with an AEM and a CEM using the same conditions as in experiments E2 and E3. (A) pH evolution and (B) theoretical anodic and cathodic

potentials at the corresponding pH by assuming an acetate concentration of  $1.69 \cdot 10^{-2}$  M and a hydrogen partial pressure of 0.01 atm. Anode (dashed) and cathode (dotted).

**Figure 5.10** Linear sweep voltammetry of BF without membrane ( $\circ$ ), and with an AEM at the initial ( $\square$ ) and final pHs ( $\nabla$ ) of a batch experiment (A) Current intensity profiles and (B) Electrode potentials at final pHs: anode potential (open symbols) and cathode potentials (filled symbols). Dashed lines indicate the theoretical electrode potentials under pH final conditions and an acetate concentration of  $1.69 \cdot 10^{-2}$  M and a hydrogen partial pressure of 0.01 atm.

**Figure 5.11** Coulombic efficiency (CE), cathodic gas recovery ( $r_{\text{CAT}}$ ), energy efficiencies ( $r_s$ ,  $r_E$ ,  $r_{\text{S+E}}$ ) (bars) and hydrogen production (circles). Note that CE for E9 is not plotted due to problems with the analysis.

## Chapter 6

**Figure 6.1** (A) Image and (B) Schematics of the experimental setup.

**Figure 6.2** Current intensity profiles of the two-chamber MEC in E1 (pH not controlled, dotted), E2 (cathode at pH 7.5, dashed), E3 (anode at pH 7.5, dash-dotted) and E4 (cathode and anode at pH 7.5, solid).

**Figure 6.3** Coulombic efficiency (CE), cathodic gas recovery ( $r_{\text{CAT}}$ ), energy efficiencies ( $r_s$ ,  $r_E$ ,  $r_{\text{S+E}}$ ) (bars) and hydrogen production (circles) for experiments conducted in this study.

**Figure 6.4** pH profiles of (A) E1 (pH not controlled) (B) E2 (cathode at pH 7.5), (C) E3 (anode at pH 7.5) and (D) E4 (cathode and anode at pH 7.5). Cathodic pH (solid), anodic pH (dashed) and setpoint (dotted).

**Figure 6.5** Theoretical and experimental proton production (HP) in (A) E2 (cathode at pH 7.5), (B) E3 (anode at pH 7.5) and (C) E4 (cathode and anode at pH 7.5). Cathodic  $\text{HP}_{\text{exp}}$  (solid), anodic  $\text{HP}_{\text{exp}}$  (dashed) and  $\text{HP}_{\text{theo}}$  (dotted). Positive HP (proton production) correspond to the anodic chamber and negative HP (proton consumption) to the cathodic chamber.

**Figure 6.6** Current intensity profiles of the two-chamber MEC in E5 (cathode at pH 2.0, dotted), E6 (cathode at pH 5.0, dashed), E4 (cathode at pH 7.5, solid) and E7 (cathode at pH 12.5, dash-dotted). The anodic chamber was controlled at pH 7.5.

**Figure 6.7** pH profiles of (A) E5 (cathode at pH 2.0), (B) E6 (cathode at pH 5.0) and (C) E7 (cathode at pH 12.5). Cathodic pH (solid), anodic pH (dashed) and setpoint (dotted).

**Figure 6.8** Theoretical and experimental proton production (HP) in (A) E5 (cathode at pH 2.0), (B) E6 (cathode at pH 5.0) and (C) E7 (cathode at pH 12.5). Cathodic  $HP_{exp}$  (solid), anodic  $HP_{exp}$  (dashed) and  $HP_{theo}$  (dotted). Positive HP (proton production) correspond to the anodic chamber and negative HP (proton consumption) to the cathodic chamber.

**Figure 6.9** (A) Monitoring of current intensity (solid), anode potential (dotted), and cathode potential (dashed) in a replicate of E5 with pH 7.5 in the anodic chamber and pH 2.0 in the cathodic chamber. (B) CV recorded under the same conditions as in E5.

**Figure 6.10** Current intensity (solid), cathode potential (dashed) and anode potential (dotted) of E8 with pH 7.5 in the anodic chamber and pH 2.0 in the cathodic chamber. The applied potential was 0.2 V.

**Figure 6.11** E8 (A) pH profiles. Cathodic pH (solid), anodic pH (dashed) and setpoint (dotted) (B) Theoretical and experimental proton production. Cathodic  $HP_{exp}$  (solid), anodic  $HP_{exp}$  (dashed) and  $HP_{theo}$  (dotted). Positive HP (proton production) correspond to the anodic chamber and negative HP (proton consumption) to the cathodic chamber.

**Figure 6.12** Nyquist diagrams of BF with different conductivities in the cathodic chamber: 14 ms/cm (○) and 19 ms/cm (●).

**Figure 6.13** Current intensity profiles of HC in E9 (solid) and LC in E10 (dashed). The cathodic pH was controlled at 7.5, the anodic pH at 2.0 and the applied voltage was 0.2 V.

**Figure 6.14** pH profiles of (A) E9 and (B) E10 where the anodic pH of HC and LC was controlled at 7.5 and the cathodic pH at 2.0. The applied voltage was 0.2 V. Cathodic pH (solid), anodic pH (dashed) and setpoint (dotted).

**Figure 6.15** Coulombic efficiency (CE), cathodic gas recovery ( $r_{\text{CAT}}$ ), energy efficiencies ( $r_{\text{E}}$ ,  $r_{\text{S+E}}$ ) (bars) and hydrogen production (circles) for E9 and E10.

**Figure 6.16** LSV recorded in BF with the anodic pH controlled at 7.5 and cheese brine as catholyte.

**Figure 6.17** (A) Monitoring of current intensity (solid) and cell applied potential (dashed) in E11 with pH 7.5 in the anodic chamber and cheese brine as catholyte (B) pH profiles of the experiments. Cathodic pH (solid), anodic pH (dashed) and setpoint (dotted).

## Chapter 7

**Figure 7.1** Schematic diagram of the MEC prototype.

**Figure 7.2** Current intensity, anode potential and applied potential before cell design modifications in the preliminary prototype.

**Figure 7.3** (A) Current intensity, anode potential, applied potential and (B) acetate concentration profiles during inoculation of MEC with anaerobic sludge, cycles 1-3.

**Figure 7.4** (A) Current intensity, anode potential, applied potential, (B) acetate concentration and (C) hydrogen production rate profiles of MEC with acetate with substrate, cycles 4-7.

**Figure 7.5** (A) Current intensity, anode potential, applied potential, (B) acetate and glucose concentration and (C) hydrogen production rate profiles of MEC after changing the carbon source, cycles 8-10.

**Figure 7.6** Evaluating starvation in MEC with an applied voltage of 0.8 V ( $\text{MEC}_{\text{AV}}$ ) (A) Current intensity and (B) anode potential. Note that from days 14 to 20 the anode potential could not be monitored.

**Figure 7.7** Coulombic efficiency (CE), cathodic gas recovery ( $r_{\text{CAT}}$ ), energy efficiencies ( $r_{\text{E}}$  and  $r_{\text{S+E}}$ ) and hydrogen production after different starvation periods at an applied voltage of 0.8 V ( $\text{MEC}_{\text{AV}}$ ).

**Figure 7.8** Evaluating starvation in MEC without any applied voltage ( $\text{MEC}_{\text{WV}}$ ).

**Figure 7.9** Coulombic efficiency (CE), cathodic gas recovery ( $r_{\text{CAT}}$ ), energy efficiencies ( $r_{\text{E}}$  and  $r_{\text{S+E}}$ ) and hydrogen production after different starvation periods without any applied voltage ( $\text{MEC}_{\text{wv}}$ ).



## Chapter 1

**Table 1.1** Electrode half-reactions in MFC and standard reduction potentials.

**Table 1.2** Electrode half-reactions in MEC and standard reduction potentials.

**Table 1.3** Major achievements and applications of BES.

## Chapter 3

**Table 3.1** Summary of the parameter values for acetate and glucose.

## Chapter 4

**Table 4.1** Stoichiometry of the possible reactions occurring in an MEC.

**Table 4.2** Nomenclature and description of parameters.

**Table 4.3** Summary of the electron equivalent balances during a cycle with H<sub>2</sub>-recycling.

**Table 4.4** Summary of the results in a cycle with methanogenic activity.

## Chapter 5

**Table 5.1** Summary of the experimental conditions of batch experiments E1 to E9.

## Chapter 6

**Table 6.1** Summary of the experimental conditions of batch experiments E1 to E11.

## Chapter 7

**Table 7.1** Summary of the efficiencies in batch cycles 1 to 10.

**Table 7.2** Glucose consumption pathways in bioelectrochemical systems [171].

**Table 7.3** Comparison of this work with other studies dealing with pilot-scale or semi-pilot MEC.



## List of Acronyms and Abbreviations

---

A	ampere
AC	alternating current
Ac <sup>-</sup>	acetate
AC-MFC	air-cathode microbial fuel cell
AEM	anion exchange membrane
ARB	anode respiring bacteria
BES	bioelectrochemical system(s)
BF	buffered
C	coulomb
CA	chronoamperometry
CC-MEC	concentric microbial electrolysis cell
CE	coulombic efficiency
CEM	cation exchange membrane
COD	chemical oxygen demand
CV	cyclic voltammetry
E	potential
EIS	electrochemical impedance spectroscopy
EET	extracellular electron transfer
F	Faraday's constant (96485 C/mol e <sup>-</sup> )
HC	high conductivity
HER	hydrogen evolution reaction
HP	proton production
I	current intensity
IDEA	Instituto para la diversificación y ahorro de la energía
IEM	ion exchange membrane
INE	National Statistics Institute
LC	low conductivity
LSV	linear sweep voltammetry
MEC	microbial electrolysis cell(s)
MEC <sub>AV</sub>	microbial electrolysis cell with applied voltage (starvation tests)
MEC <sub>WV</sub>	microbial electrolysis cell without applied voltage (starvation tests)
MFC	microbial fuel cell(s)

OC	open circuit
OCV	open circuit voltage
ORR	oxygen reduction reaction
P	power
PBS	phosphate buffered saline
PS-MEC	pilot scale microbial electrolysis cell
PTFE	polytetrafluoroethylene (Teflon)
$r_{\text{CAT}}$	cathodic gas recovery
$r_{\text{E}}$	energy recovery with respect to the electrical input
$r_{\text{E+S}}$	energy recovery with respect to both the electrical input and the energy content of the substrate
$R_{\text{ext}}$	external resistance
$R_{\text{int}}$	internal resistance
$r_{\text{S}}$	energy recovery with respect to the energy content of the substrate
Sed-MFC	sediment microbial fuel cell
SHE	standard hydrogen electrode
SSAC-MFC	small-scale air-cathode microbial fuel cell
SS-MEC	small-scale microbial electrolysis cell
t	time
V	voltage / volt
W	watt
WM	without membrane
$Z'$	real part of the impedance
$Z''$	imaginary part of the impedance
$\Omega$	ohm
$\eta$	overpotential

**Activation losses:** voltage required to overcome the activation energy of an electrochemical reaction on a catalytic surface.

**Anaerobic digestion:** wastewater treatment in which microorganisms convert biodegradable material into methane in the absence of oxygen.

**Anaerobic digestion sludge:** anaerobic digestion mixed liquor containing non-digested organic matter and microorganisms responsible of anaerobic digestion.

**Anion exchange membrane (AEM):** type of membrane that is selectively permeable to anions.

**Anode:** electrode of an electrochemical system at which an oxidation reaction takes place.

**Anode respiring bacteria (ARB):** bacteria capable of transferring electrons out of the cell, thus coupling their metabolic pathways to external electron acceptors.

**Applied voltage:** voltage provided from an external energy source to drive the reactions in a microbial electrolysis cells.

**Bioelectrochemical system:** an electrochemical system in which electrochemically active microorganisms catalyse oxidation or reduction reactions at an electrode surface.

**Biofilm:** complex communities of microorganisms growing embedded within a self-produced matrix of extracellular polymeric substance on a solid support.

**Buffer solution:** aqueous solution consisting of a mixture of a weak acid and its conjugate base (or vice versa) used to prevent changes in the pH of a solution.

**Capacitive current:** current that does not involve any chemical reactions, but the accumulation or removal of electrical charges on the electrode and in the electrolyte solution near the electrode.

**Cation exchange membrane (CEM):** type of membrane that is selectively permeable to cations.

**Cathode:** electrode of an electrochemical system at which a reduction reaction takes place.

**Cathodic gas recovery ( $r_{\text{CAT}}$ ):** ratio of coulombs consumed in hydrogen production to coulombs arriving to the cathode as current intensity.

**Chemical oxygen demand (COD):** measure used to indicate the amount of organic compounds in water. It is expressed in milligrams of oxygen per liter (mg/L), which is the amount of oxygen needed to completely oxidize the organic compounds to carbon dioxide.

**Concentration losses:** potential losses caused by reactant or product diffusion limitations between the bulk solution and the electrode surface.

**Conductivity:** measure of the ability of an electrolyte solution to conduct electricity.

**Coulomb:** charge transported by a constant current of one ampere in one second and SI unit of electric charge.

**Coulombic efficiency:** ratio of coulombs recovered as current intensity to coulombs contained in the substrate oxidized.

**Cyclic voltammetry:** electrochemical technique used to characterize electron transfer processes in which a cyclic potential sweep is imposed on the working electrode, i.e. the electrode of study, and the response of the system in terms of current intensity is monitored.

**Diffusion:** net movement of a substance by gradient of concentration.

**Electrochemical impedance spectroscopy:** electrochemical technique in which the impedance of an electrochemical system is measured over a range of frequencies.

**Electrolyte:** chemical medium that allows the flow of electrical charge between the cathode and anode.

**Electromotive force:** difference between the cathodic and the anodic potentials, which is positive for spontaneous processes and negative for nonspontaneous processes.

**Electron shuttle:** soluble mediator that ARB use for extracellular electron transfer.

**Energy recovery:** amount of energy added to the system by both the power source and the substrate recovered as hydrogen.

**Exoelectrogenic bacteria:** see ARB.

**Extracellular electron transfer:** process in which electrons derived from the oxidation of electron donors are transferred out of the cell to reduce an electron acceptor.

**Faradaic current:** current generated by the oxidation or reduction of some chemical substance at an electrode.

**Fermentation:** metabolic process that converts complex organic compounds into relatively simple substances in the absence of an exogenous electron acceptor.

**Hydrogen recycling phenomena:** scenario in which the electrochemically produced hydrogen is used by either H<sub>2</sub>-oxidizing bacteria to produce current intensity or homoacetogens to produce acetate, which in turn, can be consumed by ARB to further generate current intensity. Under this situation batch cycles are longer, thus consuming higher amounts of electrical energy and the hydrogen recovery is very low.

**Homoacetogenesis:** microbial formation of acetate using an electron donor such as hydrogen.

**H<sub>2</sub>-oxidizing bacteria:** ARB with the ability of using hydrogen as electron donor.

**Linear sweep voltammetry (LSV):** electrochemical technique used to characterize electron transfer processes in which the potential of the working electrode is changed in a ramped linear fashion and the response of the system in terms of current intensity is monitored.

**Methanogenesis:** microbial production of methane.

**Methanogens:** microorganisms that produce methane as a metabolic byproduct in anoxic conditions. Methane can be produced from acetate (acetoclastic methanogens) or from the reduction of carbon dioxide with hydrogen (hydrogenotrophic methanogens).

**Microbial fuel cell:** bioelectrochemical system in which the chemical energy stored in organic compounds can be directly converted into electrical energy.

**Microbial electrolysis cell:** bioelectrochemical system in which value-added products can be generated from organic compounds by applying voltage.

**Migration:** motion of charged species as a result of an electric field.

**Nanowire:** electrically conductive appendages that ARB use for extracellular electron transfer.

**Ohmic losses:** potential losses caused by the resistance to the flow of ions in the electrolyte and through the ion exchange membrane (if present) and the resistance to the flow of electrons through the electrodes and interconnections.

**Open circuit / open circuit voltage (OC/OCV):** difference of electrical potential between the cathode and the anode of an electrochemical system when disconnected from any circuit.

**Overpotential:** difference between the thermodynamically determined reduction potential of a half-reaction and the potential at which the half-reaction actually occurs.

**Overshoot:** rapid drop in voltage at high current intensities occurred during polarization curves.

**Polarization curve:** cell potential vs. current intensity plot used to characterize the behaviour of an electrochemical system and obtained by gradually changing the external resistance from high to low values.

**Reference electrode:** electrode with a stable and well-known electrode potential. The stability of the electrode potential is reached by maintaining constant the concentrations of each participant of the redox reaction.

**Single-chamber microbial electrolysis cell:** bioelectrochemical system lacking a membrane that physically separates oxidation and reduction reaction products. A single-chamber system can also consist of a direct assembly of one of the electrodes and a membrane not leaving space for the corresponding electrolyte.

**Standard hydrogen electrode:** redox electrode which forms the basis of the thermodynamic scale of oxidation-reduction potentials. By convention, it is zero at all temperatures to form a basis for comparison with all other electrode reactions.

**Starvation:** severe or total lack of nutrients needed for living.

**Two-chamber microbial electrolysis cell:** bioelectrochemical system with a membrane that physically separates oxidation and reduction reaction products.





# APPENDIX

---

Understanding limitations of CV in high-surface bioanodes



Cyclic voltammetry has become a standard tool in the study of bioelectrochemical systems because it is a non-destructive technique that provides useful information about the electron transfer processes under different operational conditions. However, when applied to high-surface electrodes, the scan rate must be severely diminished because otherwise, the capacitive current may mask the faradaic current. This low scan rate results in an increase of the experiment duration that may lead to significant alteration of the initial conditions. To investigate this, the repeatability of cyclic voltammetry was examined in air cathode microbial fuel cells operating in batch mode and at low anode potentials. Consecutive cyclic voltammetries were recorded at different scan rates, showing that a scan rate of 0.1 mV/s was low enough to produce alterations in the performance of the system, especially at high anode potentials where the current intensity was higher in the subsequent replicates. The results indicate that far from other reasons as hydrogen accumulation in the cell or growth of the biomass during CV recording, significant changes in the capability of bacteria to work at high anode potentials were produced.

## A.1 Introduction

The application of standard electrochemical tools such as cyclic voltammetry (CV) is nowadays a very common practice in the study of bioelectrochemical systems (BES) and can help gaining insight into the electron transfer processes [1]. Due to the upward trend in its use, some works have been published for didactic purposes, which provide some guidelines for researchers in the field for the correct use of this technique [2, 3].

CV experiments have been mostly applied in lab-scale BES to: (i) study the mechanisms of electron transfer between the biofilm and the electrode, (ii) determine the enzymes/proteins involved in the process and (iii) evaluate the performance of different cathode materials.

In Fricke, et al. [1], for instance, CV was recorded at different stages of microbial growth and metabolic activity to obtain information on the anodic electron transfer processes of *Geobacter sulfurreducens* in microbial fuel cells. Similarly, Richter, et al. [4] conducted CV

experiments on biofilms of wild type and mutant *Geobacter sulfurreducens* to gain insight on the role of different proteins on the anodic electron transfer. In that study, a multistep extracellular electron transfer mechanism was proposed. The effects of setting the anode potential at different values was also determined by means of CV [5, 6]. More recently, Yoho, et al. [7] combined CV with EIS to demonstrate that *Geobacter sulfurreducens* was able to change its electron transport pathway based on the anode potential. The performance of carbon,  $\text{Mn}_2\text{O}_3$  and  $\text{Fe}_2\text{O}_3$  as cathode materials in MFC was also assessed by conducting CV experiments [8].

All these works showed that CV is a very useful tool when working with BES from which much information can be deduced. One of the key parameters when performing CV is the scan rate, i.e. the rate of the sweep of potential. CV in BES is usually recorded at a low scan rate such as 1 mV/s, due to the slow kinetics [9]. If the potential swept is too fast, it can exceed the whole process kinetics and cause insufficient time for current stabilization at each potential. Decreasing the scan rate has also the advantage of a low capacitive current due to the double-layer effects. Unlike the faradaic current, capacitive current is not as a result of any chemical reaction, but due to the accumulation or removal of electrical charges on the electrode and in the interface between the electrode and the electrolyte solution. There is always some capacitive current when the potential of an electrode immersed in an electrolyte solution is changed. In BES, capacitive current should be minimized as much as possible, as this is not as a result of substrate oxidation and it can mask important information of the process. Capacitive current can be identified because it does not reach a limiting current and because it is still present in the absence of substrate. Furthermore, it is proportional to the electrode surface area and it is especially high in 3D electrodes such as graphite fiber brushes [2]. However, the drawbacks of working at low scan rates are the increase of the experiments duration and a possible induction of biological changes [2].

## A.2 Objectives

The aim of this study is to test the applicability and the reliability of the results of CV in our air-cathode MFC(AC-MFC).

A low scan rate must be used due to the large anodic surface area in these cells. Therefore, it will be investigated whether operating at low scan rates and thus, performing long CV can alter the system performance. For this purpose, several hypotheses to describe the experimental profiles of sequential CV in air cathode microbial fuel cells are put forward and discussed.

## A.3 Materials and Methods

### A.3.1 Reactors description and medium composition

Both air-cathode MFC (AC-MFC) and small-scale air-cathode MFC (SSAC-MFC) were used to conduct the experiments (see Materials and Methods in Chapter 3). MFC worked with an external resistance of 1000  $\Omega$  under daily operation (unless otherwise specified), which resulted in an anode potential of around -0.25 V vs SHE.

The synthetic medium described in Chapter 3 was used with acetate as substrate. The methanogenic inhibitor 2-bromoethanesulfonate was added at a concentration of 10 mM.

### A.3.2 Electrochemical analyses

CV experiments were conducted in three-electrode mode at a scan rate of 0.1 mV/s unless otherwise specified. Prior to each set of replicates, culture medium was renewed to avoid acetate depletion during the experiments and cells were sparged with nitrogen for 10 minutes to remove dissolved oxygen. MFC were then connected to its usual external resistance and once steady-state was reached, experiments were conducted. Before any CV replicate the cell was left 30 minutes in OC. Moreover, in some cases, periods (1 or 5 h) in which the cell worked at different anode potentials were also interspersed among replicates.

## A.4 Results and Discussion

### A.4.1 Scan rate and capacitive current

The first tests at the beginning of this thesis were carried out in AC-MFC and consequently with graphite fiber brushes of  $\approx 0.8 \text{ m}^2$  of surface area. CV were recorded at different scan rates to analyse the system response in each case and determine the most

convenient scan rate for AC-MFC (Figure A.1). At the highest scan rates (10 and 5 mV/s) capacitive current was much higher than faradaic current, thus information regarding the anodic processes could not be drawn from CV. Capacitive current can be easily recognized because, as stated in the introduction, it did not reach a limiting current, but it increased during the forward scan (charge accumulation) and then decreased during the reverse scan (charge release). Capacitive current drastically decreases at 1 mV/s, but still the capacitive current seemed to overlap the signal of the reaction of interest. For this reason, when studying the performance of AC-MFC an scan rate of 0.1 mV/s may be more appropriate, at expenses of long experiments up to 5 hours.

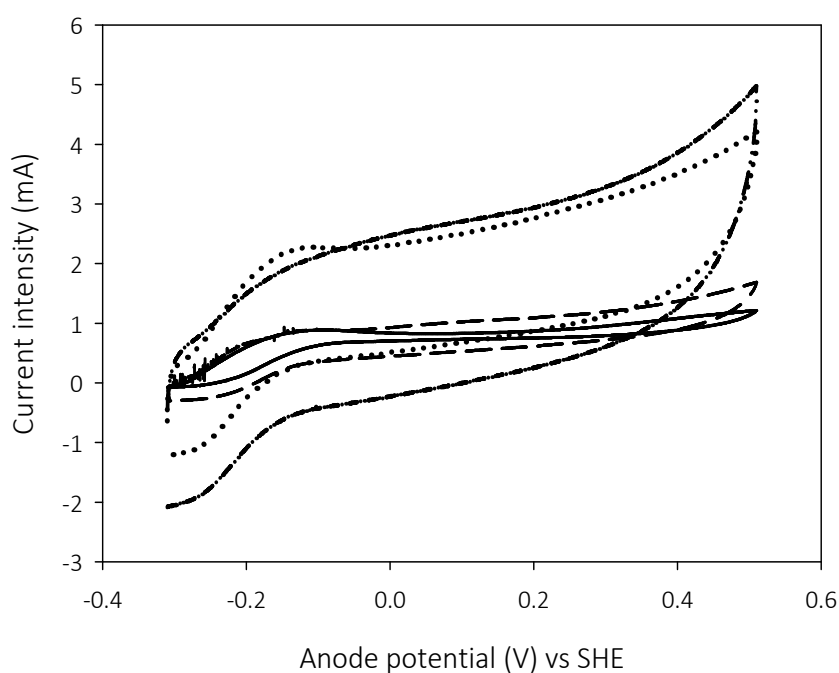


**Figure A.1** CV recorded in an AC-MFC fed with acetate at different scan rates: 10 mV/s (dash-dotted), 5 mV/s (dotted), 1 mV/s (dashed) and 0.1 mV/s (solid).

#### A.4.2 Effects of running CV at low scan rates

As previously stated, the high anodic surface area in an AC-MFC (and thus, a high capacitive current) forced to decrease the scan rate to 0.1 mV/s when conducting CV. However, long experiments can lead to biological variations.

Three consecutive replicates were recorded in SSAC-MFC at different scan rates (2, 1, 0.5 and 0.1 mV/s) to study the extent to which recording of CV might affect the performance of the cells. All the experiments presented from this point were conducted in SS-MFC

(unless otherwise specified) to avoid high capacitive currents even at 2 and 1 mV/s (because of its lower anodic surface area,  $0.18 \text{ m}^2$ ), and due to its more robust design compared to the AC-MFC. Differences in the successive replicates were expected if the performance of CV altered the performance of the cell. Figure A.2 shows the CV replicates performed at the four scan rates. For all the scan rates tested, the current intensity was always higher in the subsequent replicates. Moreover, the lower the scan rate and thus, the longer the experiment, the more significant these differences were, suggesting possible changes in the system, particularly at 0.1 mV/s. It has to be noted that during each of the experiments at 0.1 mV/s, SS-MFC operated for more than 4 hours at anode potentials higher than  $-0.25 \text{ V vs SHE}$  (its value under daily operation with  $1000 \Omega$  of external resistance), whereas experiments at 2, 1 and 0.5 mV/s lasted only around 15 min, 30 min and 1 h, respectively.

The more significant differences between replicates (particularly in Figure A.2D) were observed at anode potentials higher than  $-0.20 \text{ V vs SHE}$ . Furthermore, the SS-MFC reached current intensities close to 4 mA at the scan rates 2, 1 and 0.5 mV/s, whereas current intensity reached a value close to 10 mA at a scan rate of 0.1 mV/s.

According to the results, the behaviour of the cell changed during the experiments. These changes may have been a result of i) changes in external conditions such as pH or conductivity ii) hydrogen production/accumulation and subsequent consumption by ARB iii) synthesis of redox compounds, which shuttle electrons between bacterial cells and the anode, iv) biomass growth or v) adaptation of the microorganisms to higher anode potentials during the CV.

Since the most significant differences between replicates were found at 0.1 mV/s, all experiments to determine the source of these changes were conducted at this scan rate.

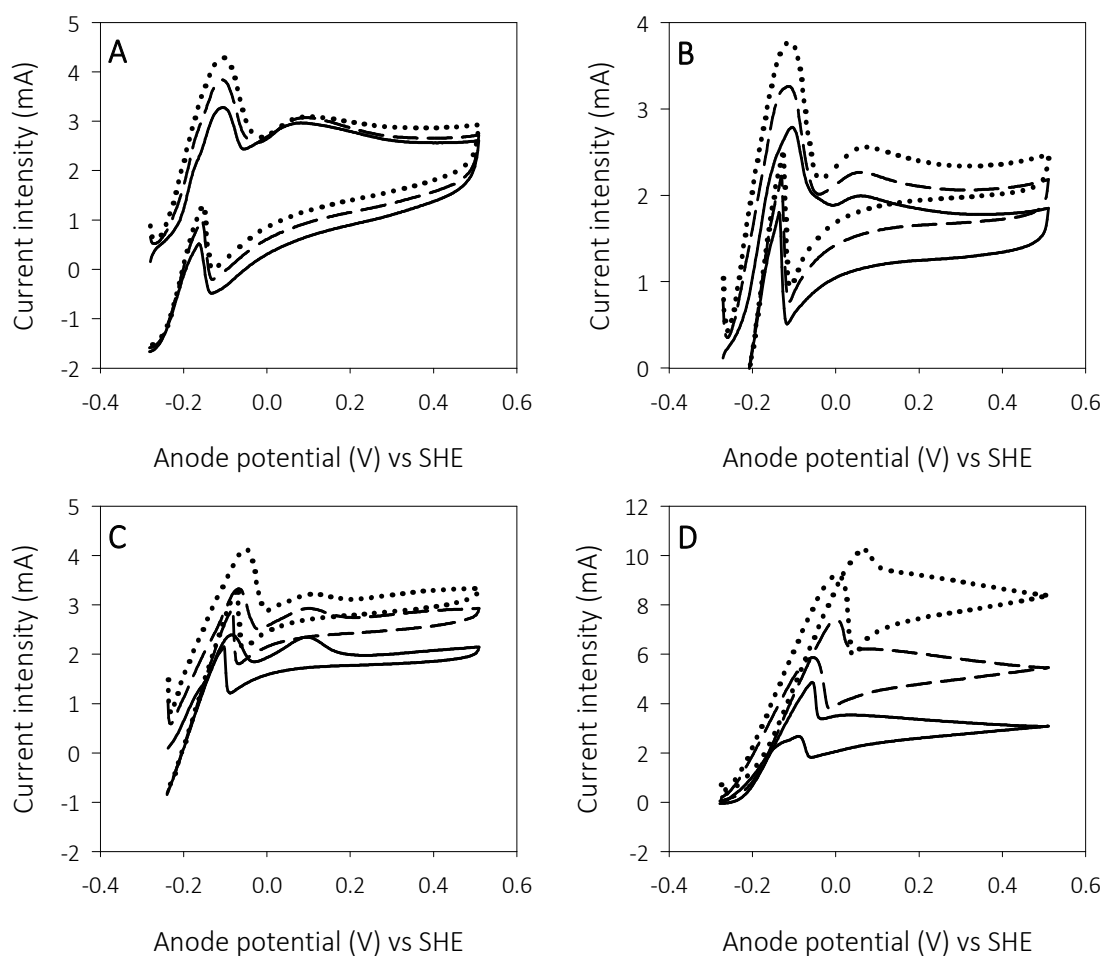


**Figure A.2** CV replicates performed at scan rates (A) 2 mV/s (B) 1 mV/s (C) 0.5 mV/s and (D) 0.1 mV/s. First replicate (solid), second replicate (dashed), third replicate (dotted). Note different scales in current intensity.

#### A.4.3 Possible changes in pH and conductivity

Possible pH or conductivity changes during the experiments were ruled out through periodical measurements at the beginning and at the end of CV experiments. Moreover, as previously discussed in the General Introduction in Chapter 1, protons are produced during the oxidation reaction of acetate. Hence, proton transport limitations out of the biofilm could eventually drive to a local pH decrease within the biofilm. This local pH decrease, however, could not be measured, but if it had significantly affected the performance of the cell, a lower response rather than a higher one would have been expected in subsequent replicates. The same effect would have been also expected for a local pH increase due to proton consumption in the cathodic reaction.



#### A.4.4 Possible accumulation of hydrogen

The possible lack of repeatability caused by the production of hydrogen at the cathode was also studied. If the cathodic reaction had been limited by oxygen during the recording of CV, hydrogen could have been produced given that a voltage is being applied by the potentiostat. Thus, the performance of the cell could have been affected due to the capability of some ARB to consume hydrogen [10]. In this sense, the increase of the current intensity from the first to the subsequent replicates could have been produced as a consequence of hydrogen accumulation in the cell.

A CV was recorded following the same procedure as in the previous experiments. However, the cathodic potential was also monitored during the whole experiment. Figure A.3A shows the anode and cathode potentials over the time during the CV as well as the theoretical cathodic potential to generate hydrogen calculated at 298 K, a pH of 7.5 and a hydrogen partial pressure of 1 atm. The cathode potential was lower than the theoretical potential for hydrogen production practically from the beginning of the reverse scan, and thus, hydrogen could have been generated. A second replicate was recorded to rule out hydrogen as a cause for the lack of repeatability between replicates. Hence, nitrogen was sparged in between replicates to eliminate, if present, the accumulated hydrogen by stripping. As it can be seen in Figure A.3B, the current intensity in the second replicate was still higher than in the first one, so hydrogen could not be the cause of the lack of repeatability in CV.

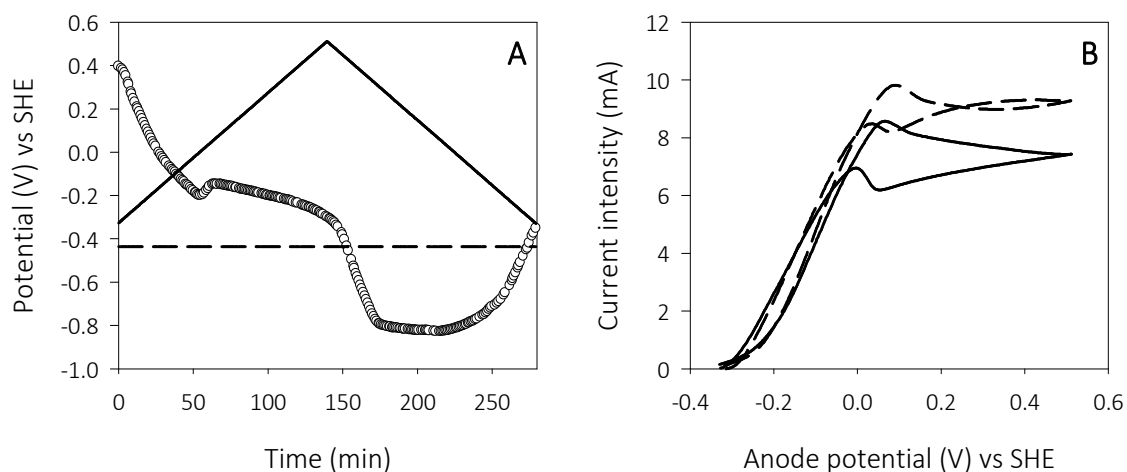


**Figure A.3** Evaluation of possible hydrogen production during CV recording (A) Anode potential (solid), cathode potential (○) and theoretical cathode potential to generate hydrogen (dashed) (B) CV replicates with nitrogen sparging in between them. First replicate (solid), second replicate (dashed).

#### A.4.5 Possible electron-mediators production

As stated in the General introduction in Chapter 1, the extracellular electron transfer (EET) from the anode respiring bacteria (ARB) to the anode can occur through direct transfer (via c-type cytochromes [11], a conductive biofilm matrix or nanowires [12, 13]) or indirect transfer by means of electron shuttles [14]. Therefore, it was hypothesized that if the EET in our cells was mediated by electron shuttles, the observed lack of repeatability in CV experiments could be related to the mediator-producing capacity at high anode potentials. Hence, a subsequent accumulation of mediators in the culture medium could produce an enhancement of the current intensity.

To test this hypothesis, the relevance of mediators in the anodic electron transfer mechanism in our MFC was assessed. For this purpose, the current intensity recovery after two different perturbations was monitored: (i) renewing the culture medium and (ii) removing and re-adding the same culture medium. After each medium addition, cells were sparged with nitrogen for 10 minutes.

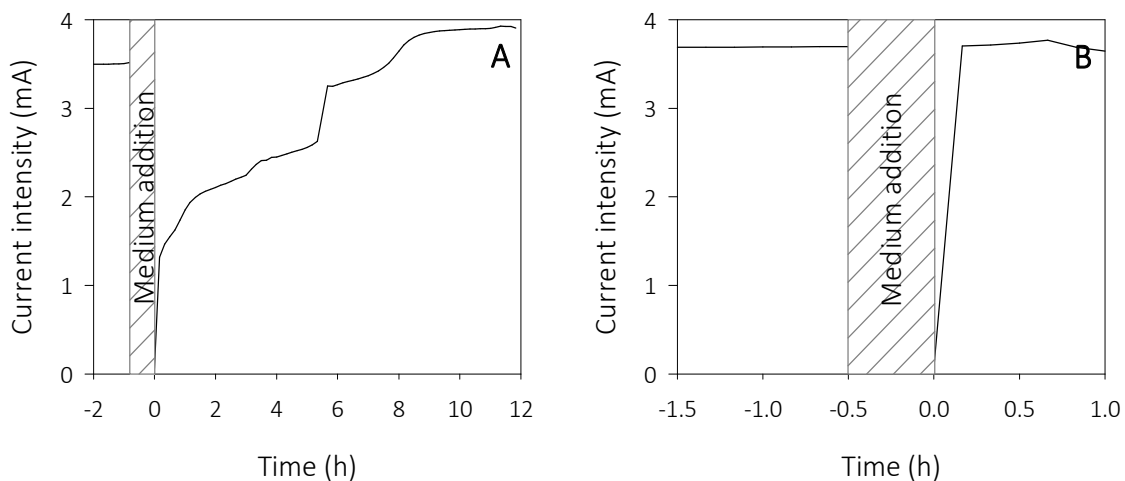


**Figure A.4** Experimental current intensity profiles of MFC before and after (A) renewing the culture medium and (B) removing and re-adding the same culture medium. Cells were connected again at time 0 h.

Figure A.4A shows that the MFC needed 9 hours approximately to recover its initial current intensity values when culture medium was refreshed. In contrast, when the same medium was re-added, the cell recovered almost instantly (Figure A.4B). These results were different from others found in the literature. In Bond and Lovley [15], it took 10 days for *Geothrix fermentans* to recover its original power production after replacement of the medium, which evidenced electron shuttles as mechanism for EET. The recovery period in this case was much lower and exoelectrogenic activity was detected from the beginning of the cycle, which suggest that electron mediators had not a significant role in the EET process. Differences between both experiments here might have been caused by lower temperature of the fresh medium. Therefore, the experimental results allow ruling out changes in the mediator-production capacity as a cause for the change of performance during the experiments.

#### A.4.6 Biological changes: growth vs adaptation

Biomass growth during the experiments could theoretically agree with the experimental results, particularly when ARB had been growing under anode potential limitation during their daily operation. Hence, given the fact that anode potential increased during the CV experiments and that these experiments were quite long, ARB growth could be significant.

Adaptation of bacteria to high anode potentials and thus, to high current intensities has been already reported. Zhu, et al. [16] stated that biofilms acclimated to high anode potentials can generate higher current intensities, since bacteria express more electron transfer component, i.e. organic or inorganic components used to transfer electrons to a final electron acceptor. This dynamic behaviour of bacteria was also studied in polarization and power curves, where the occurrence of power overshoot (caused by a rapid decrease in voltage and current intensity) was eliminated by allowing sufficient time for bacteria to adjust to a change in the external resistance [17] or by simply adapting the reactors to low external resistances [18]. In another study Zhu, et al. [6] claimed that ARB were able to self-regulate electron transfer pathways to adapt to different anode potentials. This observation was corroborated in Yoho, et al. [7], where the potential-dependency of two different electron transport pathways in a pure culture of *Geobacter sulfurreducens* was proved. In the same study it was stated that a shift between these two pathways could be accomplished in a matter of minutes.

Previous experiments showed that when recording CV at 0.1 mV/s, the current intensity achieved in a certain replicate was higher than in the previous one. To discern between growth and adaptation of the biomass, CV were recorded by interspersing in between replicates periods of 0 h (initial), 1h and 5 h, in which the anode potential was set at -0.25 V vs SHE (its value under daily operation). According to the previous experiments, changes occurring in the system were produced in a period of time of 5 hours. In this manner, it was hypothesized that if bacteria were able to acclimate or adapt to high anode potentials in such a low time, by operating at low anode potentials for a similar period of time, adaptation to low anode potentials could also occur. Therefore, the current intensity would not increase from one replicate to the other, since the cell would have returned to its initial conditions by operating at its usual anode potential.

In contrast, if changes were related to biomass growth, the electroactivity of bacteria at high anode potentials should not be affected by working at low anode potentials for a short period of time. Thus, a higher current intensity could be likewise expected in the subsequent CV replicates.

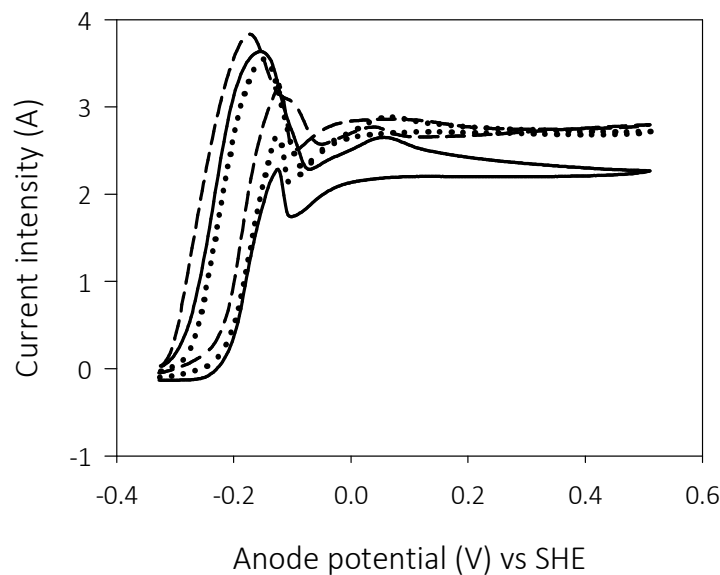


**Figure A.5** CV experiments after setting the anode potential at its typical operation value for 0 h (solid), 1 h (dashed) and 5 h (dotted).

Figure A.5 shows the three consecutive CV replicates performed with interspersed periods of 0, 1 and 5 h, in which the anode potential was set at  $-0.25$  V vs SHE. Current intensity after operating at this anode potential for 1 h was higher than in the initial CV replicate, which could *a priori* suggest biomass growth during the CV replicates. However, the current intensity profile after working at an anode potential of  $-0.25$  V vs SHE for 5 h was very similar to the one in the previous replicate (1 h). These results suggest bacterial adaptation based on the anode potential as a more likely option rather than biomass growth for the lack of repeatability in CV replicates, since operating at a low anode potential for 5 hours has avoided a higher current intensity in the third replicate. Additional tests allowed concluding that substrate limitation was not the reason why the intensity did not increase in the CV replicate after 5 h at  $-0.25$  V vs SHE (results not shown).

#### A.4.7 Adaptation of bacteria to high anode potentials

The results obtained so far seemed to indicate that the differences between CV replicates were mainly caused by an adaptation of ARB to high anode potentials. As previously stated, the MFC used in this study operated with an external resistance of  $1000 \Omega$ , which resulted in an anode potential around  $-0.25$  V vs SHE. In this manner, during the long CV

experiments bacteria would have probably adapted to work at higher anode potentials. In this context, two consecutive CV replicates were recorded after setting the anode potential at 0.21 V vs SHE (which we considered a high anode potential) for different periods of time. Figure A.6 displays the replicates after 1 and 5 hours operating at this anode potential. In the first case, the MFC still showed a higher response in the second replicate, but MFC exhibited practically the same response in both replicates after 5 hours at an anode potential of 0.21 V vs SHE. Figure A.6C shows the current intensity evolution over time previous to any CV experiment when the anode was poised at this potential for 1 and 5 hours. As observed, after an initial drop, the current intensity followed an increasing trend and after 5 hours, it finally stabilized. Thus, lack of repeatability after 1 hour could be expected, since at that point the current intensity was still increasing.

Most of the voltammograms presented in this work exhibited a peak/decrease in current intensity despite being recorded at a very slow scan rate (0.1 mV/s). However, in those replicates recorded after operating MFC at an anode potential of 0.21 V vs SHE (Figure A.6) peaks seemed to disappear. These results are in agreement with those in Yoho, et al. [7], in which a current intensity decrease in voltammograms was observed for biofilms grown at a low anode potential (-0.145 V vs SHE). In that study, a shift between electron transport pathways was proposed as a cause for this drop in current intensity. Therefore, it seems logical that by operating at high anode potentials for a certain period of time, peaks in current intensity did not appear.

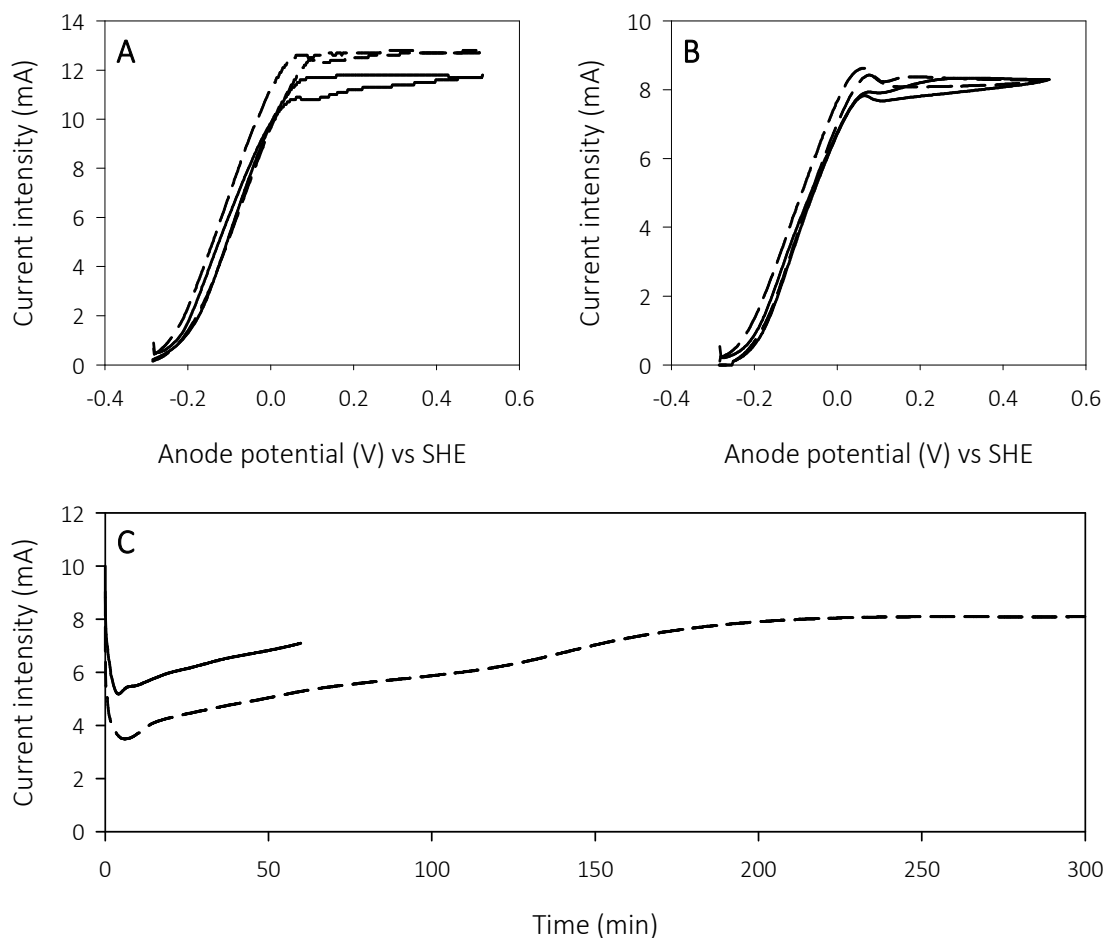


**Figure A.6** CV replicates recorded after setting the anode potential at 0.21 V vs SHE for (A) 1 h and (B) 5 h. First replicate (solid) and second replicate (dashed). (C) Current intensity evolution at 0.21 V vs SHE.

Differences between CV replicates recorded at 0.1 mV/s were minimal when MFC had been working at high anode potentials (0.21 V vs SHE). As previously stated, our cells worked with an external resistance of 1000  $\Omega$  under daily operation, which resulted in an anode potential of -0.25 V vs SHE. Hence, it was finally tested whether the differences between consecutive CV replicates could be likewise eliminated by working at low external resistances. Figure A.7 displays two consecutive CV replicates of different AC-MFC, which had been working with external resistances of 12  $\Omega$ , 50  $\Omega$  and 470  $\Omega$  for over two months. Current intensity in the second replicate was still higher than in the first one in all cases, despite the higher current intensities achieved during daily operation (6, 4 and 1.75 mA for 12  $\Omega$ , 50  $\Omega$  and 470  $\Omega$ , respectively, whereas only 0.5 mA for 1000  $\Omega$ ). However, as the anodic overpotential was relatively low, the anode potential only ranged

from  $-0.18$  to  $-0.25$  V vs SHE for the lowest and the highest external resistance, respectively. Therefore, lower external resistances did not avoid lack of repeatability in CV experiments and a potentiostat would be required to allow ARB adaptation to high anode potentials.

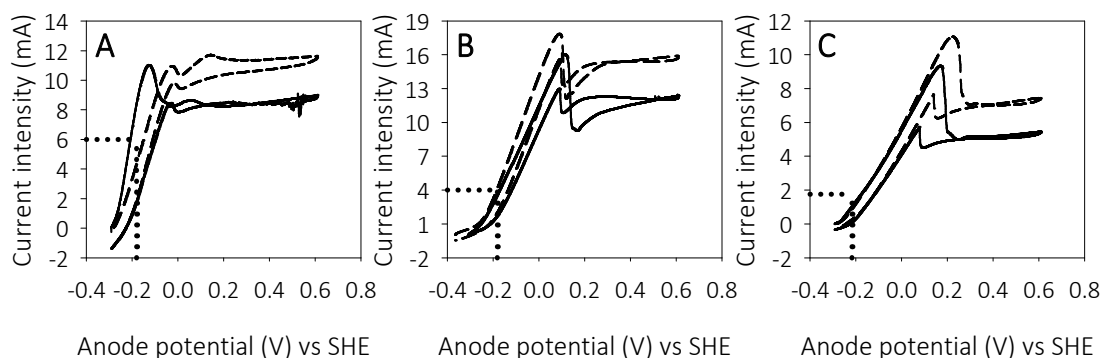


**Figure A.7** CV replicates performed at  $0.1$  mV/s in cells with an external resistance of (A)  $12 \Omega$  (B)  $50 \Omega$  and (C)  $470 \Omega$  under daily operation. First replicate (solid), second replicate (dashed) and anode potential and current intensity under daily operation (dotted).

## A.5 Conclusions

In this study, it has been experimentally demonstrated that the use of AC-MFC with high-surface electrodes and usually operated at low anode potentials is not suitable for fundamental research if the use of electrochemical techniques such as CV is required. Under these conditions, very low scan rates had to be used for a better faradaic/capacitive current ratio. This resulted in large experiments, during which biological changes occurred.

The results evidenced that the recording of CV at very low scan rates altered the system performance. Different current intensity profiles were obtained in subsequent replicates, which appeared to be caused by changes in the capability of bacteria to work at high anode potentials. Differences between replicates could be eliminated by either operating MFC at high anode potentials such as  $0.21$  V vs SHE for sufficient time or operating the cells at their usual anode potential in between replicates. However the response of the system will be different in each case, being the current intensity at high anode potentials much higher in the former case.



Therefore, analysis of CV should be carefully done and as long as possible experiments should be performed in small-scale cells, where the scan rate could be increased to 1 mV/s if required.

## References

- [1] K. Fricke, F. Harnisch, U. Schroder, On the use of cyclic voltammetry for the study of anodic electron transfer in microbial fuel cells, *Energ Environ Sci*, 1 (2008) 144-147.
- [2] F. Harnisch, S. Freguia, A Basic Tutorial on Cyclic Voltammetry for the Investigation of Electroactive Microbial Biofilms, *Chem-Asian J*, 7 (2012) 466-475.
- [3] F. Zhao, R.C.T. Slade, J.R. Varcoe, Techniques for the study and development of microbial fuel cells: an electrochemical perspective, *Chemical Society Reviews*, 38 (2009) 1926-1939.
- [4] H. Richter, K.P. Nevin, H. Jia, D.A. Lowy, D.R. Lovley, L.M. Tender, Cyclic voltammetry of biofilms of wild type and mutant *Geobacter sulfurreducens* on fuel cell anodes indicates possible roles of OmcB, OmcZ, type IV pili, and protons in extracellular electron transfer, *Energ Environ Sci*, 2 (2009) 506-516.
- [5] C.I. Torres, R. Krajmalnik-Brown, P. Parameswaran, A.K. Marcus, G. Wanger, Y.A. Gorby, B.E. Rittmann, Selecting Anode-Respiring Bacteria Based on Anode Potential: Phylogenetic, Electrochemical, and Microscopic Characterization, *Environ Sci Technol*, 43 (2009) 9519-9524.
- [6] X. Zhu, M.D. Yates, M.C. Hatzell, H. Ananda Rao, P.E. Saikaly, B.E. Logan, Microbial Community Composition Is Unaffected by Anode Potential, *Environ Sci Technol*, 48 (2013) 1352-1358.
- [7] R.A. Yoho, S.C. Papat, C.I. Torres, Dynamic Potential-Dependent Electron Transport Pathway Shifts in Anode Biofilms of *Geobacter sulfurreducens*, *Chemosuschem*, 7 (2014) 3413-3419.
- [8] E. Martin, B. Tartakovsky, O. Savadogo, Cathode materials evaluation in microbial fuel cells: A comparison of carbon,  $Mn_2O_3$ ,  $Fe_2O_3$  and platinum materials, *Electrochim Acta*, 58 (2011) 58-66.

- [9] E. Marsili, J.B. Rollefson, D.B. Baron, R.M. Hozalski, D.R. Bond, Microbial Biofilm Voltammetry: Direct Electrochemical Characterization of Catalytic Electrode-Attached Biofilms, *Appl Environ Microb*, 74 (2008) 7329-7337.
- [10] H.S. Lee, B.E. Rittmann, Significance of Biological Hydrogen Oxidation in a Continuous Single-Chamber Microbial Electrolysis Cell, *Environ Sci Technol*, 44 (2010) 948-954.
- [11] C.R. Myers, J.M. Myers, Localization of cytochromes to the outer membrane of anaerobically grown *Shewanella putrefaciens* MR-1, *J Bacteriol*, 174 (1992) 3429-3438.
- [12] G. Reguera, K.D. McCarthy, T. Mehta, J.S. Nicoll, M.T. Tuominen, D.R. Lovley, Extracellular electron transfer via microbial nanowires, *Nature*, 435 (2005) 1098-1101.
- [13] Y.A. Gorby, S. Yanina, J.S. McLean, K.M. Rosso, D. Moyles, A. Dohnalkova, T.J. Beveridge, I.S. Chang, B.H. Kim, K.S. Kim, D.E. Culley, S.B. Reed, M.F. Romine, D.A. Saffarini, E.A. Hill, L. Shi, D.A. Elias, D.W. Kennedy, G. Pinchuk, K. Watanabe, S. Ishii, B. Logan, K.H. Nealson, J.K. Fredrickson, Electrically conductive bacterial nanowires produced by *Shewanella oneidensis* strain MR-1 and other microorganisms, *P Natl Acad Sci USA*, 103 (2006) 11358-11363.
- [14] D.R. Lovley, Bug juice: harvesting electricity with microorganisms, *Nat Rev Micro*, 4 (2006) 497-508.
- [15] D.R. Bond, D.R. Lovley, Evidence for Involvement of an Electron Shuttle in Electricity Generation by *Geothrix fermentans*, *Appl Environ Microb*, 71 (2005) 2186-2189.
- [16] X. Zhu, J.C. Tokash, Y. Hong, B.E. Logan, Controlling the occurrence of power overshoot by adapting microbial fuel cells to high anode potentials, *Bioelectrochemistry*, 90 (2013) 30-35.
- [17] V.J. Watson, B.E. Logan, Analysis of polarization methods for elimination of power overshoot in microbial fuel cells, *Electrochem Commun*, 13 (2011) 54-56.
- [18] Y.Y. Hong, D.F. Call, C.M. Werner, B.E. Logan, Adaptation to high current using low external resistances eliminates power overshoot in microbial fuel cells, *Biosens Bioelectron*, 28 (2011) 71-76.

Name: Yolanda Ruiz Franco

Date of birth: March 5, 1986 (Barcelona, Spain)

Email: yolanda.ruiz.franco@gmail.com



---

## EDUCATION

---

- 2011- Present      PhD student in Environmental Science and Technology.  
Universitat Autònoma de Barcelona.  
Title: "Scale-up opportunities of microbial electrolysis cells for hydrogen production from wastewater".
- 2010-2011      Master in Environmental Studies, Environmental Technology.  
Universitat Autònoma de Barcelona.  
Title: "Examining the potential applications of low scan cyclic voltammetry in mixed culture bioelectrochemical systems".
- 2004-2009      Engineer's degree, Chemical Engineering.  
Universitat Autònoma de Barcelona

---

## WORK EXPERIENCE

---

- 2011-Present      PhD grant (FPU – Ministerio de educación, cultura y deporte).
- 2009-2010      Simulation Engineer at Inprocess Technology & Consulting Group, S.L.

---

## LANGUAGES AND COMPUTER SKILLS

---

Catalan and Spanish (mother tongues)

English (advanced)

German (intermediate)

Windows and Office products (Advanced level), Sigmaplot (Advanced level), MATLAB (medium level), AutoCAD (medium level) and Aspen HYSYS (medium level).

## **PUBLICATIONS IN JOURNALS**

---

Ruiz, Y., Baeza, J. A., Guisasola, A. Enhanced performance of bioelectrochemical hydrogen production using a pH control strategy. *ChemSusChem* 2015, 8 (2), 389–397.

Ruiz, Y., Baeza, J. A., Guisasola, A. Revealing the proliferation of hydrogen scavengers in a single-chamber microbial electrolysis cell using electron balances. *International Journal of Hydrogen Energy* 2013, 38 (16), 15917–15927.

Ribot-Llobet, E., Montpart, N., Ruiz-Franco, Y., Rago, L., Lafuente, J., Baeza, J. A., Guisasola, A. Obtaining microbial communities with exoelectrogenic activity from anaerobic sludge using a simplified procedure. *Journal of Chemical Technology and Biotechnology* 2014, 89 (11), 1727–1732.

## **PUBLICATIONS SUBMITTED/ IN PREPARATION**

---

Ruiz, Y., Ribot-Llobet, E., Baeza, J. A., Guisasola, A. Performance of bioelectrochemical systems after different starvation periods. Submitted

Ruiz, Y., Baeza, J. A., Guisasola, A. Microbial electrolysis cell performance using non-buffered and low conductivity wastewaters. In preparation

## **CONFERENCES**

---

Ruiz, Y., Rago, L., Cortés, P., Baeza, J.A. and Guisasola, A. Identifying hydrogen scavengers in a single-chamber membrane-less microbial electrolysis cell. 4<sup>th</sup> International MFC Conference, Cairns, Australia 2013. Poster presentation.

Ruiz, Y., Baeza, J. A., Guisasola, A. High hydrogen production at a very low applied potential through pH control strategies. 2nd European meeting of the International Society for Microbial Electrochemistry and Technology, Alcalá de Henares, Spain 2014. Poster presentation







